Synthesis and reactivity of novel ONN- and ONO-palladium(II) pincer complexes; applications in CH-halogenation of aryl-pyridones

Thesis submitted for the degree of Doctor of Philosophy at University of Leicester

Singh, Amandeep

Department of Chemistry

10th of October 2017

UNIVERSITY OF LEICESTER

Synthesis and reactivity of novel ONN- and ONO-palladium(II) pincer complexes; applications in CH-halogenation of aryl-pyridones

Amandeep Singh

Abstract

In this thesis, a library of novel unsymmetrical tridentate NNO- and ONO'-type ligands are synthesized and complexed with sources of palladium(II) with a view to exploring the reactivity of the so-formed pincer complexes and their role in CH-halogenation.

Chapter 1 presents a general introduction to pincer chemistry with the emphasis being placed on pincer ligands in which a pyridine unit defines the central donor atom and metals drawn from the platinum group and in particular palladium.

In chapter two the synthesis and characterization of four unsymmetrical ONN-type pincer pro-ligands is described, two of which possess donor units that are capable of inducing hydrogen-bonding interactions. The phenomenon of complex self-dimerization via hydrogen bonding is demonstrated as is its inhibition through suitably placed steric bulk. Ligand exchange reactions of an acetate group with a halide, pyridonate, phenolate, carboxylate are reported and the intra- and intermolecular NH···A interactions studied.

Chapter 3 describes the synthesis of four examples of ONO'-type pro-ligands and their ability to act as dianionic ligands when bound to soft palladium(II) in the form of dimers and tetramers. Means of breaking the dimeric species to form well-defined ONO'-PdL (L = pyridines, pyridones) type complexes have been developed as has their amenability to protonation reactions and to form non-covalent interactions.

Chapter 4 documents the rich stoichiometric reactivity of 6-phenyl-2-pyridone with $Pd(OAc)_2$ yielding products the result of CH, OH or NH activation. Furthermore, the ability of $Pd(OAc)_2$ to mediate the catalytic halogenation (bromination, chlorination, fluorination) of 6-phenyl-2-pyridone is probed. In addition, the capacity of ONO'- and ONN-palladium pincers to generate complexes with 6-phenyl-2-pyridone is studied. Finally, the screening of selected palladium pincer complexes prepared in chapters 2 and 3 as catalysts in CH-bromination of 6-phenyl-2-pyridone is disclosed and the results compared to that observed with $Pd(OAc)_2$. Full experimental details are given in Chapter 5.

Acknowledgements

I would like to thank Dr. Gregory A. Solan and Prof. Eric E. Hope for their guidance and support throughout my PhD studies at the University of Leicester. I acknowledge with my highest regards the help provided in my stressful periods during my stay in the inorganic lab. I pay my thanks to Mr. Kuldip Singh, Dr. Gerry Griffith and Mr. Mick Lee for their help with crystallography, NMR spectroscopy and mass spectrometry, respectively. I would like to thank Barbara Villa Marcos, Charles Ellul and Luka Wright for their advice and support during lab work and chemistry discussions.

I also want to thank my fellow PhD students Mona, Amina, Meshari, Rena and Martyna for their support and creating lab a helping and good place to work. I also want to extend my thanks to various MChem students including Billy and Stephen for creating a very encouraging environment in our lab.

Finally, I thank my parents for their continuous confidence in me although I have been a consistent under performer. Without their encouragement, I simply could not have completed this thesis. At the end I would like to express appreciation to my beloved wife Raman who spent sleepless nights with and was always my support in the moments when there was no one to answer my queries.

Contents

Abbreviations

HSAB	Hard/Soft acid base principle
°	Degrees
Å	Angstrom
app.	apparent
Ar	Aryl
AMLA	Ambiphilic Metal Ligand Activation
ASAP	Atmospheric Solids Analysis Probe
br s	Broad singlet
ca.	*circa*
cf.	Confer (compare)
COSY	Correlated spectroscopy
Cp	cyclopentadiene
^{o}C	Degrees Centigrade
d	doublet
DCM	dichloromethane
dd	Doublet of doublets
ddd	Doublet of doublet of doublets
dt	Doublet of triplets
eq.	equivalents
ESI	Electrospray Ionisation
ES-MS	Electrospray Mass Spectrometry
FAB	Fast Atom Bombardment
FT	Fourier Transform

g	grams
GCMS	Gas Chromatography-Mass Spectrometry
h	hours
HOAc	Acetic Acid
HR	High Resolution
HSAB	Hard/Soft acid and base principle
IR	Infra-Red
J	Joules
M	Molar Concentration
m	Multiplet
m/z	Mass/Charge Ratio
Me	Methyl Fragment
MeCN	Acetonitrile
MHz	Mega Hertz
Mp	Melting Point
MS	Mass Spectrometry
NHC	N-Heterocyclic carbene
NMR	Nuclear Magnetic Resonance
OAc	Acetate
OTf	Triflate (trifluoromethane sulfonate)
ppm	Parts Per Million
pr	Propyl Fragment
py	Pyridyl Fragment
R	Alkyl Fragment
s	Singlet

sept.	Septet
SET	Single Electron Transfer
^{t}Bu	*t*- butyl fragment
td	Triplet of doublets
THF	Tetrahydrofuran
TMA	Trimethylaluminium
v/v	Volume/Volume
δ	Chemical Shift

Chapter 1
Pincer complexes and their applications

Chapter 1

Pincer complexes and their applications

1.1 Introduction

Pincer compounds have emerged in recent years as a hot topic of research with tremendous possibilities in areas such as synthesis, catalysis and material science. A large number of pincer complexes have been synthesised and employed in various types of catalytic processes. Pincer complexes, as the name suggests, are complexes with pincer-shaped tridentate ligands bound to a metal centre.[1]

The enhanced stability of a complex containing a tridentate pincer ligand over those containing mono- and/or bi-dentate ligands, as well as other reaction specific favourable properties, make them attractive candidates to be used as catalysts. Inspired by the mode of action of enzymes, organometallic chemists are showing interest in introducing new properties to their organometallic complexes to achieve similar high reactivity and selectivity under milder conditions. In addition to binding pocket and chelate control, other molecular recognition factors such as hydrogen bonding, aromatic stacking, solvophobic effects are features that could be added to the pincer framework to seek higher efficiency and selectivity.[2, 3]

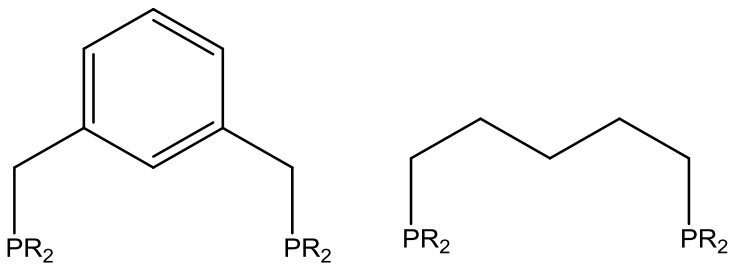

Fig. 1.1 PCP-type pincer ligands first reported by Shaw *et al.*[4]

In 1976 Moulton and Shaw first synthesized pincer ligands of the symmetric PCP-type with phosphines as the neutral exterior donors and an aryl carbon as the central monoanionic sigma donor (Fig 1.1).[4] PCP-type pincers containing an aliphatic carbon as the central sigma donor have also been reported but their chemistry has not been nearly as well developed when compared their aryl counterparts.[5, 6] The relative ease of CH activation of the central aryl C-H bond compared to their aliphatic derivatives, coupled

with the stable planar geometry of the resulting aryl pincer complex, is a likely reason for the scarcity of aliphatic pincer complexes.[7]

Although the first examples of pincer complexes were first prepared in 1976, they did not gain significant attention until their application as robust catalysts, sensors and switches for sulphurdioxide detection were first recognised.[8] In these emerging pincer systems the central metal atom was bound by a covalent bond while the phosphine donors were bound by dative bonds to a metal centre. This unique binding of the tridentate ligands in a meridional fashion gives them a perfect balance between complex stability and ability to mediate difficult transformations as a catalyst.[3, 6]

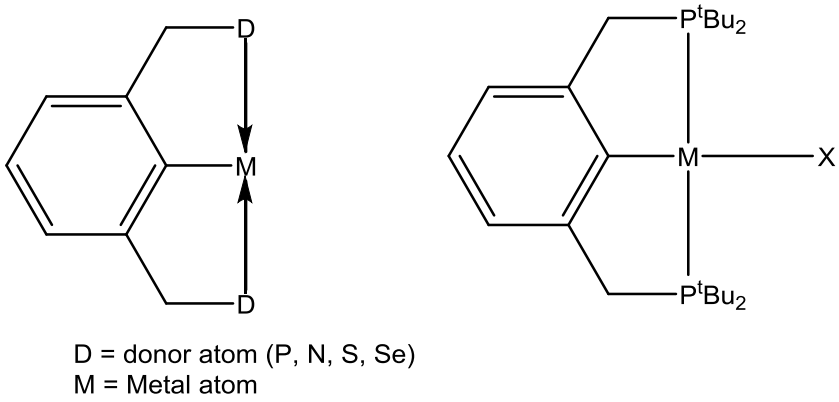

Fig. 1.2 i) General representation of a DCD-type symmetric pincer complex and ii) the first reported pincer complex.[4]

In general, DCD-type symmetrical pincer ligands (where D is a neutral P, N, S or Se donor atom) form stable complexes due to the strong central carbon-metal bond, while their planar coordination leads to high thermal stability (Fig 1.2). High thermal and air moisture stability makes pincer complexes easy to handle and store. Furthermore, thermally stable and robust catalysts are always needed for transformations requiring high activation energy.[9]

The ligand skeleton provides numerous options to modulate the properties of a pincer complex which may be required by the particular transformation.[10] For example:

1. The neutral donor arm could provide a chiral pocket around the metal centre, thus providing asymmetric control with reactions taking place at the metal centre.

2. The choice of exterior donor atoms can be tuned as soft or hard donors depending on the metal centre or reaction requirement. In addition, the donor atoms can provide steric control near the metal centre.
3. The pincer ligand can provide a pocket for binding the reactant, a tunable size for the incoming reactants and sites for counterions and ancillary ligands.
4. Also R groups can be added to the central aryl ring to provide support to the pincer complex or to allow a means of tuning the electronic properties of the ring.

1.2 Symmetrical DCD-type pincer complexes

In addition to well-studied symmetrical PCP pincer complexes, complexes with pincer ligands such as SCS, NCN and SeCSe have also been thoroughly explored due to their properties in synthesis, catalysis and material science.[4, 10-13] These symmetrical aryl-based DCD-type pincer complexes have found use as catalysts for many desirable transformations. For example, the SeCSe-Pd(II) pincer complex shown in Scheme 1.1 is air and moisture stable and is an efficient catalyst for the allylation reaction of aldehyde with allyltributyltin.[12] Similar allylation is also reported by a NCN-Pd(II) pincer complex.[13]

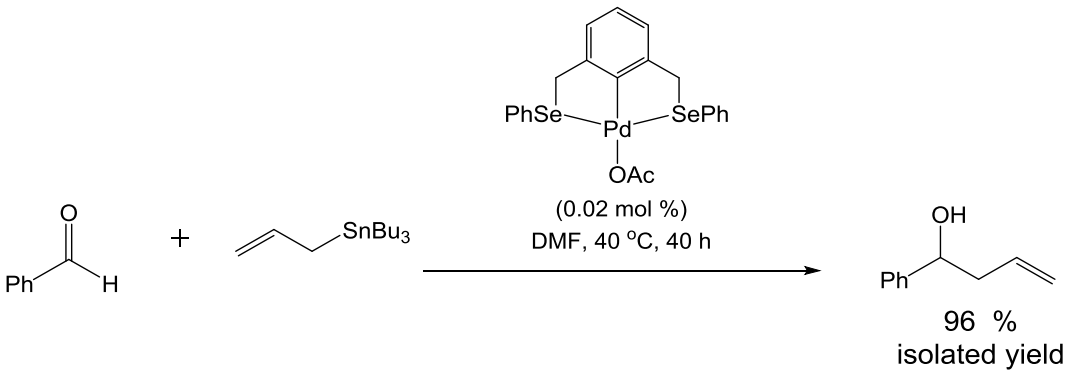

Scheme 1.1 Allylation of aldehydes with allyltributyltin catalysed by a SeCSe-Pd(II) pincer complex

1.3 Unsymmetrical DCD'-type pincer complexes

In earlier studies symmetrical pincer complexes were considered more stable and as a result have been studied more extensively when compared to their unsymmetrical counterparts. Nevertheless unsymmetrical pincer complexes have also been reported and have their own unique properties. They can be formed by different side donor atoms or

with the same donor atoms but with different sized chelate rings formed with the metal. Some examples of unsymmetrical palladium pincers are shown in Fig. 1.3.[14, 15]

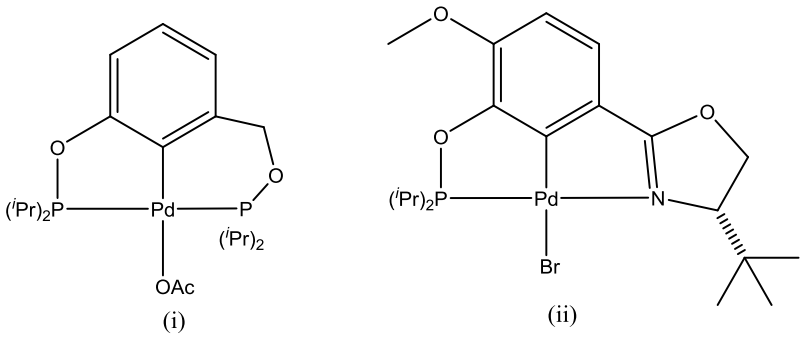

Fig. 1.3 Unsymmetrical palladium pincer complexes: i) with different chelate ring sizes and ii) with two different donor atoms

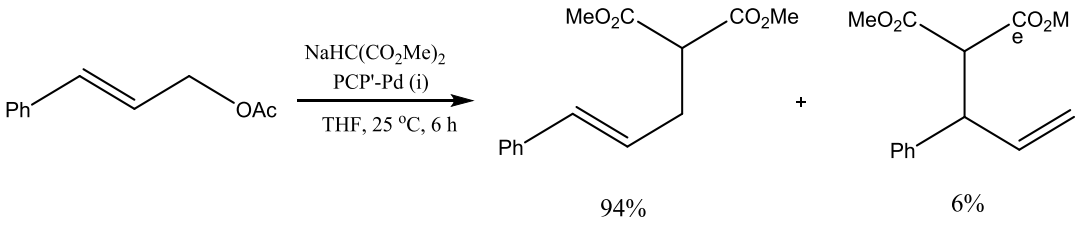

Scheme 1.2 Regioselectivity in the allylic alkylation of cinnamyl acetate with sodium dimethyl malonate with the unsymmetrical palladium pincer (i) shown in Fig. 1.3

It was found that unsymmetrical palladium pincer (i) (in Fig. 1.3) proved a more efficient catalyst when compared to the symmetric derivative in the allylic alkylation of cinnamyl acetate with sodium malonate. It was suggested that increased reactivity of (i) is due to an increase in the flexibility of the complex due to increased ring size, and an increase in the P-M-P angle.[14]

1.4 Pyridine-based pincer complexes

Pincer complexes with a pyridine nitrogen as the central donor atom are relatively rare in comparison with their aryl counterparts. Even so these DND-type complexes are of high interest due to their interesting properties they offer towards catalysis, synthesis and electroluminescent materials.[3, 8, 16, 17] A wide range of symmetrical pincers with a central pyridine nitrogen have now been reported including those based on PNP[18], NNN, CNC[19] and SNS.[20] Indeed these pyridine-based pincer complexes have been of great interest due to their utility in catalysis, new materials and ease of synthesis.

For example, the pyridine-based PNP-Ir(III) complex constitutes an almost perfect catalyst for the hydrogenation of carbon dioxide in the presence of potassium hydroxide to form potassium formate with turnover numbers up to 3,500,000 and turnover frequencies of 150,000 h^{-1}.[21]

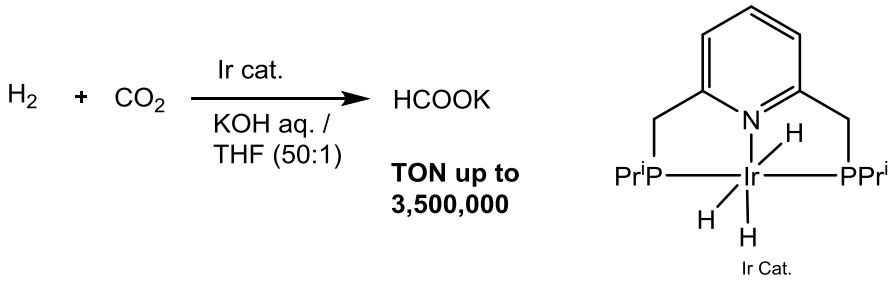

Scheme 1.3 Hydrogenation of carbon dioxide with PNP-Ir(III) pincer catalyst[21]

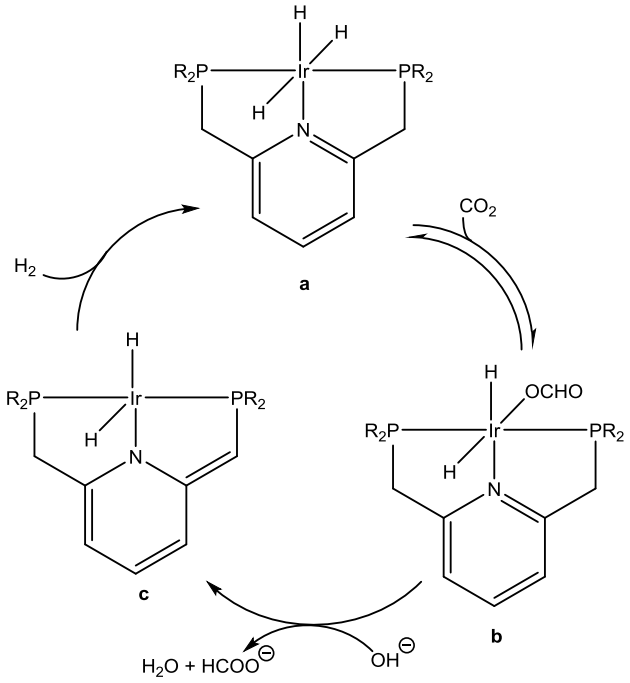

Scheme 1.4 Possible mechanism for the PNP-Ir mediated hydrogenation of carbon dioxide[21]

The reason for the exceptional performance of this iridium catalyst is due to the unique property of the pincer ligand enabling it to work together with the metal centre to activate H_2 molecules. The pyridine ring can lose aromatization (**c** in Scheme 1.4) in the catalytic cycle thus making an empty site for the new hydrogen molecule to be activated in the next step (**a**). This ligand participation through aromatization-dearomatisation of a pyridine ring has revolutionized the hydrogenation of molecules such as carbon dioxide.[22]

In a similar way, it has been demonstrated that symmetrical PNP-pincer complexes of palladium and platinum are capable of undergoing single or double deprotonations to form neutral or anionic complexes again showing the non-innocence of the pincer ligand (Scheme 1.5).[18, 23] Hence it can be seen that the presence of pyridine as a central donor in a pincer complex can introduce bifunctional properties to the complex to allow it to carry out potentially challenging transformations.

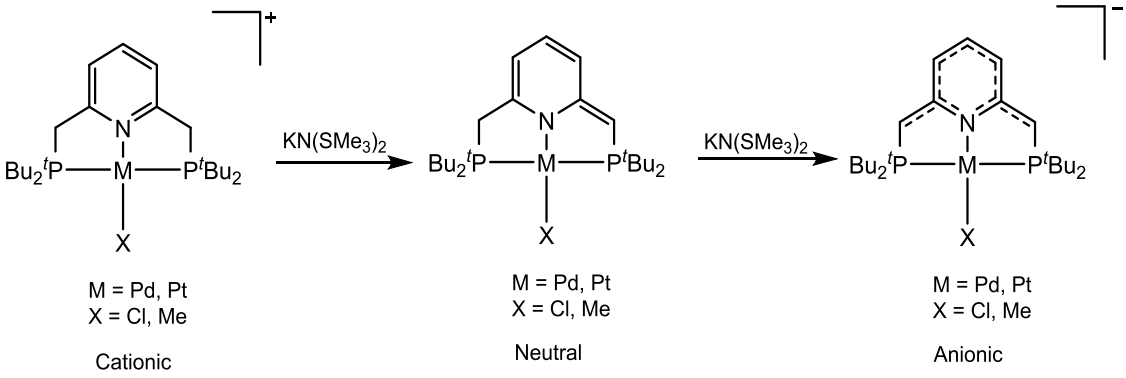

Scheme 1.5 Symmetrical PNP-pincer complexes in single- and double-deprotonation reactions

As with their PNP counterparts, other pincer ligands such as the SNS-type have shown their non-innocent behaviour in the formation of complexes (Scheme 1.6). It was established that the resulting anionic SNC-Pd alkyl complex was an active catalyst in a Negishi coupling reaction.[20, 24]

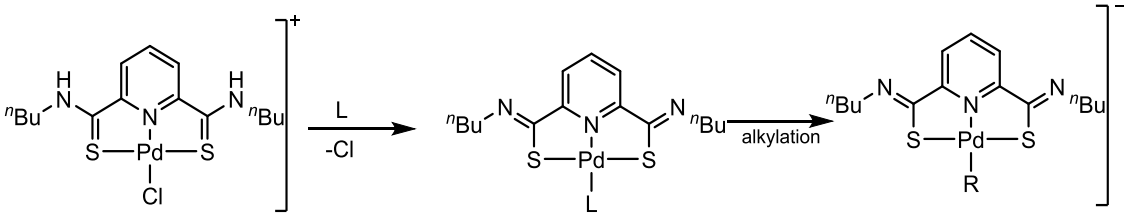

Scheme 1.6 Deprotonation followed by ligand exchange leading to an anionic SNS-Pd alkyl complex

1.5 Unsymmetrical pyridine-based pincer complexes

Like carbon-based pincer ligands, pyridine-based pincers can be of the symmetrical (DND) or unsymmetrical type; the unsymmetrical variant most often coming in the form of inequivalent exterior donor atoms (DND') (Fig. 1.4).

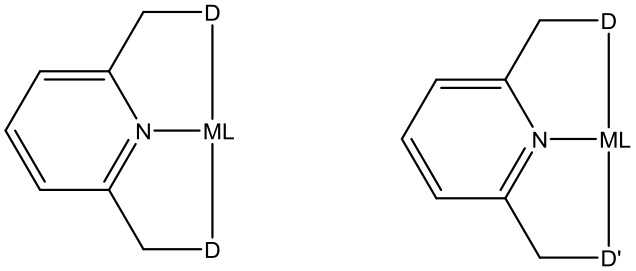

Fig. 1.4 Representations of pyridine-based symmetrical and unsymmetrical pincer complexes.[22]

Unsymmetrical DND'-type pincer complexes have tended to be quite scarce when compared to their symmetrical counterparts until recently where some examples of their applications as catalysts in otherwise challenging transformations have emerged in the literature.[25] Their ability to allow the pincer ligand and the metal centre to work simultaneously to activate otherwise near inert bonds is of great interest. One such example where the NNP-ligand is non-innocent in a complex and undergoes aromatization-dearomatization of the pyridine ring in hydrogenation reactions of organic carbonates, carbamates and formates is shown in Scheme 1.7.[26]

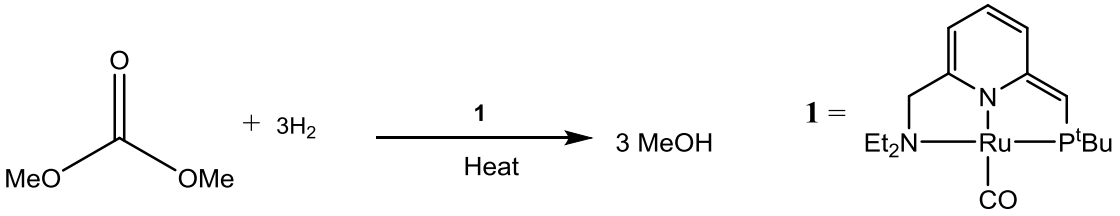

Scheme 1.7 Hydrogenation of dimethyl carbonate to methanol mediated by bifunctional **1**[20]

The proposed mechanism involves aromatization-dearomatization of **1** (Scheme 1.8). The first step involves the addition of a hydrogen molecule to de-aromatized **1** to form aromatized **2**. Hydride transfer to the carbonyl group in dimethylformate to form intermediate **3** with a carbonate ligand which in turn loses methanol to give dearomatized **4**. The next step involves addition of hydrogen which results in aromatization and reduction of the carbonyl ligand to form **5**. Methanol is formed leaving an alkene as ligand with the complex in the dearomatized state **6** which undergoes hydrogenation to give the methoxy intermediate **7**. Methanol is then lost affording **7** which can regenerate dearomatized **1**.

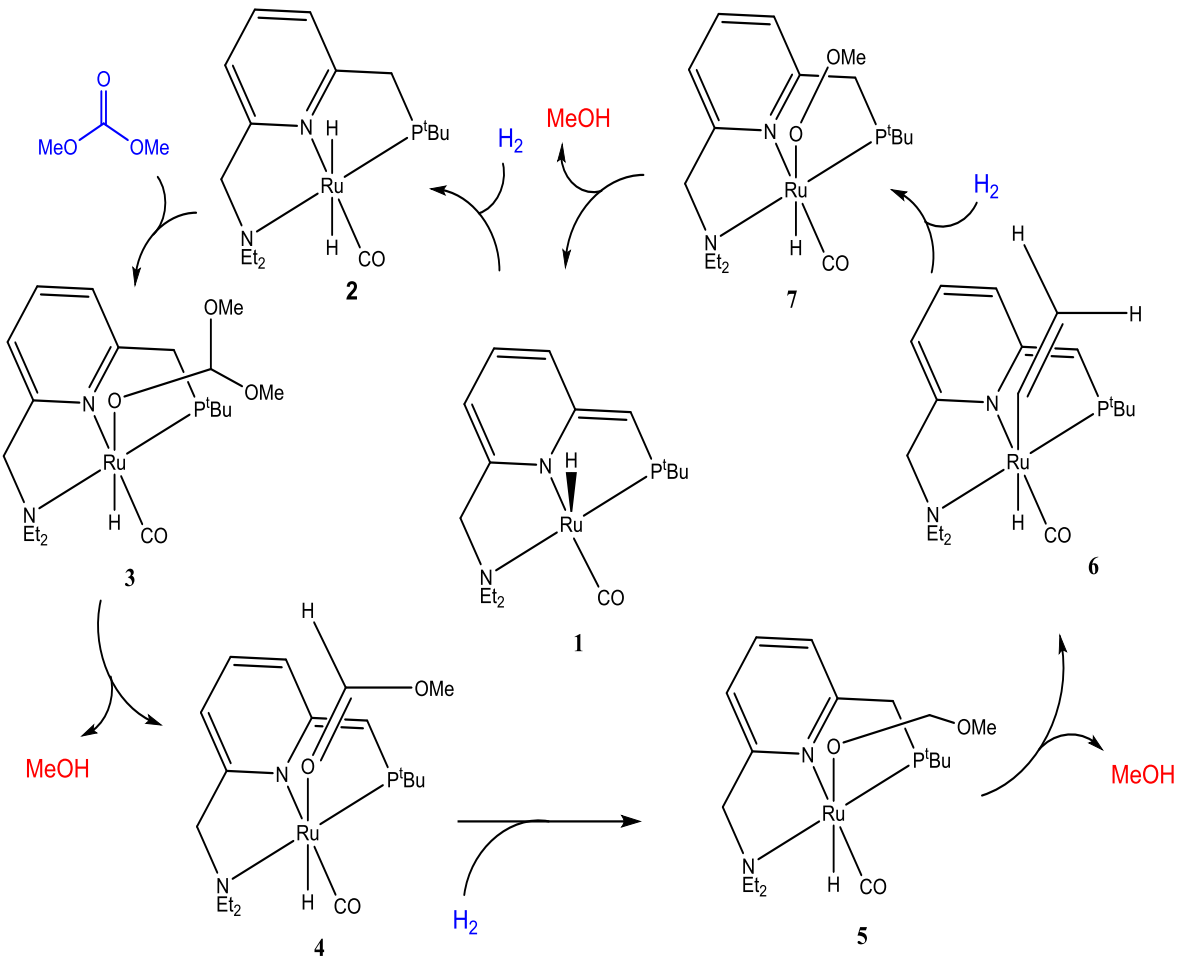

Scheme 1.8 Mechanism for the hydrogenation of dimethyl carbonate via aromatization-dearomatization of NNP-Ru complex **1**

Further development of pyridine-based pincer complexes capable of aromatisation-dearomatisation processes has led to systems able to activate strong bonds such as C-H, H-H, N-H and O-H bonds (Scheme 1.9). Based on the targeted transformation the design of a pyridine-based pincer complex could be modified to achieve the desired reactions such as reversible proton transfer reactions to substrates. These stable pincers are seen as a benign approaches to carry out difficult transformations.[22]

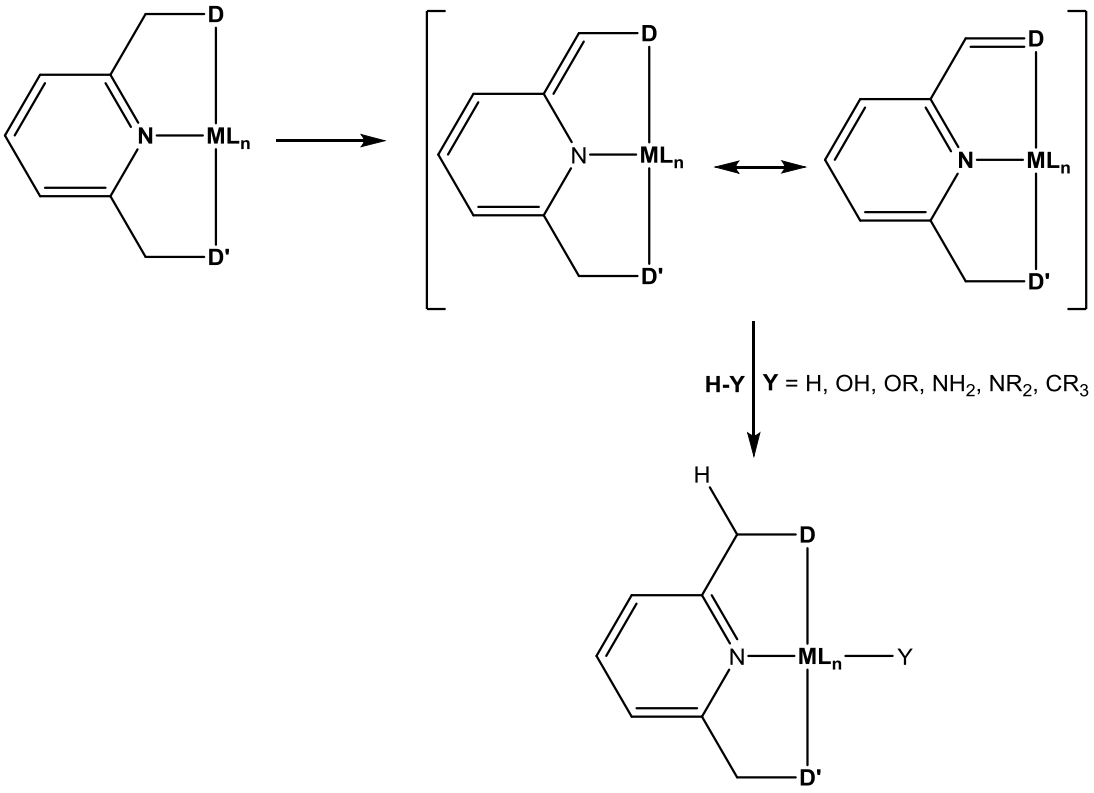

Scheme 1.9 Application of metal-ligand cooperation via aromatization-dearomatization to various activation processes

1.6 Formation of palladium(IV) species bearing unsymmetrical pincer ligands

Higher oxidation state transition metal chemistry is usually considered as interesting field due to its potential capacity to carry out challenging transformations. Palladium(IV) chemistry has gained interest due to its ability to perform transformations which are not achieved by the traditional Pd(II)/Pd(0) cycle.[27, 28] However there are very few examples in literature where Pd(IV) species or complexes have been detected or isolated.[29]

In early work van Koten has reported a Pd(IV) complex formed by the oxidative addition of chlorine to a CNN'-palladium complex (non-pyridine based). It was found that the Pd(IV) complex readily decomposed via reductive elimination to form a C-Cl bond (Scheme 1.10).[30] The Pd(IV) species formed using iodine was even more unstable and instantaneously resulting in reductive elimination.

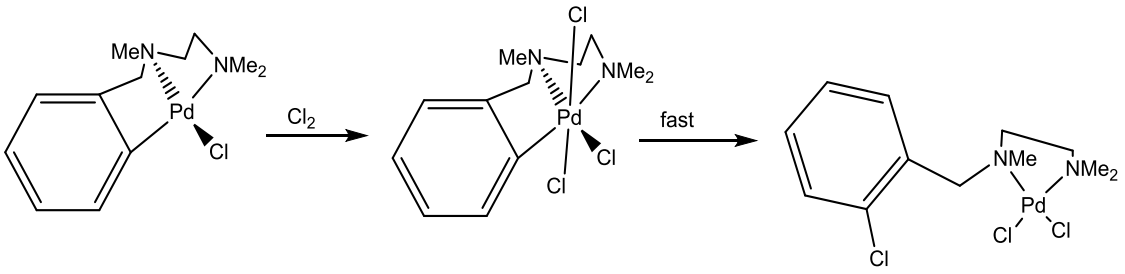

Scheme 1.10 Formation of a Pd(IV) intermediate on a CNN-Pd pincer complex

Hence unsymmetrical pyridine-based pincer complexes offer vast opportunities to tune the electronic properties at the metal centre, which can result in the detection of higher oxidation state complexes, which are otherwise hard to detect. One such example, reported by Vicente *et al*., is shown in Scheme 1.11, in which oxidative addition of an aryl halide to Pd(II) generates a Pd (IV) complex.[31]

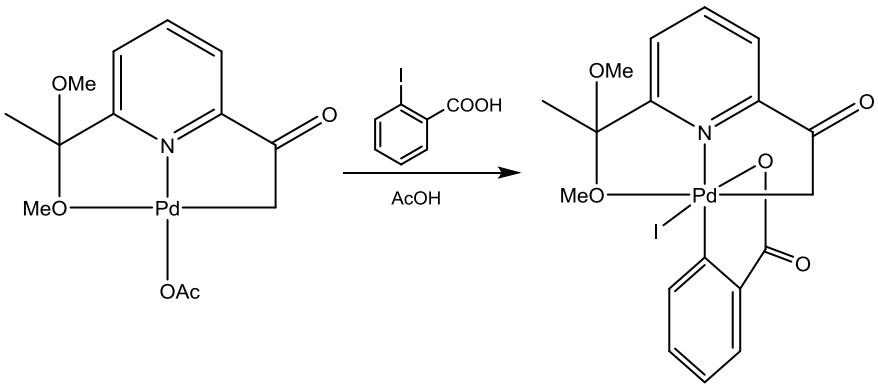

Scheme 1.11 Formation of a Pd(IV) ONC-pincer complex by the oxidative addition of aryl-halide to palladium(II) centre.

The formation and characterization of palladium(IV) species further provides support in favour of Pd(II)/Pd(IV) cycles being involved in many well-known catalytic transformations. The Vicente group also demonstrated that the involvement of Pd(IV) species in Heck coupling reactions.[32] It seems that these particular ONC pincer ligands provide suitable electronic and steric properties to allow the isolation of stable Pd(IV) species that can then be used in coupling reactions.[33]

1.7 Pincer complexes as green catalysts

Pincer complexes as catalysts have made significant improvements to fundamental reactions such as the synthesis of esters, acetals, amides, amines and peptides due to their ability to reduce the amount of undesirable by-products that can be problematic with conventional routes. Traditional methods usually are multistep, involving stoichiometric

amounts of acids, bases and expensive reagents thus producing large amounts of hazardous waste (Scheme 1.12).[32]

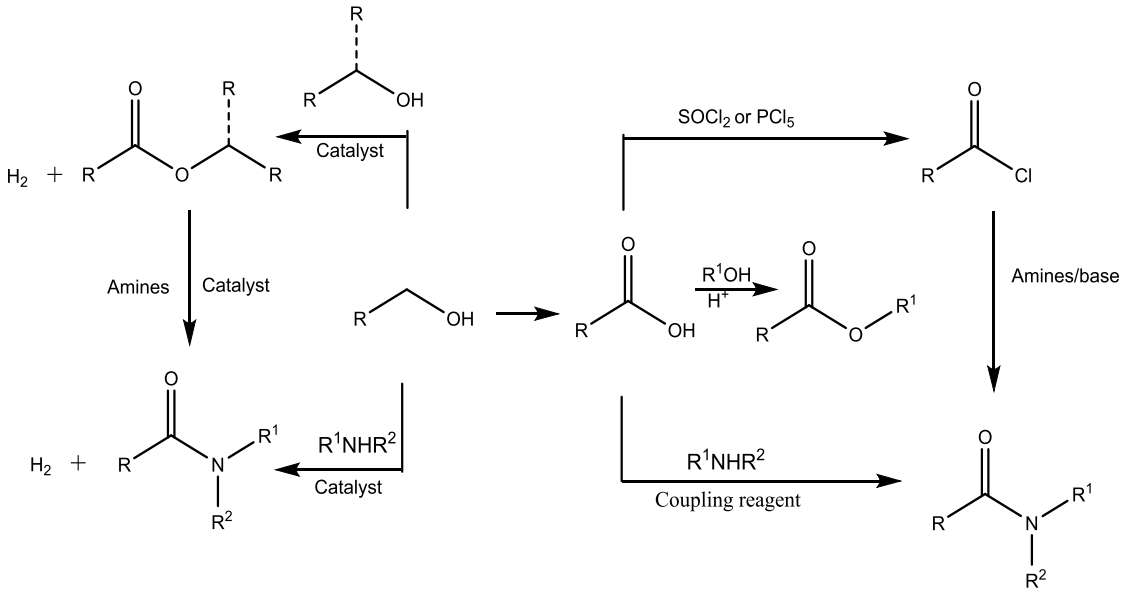

Scheme 1.12 Applications of pincer-based catalysts to fundamental organic transformations

Pincer complexes have also been applied as catalysts in traditional Suzuki coupling reactions and promising results in aqueous solvents and under mild conditions have been observed (Scheme 1.13).[33, 34]

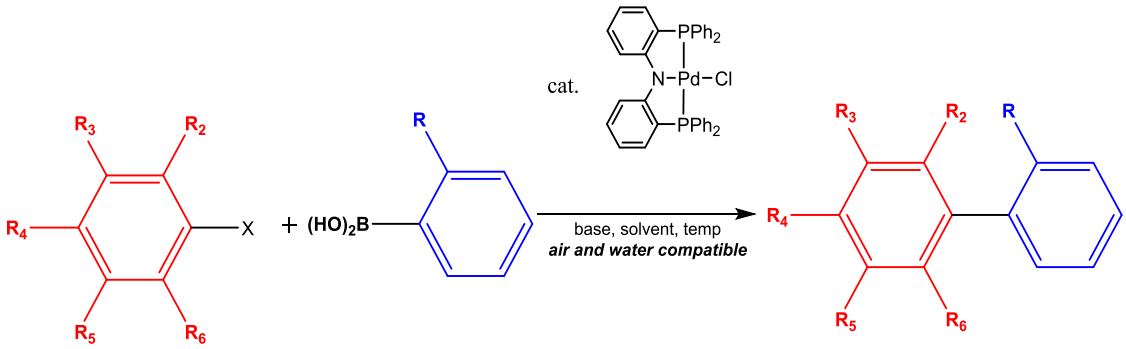

Scheme 1.13 Pincer complexes in Suzuki coupling reaction under mild conditions

1.8 Pincer complexes and hydrogen bonding effects

So far pincer ligands have been seen to not only impart stability to a complex, but also be used in a more functional role to mediate interactively chemical transformations. Currently, there is considerable interest in adding properties to the pincer framework

specific to the particular catalysis such as hydrogen bonding, proton/electron responsiveness, photo responsiveness or molecular recognition function. Hydrogen bonding interactions are short-range interaction between an electronegative atom and a partially positive hydrogen.[35-37] This type of bonding is a highly important property, but its use in organometallic catalysis is still limited. In organometallic chemistry hydrogen bonding can be used as a molecular recognition factor in which a hydrogen bond can guide an incoming substrate/ligand to the binding metal site by interacting with ligands already bound to the metal centre.

The interaction imparted by a hydrogen bonding can provide a favourable push in more difficult transformations. In one such example, the conversion of carbon dioxide into formic acid is thermodynamically unfavourable. However, with the introduction of an amine hydrogen bond donor in the pincer ligand, the iridium formate complex was isolated (Scheme 1.14). Furthermore, as expected, the formate complex formed was the most water soluble due to the presence of hydrogen bonding interactions.[38]

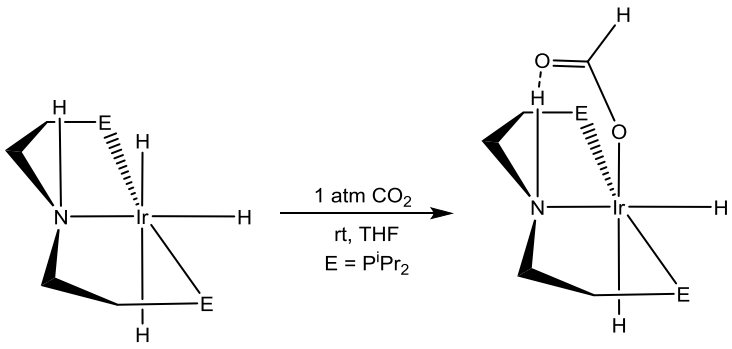

Scheme 1.14 Stabilization of a formate intermediate through NH···O hydrogen bonding

1.9 Aims and objectives of thesis

Two synthetic chapters of this thesis are concerned with the preparation of a range of novel pyridine-based pincer pro-ligands of the type, ONN, ONO', with the aim to explore their use as either monoanionic or dianionic ligands for palladium(II) (Fig. 1.5). Ligand exchange reactions of the so-formed pincer complexes with anionic and neutral monodentate ligands are reported and potential hydrogen bond interactions probed. In addition, a third synthetic chapter is dedicated to exploring the stoichiometric CH

activation of 6-phenyl-2-pyridone using palladium(II) acetate. The catalytic potential of palladium(II) acetate in the CH halogenation (bromination, chlorination and fluorination) of 6-phenyl-2-pyridone is also disclosed and compared with the catalytic performance of a selection of the ONN-Pd and ONO'-Pd complexes developed in the thesis.

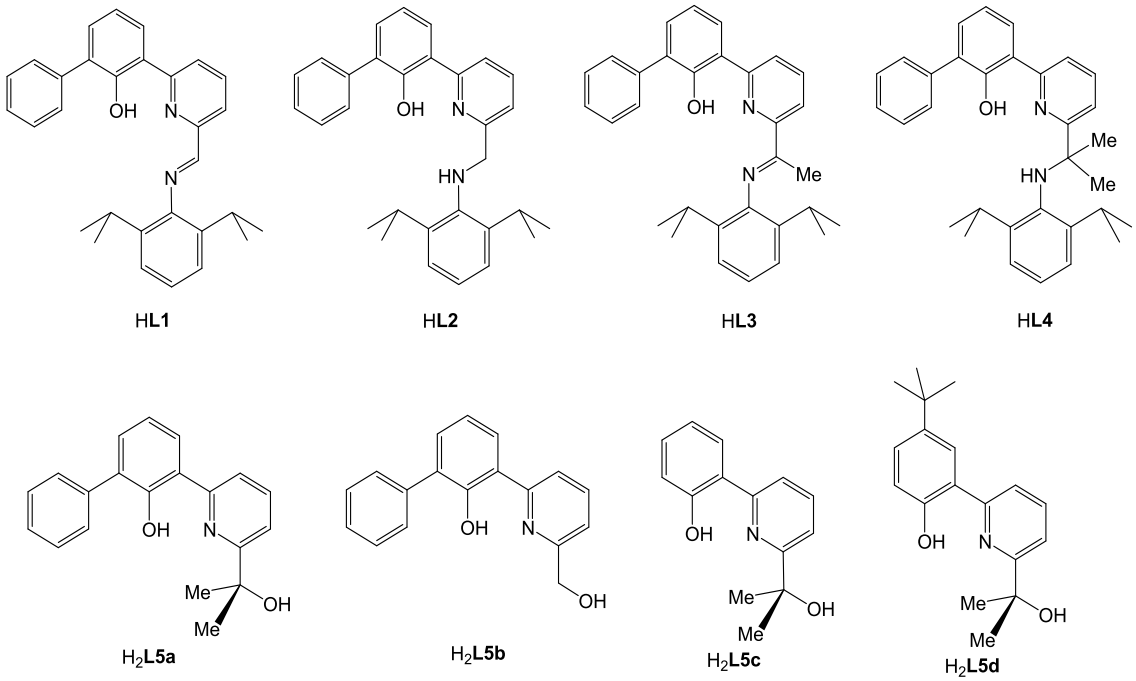

Figure 1.5 Pincer pro-ligands, H**L1** – H**L4** and H_2**L5**, to be synthesised and explored as sources of mono- or di-anionic ligands for palladium(II)

In Chapter 2, four examples of ONN-type pincer pro-ligand, H**L1** – H**L4**, differing in the exterior nitrogen donor (amine versus imine) and the substituents on the group adjacent to the nitrogen donor, are prepared and fully characterized. Their capacity to act as monoanionic ligands on treatment with palladium(II) acetate is investigated, while the potential of the exterior NH group to serve as a directional hydrogen bond donor (D) to acceptor atoms (e.g., A = oxygen) in neighbouring complexes or incoming substrates/ligands is examined. Comparisons are made with regard to the variation in nitrogen donor (imine/amine) on coordination and hydrogen bonding properties. The reactivity of the ONN-Pd complexes towards ligands well-known for undergoing hydrogen bonding interactions such as pyridones and carboxylates is systematically explored. The extent of hydrogen bonding is evaluated by comparing the chemical shift of the N*H* proton in their ^{1}H NMR spectra.

In Chapter 3, four examples of ONO'-type pincer pro-ligands, H_2**L5a** – H_2**L5d**, differing in the steric and electronic properties of either the phenol moiety or the alkyl alcohol are synthesized and fully characterized. Their unusual ability to act as unsymmetrical dianionic pincer ligands on reaction with palladium(II) acetate is reported and compared with unsuccessful attempts to make their symmetrical counterparts. The presence of inequivalent O-donors and their relative ability to serve as hydrogen bond acceptors (A) with a range of incoming ligands/substrates is studied; their proton responsiveness is also be explored.

In Chapter 4, the CH activation of biologically relevant 6-phenyl-2-pyridone is firstly explored using stoichiometric amounts of palladium(II) acetate. Unexpectedly a number of reaction pathways are possible dependent on CH, OH or NH activation leading to a wide variety of new palladium(II) complexes. A section is also dedicated to exploring the use of palladium(II) acetate as a catalyst in the CH halogenation (bromination, chlorination and fluorination) of 6-phenyl-2-pyridone and using N-bromosuccinamide, N-chlorosuccinamide or Selectfluor^{TM} as the oxidising/halogenating reagent. An evaluation of selected palladium pincer complexes prepared in chapters 2 and 3 as catalysts in CH bromination is also disclosed.

Chapter 5 gives the experimental and characterization details for all the complexes, pro-ligands and catalytic studies reported in Chapters 2-4.

1.10 References

1. *Pincer and Pincer-Type Complexes*, John Wiley & Sons, Germany, 2014.
2. S. Das, G. W. Brudvig and R. H. Crabtree, *Chem. Commun.*, 2008, 413-424.
3. *The Chemistry of Pincer Compounds*, Elsevier Science, Amsterdam, 2007.
4. C. J. Moulton and B. L. Shaw, *J. Chem. Soc., Dalton Trans.*, 1976, 1020-1024.
5. H. D. Empsall, E. M. Hyde, R. Markham, W. S. McDonald, M. C. Norton, B. L. Shaw and B. Weeks, *J. Chem. Soc., Chem. Commun.*, 1977, 589-590.
6. M. E. van der Boom and D. Milstein, *Chem. Rev.*, 2003, **103**, 1759-1792.
7. O. F. Wendt, K. J. Szabó and K. J. Szabo, *Pincer and Pincer-Type Complexes*, John Wiley & Sons, Incorporated, Somerset, GERMANY, 2014.
8. M. Albrecht and G. van Koten, *Angew. Chem., Int. Ed.*, 2001, **40**, 3750-3781.
9. N. Selander and K. J. Szabó, *Chem. Rev.*, 2011, **111**, 2048-2076.
10. M. Albrecht, B. M. Kocks, A. L. Spek and G. van Koten, *J. Organomet. Chem.*, 2001, **624**, 271-286.
11. D. Morales-Morales, R. Redon, C. Yung and C. M. Jensen, *Chem. Commun.*, 2000, 1619-1620.
12. Q. Yao and M. Sheets, *J. Org. Chem.*, 2006, **71**, 5384-5387.
13. *Additions of Allyl, Allenyl, and Propargylstannanes to Aldehydes and Imines*, John Wiley & Sons, 2004.
14. Z. Wang, M. R. Eberhard, C. M. Jensen, S. Matsukawa and Y. Yamamoto, *J. Organomet. Chem.*, 2003, **681**, 189-195.
15. Y. Motoyama, K. Shimozono and H. Nishiyama, *Inorg. Chim. Acta*, 2006, **359**, 1725-1730.
16. A. M. Prokhorov, T. Hofbeck, R. Czerwieniec, A. F. Suleymanova, D. N. Kozhevnikov and H. Yersin, *J. Am. Chem. Soc.*, 2014, **136**, 9637-9642.
17. K. J. S. Lukasz T. Pilarski, *Curr. Org. Chem.*, 2011, **15**, 3389.
18. M. Feller, E. Ben-Ari, M. A. Iron, Y. Diskin-Posner, G. Leitus, L. J. W. Shimon, L. Konstantinovski and D. Milstein, *Inorg. Chem.*, 2010, **49**, 1615-1625.
19. A. A. Danopoulos, N. Tsoureas, J. C. Green and M. B. Hursthouse, *Chem. Commun.*, 2003, 756-757.
20. J. Liu, H. Wang, H. Zhang, X. Wu, H. Zhang, Y. Deng, Z. Yang and A. Lei, *Chem. Eur. J*, 2009, **15**, 4437-4445.
21. R. Tanaka, M. Yamashita and K. Nozaki, *J. Am. Chem. Soc.*, 2009, **131**, 14168-14169.
22. C. Gunanathan and D. Milstein, *Acc. Chem. Res.*, 2011, **44**, 588-602.
23. J. I. van der Vlugt, M. A. Siegler, M. Janssen, D. Vogt and A. L. Spek, *Organometallics*, 2009, **28**, 7025-7032.
24. H. Wang, J. Liu, Y. Deng, T. Min, G. Yu, X. Wu, Z. Yang and A. Lei, *Chem. Eur. J*, 2009, **15**, 1499-1507.
25. D. Milstein, *Philo. Trans. of the Royal Soc.*, 2015, **373**.
26. E. Balaraman, C. Gunanathan, J. Zhang, L. J. W. Shimon and D. Milstein, *Nat Chem*, 2011, **3**, 609-614.
27. H. Sun, Y. Zhang, P. Chen, Y.-D. Wu, X. Zhang and Y. Huang, *Adv. Synth. Catal.*, 2016, **358**, 1946-1957.
28. P. Sehnal, R. J. K. Taylor and I. J. S. Fairlamb, *Chem. Rev.*, 2010, **110**, 824-889.
29. O. Blacque and C. M. Frech, *Chem. Eur. J* 2010, **16**, 1521-1531.
30. P. L. Alsters, P. F. Engel, M. P. Hogerheide, M. Copijn, A. L. Spek and G. van Koten, *Organometallics*, 1993, **12**, 1831-1844.
31. J. Vicente, A. Arcas, F. Juliá-Hernández and D. Bautista, *Inorg. Chem.*, 2011, **50**, 5339-5341.
32. *Comprehensive organic transformations : a guide to functional group preparations*, Cambridge : VCH Publishers New York, 1989.
33. L.-C. Liang, P.-S. Chien and L.-H. Song, *J. Organomet. Chem.*, 2016, **804**, 30-34.
34. A. Vignesh, W. Kaminsky and N. Dharmaraj, *ChemCatChem*, 2017, **9**, 910-914.

35. R. H. Crabtree, *New J. Chem.*, 2011, **35**, 18-23.
36. L. M. Epstein and E. S. Shubina, *Coord. Chem. Rev.*, 2002, **231**, 165-181.
37. E. Arunan, R. Desiraju Gautam, A. Klein Roger, J. Sadlej, S. Scheiner, I. Alkorta, C. Clary David, H. Crabtree Robert, J. Dannenberg Joseph, P. Hobza, G. Kjaergaard Henrik, C. Legon Anthony, B. Mennucci and J. Nesbitt David, in *Pure Appl. Chem.*, 2011, vol. 83, p. 1619.
38. T. J. Schmeier, G. E. Dobereiner, R. H. Crabtree and N. Hazari, *J. Am. Chem. Soc.*, 2011, **133**, 9274-9277.

Chapter 2

NNO-palladium pincer complexes with hydrogen-bonding interactions

Chapter 2

NNO-palladium pincer complexes with hydrogen-bonding interactions

2.1. Introduction

Besides the enhanced stability imparted by the tridentate pincer complex, as compared to mono- and bi-dentate ligand counterparts, there are other reaction specific favourable properties that make them more desirable as catalysts.

Despite the importance of hydrogen bonding in natural systems, its use in organometallic catalysis still remains relatively scarce. In principle, hydrogen bonding in organometallic chemistry can be used as a molecular recognition factor where the hydrogen bond can guide the incoming substrate (or ligand) to the binding metal site by interacting with ligands already bound to metal centre. For example iridium complex (**a**) (Fig. 2.1) can only be formed if there is an amine group present to allow hydrogen bonding with the HF ligand bound to the metal centre.[1]

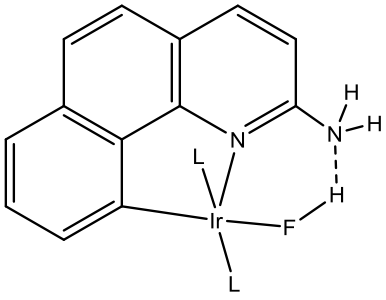

(a)

Figure 2.1. Effect of an amine group on the formation of iridium-HF complex (**a**); L = PPh_3

Organometallic catalysis has gained considerable recognition over the past 60 years due to its capacity to carry out difficult transformations under mild conditions.[2-5] In general reactions occur at the metal centre and the supporting ligands plays an important role in tuning the electronic and steric properties so as to enable the reaction to occur. Despite there being extensive research carried out on this type of catalysis, there is still a need to develop more selective and efficient organometallic catalysts that operate under even milder conditions.[6] To fulfill the ever growing demand for new and improved transformations, novel properties such as multifunctionalisation and self-assembly are starting to be introduced to both the ligands and complexes.[7] Indeed new inorganic catalysts have been developed that make use of metal-ligand cooperation (in case of self-

assembly) and metal-ligand cooperation in multifunctional complexes to accomplish the desired transformation (Scheme 2.1).

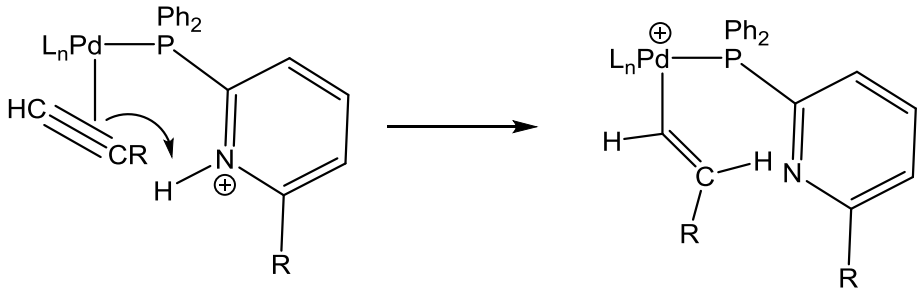

Scheme 2.1. Example of bifunctional catalysis in alkyne hydrogenation by metal-ligand cooperation[8]

2.1.1. Self-assembly of complexes

Self-assembly of organic molecules is seen as an important property as a result of its effect on reaction pathways. In self-assembly, ligands or complexes are aligned with each other by mild hydrogen bonding of their functional groups in contrast to covalent bonds. These mild non-covalent forces link individual ligands/catalysts to supramolecular reaction centers in a transition state and may enhance catalyst efficiencies.[9] Ligands represent a starting point to impart multifunctional and self-assembly concepts to a metal complex for catalysis. In addition to chelating atoms, other functional groups could be attached to the ligand skeleton to achieve the desired properties in a complex. Amine or imine groups are very important in organometallic chemistry on account of the properties they can introduce to a complex in addition to chelation to the metal centre.[9]

2.1.2. R_2NH or RNH_2 groups as ideal hydrogen bond donors

Primary or secondary amine groups are well-known to act as donors to a metal centre but what makes them special is their unique ability to act as a hydrogen bond donor, acceptor and proton source. It can provide cooperation in catalysis by self-aligning ligands and catalysts in reaction mixtures, hence it may play a role in multifunctionalised catalysis. Fortunately, R_2NH or RNH_2 moieties are stable and can be easily installed within a multidentate ligand structure which makes them ideal functional groups to be incorporated within multifunctional ligands and catalysts.[10-12] Depending on the location of the amine group in a complex, it can contribute in number of ways.

2.1.3. Mode of interaction of an amine moiety

The R_2NH or RNH_2 moieties can interact with a metal centre or substrate to influence the reaction in five known modes.

1. *Direct M-NR_2H catalysis*: The nitrogen atom of the amine group is attached directly to the metal atom and can cooperate in the reaction by interacting with substrates attached to the metal atom (Fig. 2.2).

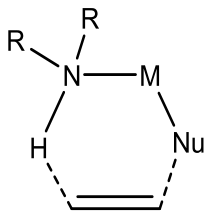

Figure 2.2. Cooperation of a M-bound NR_2H moiety with an incoming substrate

The most relevant example of M-NR_2H-type catalysis comes from the work of Noyori on the hydrogenation of acetophenone to give 1-phenylethanol using $[RuCl_2(PPh_3)_3]$ as the pre-catalyst (Scheme 2.2). High catalytic activity was observed on addition of diethylenediamine (dien) to the reaction mixture. Later it was found that the active catalyst was in fact $[(dien)Ru(PPh_3)_2Cl_2]$ containing an N,N-bound diethylenediamine. The mechanistic studies further explained the importance of the role of the bound primary amine moieties in the catalytic cycle.[13-27]

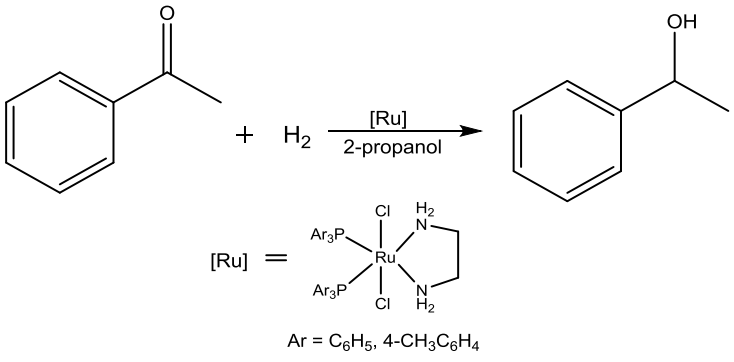

Scheme 2.2. Hydrogenation of acetophenone mediated by $[(dien)Ru(PPh_3)_2Cl_2]$

2. *Remote M-L-NR_2H Catalysis:* In addition to participating directly in a reaction while bound to the metal centre, the amine moiety can also participate by aligning with other

ligands or substrates more remotely (Scheme 2.3).[28] It can act as a recognition factor for desired substrates thus helping them to align in close proximity to the metal centre. In this way, the NR_2H group stays away from metal centre but influences the reaction from the outer sphere. Results obtained from using the hydrogen bond donor and acceptor phosphine ligand **A** gave 80% conversion in rhodium-catalysed alkene hydroformylation, whereas when the non-functional triphenylphosphine was used as the ligand low conversion was noted (Table 2.1).

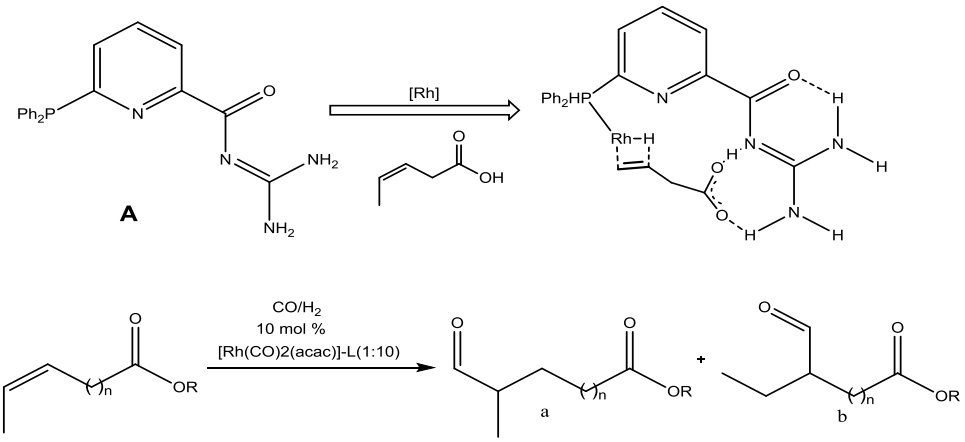

Entry	L	Substrate	Conversion [%]	a:b
1	**A**	*n* = 1, R = H	80.5	11:1
2	PPh_3	*n* = 1, R = H	20	1:1.7

Yield determined by ^{1}HNMR spectroscopy

Table 2.1. Effect of ligands on reaction activity and selectivity

3. *Assembly of Ligands by $NR_2H\cdots O$ hydrogen bonding interactions:* The amine unit in association with a suitable hydrogen acceptor is well known to facilitate dimerisation of neighbouring organic molecules through self-assembly. In this context 2-pyridone or its tautomeric isomer 2-hydroxypyridine can readily assemble in three ways depending on the tautomeric forms involved (Fig. 2.3).

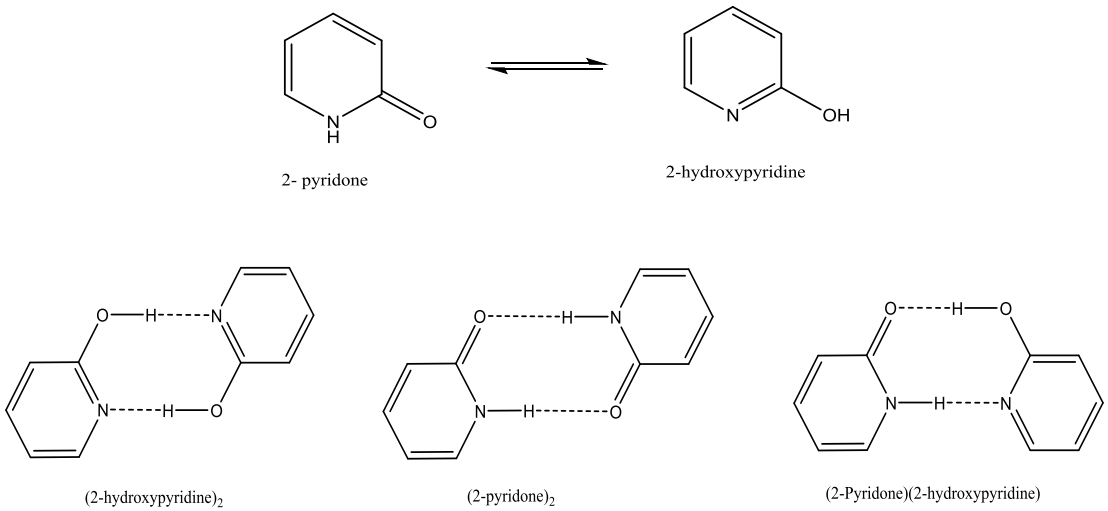

Figure 2.3. The two tautomers of 2-pyridone and the potential hydrogen-bonded assemblies.

This type of association involving pyridone tautomers has been used effectively in inorganic catalysis. For example, Breit *et al.* reported rhodium catalysts, incorporating pseudo-bidentate phosphine ligands that are held together by their self-assembled pyridone moieties, that proved to be very effective in alkene hydroformylation (Scheme 2.3).[29-36]

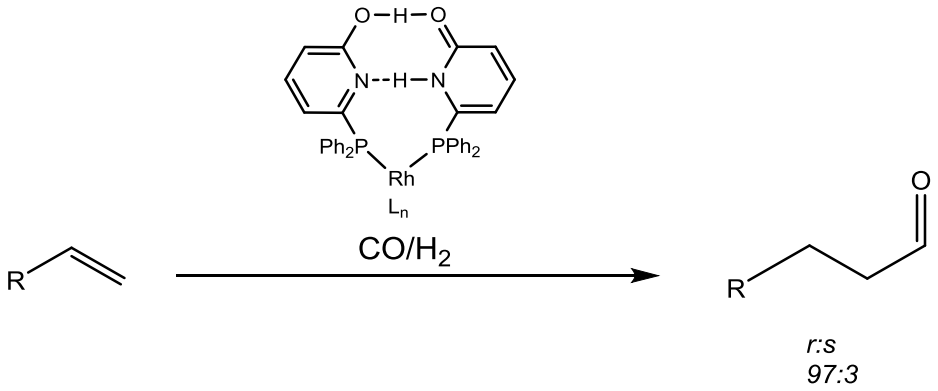

Scheme 2.3. Hydroformylation using a rhodium catalyst based on self-assembled pyridones

4. Assembly of catalysts by hydrogen bonding: As discussed earlier, metal-ligand cooperation to facilitate a metal-catalysed organic transformation, for example by bringing the incoming substrate close to the metal centre by hydrogen bonding or forming a flexible chelate through hydrogen bonding. In addition to metal-ligand cooperation, metal-metal cooperation is highly desirable as bimetallic catalysis are widespread and can be highly efficient.[37] Traditionally, two metal complexes can be brought together in close proximity through covalent bonds. More recently, strategically placed hydrogen

bond donor and acceptor groups within the neighbouring ligand frames can be used to assemble pseudo-bimetallic catalysts. Notably, the enantioselectivity of a Henry reaction was improved significantly when a cobalt catalyst composed of two Co-salen units linked together by hydrogen bonding was employed (Fig. 2.4); the corresponding mono-metallic Co(II) complex proved inferior in the same transformation.[38, 39] In the bimetallic case, assembly of the catalysts is facilitated by two sets of remotely positioned intermolecular $NR_2H\cdots O$ hydrogen bond interactions allowing the cobalt species to perfectly align.

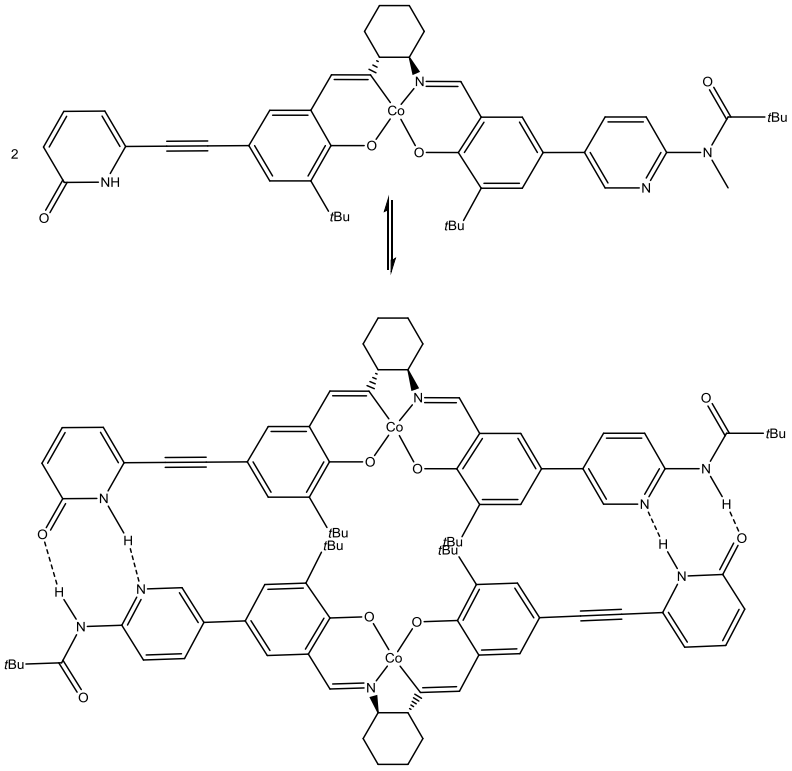

Fig. 2.4. Bimetallic assembly due to remotely positioned NH hydrogen bonding interactions.[38]

5. *Immobilization of homogeneous catalysts by using hydrogen bonding:* Separation of a catalyst is an important step to allow recycling of an expensive catalyst. Usually the catalyst is bound to a supporting surface via a covalent bond, which in turn requires steps to allow its synthesis.[40, 41] Recently, non-covalent bonds such as hydrogen bonding between a catalyst and a supporting surface has provided an attractive tool to remove the catalyst after the reaction has occurred (Fig. 2.5). For example, It has been shown that a silica-supported palladium catalyst bound through hydrogen bonding can be firstly used in nucleophilic substitution and then readily released from the silica support and then replaced with a rhodium catalyst which then can be used in hydroformylation.[42]

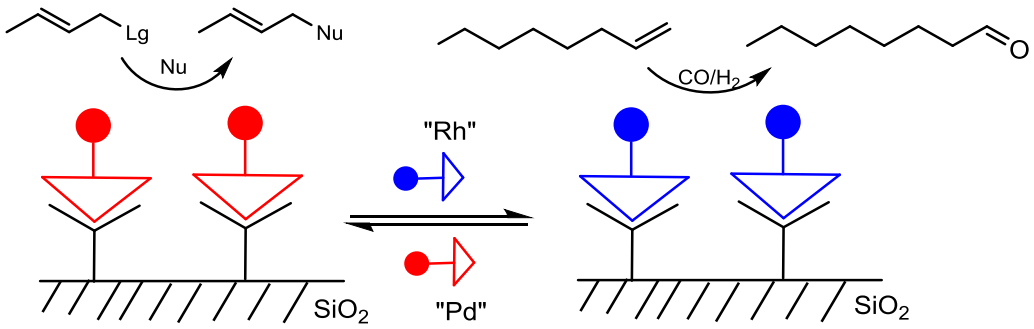

Figure 2.5. Catalyst immobilisation through hydrogen bonding; application to dual catalyst transformations

2.1.4. Importance of the hydroxyl functional group

In addition to the versatile amine functional group, the hydroxyl group is another important group that has been shown to impart bifunctional properties to a ligand system. The properties such as hydrogen bonding, water solubility, acid-base reactivity and in its deprotonated state coordinate to metals as strong donor.[43] The ability of the hydroxyl group to transfer protons in reactions has earned this group a reputation as an essential component in functional catalysis (see for Scheme 2.4).[44, 45]

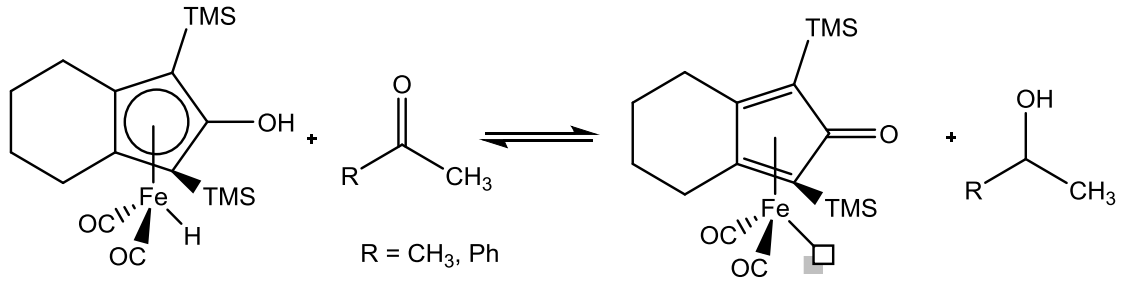

Scheme 2.4. Hydrogenation of ketones by an iron catalyst containing an active hydroxyl ligand.[45]

2.2. Aims of this chapter

The overall aim of this chapter is to develop unsymmetrical pincer-type ligands that when complexed with palladium are capable of creating a sterically protected pocket around the metal centre that can mediate self-assembly or complex-substrate/ligand hydrogen bonding interactions (Figure 2.6).

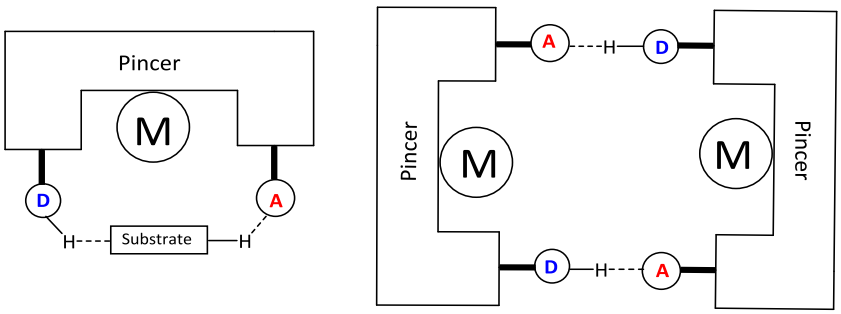

Figure 2.6. Representation of the target hydrogen bonding interactions; (**D**) and (**A**) define the donor and acceptor moieties built into the unsymmetrical pincer arms.

In order to realise this objective we have targeted four monoanionic NNO-pincer ligands, two of which provide the potential to give $NR_2H\cdots A$ type interactions (**L2** and **L4** in Figure 2.7) and, for comparison purposes, two others that will be unlikely to (**L1** and **L3** in Figure 2.7).

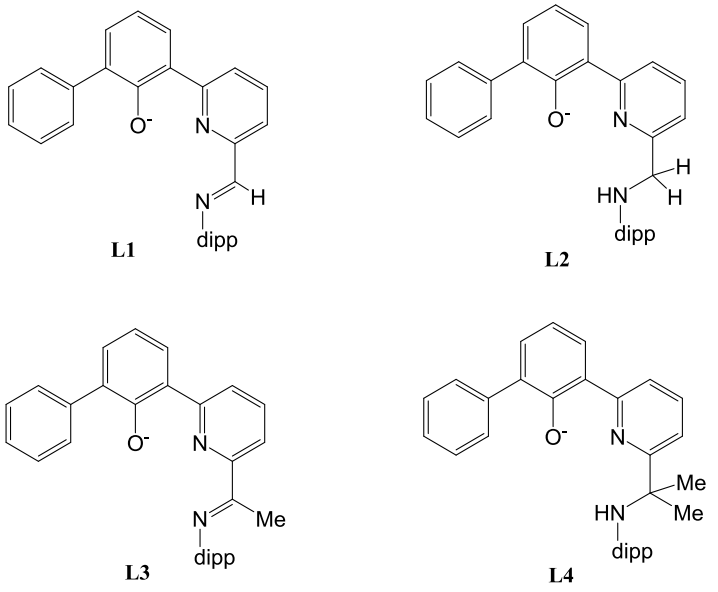

Figure 2.7. Monoanionic 2-(3-biphenyl-2-olate)-6-imine-pyridines (**L1**), 2-(3-biphenyl-2-olate)-6-methyllamine-pyridine (**L2**), 2-(3-biphenyl-2-olate)-6-methyliminepyridines (**L3**), 2-(3-biphenyl-2-olate)-6-(dimethylamine)pyridine (**L4**); dipp = 2,6-diisopropylphenyl

Specifically, we aim to prepare square planar NNO-bound palladium(II)-X complexes (X = halide, pyridonate, carboxylate and triflate) and explore not only the effect of the NNO ligand to promote hydrogen bond interactions but also the influence the X-donor may have on these interactions. Furthermore, some effort will be made to explore the

steric effort of the substituents belonging to the methyl group (CH_2 *vs.* CMe_2) adjacent to the NH donor in **L2** and **L4**.

All the ligands and complexes are new and are fully characterised by spectrometric (ESI, HRMS) and spectroscopic (^{1}H, ^{13}C NMR, IR) techniques as well as by single crystal X-ray diffraction.

2.3. Results and discussion

2.3.1. Preparation of pro-ligands HL1 – HL4

The 2-(3-biphenyl-2-ol)-6-aldimine-pyridine, 2-(3-$C_{12}H_8$-2-OH)-6-(CH=NAr)C_5H_3N (Ar = 2,6-*i*-$Pr_2C_6H_3$ (H**L1**), was prepared in three steps involving Suzuki cross-coupling of 2-methoxybiphenyl-3-ylboronic acid and 2-bromo-6-formylpyridine, BBr_3-mediated deprotection and condensation with 2,6-diisopropylaniline in good overall yield (Scheme 2.5).[46] The imine group in H**L1** can be easily reduced to the amine by using lithium aluminium hydride as the reducing agent to give 2-(3-biphenyl-2-ol)-6-methylamine-pyridine, 2-($C_{12}H_8$-2-OH)-6-CH_2-NHAr)C_5H_3N (Ar = 2,6-*i*-$Pr_2C_6H_3$) (H**L2**).

Similarly, the ketimine analogue, 2-($C_{12}H_8$-2-OH)-6-(CMe=NAr)C_5H_3N (Ar = 2,6-*i*-$Pr_2C_6H_3$) (H**L3**), has been prepared in this case by two steps involving Suzuki coupling of 2-hydroxy-biphenyl-3-ylboronic with 2-bromo-6-acetylpyridine followed by the condensation reaction of the resulting ketone, 2-(3'-phenyl-2'-phenol)-6-acetylpyridine, with 2,6-diisopropylaniline (Scheme 2.6). The imine group in H**L3** can be readily methylated/reduced by treating H**L3** with trimethylaluminium and then hydrolysing the aluminium intermediate affording, 2-($C_{12}H_8$-2-OH)-6-(CMe_2-NHAr)C_5H_3N (Ar = 2,6-*i*-$Pr_2C_6H_3$) (H**L4**).

The four new compounds, H**L1**, H**L2**, H**L3**, and H**L4** have been characterised using a combination of mass spectrometry, melting point, IR, ^{1}H NMR and ^{13}C NMR spectroscopy (see experimental section).

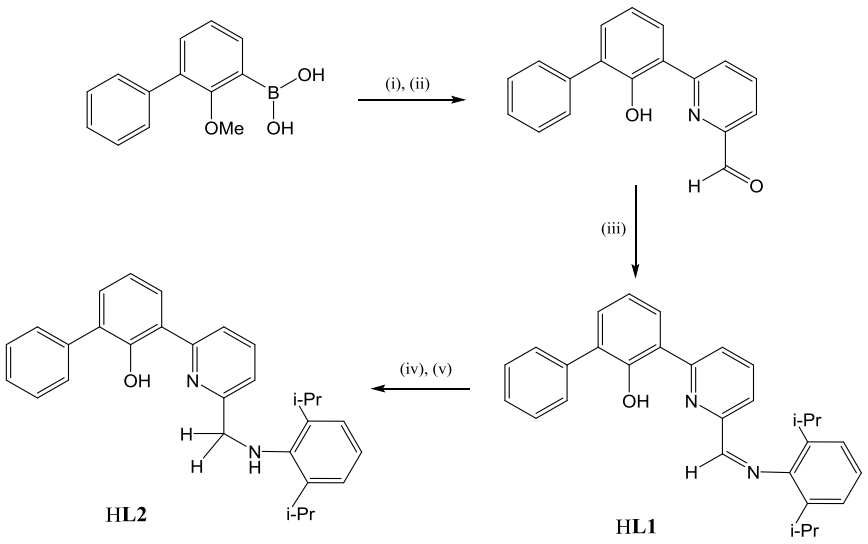

Scheme 2.5. Reagents and conditions: (i) 2-Br-6-(CHO)C_5H_3N, cat. $Pd(PPh_3)_4$, toluene, 2M K_2CO_3 (aq), ethanol; (ii) BBr_3, CH_2Cl_2, -78 ^oC; (iii) $ArNH_2$, ethanol, 40 ^oC; (iv) $LiAlH_4$, THF, -78 ^oC; (v) H_2O

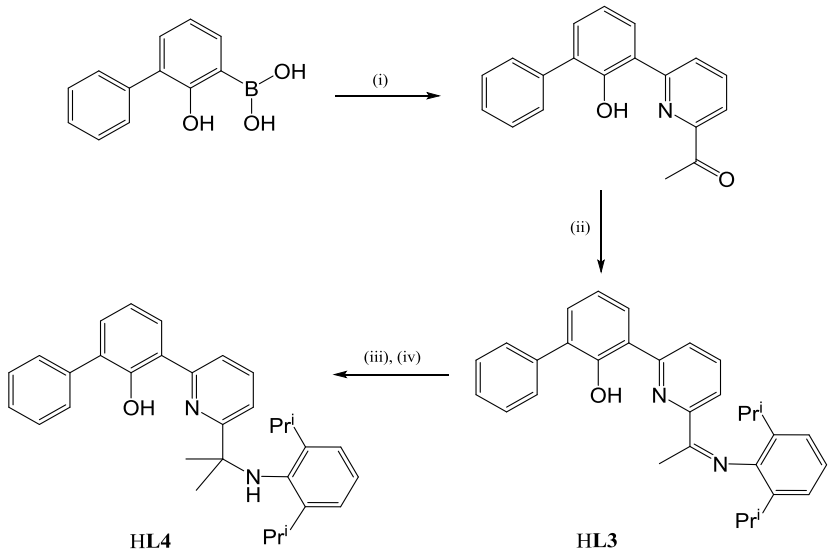

Scheme 2.6. Reagents and conditions: (i) 2-Br-6-(CMeO)C_5H_3N, cat. $Pd(PPh_3)_4$, toluene, 2M K_2CO_3 (aq), ethanol, 90 ^oC; (ii) 2,6-i-$Pr_2C_6H_3NH_2$, methanol, reflux; (iii) $5AlMe_3$, toluene, reflux; (iv) H_2O

Molecular ion peaks were detected for all four pro-ligands, H**L1**, H**L2**, H**L3** and H**L4**, in their electrospray mass spectra and downfield proton chemical shifts for the phenolic protons were clearly evident (14.5 - 15.0 ppm). The downfield position of these OH protons can be attributed to hydrogen bonding with the neighbouring pyridine nitrogen. In addition, broad υ(OH) absorption bands centred at *ca.* 2600 cm^{-1} in their IR spectra are consistent with strong intramolecular hydrogen bonds. The IR spectra for H**L1** and H**L3** also reveal $\upsilon(C{=}N)_{imine}$ absorption bands at *ca.* 1640 cm^{-1} that are absent in H**L2** and H**L4**. In the ^1H

NMR spectrum of H**L2**, the amine proton appears as a broad singlet at *ca.* 3.45 ppm while H**L4** it can be seen at 3.38 ppm. The isopropyl methyl groups take the form of closely located doublets while the C*H*Me$_2$ protons are seen as an apparent septet. The structures of H**L1** and H**L3** were further confirmed by single crystal X-ray determinations.

The molecular structures of H**L1** and H**L3** are shown in Figures 2.8 and 2.9, respectively; selected bond lengths and angles are listed in Tables 2.2 and 2.3. Both H**L1** and H**L3** consist of a central pyridine ring with a 3-biphenyl-2-ol group at the 2-position and at the 6-position a *trans*-configured N-arylimine unit [aldimine (H**L1**) and ketimine (H**L3**)]. In both structures the pyridine nitrogen adopts a *cis*-configuration with respect to the phenol group to enable strong N···HO hydrogen bonding interactions [O(1)···N(1) 2.540 (H**L1**), 2.563 Å (H**L3**)]. The imine C-N bond distances fall between 1.262(3) and 1.293(9) Å and are consistent with double bond character. In both structures some tilting of the 3-phenyl group with respect to the phenol group is apparent [C(1)-C(2)-C(25)-C(26) 48.33^o (H**L1**); C(1)-C(6)-C(7)-C(12) 57.12^o (H**L3**)], which is comparable in size to that seen in free 2-hydroxybiphenyl.[47-49]

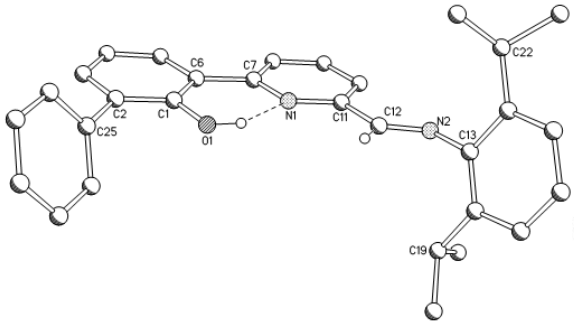

Figure 2.8. Molecular structure of H**L1**, including a partial atom numbering scheme. All hydrogen atoms, apart from H1 and H12, have been omitted for clarity.

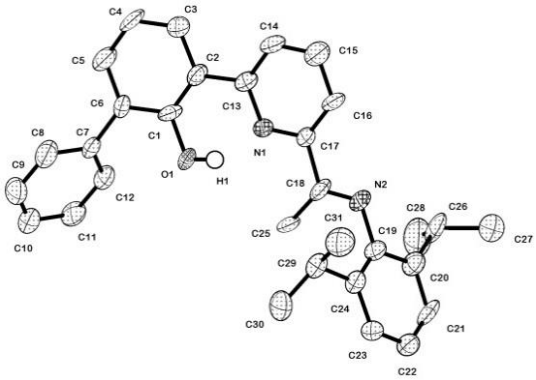

Figure 2.9. Molecular structure of H**L3**, including a partial atom numbering scheme. All hydrogen atoms, apart from H1 have been omitted for clarity.

Table 2.2. Selected bond distances (Å) and angles (^{o}) for H**L1**

Bond lengths	
C(1)-O(1)	1.348(3)
C(2)-C(25)	1.489(4)
C(6)-C(7)	1.482(3)
C(12)-N(2)	1.262(3)
C(13)-N(2)	1.429(3)
Bond angles	
C(11)-C(12)-N(2)	122.0(2)

C(12)-N(2)-C(13)	119.2(2)

Table 2.3. Selected bond lengths (Å) and angles (°) for H**L3**

Bond lengths	
C(1)-O(1)	1.353(7)
C(2)-C(13)	1.500(9)
C(6)-C(7)	1.478(9)
C(18)-N(2)	1.293(9)
C(19)-N(2)	1.434(9)
Bond angles	
C(17)-C(18)-N(2)	116.7(7)
C(18)-N(2)-C(19)	118.7(6)

2.3.2. Complexation reactions of HL1

Treatment of H**L1** with $Pd(OAc)_2$ in toluene at 60 °C results in deprotonation and the formation of **L1**PdOAc (**1a**) in good yield (Scheme 2.7). Its chloride analogue, **L1**PdCl (**1b**), can be prepared directly by reacting H**L1** with $(MeCN)_2PdCl_2$ in tetrahydrofuran at room temperature or simply by stirring a solution of **1a** in chloroform with aqueous sodium chloride in (Scheme 2.8). Both **1a** and **1b** were characterised using FAB mass spectrometry, NMR and IR spectroscopy as well as by elemental analysis. X-ray diffraction studies have been performed on single crystals of **1a**.

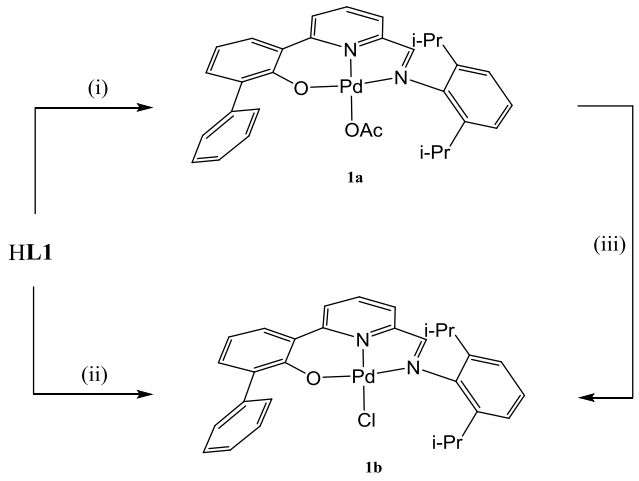

Scheme 2.7. Reagents and conditions: (i) $Pd(OAc)_2$, toluene, 60 °C; (ii) $(MeCN)_2PdCl_2$, THF, RT; (iii) NaCl(aq), $CHCl_3$, RT

The absence of a downfield OH peak from the pro-ligand H**L1** in the ^1H NMR spectra of **1a** and **1b** is consistent with successful deprotonation. Two distinct doublets are seen for

the isopropyl methyl groups in their ^{1}H NMR spectra consistent with some restricted rotation about their N-aryl bond in solution; the acetate resonance is clearly visible at 1.65 ppm in **1a**, while the aldimine proton is slightly shifted in comparison with H**L1**. Both complexes give fragmentation peaks in their mass spectra corresponding the loss of an acetate or a chloride from their molecular ion. In their IR spectra, the $\upsilon(C=N)_{imine}$ absorption bands are shifted by *ca.* 20 cm^{-1} to lower wavenumber compared to that seen in H**L1** consistent with effective coordination of the imine nitrogen.

The molecular structure of **1a** is shown in Fig. 2.10; selected bond distances are compiled in Table 2.4. Two independent molecules (A and B) are found within the asymmetric unit that display only modest differences. The structure consists of a single palladium centre bound by a tridentate monoanionic pincer ligand 2-(3-biphenyl-2-olate)-6-iminepyridine (**L1**) along with an O-bound acetate to complete a distorted square planar geometry. The imine-based tridentate ONN-ligand forms two different sized chelate rings (5- and 6-membered) with the palladium centre. The bite angle of the 6-membered ring [O(1)-Pd(1)-N(1) is $94.5(2)_A$, $92.9(2)_B$] is more compatible with a square planar geometry than for the 5-membered ring [N(2)-Pd(1)-N(1) $83.1(3)_A$, $83.8(3)_B$]. The phenolate ring unit is slightly twisted with respect to the adjacent pyridine ring as evidenced by the torsion angle N(1)-C(13)-C(2)-C(1) $9.2(11)_A$, $8.8(11)_B$. The bond distances with respect to the palladium centre fall in the order: Pd(1)-O(1) $1.934(5)_A/1.948(5)_B$ < Pd(1)-N(1)$1.958(6)_{A/B}$ < Pd(1)-N(2) $1.973(6)_A/1.993(6)_B$. A similar complex [2-(2,2-bipyridin-6-yl)phenolate]PdCl reported comparable crystallographic data to **1a**.[50] No evidence for intramolecular nor intermolecular hydrogen bonding could be observed.

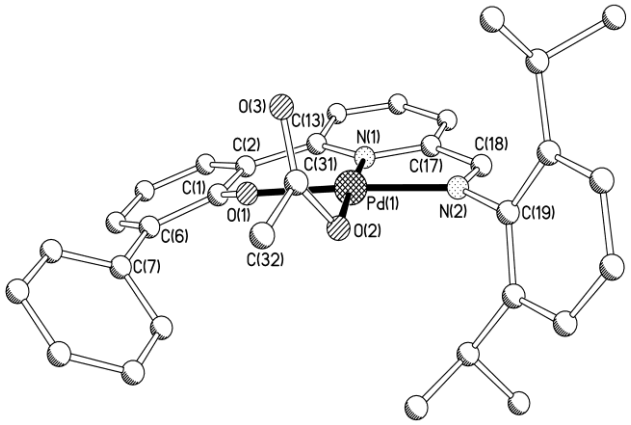

Figure 2.10. Molecular structure of **1a** (*molecule A*) including a partial atom numbering scheme. All hydrogen atoms have been omitted for clarity.

Table 2.4. Selected bond distances (Å) and angles (°) for **1a**

	Bond lengths	
	Molecule A	*Molecule B*
Pd(1)-O(1)	1.934(5)	1.948(5)
Pd(1)-O(2)	1.997(5)	2.004(5)
Pd(1)-N(1)	1.958(6)	1.958(6)
Pd(1)-N(2)	1.973(6)	1.993(6)
C(18)-N(2)	1.292(8)	1.297(8)
C(6)-C(7)	1.483(10)	1.503(11)
C(31)-O(2)	1.303(9)	1.293(9)
C(31)-O(3)	1.225(9)	1.224(8)
	Bond angles	
N(1)-Pd(1)-N(2)	83.1(3)	83.8(3)
N(1)-Pd(1)-O(1)	94.5(2)	92.9(2)
N(2)-Pd(1)-O(2)	95.0(2)	94.7(2)
O(1)-Pd(1)-O(2)	87.3(2)	88.6(2)
N(1)-Pd(1)-O(2)	176.8(2)	178.2(2)

2.3.3. Complexation reactions of HL2: introduction of a hydrogen bond donor

H**L2** contains an amine moiety that can potentially serve as a hydrogen bond acceptor and, when deprotonated, it also contains a phenoxide oxygen that could act as a hydrogen bond acceptor. In principle, **L2** presents a good candidate for hydrogen bonding interactions with incoming ligands/substrates or self-assembly of ligands or complexes.

The synthesis of [{2-(3-$C_{12}H_8$-2-O)-6-(CH_2-NHAr)C_5H_3N}Pd(OAc)] (Ar = 2,6-*i*-$Pr_2C_6H_3$ (**2a**)) was performed by reacting H**L2** with $Pd(OAc)_2$ at 0 °C in toluene (Scheme

2.8). Conversion of **2a** to its chloride counterpart **2b** can be achieved quantitatively by using a similar procedure to that employed for **1b**. Alternatively **2b** can be made more directly by reacting H**L2** with $(MeCN)_2PdCl_2$.

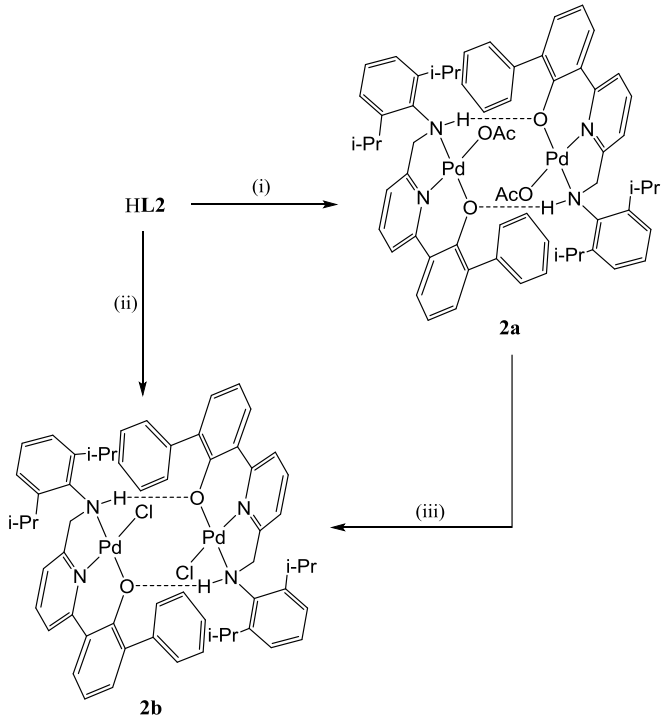

Scheme 2.8. Reagents and conditions: (i) $Pd(OAc)_2$, toluene, 0 °C; (ii) $(MeCN)_2PdCl_2$, THF, RT; (iii) NaCl(aq), $CHCl_3$

The molecular structure of **2a** is shown in Fig. 2.11; selected bond lengths and bond angles are collected in Table 2.5. The structure of **2a** consists of two square planar {2-(3-biphenyl-2-olate)-6-alkylamine-pyridine}Pd(OAc) monomeric units that assemble through NH···O hydrogen bonding interactions involving amine NH and phenolate oxygen atoms in neighbouring molecules [N(2)···O(1A) 3.038 Å].[51, 52] The acetate group within each unit acts as a monodentate ligand and is devoid of hydrogen bonding interactions. The palladium-palladium separation (3.284 Å) was slightly longer than the sum of the van der Waals radii (3.26 Å).

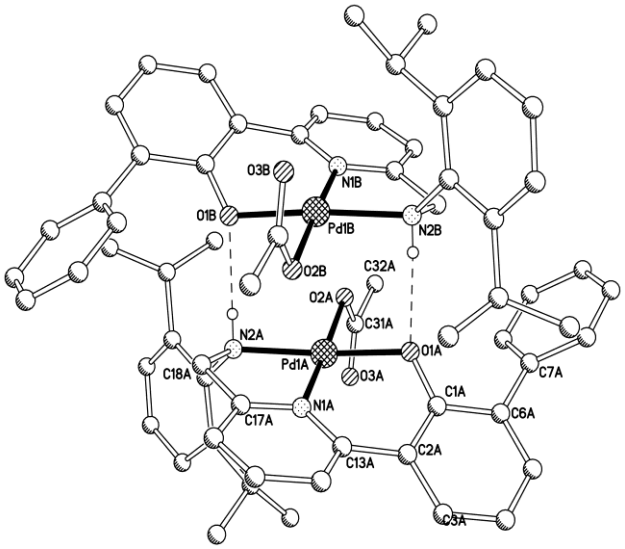

Figure 2.11. Molecular structure of **2a** including a partial atom numbering scheme. All hydrogen atoms have been omitted for clarity.

Table 2.5 Selected bond distances (Å) and angles (°) for **2a**

Bond lengths	
Pd(1)-O(1)	1.990(4)
Pd(1)-O(2)	2.019(4)
Pd(1)-N(1)	1.955(5)
Pd(1)-N(2)	2.078(4)
C(18)-N(2)	1.505(6)
C(6)-C(7)	1.477(8)
C(31)-O(2)	1.257(7)
C(31)-O(3)	1.221(7)
Pd(1)···Pd(1A)	3.284
Bond angles	
N(1)-Pd(1)-N(2)	84.59(19)
N(1)-Pd(1)-O(1)	90.48(18)
N(2)-Pd(1)-O(2)	94.99(17)
O(1)-Pd(1)-O(2)	89.43(15)
N(1)-Pd(1)-O(2)	176.25(19)

Compounds **2a** and **2b** all show fragmentation peaks corresponding to the loss of an acetate or chloride group from both the dimeric and monomeric species in their ESI mass spectra. The methylene C*H*$_2$-NH protons in the ^{1}H NMR spectra are inequivalent and appear as two doublet of doublets [at 4.58 and 4.16 ppm (**2a**); at 4.99 and 3.34 ppm (**2b**)]. Each isopropyl-methyl proton in **2a** and **2b** are inequivalent leading to four separate doublets. The NH proton in each complex is shifted by *ca.* 4 ppm downfield compared to that observed in the free pro-ligand, supportive of a hydrogen bonding interaction being maintained in solution.

2.3.4. Complexation reactions of HL3

Similar to **L1**, **L3** is potentially a pyridine-based ONN type pincer ligand with one imine arm and phenoxide as the other donor arm. Unlike **L1**, **L3** contains a ketimine nitrogen instead of an aldimine nitrogen donor.

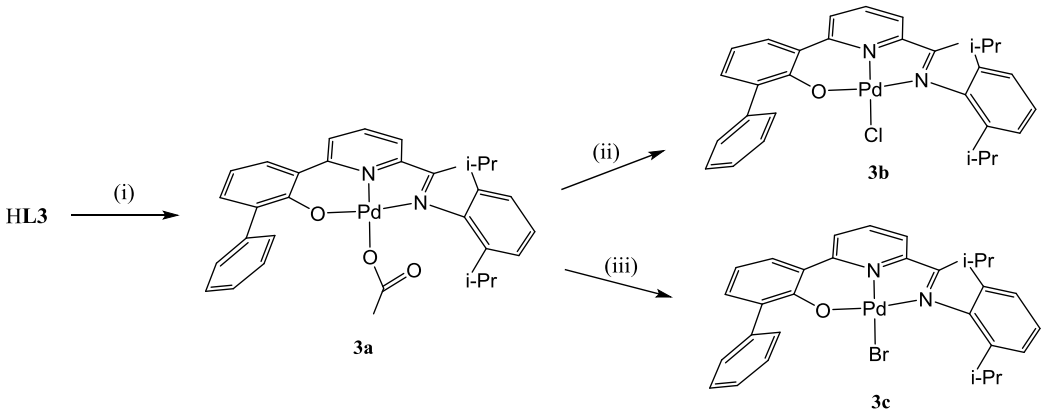

Scheme 2.9. Reagents and conditions: (i) $Pd(OAc)_2$, toluene, 60 ^oC; (ii) NaCl(aq), $CHCl_3$, RT; (iii) NaBr(aq), $CHCl_3$, RT

Reaction of H**L3** with palladium acetate at 60 ^oC in toluene resulted in removal of the phenolic hydrogen peak (14.45 ppm) in its ^1H NMR spectrum suggesting all free ligand has been deprotonated to form **L3**Pd(OAc) (**3a**). Complex **3a** could be converted quantitatively to **L3**PdCl (**3b**) and **L3**PdBr (**3c**) by treatment with an aqueous solution of the corresponding sodium salt (**3b** (NaCl), **3c** (NaBr)). All imine complexes **3a**, **3b** and **3c** have been fully characterised by NMR spectroscopy and by mass spectrometry. In addition, crystals of **3b** and **3c** suitable for X-ray diffraction studies were grown by slow diffusion of petroleum ether into a solution of the corresponding complex in chloroform.

Molecular structures of **3b** and **3c** are similar and will be discussed together. Views of **3b** and **3c** are shown in Figs. 2.12 and 2.13; selected bond distances and angles are collected in Table 2.6. Each structure consists of a single palladium centre bound by a tridentate monoanionic pincer ligand 2-(3-biphenyl-2-olate)-6-iminepyridine (**L3**) along with a halide ligand to complete a distorted square planar geometry. The bite angle of the 6- and 5-membered chelate rings are similar to that observed in **1a** and the bond distances with respect to the palladium centre fall in a similar order: Pd(1)-O(1) < Pd(1)-$N(1)_{pyridine}$ < Pd(1)-$N(2)_{imine}$. As expected this Pd-I distance is longer than the Pd-Cl distance. There is no evidence for any significant intramolecular contacts.

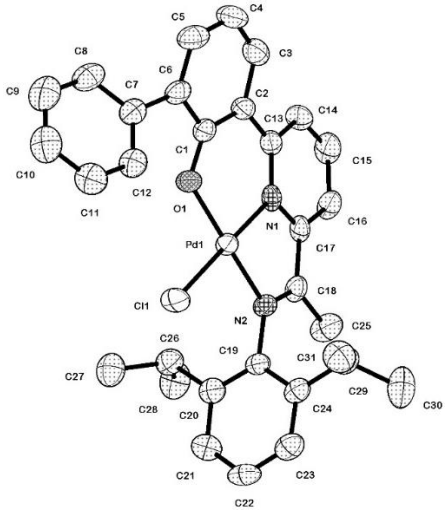

Figure 2.12. Molecular structure of **3b**, including a partial atom numbering scheme. All hydrogen atoms have been omitted for clarity.

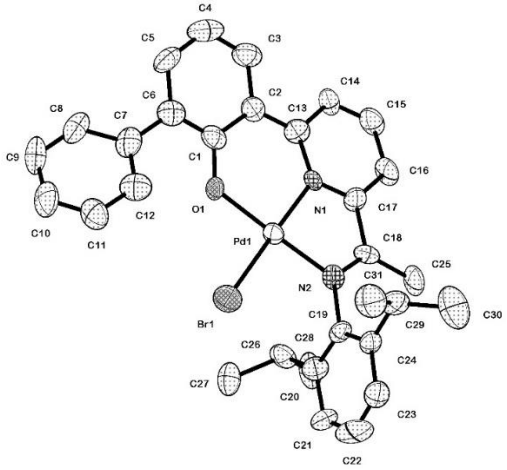

Figure 2.13. Molecular structure of **3c**, including a partial atom numbering scheme. All hydrogen atoms have been omitted for clarity.

Table 2.6 Selected bond distances (Å) and angles (°) for **3b** and **3c**

	Bond lengths	
	3b	**3c**
Pd(1)-O(1)	1.944(3)	1.937(8)
Pd(1)-N(1)	1.983(4)	1.992(9)
Pd(1)-N(2)	1.999(4)	1.982(11)
C(18)-N(2)	1.299(5)	1.301(15)
C(6)-C(7)	1.501(7)	1.47(2)
Pd(1)-X(1)	2.2956(12)	2.386(2)
	Bond angles	
N(1)-Pd(1)-N(2)	82.35(16)	82.0(4)
N(1)-Pd(1)-O(1)	93.47(15)	93.7(4)
O(1)-Pd(1)-X(1)	88.00(10)	87.4(2)
N(1)-Pd(1)-X(1)	178.27(12)	178.8(3)
N(2)-Pd(1)-X(1)	96.12(11)	96.8(3)

(X = Cl for **3b**, X = Br for **3c**)

In the ^{1}H NMR spectra of **3a** – **3c**, the imine methyl group is clearly visible at *ca.* 2.2 ppm, while the acetate resonance in **3a** can be seen at 1.70 ppm. Four separate doublet resonances are seen for the CH*Me*$_2$ protons supportive of restricted rotation about the N-2,6-diisopropylphenyl bond. All three complexes give fragmentation peaks in their mass spectra corresponding the loss of an acetate or a halide from their molecular ion. In their IR spectra, the $\upsilon(C{=}N)_{imine}$ absorption bands are shifted by *ca.* 20 cm^{-1} to lower wavenumber compared to that seen in H**L3** consistent with effective coordination of the imine nitrogen.

2.3.5. Complexation reactions of HL4: introduction of a hydrogen bond donor

2.3.5.1 Preparation of L4PdX (X = OAc (4a), Cl (4b), I (4c))

To explore the effect of replacing a CH_2 group with CMe_2 on the hydrogen bonding interactions that led to self-dimerization in **2a** and **2b**, we now explore the chemistry of H**L4** with palladium(II) acetate. Hence, the reaction of H**L4** with $Pd(OAc)_2$ at 60 °C in toluene gave, on work-up, **L4**Pd(OAc) (Ar = 2,6-*i*-$Pr_2C_6H_3$) (**4a**), in good yield (Scheme 2.10).[53] Complex **4a** can be readily converted to chloride **4b** or iodide **4c** in high yield by stirring **4a** with brine or aqueous sodium iodide in $CHCl_3$. All three complexes, **4a** – **4c** are air stable and have been characterised using a combination of FAB mass spectrometry, IR, and NMR (^1H, ^{13}C) spectroscopy and elemental analyses (see experimental section). In addition, crystals of each complex have been subject of single crystal X-ray diffraction studies.

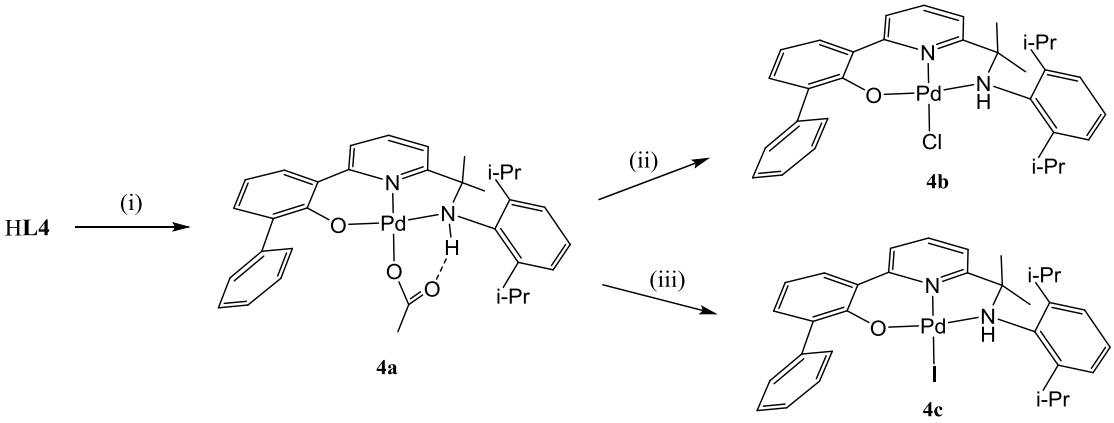

Scheme 2.10. Reagents and conditions: (i) $Pd(OAc)_2$, toluene, 60 °C; (ii) NaCl(aq), $CHCl_3$, RT; (iii) NaI(aq), $CHCl_3$, RT

Crystals of **4a**·OH_2 suitable for an X-ray determination were grown from chloroform. There are three independent molecules for **4a**·OH_2 in the unit cell (molecules *A*-*C*) that differ in the nature of the hydrogen bonding; the packing diagram for **4a**·OH_2 is shown in Figure 2.14b. A view of solely molecule *B* is shown in Fig 2.14a; selected bond distances and angles are collected in Table 2.7. The structure consists of a palladium centre bound by a tridentate **L4** and a monodentate acetate to complete a distorted square planar geometry. In molecule *B*, an intramolecular H-bonding interaction exists between the pendant O of the acetate and NH proton of the amine group (N···O 2.931 Å). In contrast, molecules *A* and *C* in **4a**·OH_2 are associated together via one molecule of water which H-bonds to the pendant oxygen atoms of the neighbouring acetate ligands. The Pd-N(amine)

bond distance is the longest of the three metal-ligand interactions involving the ONN-ligand followed by the Pd-N(pyridine) distance and then by the Pd-O(phenolate) distance which is best exemplified [Pd(1)-N(2)$_{amine}$ 2.023(12) > Pd(1)-N(1)$_{pyridine}$ 1.977(13) > Pd(1)-O(1)$_{phenolate}$ 1.964(10) Å]. Some twisting of the phenolate unit with respect to pyridyl group was seen in both structures similar to the observed in free 2-phenylphenol.[15] Interestingly, crystals of water-free **4a** were grown from benzene and revealed uniquely molecule *B* in the asymmetric unit; the bond parameters otherwise are essentially similar.

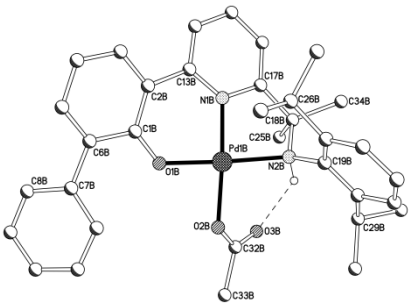

Figure 2.14a. Molecular structure of **4a**·OH_2 (*molecule B*) including a partial atom numbering scheme. All hydrogen atoms, apart from the NH proton, have been omitted for clarity.

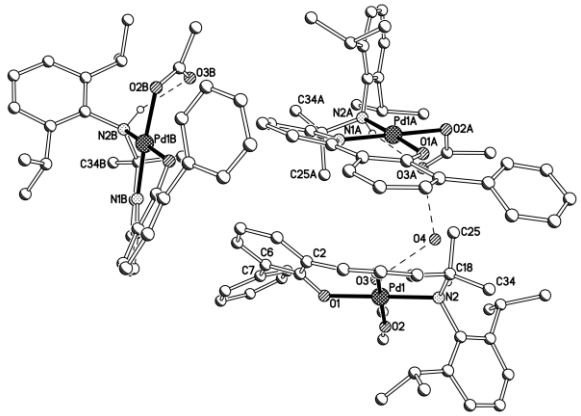

Figure 2.14b. Packing diagram of the three independent molecules in **4a**·OH_2

Table 2.7. Bond lengths (Å) and angles (°) for **4a**·OH_2

	Molecule A	*Molecule B*	*Molecule C*
Bond lengths			
Pd-O(1)	1.964(10)	1.937(10)	1.911(10)
Pd-O(2)	2.030(10)	2.046(10)	1.985(11)
Pd-N(1)	1.977(13)	1.988(13)	1.966(14)
Pd-N(2)	2.023(12)	2.056(12)	2.062(12)
Bond angles			
N(1)-Pd-N(2)	84.2(6)	84.7(5)	84.8(6)
N(1)-Pd-O(1)	94.2(5)	94.0(5)	91.8(6)
O(1)-Pd-O(2)	88.4(4)	88.1(5)	84.7(5)
N(2)-Pd-O(2)	93.1(5)	93.1(5)	98.4(5)
N(1)-Pd-O(2)	171.6(5)	177.7(5)	175.6(5)

A perspective of **4b** is given in Fig. 2.15; selected bond distances and angles are compiled in Table 2.8. Data for structurally related **4c** is presented in a separate section. The structure of **4b** resembles **4a**, with three coordination sites filled by the tridentate NNO ligand, but differs in that the acetate group has been replaced by a chloride ligand. In this case no NH hydrogen bonding interaction with an acceptor atom is apparent.

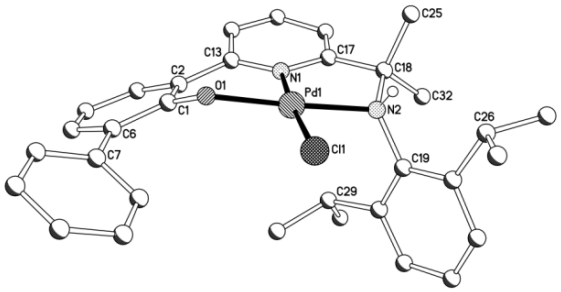

Figure 2.15. Molecular structure of **4b** including a partial atom numbering scheme. All hydrogen atoms, apart from the NH proton, have been omitted for clarity.

Table 2.8. Bond lengths (Å) and angles (°) for **4b**

Bond lengths	
Pd(1)-O(1)	1.979(2)
Pd(1)-Cl(1)	2.3087(11)
Pd(1)-N(1)	1.987(3)
Pd(1)-N(2)	2.043(3)
Bond angles	
O(1)-Pd(1)-N(1)	93.49(11)
O(1)-Pd(1)-N(2)	176.99(11)
N(1)-Pd(1)-N(2)	84.27(12)
O(1)-Pd(1)-Cl(1)	91.30(7)
N(1)-Pd(1)-Cl(1)	175.20(9)

The solid state structures for **4a** – **4c** are maintained in solution with the NH protons for **4a** and **4b** seen at 6.22 and 6.05 ppm in their ^{1}H NMR spectrum of, while in **4a** the NH proton is more downfield shifted as broad resonances at *ca* 8.72 ppm consistent with the NH···O bonding seen in the solid state. The FAB mass spectrum reveals molecular ion peaks and fragments corresponding to then loss of OAc, Cl or I for **4a**, **4b** and **4c**, respectively.

Clearly the introduction of methyl groups on the carbon atom adjacent to NH group in **4a** has resulted in the breaking of the dimeric assembly seen in **2a**. This could be due to increased steric bulk near the NH hydrogen bond donor or due to a change in electronic properties at the metal centre. Furthermore, this inability for the NH group to hydrogen

bond with a phenolate-oxygen in a neighbouring molecule (*cf.* **2a**) has resulted in the NH group seeking an alternative hydrogen-bond acceptor (e.g. water, acetate). In the absence of an acetate ligand the amine moiety can also opt not to undergo hydrogen bonding interactions (see **4b** and **4c**).

2.3.5.2 Preparation of L4Pd(xhp) (xhp = hp (5a), mhp (5b), chp (5c), fhp (5d))

Given the propensity of the acetate complexes of **L4**, to undergo intramolecular NH···O hydrogen bonding, we decided to examine the effect of a range of electronically different pyridonate ligands as the monoanionic X donor. Gratifyingly, four pyridonate derivatives, **L4**Pd(xhp) (xhp = hp (**5a**), CH_3 (**5b**), Cl (**5c**), F (**5d**)) differing in the nature of the ortho-substituent, could be prepared in high yield by the reaction of **4a** with Hxhp (x = H, CH_3, Cl, F) in toluene at room temperature (Scheme 2.11). All pyridonate complexes were fully characterised using ^{1}H NMR, ^{13}C NMR, FAB, ESIMS, and micro-analysis (**5b**, **5d**). In addition, crystals of **5a**, **5b** and **5d** suitable for an X-ray diffraction determination were grown.

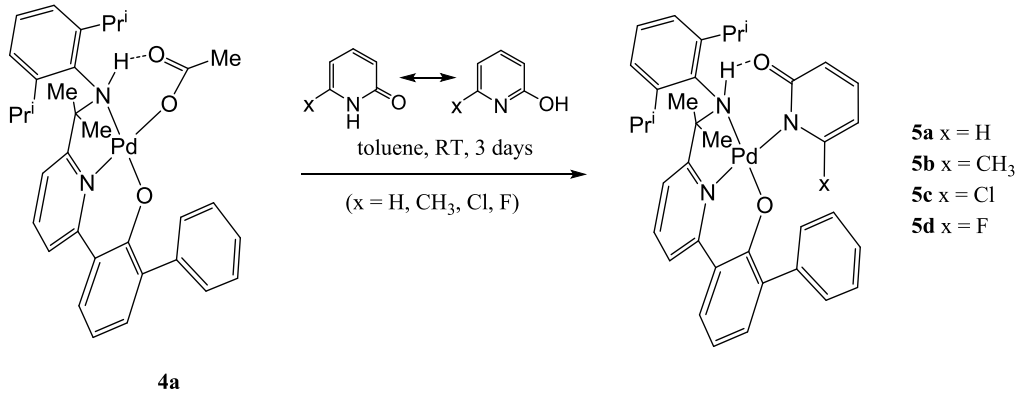

Scheme 2.11. Reaction of **4a** with 2-pyridones (Hxhp)

The X-ray structures of **5a**, **5b** and **5d** are shown in Figure 2.16; selected bond distances and bond angles are collected in Table 2.9. Each structure consists of a palladium centre bound by a tridentate **L4** ligand and a N-bound pyridonate ligand to complete a distorted square planar geometry.

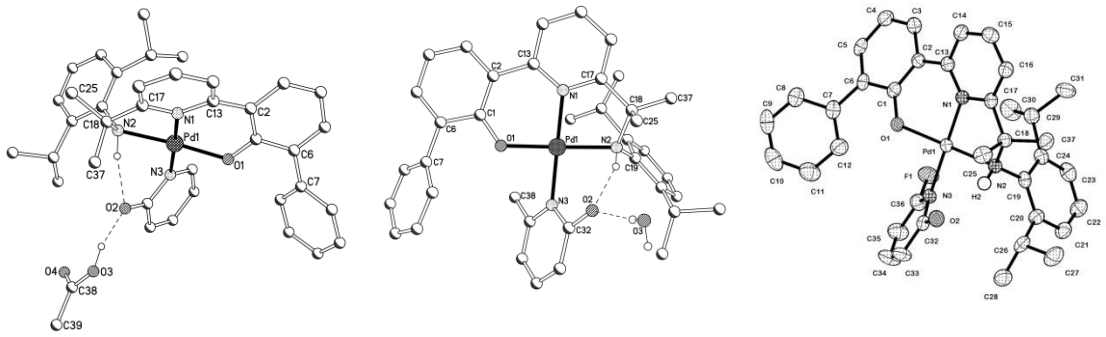

Figure 2.16 Molecular structure of **5a**, **5b** and **5d** including a partial atom numbering scheme. All hydrogen atoms, apart from the NH protons, have been omitted for clarity.

Table 2.9. Selected bond distances (Å) and angles (°) for **5a**, **5b** and **5d**

	5a	**5b**	**5d**
	Bond lengths		
Pd(1)-N(1)	1.967(5)	1.990(4)	1.969(4)
Pd(1)-O(1)	1.974(4)	1.949(4)	1.983(3)
Pd(1)-N(3)	2.019(5)	2.036(4)	2.031(4)
Pd(1)-N(2)	2.062(4)	2.063(4)	2.049(4)
Pd(1)-H(2)	2.1190	2.1635	2.264
N(2)-C(19)	1.491(7)	1.457(6)	1.464(5)
N(2)-C(18)	1.525(7)	1.546(6)	1.545(5)
	Bond angles		
N(1)-Pd(1)-O(1)	93.83(18)	93.26(17)	91.82(14)
N(1)-Pd(1)-N(3)	175.6(2)	174.85(18)	176.04(15)
O(1)-Pd(1)-N(3)	87.00(17)	86.66(16)	89.37(14)
N(1)-Pd(1)-N(2)	83.48(19)	84.80(18)	85.37(15)
O(1)-Pd(1)-N(2)	173.59(17)	174.60(16)	172.72(13)

In all cases, significant intramolecular H-bonding exists between the pyridonate O and the amine hydrogen atom ($NH_{amine}\cdots O_{pyridonate}$ = 2.848 - 2.904 Å). In addition for **5a** and **5b**, a secondary H-bond interaction between pyridonate oxygen and a hydrogen atom of a polar molecule is seen in the X-ray unit cell. In **5a** a molecule of acetic acid (O(2)···O(3) 2.556 Å) and in **5b** a water molecule (O(2)…O(3) 2.701 Å) was observed which is comparable to the intermolecular distance between two molecules of water. The H-bond interactions are also supported by amine NH (*ca.* 9.05-10.38 ppm) downfield shifts in the ^{1}H NMR spectra which provides a measure of the H-bonding interactions.[16] Replacing an O-bound acetate in **4a** for an N-bound pyridonate has little effect on the *trans* Pd-N(pyridine) distance [1.966(14) – 1.988(13) Å (**4a**) vs. 1.967(5) (**5a**), 1.990(4) (**5b**), 1.969(4) (**5d**) Å]. Also a torsion angle of N(2)-Pd(1)-N(3)-C(32) for 57.1 (**5a**), 61.1 (**5b**), 63.7 (**5d**) shows the effect of substituents on the binding of the pyridonates.

In the ^{1}H NMR spectra of each pyridonate complex (**5a, 5b, 5c, 5d**) the NH proton is shifted downfield as compared to the starting material **4a.** Complexes **5a**, **5b**, **5c** and **5d** all show molecular peaks in their FAB mass spectra (TOFMS for **5d**) along with fragmentation peaks corresponding to the loss of pyridonate ligands. In all four pyridonate complexes four distinct doublets are seen for the isopropyl methyl groups in their ^{1}H NMR spectra consistent with some restricted rotation about the *N*-aryl bond in solution.

2.3.5.3 Reaction of 4a with phenols C_6R_5OH (R = H, F)

To probe the use of **4a** as a precursor to other **L4**PdX complexes and to examine the effect of a bound oxygen on potential NH···O interactions, we studied its reactivity towards two types of phenol. Hence, reaction of pentafluorophenol with **4a** at room temperature in toluene gave **L4**Pd(OC_6F_5) (Ar = 2,6-*i*-$Pr_2C_6H_3$) (**6**) in good yield (Scheme 2.12). On the other hand no reaction occurred on treating **4a** with phenol. Complex **4a** is unreactive towards phenol even at high temperatures, highlighting the reduced acidity of phenol hindering the activation of the O-H bond. By contrast the O-H bond of pentafluorophenol is reactive enough to be activated at room temperature. Complex **6** is air stable and has been characterised using a combination of FAB mass spectrometry, IR and NMR (^{1}H and ^{13}C) spectroscopy and elemental analyses (see experimental section).

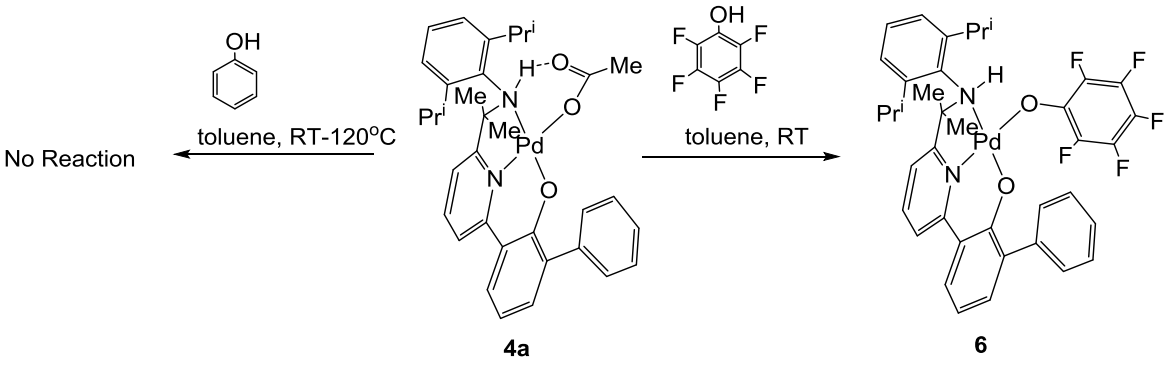

Scheme 2.12. Comparative reactivity of **4a** towards pentafluorophenol and phenol.

The ^{1}H NMR spectrum of **6** shows four distinct doublets for the isopropyl methyl groups suggesting some restricted rotation about the *N*-aryl bond in solution. The N*H* signal can be seen at δ *ca.* 6.41 as compared to δ *ca.* 8.72 in **4a** in their ^{1}H NMR spectra, suggesting no or limited H-bonding in **6**. In the ^{19}F NMR spectrum of **6**, three highly coupled fluorine resonances are seen at δ −178.6, δ −168.9 and δ −162.3. The FAB mass spectrum reveals molecular peak and a fragmentation peak corresponding to the loss of a

pentafluorophenolate ligand. Inspection of the literature reveals only a few examples of palladium complexes containing a pentafluorophenolate ligand.[17-18].

2.3.5.4 Preparation of L4Pd(X) (X = $O_2CC_6H_4$-2-I (7a), O_2CCF_3 (7b), O_3SCF_3 (7c))

Given the ability of the pendant acetate oxygen atom in **4a** to undergo strong NH···O interactions that can be monitored using ^{1}H NMR spectroscopy, we decided to investigate other **L4**Pd complexes bearing both a bound oxygen and a pendant oxygen. Thus, treatment of **4a** with either 2-iodobenzoic acid, trifloroacetic acid or triflic acid at room temperature in toluene were attempted and found to form **L4**Pd(X) (X = $O_2CC_6H_4$-2-I (**7a**), O_2CCF_3 (**7b**), O_3SCF_3 (**7c**)) in reasonable yield, respectively (Scheme 2.13). Complexes **7a**, **7b** and **7c** have been fully characterised and, in addition, **7a** and **7b** have been the subject of single crystal X-ray diffraction studies.

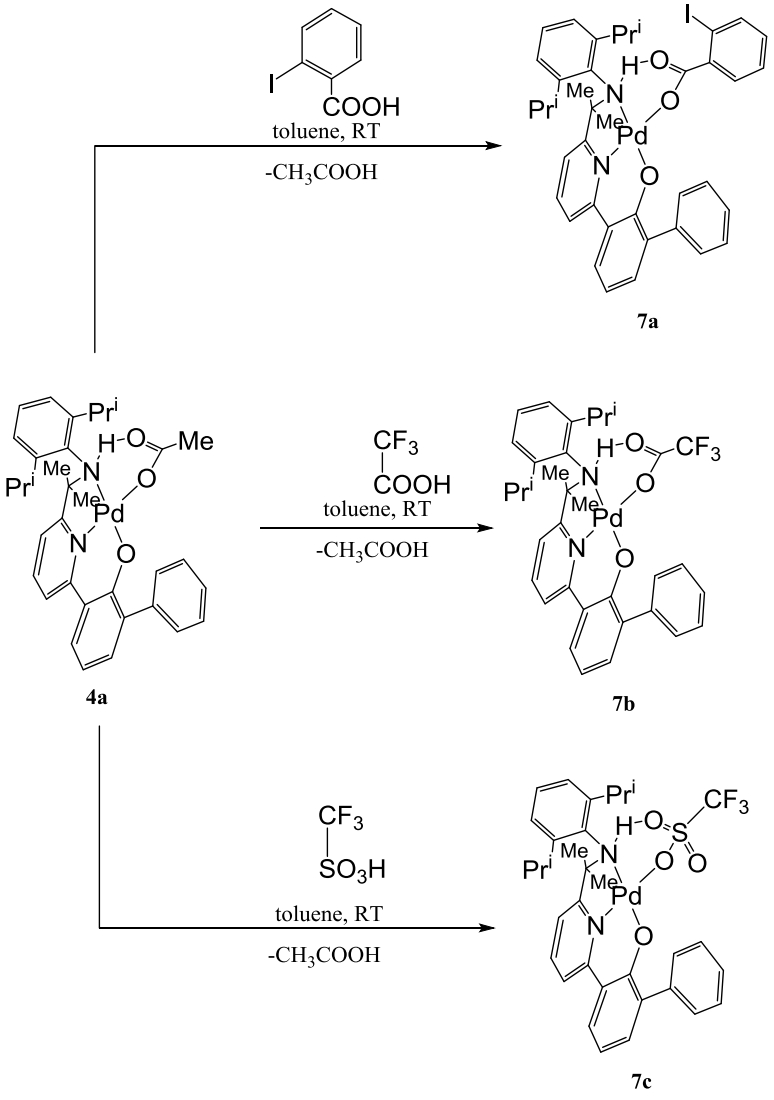

Scheme 2.13. Reactions of **4a** with 2-iodobenzoic acid, trifloroacetic acid and triflic acid.

The molecular structure of **7a** is shown in Fig. 2.17; selected bond distances and angles are collected in Table 2.10. The structure comprises a palladium centre bound by a tridentate **L4** and an O-bound carboxylate ligand to complete a distorted square planar geometry. An interaction of the NH group belonging to **L4** is clearly observable with the pendant oxygen of the iodobenzoate (N···O 2.860 Å). The aryl iodide moiety adopts a configuration cis to the pendant oxygen atom.

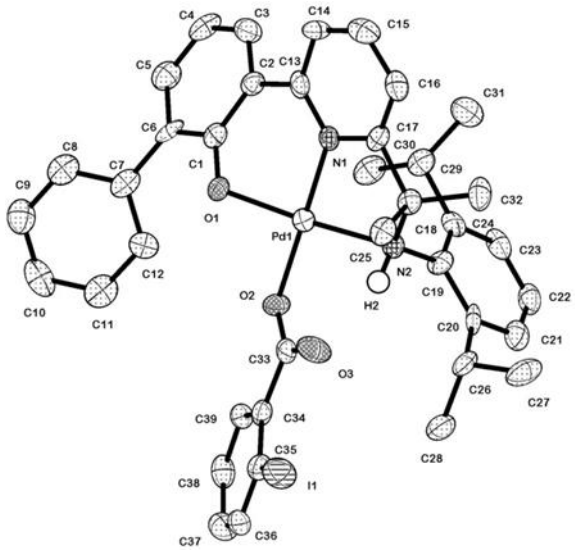

Figure 2.17 Molecular structure of **7a** including a full atom numbering scheme. All hydrogen atoms, apart from the NH protons, have been omitted for clarity.

Table 2.10. Selected bond distances (Å) and angles (°) for **7a**

Bond lengths	
Pd(1)-O(1)	1.970(5)
Pd(1)-O(2)	2.023(5)
Pd(1)-N(1)	1.952(6)
Pd(1)-N(2)	2.073(5)
Bond angles	
N(1)-Pd(1)-O(1)	90.6(2)
O(1)-Pd(1)-O(2)	88.93(19)
N(1)-Pd(1)-N(2)	83.4(2)
O(1)-Pd(1)-O(2)	88.93(19)

Crystals of **7b** suitable for X-ray diffraction studies were grown from slow diffusion of hexane and chloroform. The molecular structure of **7b** is shown in Fig 2.18a and selected bond distances and angles are collected in Table 2.11. Again a distorted square planar geometry is adopted by the palladium centre with **L4** filling three coordination sites and an

oxygen of the CF_3COO group the fourth. Unexpectedly, the pendant oxygen of the CF_3COO group is not involved in a hydrogen bonding interaction with the NH proton instead adopting a remote position. Curiously, there were some long distance $NH\cdots O_{phenolate}$ interactions (N···O 4.017 Å) similar to that observed in **2a** (Fig. 2.18b) which are likely due to crystal packing properties.

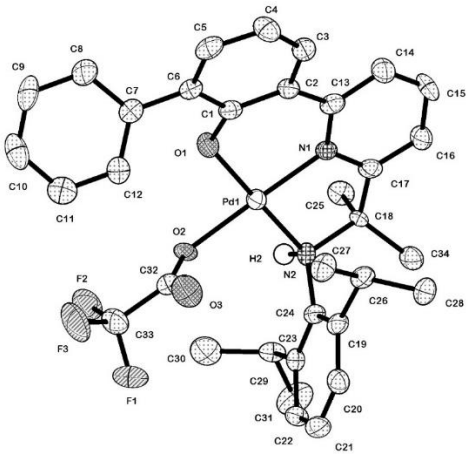

Figure 2.18a. Molecular structure of **7b** including a full atom numbering scheme. All hydrogen atoms, apart from the NH protons, have been omitted for clarity

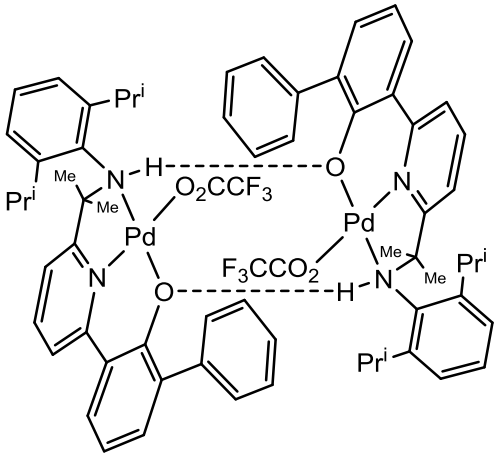

Figure 2.18b. Representation of the long range $NH\cdots O_{phenolate}$ interactions in **7b** found in the packing

Table 2.11. Selected bond distances (Å) and angles (°) for **7b**

Bond lengths	
Pd(1)-O(1)	1.950(3)
Pd(1)-O(2)	2.034(4)
Pd(1)-N(1)	1.959(4)
Pd(1)-N(2)	2.032(4)
Bond angles	
N(1)-Pd(1)-O(1)	94.01(16)
O(1)-Pd(1)-O(2)	89.91(15)
N(1)-Pd(1)-N(2)	85.45(17)
O(1)-Pd(1)-N(2)	177.46(17)

All three complexes, **7a** – **7c**, display fragmentation peaks corresponding to the loss of a 2-iodobenzoate, trifloroacetate or a triflate ligand. In their ^{1}H NMR spectra the NH protons can be seen at 8.20 (**7a**), 7.57 (**7b**) and 6.26 (**7c**) ppm, which compares to the more downfield chemical shift observed in **4a** (8.72 ppm).

For **7a**, we were also interested in whether heating **7a** would lead to oxidative addition across the aryl-I bond.[54] On heating **7a** at 60 - 110 °C in toluene for up to five days the only

complex that could be identified as growing in the ^{1}H NMR spectrum was iodide-containing **4c** (Scheme 2.14).

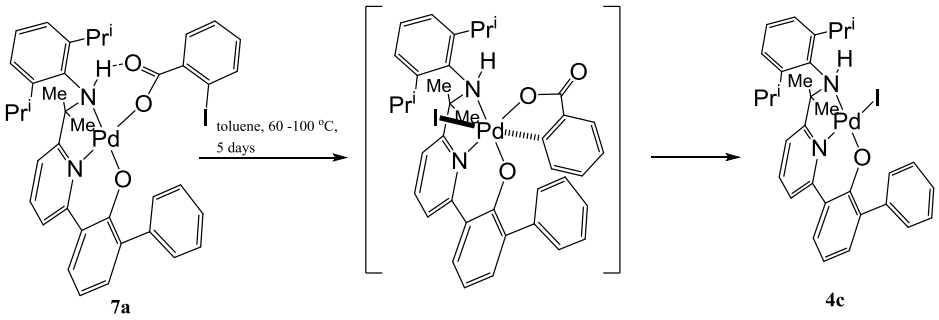

Scheme 2.14. Thermolysis of **7a** between 60 – 110 °C affording **4c** via a proposed Pd(IV) intermediate

One possible explanation accounting for the formation of **4c** is that oxidative addition of iodobenzoate occurred generating a palladium(IV) intermediate that then underwent reductive elimination to give **4c**. Unfortunately attempts at trying to isolate the reductively eliminated organic species failed. Prolonged standing of the reaction mixture obtained after 5 days gave crystals of **4c** that were suitable for an X-ray determination.

The molecular structure of **4c** is shown in Fig. 2.19; selected bond distances and angles are collected in Table 2.12. The structure resembles **4b** and indeed apart from the palladium-halide distance [Pd(1)-I(1) 2.5789(8) Å (**4c**) vs. Pd(1)-Cl(1) 2.3087(11) Å (**4b**)] shows little variation.

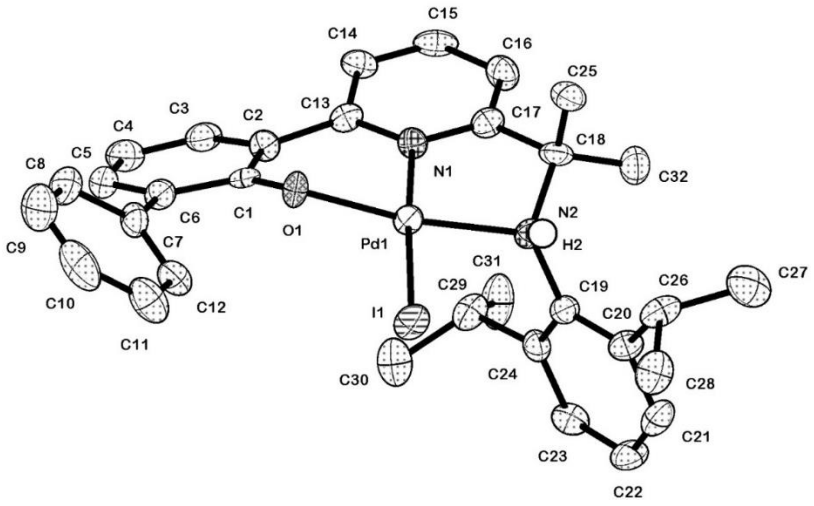

Figure 2.19. Molecular structure of **4c** including a full atom numbering scheme. All hydrogen atoms, apart from the NH protons, have been omitted for clarity

Table 2.12. Selected bond distances (Å) and angles (°) for **4c**

Bond lengths	
Pd(1)-O(1)	1.971(3)
Pd(1)-I(1)	2.5789(8)
Pd(1)-N(1)	2.006(5)
Pd(1)-N(2)	2.055(4)
Bond angles	
O(1)-Pd(1)-N(1)	91.18(17)
O(1)-Pd(1)-N(2)	171.55(16)
N(1)-Pd(1)-N(2)	83.91(17)
O(1)-Pd(1)-I(1)	92.56(11)
N(1)-Pd(1)-I(1)	176.21(13)

2.3.5.5 Reactions of 4 with silver salts

To explore the potential of the NNO-complexes, **L4**PdX (X = OAc (**4a**), Cl (**4b**)), to act as precursors to cation-anion pairs, we studied their reactions with silver salts including silver triflate, silver hexafluorphosphate and silver tetrafloroborate. Firstly, we examined the reaction **4a** was reacted with $AgSO_3CF_3$ (ca, 5 eq.) in $CDCl_3$. Unexpectedly, on work-up, the Pd_2Ag_3 cluster **8** was isolated (Scheme 2.20). It was also found that different size clusters (with different number of metal centres) could be also formed by using different molar ratios of $AgSO_3CF_3$. In this work we only report complex $[(\mathbf{L4})_2Pd_2Ag_3(OAc)_2(O_3SCF_3)(OH_2)][O_3SCF_3]_2$ (**8**) which has been characterised by ^1H NMR spectroscopy and by single X-ray diffraction. The molecular structure of **8** is shown in Fig. 2.20; selective bond distances and angles are collected in Table 2.13.

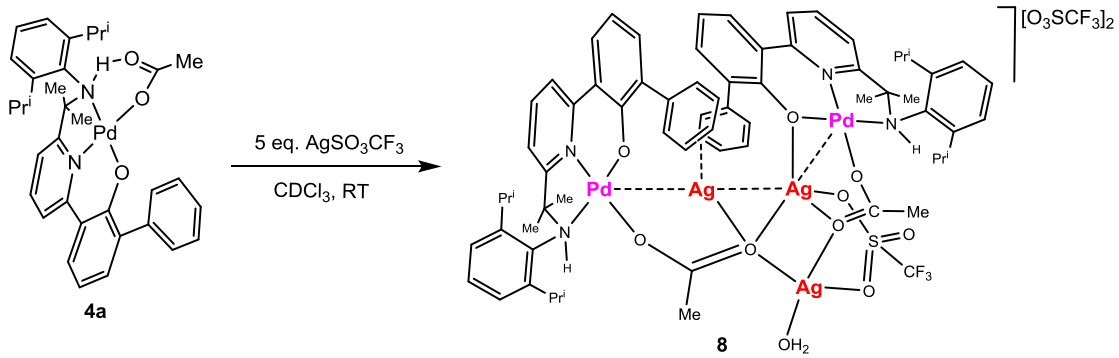

Scheme 2.17. Reaction of **4a** with $AgSO_3CF_3$ to give **8**

The structure consists of a dication and two triflate counterions. Within the dication two molecules of square planar **4a** are bridged by a $Ag_3(O_3SCF_3)(OH_2)$ unit. The pendant acetate oxygen atoms in each **4a** are used to link the three silver centres. There is also some

evidence for a π-interaction involving the pendant phenyl group in molecule of **4a** with a silver atom.

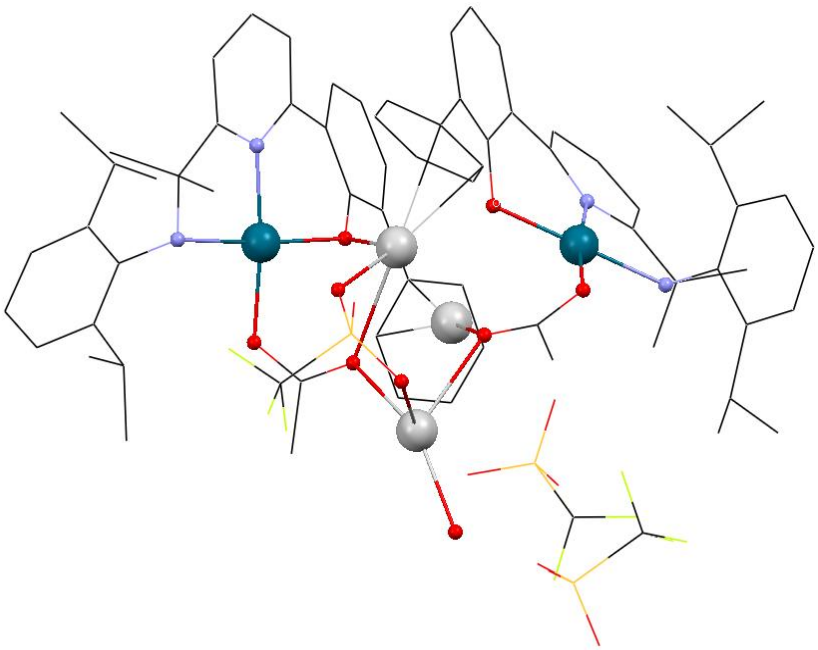

Figure 2.20. Molecular structure of $[(\mathbf{L4})_2Pd_2Ag_3(OAc)_2(O_3SCF_3)(OH_2)]^{2+}[(O_3SCF_3)_2]^{2-}$ (**8**)

Table 2.13. Selected bond distances (Å) and angles (°) for **8**

Bond lengths	
Pd(1)-O(1)	1.977(5)
Pd(1)-O(2)	2.027(4)
Pd(1)-N(1)	1.966(5)
Pd(1)-N(2)	2.027(6)
Bond angles	
O(1)-Pd(1)-N(1)	91.18(17)
O(1)-Pd(1)-N(2)	171.55(16)
N(1)-Pd(1)-N(2)	83.91(17)
O(1)-Pd(1)-I(1)	92.56(11)
N(1)-Pd(1)-I(1)	176.21(13)

Palladium-silver heterobimetallic clusters with a variety of ligands have been previously reported and are of high interest due to their high reactivity and properties.[55] There are also a few examples in the literature with Pd-Ag nanoparticles but are rare with pincer complexes of palladium.[56] It was interesting to note that the basic skeleton in **4a** has been preserved in this fast and reactive environment resulting in formation of **8**.

Given the propensity of acetate-containing **4a** to undergo cluster assembly with silver triflate, we decided to focus on the reactivity of chloride **4b** with the silver salts. Hence

reaction of **4b** with either AgO_3SCF_3, $AgPF_6$ or $AgBF_4$ in acetonitrile gave on work-up, [**L4**Pd(NCMe)][X] [X = O_3SCF_3 (**9a**), PF_6 (**9b**), BF_4 (**9c**)] in high yield (Scheme 2.18).

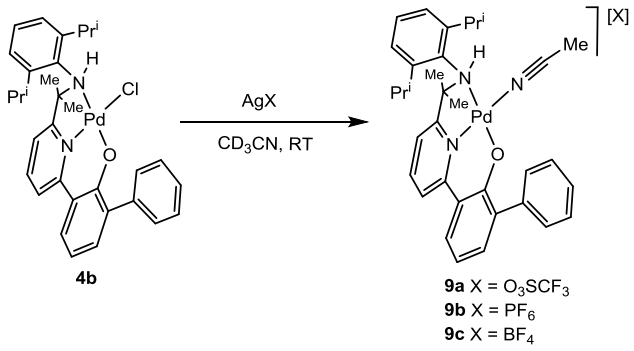

Scheme 2.18. Reaction of **4b** with AgO_3SCF_3, $AgPF_6$ or $AgBF_4$

Complexes **9a – 9c**, have been fully characterized by multinuclear NMR (^1H, ^{13}C and ^{19}F) and by mass spectrometry. In each case, the four isopropylmethyl groups are inequivalent in their ^1H NMR spectra. This inequivalency has the effect that the CMe_2NH methyl groups are also inequivalent as are the C*H*Me_2 protons. In the ^{19}F NMR spectra signals corresponding to the triflate, hexafluorophosphate and tetrafluoroborate counterions are clearly visible at δ 77.3, 72.9, 151.4, respectively. The mass spectra for **9a** and **9b** show peaks corresponding to the cationic unit while for **9c**, the fragmentation of an acetonitrile molecule also evident to give an **L4**Pd ion.

2.3.6. Comparison of NH chemical shifts for 2, 4 - 7

In an attempt to correlate the NH chemical shift found in **L2**-containing **2** and **L4**-containing **4 - 7**, with the NH···O interaction found in the solid state, Table 2.14 lists the corresponding data.

Table 2.14. Solution state versus solid state hydrogen-bonding properties

Complex	NH chemical shift (in ppm) in ^{1}H NMR spectrum[a]	NH···O interaction in solid state
2a	4.58	NH···O(phenolate)
2b	5.98	NH···O(phenolate)
4a	8.72	NH···O(acetate)
4b	6.41	NH (no observable H-bonding interactions)
4c	6.05	NH (no observable H-bonding interactions)
5a	10.38	NH···O(pyridonate)
5b	9.53	NH···O(6-methylpyridonate)
5c	9.05	NH···O(6-chloropyridonate)
5d	9.27	NH···O(6-fluoropyridonate)
6a	6.41	NH (no apparent H-bonding interactions)
7a	8.20	NH···O(2-iodobenzoate)
7b	7.57	NH···O(trifluoroacetate)
7c	6.26	NH···O(triflate)

[a] recorded in $CDCl_3$ at room temperature

Inspection of the data reveals that the NH proton can appear anywhere between 6.4 and 10.4 ppm. At the lower end of the range complexes containing no apparent NH···O hydrogen bonding interactions (**4b**, **4c**, **6a**), while at the top end of the range the pyridonate complexes (**5a** – **5d**) are found with the parent pyridonate **5a** showing the most downfield chemical shift (10.38 ppm). No obvious trend relating to the electronic properties of the ortho-substituent within the pyridonate series can be identified. Within the carboxylate series (**4a**, **7a** and **7b**), the NH resonance for the parent acetate (**4a**), is seen the most downfield (8.72 ppm) while for the trifluoactate derivative the most upfield (7.57 ppm).

2.4. Conclusions

In summary, routes to four types of sterically bulky ONN pro-ligands, H**L1**, H**L2**, H**L3** and H**L4**, differing in the nature of the exterior nitrogen donor [imine (H**L1** and H**L3**) and amine (H**L2** and H**L4**) and groups attached to this donor, have been developed. Deprotonation of the OH group in each pro-ligand in the presence of palladium(II) acetate proceeds smoothly leading to discrete (ONN)Pd(OAc) pincer complexes (**1a**, **3a**) using

H**L1** and H**L3**, while for H**L2** and H**L4** the amine-NH moieties (**2a**, **4a**) within the ONN-ligand help generate inter- or intra-molecular hydrogen-bonding interactions with acceptor atoms in neighbouring molecules (phenolate-O) or co-ligands leading to self-dimerisation or complex-ligand/solvent interactions. It is apparent that by the introduction of methyl groups near the NH group (with **L4**) inhibits self-dimerisation leading to mainly intramolecular type hydrogen bond interactions. Complex **4a** has provided a versatile starting material leading to the substitution of the acetate group for halides, pyridonates, carboxylates and triflates that have in turn revealed a range of types of NH···O type interactions in which an O-atom is present within the X-donor. Furthermore, the attempted salt elimination reaction of **4a** with silver triflate led unexpectedly to the Pd-Ag cluster **8**. Attempts at trying to correlate the degree of hydrogen bonding with NH chemical shift in the ^{1}H NMR spectra have been made.

2.5. References

1. D.-H. Lee, H. J. Kwon, B. P. Patel, L. M. Liable-Sands, A. L. Rheingold and R. H. Crabtree, *Organometallics*, 1999, **18**, 1615-1621.
2. M. Asay and D. Morales-Morales, *Dalton Trans.*, 2015, **44**, 17432-17447.
3. J. M. Serrano-Becerra and D. Morales-Morales, *Curr. Org. Synth.*, 2009, **6**, 169-192.
4. R. Cerón-Camacho, V. Gómez-Benítez, R. Le Lagadec, D. Morales-Morales and R. A. Toscano, *J. Mol. Catal. A: Chem.*, 2006, **247**, 124-129.
5. X.-Q. Gu, W. Chen, D. Morales-Morales and C. M. Jensen, *J. Mol. Catal. A: Chem.*, 2002, **189**, 119-124.
6. J. Dupont, M. Pfeffer and J. Spencer, *Eur. J. Inorg. Chem.*, 2001, **2001**, 1917-1927.
7. R. H. Crabtree, *New J. Chem.*, 2011, **35**, 18-23.
8. G. D. B., *Chem. Lett.*, 2010, **39**, 908-914.
9. B. Zhao, Z. Han and K. Ding, *Angew. Chem., Int. Ed.*, 2013, **52**, 4744-4788.
10. M. Sawamura and Y. Ito, *Chem. Rev.*, 1992, **92**, 857-871.
11. R. Noyori and S. Hashiguchi, *Acc. Chem. Res.*, 1997, **30**, 97-102.
12. R. Noyori and T. Ohkuma, *Angew. Chem., Int. Ed.*, 2001, **40**, 40-73.
13. S. E. Clapham, A. Hadzovic and R. H. Morris, *Coord. Chem. Rev.*, 2004, **248**, 2201-2237.
14. K. Abdur-Rashid, A. J. Lough and R. H. Morris, *Organometallics*, 2000, **19**, 2655-2657.
15. K. Abdur-Rashid, M. Faatz, A. J. Lough and R. H. Morris, *J. Am. Chem. Soc.*, 2001, **123**, 7473-7474.
16. K. Abdur-Rashid, A. J. Lough and R. H. Morris, *Organometallics*, 2001, **20**, 1047-1049.
17. K. Abdur-Rashid, S. E. Clapham, A. Hadzovic, J. N. Harvey, A. J. Lough and R. H. Morris, *J. Am. Chem. Soc.*, 2002, **124**, 15104-15118.
18. C. A. Sandoval, T. Ohkuma, K. Muñiz and R. Noyori, *J. Am. Chem. Soc.*, 2003, **125**, 13490-13503.
19. T. Li, R. Churlaud, A. J. Lough, K. Abdur-Rashid and R. H. Morris, *Organometallics*, 2004, **23**, 6239-6247.
20. R. Abbel, K. Abdur-Rashid, M. Faatz, A. Hadzovic, A. J. Lough and R. H. Morris, *J. Am. Chem. Soc.*, 2005, **127**, 1870-1882.
21. R. J. Hamilton and S. H. Bergens, *J. Am. Chem. Soc.*, 2006, **128**, 13700-13701.
22. A. Hadzovic, D. Song, C. M. MacLaughlin and R. H. Morris, *Organometallics*, 2007, **26**, 5987-5999.
23. Z. Chen, Y. Chen, Y. Tang and M. Lei, *Dalton Trans.*, 2010, **39**, 2036-2043.
24. S. Takebayashi, N. Dabral, M. Miskolzie and S. H. Bergens, *J. Am. Chem. Soc.*, 2011, **133**, 9666-9669.
25. M. Zimmer-De Iuliis and R. H. Morris, *J. Am. Chem. Soc.*, 2009, **131**, 11263-11269.
26. R. J. Hamilton and S. H. Bergens, *J. Am. Chem. Soc.*, 2008, **130**, 11979-11987.
27. C. A. Sandoval, Q. Shi, S. Liu and R. Noyori, *Chem. Asian J.*, 2009, **4**, 1221-1224.
28. T. Šmejkal and B. Breit, *Angew. Chem.*, 2008, **120**, 317-321.
29. C. H. Beierlein, B. Breit, R. A. Paz Schmidt and D. A. Plattner, *Organometallics*, 2010, **29**, 2521-2532.
30. B. Breit, *Angew. Chem., Int. Ed.*, 2005, **44**, 6816-6825.
31. B. Breit and W. Seiche, *J. Am. Chem. Soc.*, 2003, **125**, 6608-6609.
32. D. Fuchs, G. Rousseau, L. Diab, U. Gellrich and B. Breit, *Angew. Chem.*, 2012, **124**, 2220-2224.
33. U. Gellrich, J. Huang, W. Seiche, M. Keller, M. Meuwly and B. Breit, *J. Am. Chem. Soc.*, 2011, **133**, 964-975.
34. S. T. Kemme, T. Šmejkal and B. Breit, *Adv. Synth. Catal.*, 2008, **350**, 989-994.
35. W. Seiche, A. Schuschkowski and B. Breit, *Adv. Synth. Catal.*, 2005, **347**, 1488-1494.
36. L. P. Wolters, R. Koekkoek and F. M. Bickelhaupt, *ACS Catalysis*, 2015, **5**, 5766-5775.

37. N. Sträter, W. N. Lipscomb, T. Klabunde and B. Krebs, *Angew. Chem. Int. Ed.*, 1996, **35**, 2024-2055.
38. J. Park, K. Lang, K. A. Abboud and S. Hong, *J. Am. Chem. Soc.*, 2008, **130**, 16484-16485.
39. M. Tokunaga, J. F. Larrow, F. Kakiuchi and E. N. Jacobsen, *Science*, 1997, **277**, 936-938.
40. *Enantioselective Catalysis with Structurally Tunable Immobilized Catalysts*, Springer Berlin Heidelberg, Berlin, 2011.
41. M. Qi, P. Z. Tan, F. Xue, H. S. Malhi, Z.-X. Zhang, D. J. Young and T. S. A. Hor, *RSC Advances*, 2015, **5**, 3590-3596.
42. R. Chen, R. P. J. Bronger, P. C. J. Kamer, P. W. N. M. van Leeuwen and J. N. H. Reek, *J. Am. Chem. Soc.*, 2004, **126**, 14557-14566.
43. W.-H. Wang, J. T. Muckerman, E. Fujita and Y. Himeda, *New J. Chem.*, 2013, **37**, 1860-1866.
44. H. J. Knölker, E. Baum, H. Goesmann and R. Klauss, *Angew. Chem., Int. Ed.*, 1999, **38**, 2064-2066.
45. C. P. Casey and H. Guan, *J. Am. Chem. Soc.*, 2007, **129**, 5816-5817.
46. C. J. Davies, A. Gregory, P. Griffith, T. Perkins, K. Singh and G. A. Solan, *Tetrahedron*, 2008, **64**, 9857-9864.
47. K. B. M. Perrin, A. Thozet, in *Acta Crystallogr., Sect. C: Cryst. Struct. Commun.*, 1987, vol. 43, p. 980.
48. M. Kapon and G. M. Reisner, *Acta Crystallogr., Sect. C: Cryst. Struct. Commun.*, 1988, **44**, 2039.
49. X. H. a. C. P. B. S. Parkin, *Acta Crystallogr., Sect. B: Struct. Sci.*, 2004, **60**, 197.
50. D. Bardwell, D. Black, J. C. Jeffery and M. D. Ward, *Polyhedron*, 1993, **12**, 1577-1580.
51. *Hydrogen Bonding in Biological Structures*, Springier, 1994.
52. G. C. Pimental and A. L. McClellan, *W. H. Freeman*, 1960, 475.
53. A. H. Abadi, T. M. Ibrahim, K. M. Abouzid, J. Lehmann, H. N. Tinsley, B. D. Gary and G. A. Piazza, *Bioorg. Med. Chem.*, 2009, **17**, 5974-5982.
54. F. Juliá-Hernández, A. Arcas and J. Vicente, *Chem. Eur. J.*, 2012, **18**, 7780-7786.
55. E. A. Sales, M. de Jesus Mendes and F. Bozon-Verduraz, *J. Catal.*, 2000, **195**, 96-105.
56. J. Vicente, M. T. Chicote, S. Huertas, D. Bautista, P. G. Jones and A. K. Fischer, *Inorg. Chem.*, 2001, **40**, 2051-2057.

Chapter 3

Dianionic ONO'-palladium pincer complexes and their reactivity towards pyridines, pyridones and acids

Chapter 3

Dianionic ONO'-palladium pincer complexes and their reactivity towards pyridines, pyridones and acids

3.1. Introduction: Pyridine-based palladium pincers

A wide variety of carbon-based pincer complexes of the DCD-type (D = neutral donor atom) have been reported and used extensively in catalysis due to their cost effective synthesis and ease of preparation. Recently, pincer ligands incorporating a neutral central donor such as a pyridine nitrogen have emerged in the literature and their resultant complexes have gained growing interest due to their applications in catalysis and in the synthesis of new types of complexes. These so-called pyridine-based pincers have also proved amenable to the introduction of different functional moieties so as to potentially influence steric and electronic properties of the overall complex (Fig 3.1).[1]

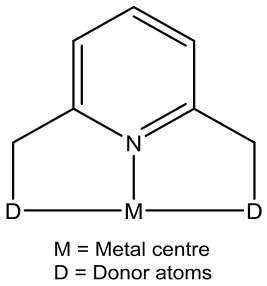

Figure 3.1. Pyridine-based DND type pincer complexes

In addition, the use of D-type coordinating atoms capable of acting as good proton donors and acceptors are highly desirable in metal complexes due to their potential in proton transfer reactions. Moreover, their presence in a metal complex can induce non-covalent interactions such as hydrogen bonding between reactants/substrates and the metal complex. These non-covalent interactions can lead to the formation of supra-molecular networks or complex-substrate interactions.[2, 3]

3.1.2. ONO-type pincers and their potential

Due to the various properties of an oxygen donor atom (see below), symmetrical ONO or unsymmetrical ONO'-type pincer ligands are highly desirable for complexation with late transition metals (Fig. 3.2). Although there is genuine potential of ONO/ONO' palladium pincer complexes in catalysis, only a few complexes have been synthesised and screened.

Palladium complexes incorporating pyridine as the central donor type have commonly been reported with N, P or S at the exterior donor atoms. As oxygen is a hard donor and according to the HSAB principle, Hard-Hard and Soft-Soft interactions are preferred, Pd-O bonds would be expected to be less stable. Unsurprisingly, pincer ligands containing a pyridine-N atom as a central donor and an oxygen-based exterior donor atoms are relatively rare.[4-11] Nevertheless the capacity of oxygen donor arms to be labile when bound to palladium (with the pyridine unit remaining bound) or to act as acceptor atoms for hydrogen bond donors makes them an attractive target.

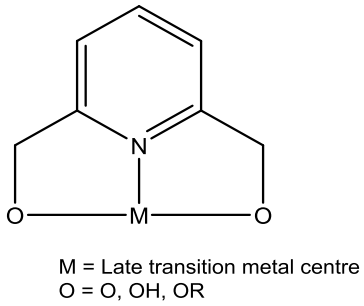

Figure 3.2. Pyridine-based ONO type pincer complexes of late transition metals

Furthermore, the exterior oxygen donor atoms (e.g., O, OH or -OR (R = hydrocarbyl)), offer vast potential for tuning the electronic properties of the pincer complex. For example, both electronic and steric properties can be tuned by varying groups on the methylene carbon adjacent to the oxygen atom. Hence oxygen donor groups due to their tremendous capacity to impart many valuable properties, are highly sought after in pincer-type chemistry. For OH-type exterior donors, their deprotonation when part of a complex could lead to non-covalent interactions such as hydrogen-bonding to substrates which may result in lower activation barriers for the proposed transformation. Additionally, if suitably tuned electronically these ONO-M complexes could act as a proton acceptor (internal base) by playing same role as an acetate in palladium-acetate catalysed C-H activation reactions.[12-14] Hence ONO-type complexes have the capacity to act as functional ligands.

Hence, the hydroxy group due to its attractive properties is a highly desirable feature for incorporation into a ligand scaffold. With regard to hydrogen bonding, the OH group can be used to stabilise certain structures or orientations, increase water stability and undergo acid-base reactions to impart pH-switchability to a ligand or complex. Furthermore, the

OH group when deprotonated can act as strong donor to a metal centre and can act as a neutral OH donor it its own right in some complexes.[15]

3.1.3. Applications of ONO-pincer complexes

In the context of C-H activation, directing groups can bind to a metal centre to bring a desired CH activation site in close proximity to the metal centre to initiate CH activation with the assistance of base to abstract a proton. This is a robust approach with high reactivity and regioselectivity due to pre-coordination of the directing group to the metal centre.[16-20] However, attaching a directing group and removal from the desired product can be a labour intensive process.[21, 22]

A new approach involving bifunctional catalysts is starting to gain attention as an alternative to traditional directing group assisted CH activation. Functionalised pincer complexes are highly desirable which can assist a metal centre under mild conditions and without the need of a directing group.[23] One approach is the participation of the pincer ligand with an incoming substrate via non-covalent interactions such as hydrogen bonding thus providing assistance to the metal centre to carry out the CH activation. In addition, if the pincer ligand has an electronegative donor it could act as internal base to abstract a proton. The conceptual representation of this approach is shown in Fig 3.3.

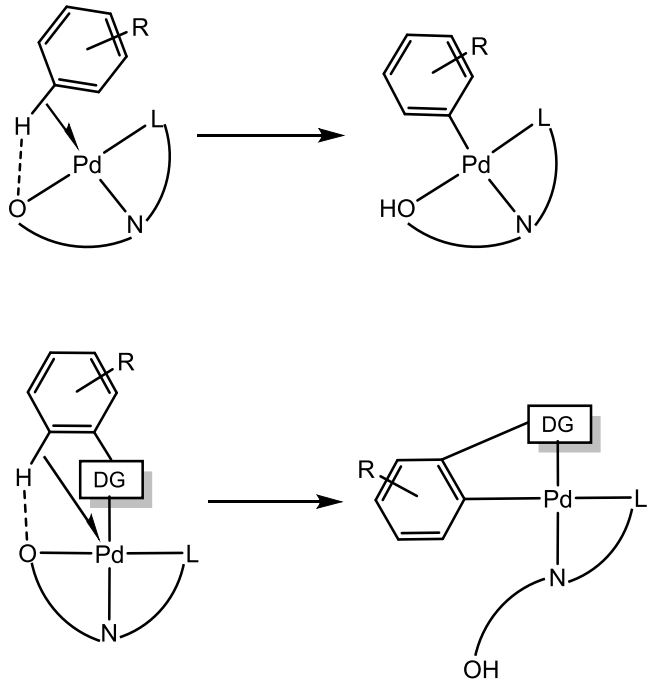

Figure 3.3. Conceptual bifunctional pincer-assisted CH activation and, for comparative purposes, traditional directing group assisted CH activation.[24]

Palladium catalysis has gained interest due to its use in hetero-atom directed CH functionalisation.[20, 25, 26] Usually, these reactions are carried out with the help of expensive and environmentally non-benign oxidants such as *N*-halosuccinamides, *N*-fluoroammonium and *N*-fluoropyridinenium salts, $PhIX_2$ (X = OOCR, Cl), peroxosulphates and alkylperoxides.[20, 27-29]

Recently, ONO-type pincer complexes have gained attention due to their capacity to perform chemically challenging transformations using air or oxygen as ‘green’ oxidants (Scheme 3.1).[13]

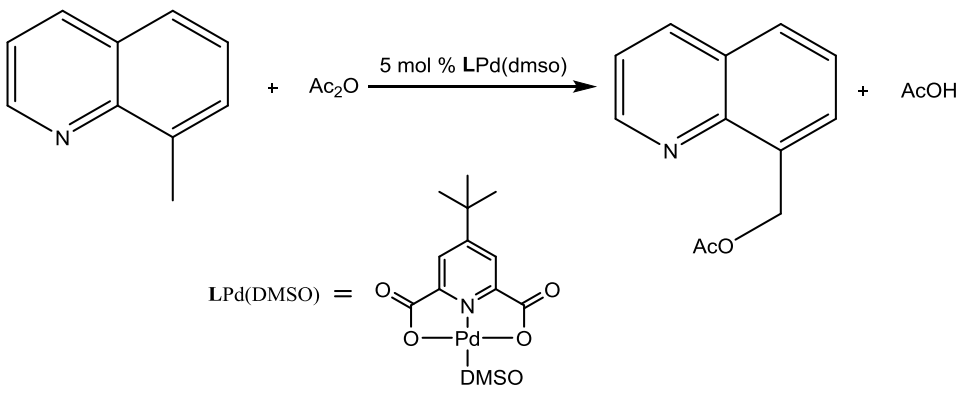

Scheme 3.1. Use of a ONO-palladium pincer in the acetoxylation of 8-methylquinoline

In this example acetoxylation of 8-methylquinoline can be readily achieved using a palladium(II) catalyst with air as the oxidant (Scheme 3.1). The active palladium(II) species contains a ONO-dicarboxylate pincer ligand that can act as an internal base to abstract a proton from the substrate.[14]

In this chapter the proposed idea is to build a library of pyridine-based ONO' unsymmetric pincer ligands with a phenoxide and an alkoxide as the exterior donor atoms. It is worthy of note that the complexation of symmetrical ONO ligands with palladium(II) as the metal centre is relatively scarce while unsymmetrical systems to the knowledge of the author have not been reported.

3.2. Aims and Objectives

From inspection of the literature, it is clear that ONO-type pincer complexes with palladium are rare, but nevertheless have desirable performance characteristics in catalytic processes.[11, 30-33] A few examples of symmetrical pyridine-based dicaboxylate Pd(II) complexes have emerged as efficient catalysts in challenging reactions (Scheme 3.1).[13] Therefore, it is of interest to target pyridine-based pincer complexes with oxygen donor arms to explore the properties imparted by this complex as a whole.

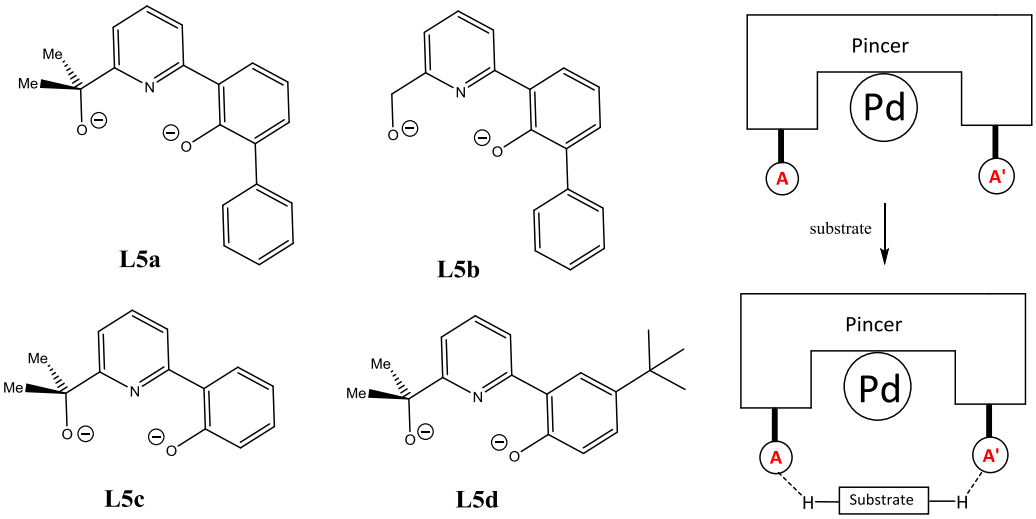

Figure 3.4. Proposed unsymmetrical ONO' ligands, **L5a** – **L5d**, and their capacity to chelate to Pd and act as hydrogen bond acceptors

The first objective of chapter 3 is to modify the ONN ligand skeleton described in chapter 2 to synthesise pyridine-based unsymmetrical ONO' dianionic ligands (**L5**) that contain a tertiary alkoxide arm in addition to a phenolate arm (Fig. 3.4.). To explore the effect of steric and electronic effects, the substitution pattern at the 3- and 5-positions of the phenolate unit were modified to include aryl (**L5a** and **L5b**) and alkyl/H groups (**L5c** and **L5d**). In addition, the substituents on the alkoxide carbon were varied (**L5a** and **L5b**). Secondly, the complexation reactions with palladium(II) acetate were explored as a means to establish the viability of **L5** as a dianionic ligand and to investigate if the changes in steric and electronic properties influence structural type. Thirdly, the reactivity of the resultant palladium complexes towards ligand exchange reactions were explored. As an overall objective, the influence of having inequivalent hard oxygen donors on complex formation was studied, e.g., in hydrogen bonding, proton transfer etc. In addition, the potential of the oxygen donor arms to act as potential hydrogen bond acceptors or serve as an internal base in the complex was probed.

3.3 Results and discussion

3.2.1. Preparation of pro-ligands HL5a, HL5b, HL5c and HL5d

The 2-(3-biphenyl-2-ol)-6-(2-hydroxypropan-2-yl)-pyridine, 2-(3-$C_{12}H_8$-2-OH)-6-(CMe_2OH)C_5H_3N (H_2**L5a**) was prepared in two steps by the Suzuki cross coupling reaction of 2-phenylphenol-boronic acid with 2-bromo-6-acetyl pyridine to form 2-(3-biphenyl-2-ol)-6-acetylpyridine, which on alkylation with $AlMe_3$ and subsequent hydrolysis gives H_2**L5a** in good overall yield (Scheme 3.2). A modified approach had to

be used to prepare 2-(3-$C_{12}H_8$-2-OH)-6-(CH_2OH)C_5H_3N (H_2**L5b**) involving protection-deprotection steps as the cross coupling of 2-phenylphenol-boronic acid with 2-bromo-6-formylpyridine gave only low yields of 2-(3-biphenyl-2-ol)-6-formylpyridine. Using the anisole boronic acid in place gave high yields of 2-(3-biphenyl-2-OMe)-6-formylpyridine which could be readily deprotected with BBr_3. Reduction of the aldehyde unit in 2-(3-biphenyl-2-ol)-6-formylpyridine with $NaBH_4$ then gave H_2**L5b** almost quantitatively (Scheme 3.3).

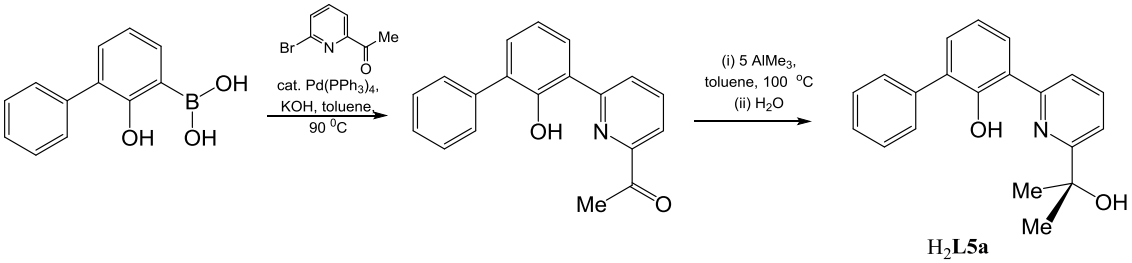

H_2**L5a**

Scheme 3.2. Synthetic route to H_2**L5a**

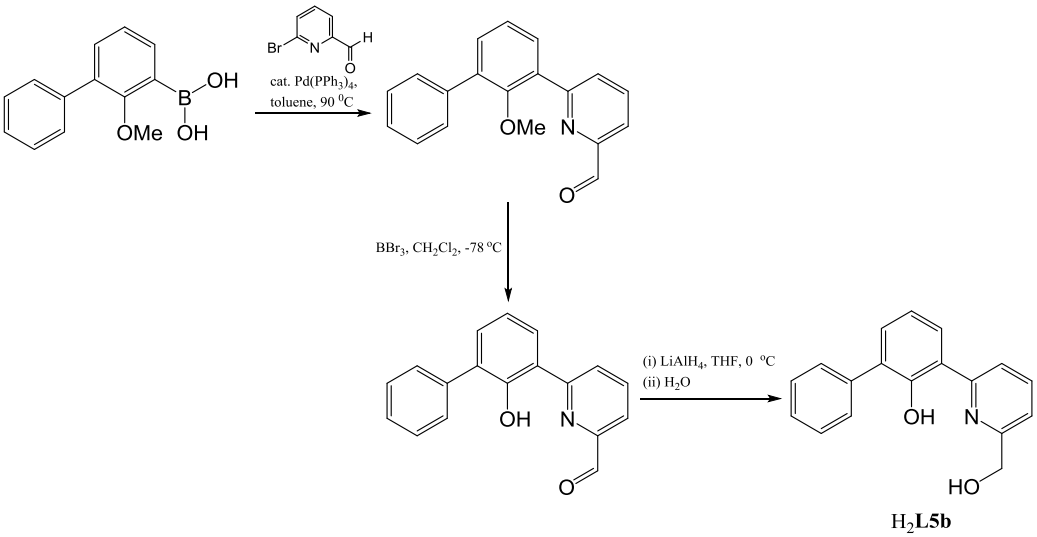

H_2**L5b**

Scheme 3.3. Synthetic route to H_2**L5b**

The other two pro-ligands, 2-(5-RC_6H_3-2-OH)-6-(CH_2OH)C_5H_3N (R = H, H_2**L5c**; C(CH_3), H_2**L5d**), were prepared in good yield based on the route given for H_2**L5a** (Fig. 3.5).

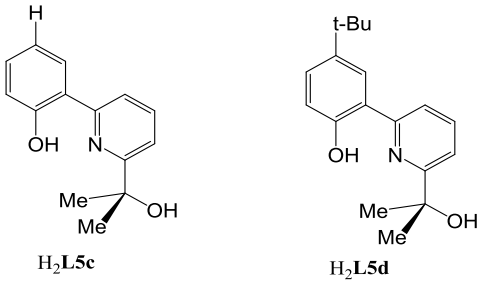

Figure 3.5. Pro-ligands H_2**L5c** and H_2**L5d**

The four new compounds, H_2**L5a**, H_2**L5b**, H_2**L5c** and H_2**L5d**, have been characterised using a combination of mass spectrometry (electrospray, high resolution), ^{1}H NMR and ^{13}C NMR spectroscopy (see experimental section). As expected, H_2**L5a**, H_2**L5b,** H_2**L5c** and H_2**L5d** all show downfield signals in their ^{1}H NMR spectra for the phenol proton (range: 10 - 15 ppm) due to intramolecular hydrogen bonding with the neighbouring pyridine nitrogen. The tertiary alcohol protons in H_2**L5a**, H_2**L5c** and H_2**L5d** could be seen more upfield in the range 3.1 - 3.8 ppm, while the primary alcohol proton in H_2**L5b** was visible at 3.5 ppm as broad singlet. Protonated molecular peaks were observed in the positive electrospray mass spectra for all four pro-ligands.

3.2.2. Preparation of [L5a/bPd]$_2$ (10a/10b) and [L5c/dPd]$_4$ (11a/11b)

Reaction of H_2**L5a** and H_2**L5b** with $Pd(OAc)_2$ at room temperature in toluene gave, on work up, the bimetallic complexes [**L5a**Pd]$_2$ (**10a**) and [**L5b**Pd]$_2$ (**10b**) in excellent yield (Scheme 3.4). By contrast the reaction of H_2**L5c** and H_2**L5d** with $Pd(OAc)_2$ gave the tetrametallic complexes [**L5c**Pd]$_4$ (**11a**) and [**L5d**Pd]$_4$ (**11b**). All four complexes are air stable and were characterised using FAB mass spectrometry, NMR and IR spectroscopy as well as by elemental analysis. X-ray diffraction studies have been performed on single crystals of **10a**, **11a** and **11b**.

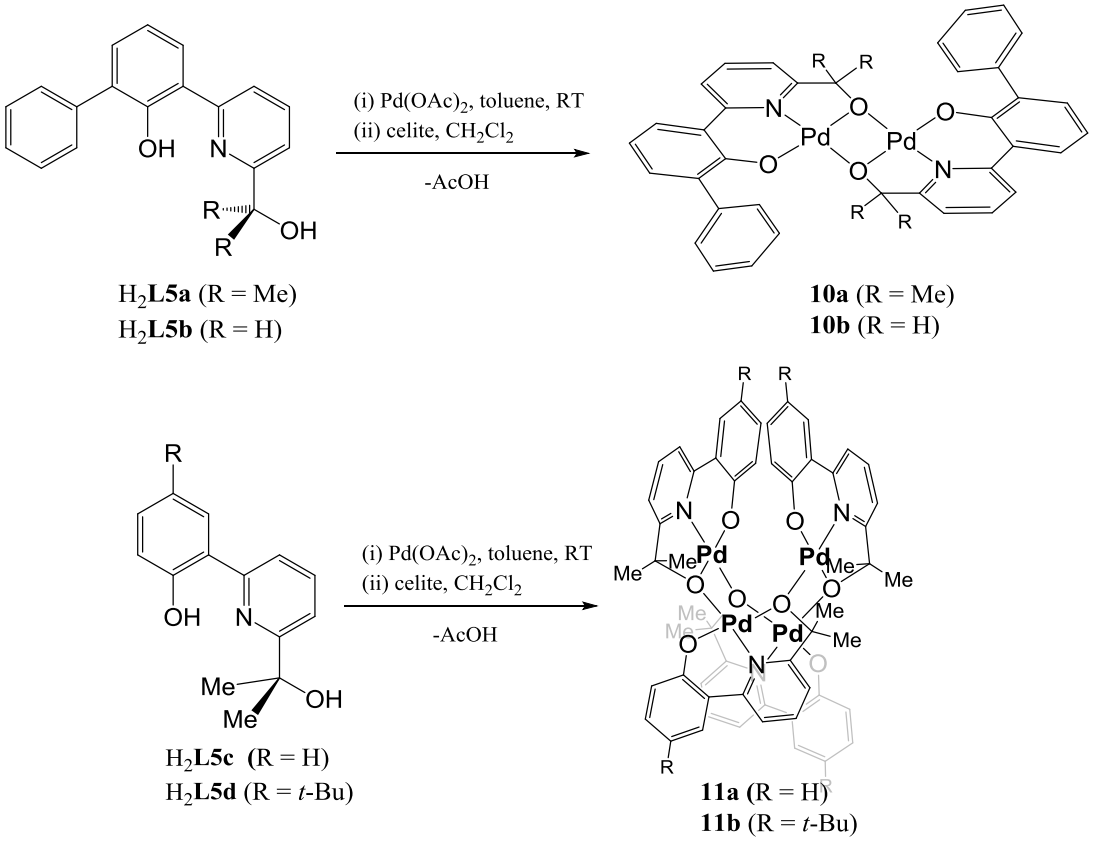

Scheme 3.4. Reactivity of H_2**L5a** – H_2**L5d** towards palladium(II) acetate

The ^{1}H NMR spectra for **10a**, **10b**, **11a** and **11b** reveal the absence of any phenolic or alkoxy protons highlighting full consumption of the corresponding ligand. In addition no acetate methyl signals were observable implying the acetate ligands have been displaced. In **10a**, **11a** and **11b**, the CMe_2 units were seen as singlet resonances. The electrospray mass spectra shows molecular ion peaks for all four complexes.

Single crystals of **10a**, suitable for a X-ray determination, were grown by slow evaporation of a toluene solution. The molecular structure is shown in Fig. 3.6; selected bond lengths and bond angles are collected in Table 3.1. The structure of **10a** consists of two palladium centres bound by tridentate **L5a** with the alkoxide oxygen acting as bridge between the two palladium centres. The solid state structure reveals slightly distorted square planar palladium(II) centres. The pyridine nitrogen to palladium centre distance is shortest (Pd(1)-N(1) 1.946(4) Å) and the alkoxide oxygen to palladium the longest (Pd(1)-O(2A) 2.049(3) Å). There are both 5-and 6-membered chelate rings formed with the tridentate ligand with the bite for the six-membered ring more suitable for the square planar requirement of the palladium(II) centre [O(1)-Pd(1)-$N(1)_{6\text{-membered}}$ 94.42(16)^o *vs.*

O(2)-Pd(1)-N(1)$_{5\text{-membered}}$ 82.00(16)^{o}. Some twisting of the phenolate unit with respect to the pyridyl plane is apparent [tors. N(1)-C(13)-C(2)-C(1) 6.0(10) 27.9(8)^{o} and is slightly more pronounced than in similar ONN type palladium(II) pincer complexes.[34] The palladium-palladium separation is 2.9729(10) Å which is at the top end of the range for previously reported covalently bridged palladium(II) dimers (2.55-3.05 Å).[35-40] Recently, computational studies carried out on palladium (II) dimers (Pd···Pd 2.55-3.05 A) showed d^8-d^8 interactions between palladium atoms but are orthogonal to square plane of palladium centers.[41]

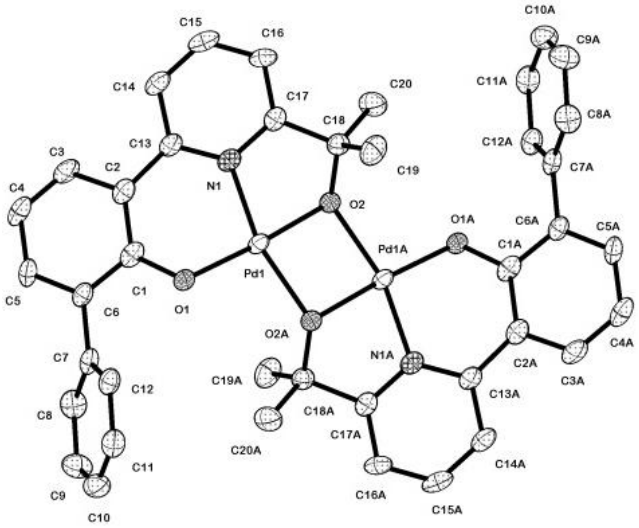

Figure 3.6. Molecular structure of **10a** including a partial atom numbering scheme. All hydrogen atoms have been omitted for clarity.

Table 3.1. Selected bond distances (Å) and angles (^{o}) for **10a**

Bond lengths	
Pd(1)-O(1)	1.971(3)
Pd(1)-O(2)	1.988(3)
Pd(1)-N(1)	1.946(4)
Pd(1)-O(2A)	2.049(3)
Pd(1)-Pd(1A)	2.9729(10)
Bond angles	
N(1)-Pd(1)-O(1)	94.42(16)
O(1)-Pd(1)-O(2A)	98.59(14)
N(1)-Pd(1)-O(2)	82.00(16)
O(1)-Pd(1)-O(2)	176.12(14)

The molecular structures of **11a** and **11b** are shown in Figs. 3.7 and 3.8; selective bond distances and angles are collected in Table 3.2. As the structures of both **11a** and **11b** are closely related they will be discussed together. The structures consist of four palladium centres bound by four ligands held together by bridging alkoxides. In both, the Pd-O(bridging) is longest of four metal-ligand bonds **11a** [Pd(1)-O(2A) 2.034(3)] and **11b** [Pd(1)-O(2A) 2.041(3)Å]. Phenolic ring is tilted [tors. C(1)-C(2)-C(7)-N(1).20.8(7)$_{\mathbf{11a}}$, 22.2(6)$_{\mathbf{11b}}$] with respect to the pyridine plane thus making square planar geometry slightly distorted. There are no non-covalent interactions within or with any other molecule.

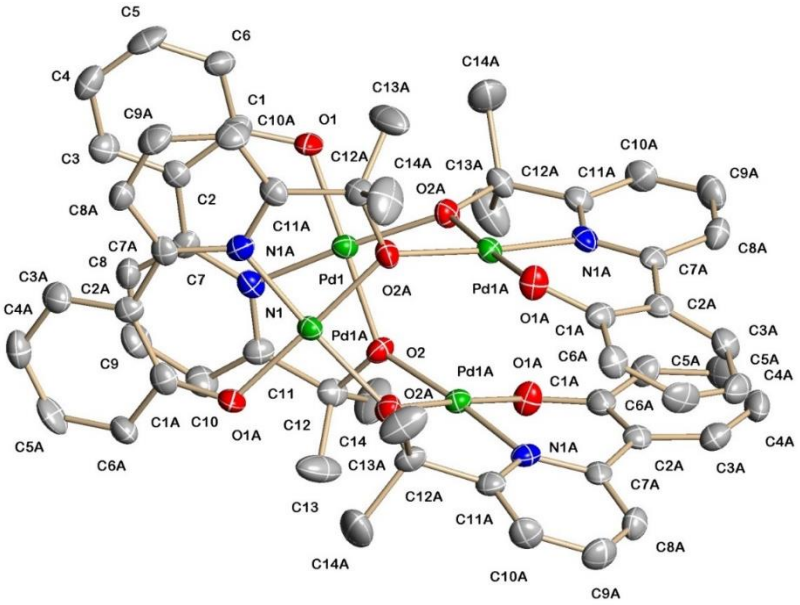

Figure 3.7. Molecular structure of **11a** including a partial atom numbering scheme. All hydrogen atoms have been omitted for clarity

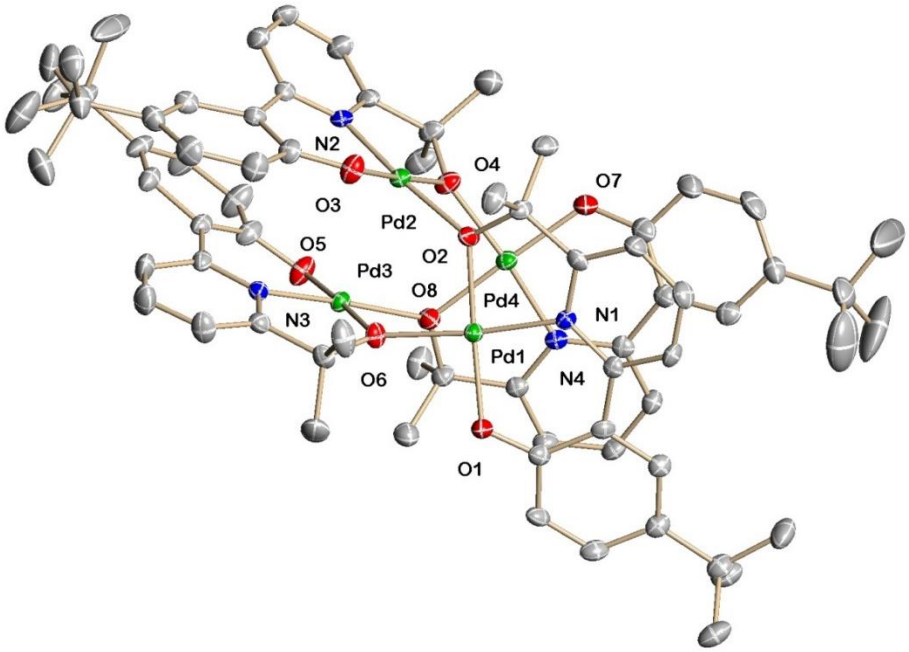

Figure 3.8. Molecular structure of **11b** including a partial atom numbering scheme. All hydrogen atoms have been omitted for clarity

Table 3.2. Selected bond lengths [Å] and bond angles [º] of **11a** and **11b**

	Selected bond lengths	
	11a	**11b**
Pd(1)-O(1)	1.958(3)	1.973(3)
Pd(1)-N(1)	1.960(4)	1.963(4)
Pd(1)-O(2)	1.984(3)	1.976(3)
Pd(1)-O(2A)	2.034(3)	2.041(3)
O(2)-Pd(1A)	2.034(3)	2.039(3)
	Selected bond angles	
O(1)-Pd(1)-N(1)	95.04(17)	94.51(13)
O(1)-Pd(1)-O(2)	177.56(15)	177.25(13)
N(1)-Pd(1)-O(2)	83.44(16)	83.04(13)
O(1)-Pd(1)-O(2)#1	88.86(15)	91.91(12
N(1)-Pd(1)-O(2)#1	175.12(17)	173.25(13)

It is interesting to note that by removing the phenyl ring from the phenolate arm of the NNO ligand in **L5a** leads to the formation of tetramers (**11a** and **11b**), instead of dimers (**10a** and **10b**). It is likely that the steric properties of phenyl group are responsible for this structural difference.

Inspection of the literature reveals only a few examples of palladium(II) complexes containing ONO-type ligands.[42, 43] This scarcity is likely due to the mis-match of hard exterior oxygen donor atoms with soft metal. It may be noted that past attempts to bind pyridine based tridentate symmetrical phenoxide or alkoxide were not successful.[44]

3.2.3. Reactivity of 10a towards pyridines

Surprisingly dimeric [**L5a**Pd]$_2$ (**10a**) proved stable at room temperature and did not undergo bridge cleavage reactions in acetonitrile even at elevated temperatures. In order to force the breaking of the alkoxy- bridged dimer, stronger donors such as pyridine, 3,5-dimethylpyridine and 3,5-dichloropyridine were attempted.

It was found that the alkoxide-bridging in **10a** could only be broken by heating it with pyridine in acetonitrile to give mononuclear **L5a**Pd(NC_5H_5) (**12a**) (Scheme 3.5). Pyridine-bound complex **12a** can also be formed via a one-pot synthesis by stirring H_2**L5a**, Pd(OAc)$_2$ and pyridine in toluene at room temperature. Similarly, **L5a**Pd(NC_5H_3-3,5-Cl_2) (**12b**) can be prepared by using a one-pot procedure from Pd(OAc)$_2$ and 3,5-dichloropyridine. It should be noted that 3,5-dichloropyridine ligand in **12b** can be replaced by the stronger pyridine ligand to obtain **12a** by ligand exchange (Scheme 3.6).

Notably, **L5a**Pd(NC_5H_3-3,5-Me_2) (**12c**) which has 3,5-dimethylpyridine as the N-bound monodentate ligand can only be prepared by using dimeric **10a** as the starting material. An attempt to make **12c** using a one-pot synthesis from Pd(OAc)$_2$ gave no reaction with H_2**L5a** but instead formed *trans*-[Pd(3,5-dimethylpyridine)$_2$(OAc)$_2$].

Complexes **12a**, **12b** and **12c** are air stable and have been characterised using a combination of FAB mass spectrometry, IR, and NMR (^{1}H, ^{13}C) spectroscopy (see experimental section). In addition, crystals of **12a** and **12b** were the subject of single crystal X-ray diffraction studies. The structure of *trans*-[Pd(3,5-dimethylpyridine)$_2$(OAc)$_2$] is presented in the Appendix)

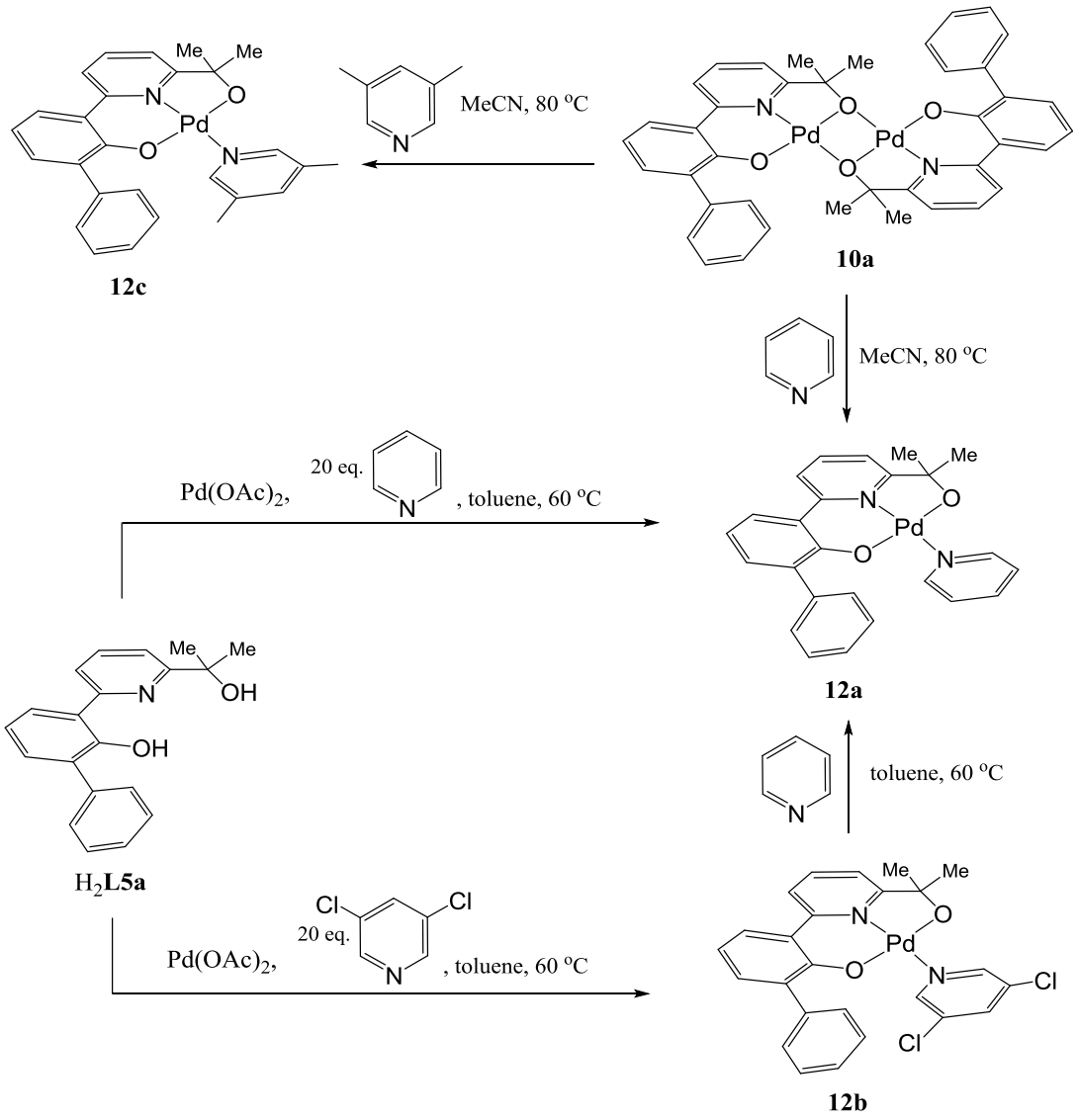

Scheme 3.5. Synthetic routes to **12a**, **12b** and **12c**

The molecular structure of complexes **12a** and **12b** are shown in Figures 3.7 – 3.8; selected bond distances and angles are compiled in Table 3.3 and 3.4. The structures are similar and will be discussed together. Each structure comprises a mononuclear palladium(II) centre bearing dianionic **L5a**, which adopts a ONO-bonding mode, and an N-bound pyridine (pyridine (**12a**), 3,5-dichloropyridine (**12b**)) ligand to complete a geometry best described as square planar. The torsion angle of the pyridine ligand in **12a** with respect to the palladium plane is 17.77° which compares to 19.32° for the 3,5-dichloropyridine in **12b**. In both **12a** and **12b** the longest bond with palladium(II) is with the monodenate pyridine ligand [Pd(1)-N(1) 2.030(6)$_{\mathbf{12a}}$, 2.024(5)$_{\mathbf{12b}}$ Å] and shortest with the central pyridine from the **L5a** skeleton [Pd(1)-N(2) 1.956(6)$_{\mathbf{12a}}$, 1.950(5)$_{\mathbf{12b}}$ Å]. In

addition, the bite angles of two chelate rings (5-membered: 83.2(2)-84.7(2)^{o} and 6-membered: 93.1(1)-94.4(2)^{o}) formed around the palladium centre leading to distortion from an ideal square planar geometry.

Palladium pincers have not been formed from symmetrical di-alcohol tridentate ligands. An attempt to form palladium pincer with 2,6-bis(1-hydroxy-1-methylethyl)pyridine resulted in alkoxide donors functions of the ligand not taking part in coordination.[44]

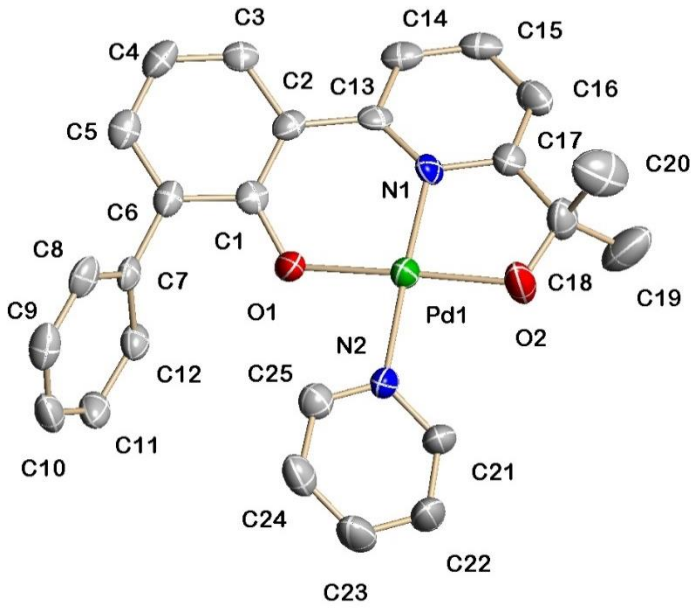

Figure 3.7. Molecular structure of **12a** including a partial atom numbering scheme. All hydrogen atoms have been omitted for clarity

Table 3.3. Selected bond distances (Å) and angles (^{o}) for **12a**

	Bond lengths	
	Molecule A	*Molecule B*
Pd(1)-O(2)	1.953(5)	1.962(5)
Pd(1)-N(1)	1.956(6)	1.965(6)
Pd(1)-O(1)	1.970(5)	1.895(4)
Pd(1)-N(2)	2.030(6)	2.054(6)
O(2)-C(18)	1.382(9)	1.416(9)
	Selected bond angles	
O(2)-Pd(1)-N(1)	84.7(2)	84.9(2)
O(2)-Pd(1)-O(1)	174.8(3)	175.7(2)
N(1)-Pd(1)-O(1)	94.4(2)	96.7(2)
O(2)-Pd(1)-N(2)	92.9(2)	90.0(2)
N(1)-Pd(1)-N(2)	177.2(3)	174.8(3)
O(1)-Pd(1)-N(2)	87.8(2)	88.4(2)

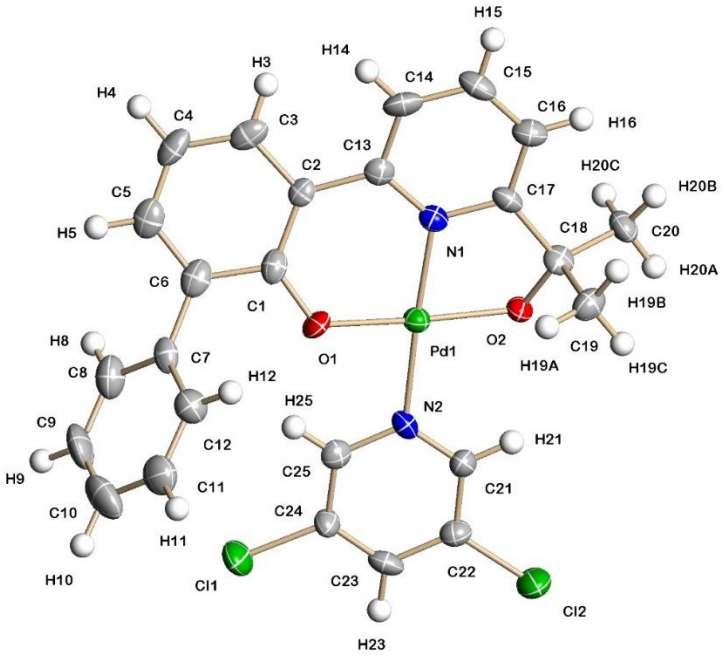

Figure 3.8. Molecular structure of **12b** including a partial atom numbering scheme. All hydrogen atoms have been omitted for clarity

Table 3.4. Selected bond distances (Å) and angles (°) for **12b**

Bond lengths	
Pd(1)-O(1)	1.951(4)
Pd(1)-O(2)	1.971(4)
Pd(1)-N(1)	1.950(5)
Pd(1)-N(2)	2.024(5)
O(2)-C(18)	1.417(7)
Bond angles	
O(2)-Pd(1)-N(1)	83.2(2)
O(2)-Pd(1)-O(1)	175.95(18)
N(1)-Pd(1)-O(1)	93.1(2)
O(2)-Pd(1)-N(2)	93.4(2)
N(1)-Pd(1)-N(2)	176.5(2)
O(1)-Pd(1)-N(2)	90.4(2)

In **12a**, **12b** and **12c**, the two methyl groups appear as 6H singlets in the region δ 1.45-1.87 due to their equivalent environments. In the ESI mass spectra peaks corresponding the molecular ion minus the pyridine unit are evident.

The formation of *trans*-[Pd(3,5-dimethylpyridine)$_2$(OAc)$_2$] over **12c** during the one-pot synthesis from Pd(OAc)$_2$ was unexpected. It is likely due to the strong donor properties

of 3,5-dimethylpyridine preferring to doubly bind to palladium. The success of this one-pot approach with pyridine or 3,5-dichloropyridine lends some support to this donor strength theory.

Given the procedures developed above to make palladium(II) complexes of the type (ONO)PdPy (see **12a**, **12b** and **12c**), it was of interest to see how robust these procedures were for introducing other nitrogen donors and in particular those that can in principle incorporate hydrogen bonding. We reasoned that anionic oxygen donors in the pincer complex would act as excellent hydrogen bond acceptors or even be basic enough to abstract a proton. To realise this goal we have targeted the use of 2-pyridones.

3.2.4. Reactivity of 10a towards pyridones

2-Pyridones are important organic compounds known for hydrogen bonding in organic chemistry. Their ability to act as both donor and acceptor atoms for hydrogen bonding is well documented.[45-47] We were interested in how a pyridone ligand would interact in the presence of an ONO'-chelate which contains, in principle, two possible hydrogen-bond acceptor atoms.

Heating a one-pot mixture of H_2**L5a,** $Pd(OAc)_2$ and Hxhp (x = H, Cl) in toluene gave pyridone complexes **L5a**Pd(Hxhp) (x = H (**13a**), Cl (**13b**)) in good yield (Scheme 3.6). Complexes **13a** and **13b** have been characterised by ^{1}H NMR, ESIMS, FABMS and have both been the subject of single crystal X-ray determinations.

The molecular structures of **13a** and **13b** are shown in Fig. 3.9 and 3.10; selected bond distances and angles are collected in Table 3.5 and 3.6. Each structure consists of a palladium centre bound by a dianionic **L5a** ligand and an N-bound neutral pyridinol ligand to complete a distorted square planar geometry. In both **13a** and **13b** the OH proton of the pyridinol is interacting through hydrogen-bonding (intramolecular in **13a** and intermolecular in **13b**). The effect of bulky chloride substituent on the pyridone can be seen from the torsion angle between palladium plane and the pyridone i.e., O(2)-Pd(1)-N(2)-C(21) 22.8^o (**13a**), 85.7^o (**13b**). Thus in **13a** the pyridinol prefers a more in-plane conformation so as to facilitate OH···alkoxide hydrogen bonding oxygen. On other hand the large torsional angle (85.7) of 6-chloro-2-pyridinol with palladium square plane

prevents the pyridinol OH undergoing intramolecular interactions in **13b**. The distance between the alkoxide oxygen and the pyridinol oxygen involved in the intramolecular hydrogen bond interactions [2.480 Å (**13a**)] and [2.448 Å..**13b**] for corresponding alkoxide oxygen and pyridone of other molecule of **13b**. These distances are less than the distances between two water molecules (~2.800 Å) which shows stronger hydrogen bonding interactions in **13a** and **13b**.[48]

As a common feature the OH of the pyridinol is bound to the alkoxide oxygen by hydrogen bonding interactions. The alkoxide oxygen appears to act as a guiding functional group to an incoming substrate or play a role in stabilising complex **13a**. It is interesting to note that introduction of chlorine atom at 6-position on pyridine lead to tilting of pyridinol ring by *ca*. 90^{o} in the solid state. The X-ray structure of **13b** showed hydrogen bonding interactions between the alkoxide oxygen of the palladium-bound tridentate H_2**L5a** ligand and the OH of pyridinol of a neighbouring molecule. It is also worth noting that the alkoxide arm is acting as the hydrogen bond acceptor in the ONO pincer complex whereas the phenoxide oxygen has not shown any such interactions due possibly to steric hindrance imparted by the phenyl ring.

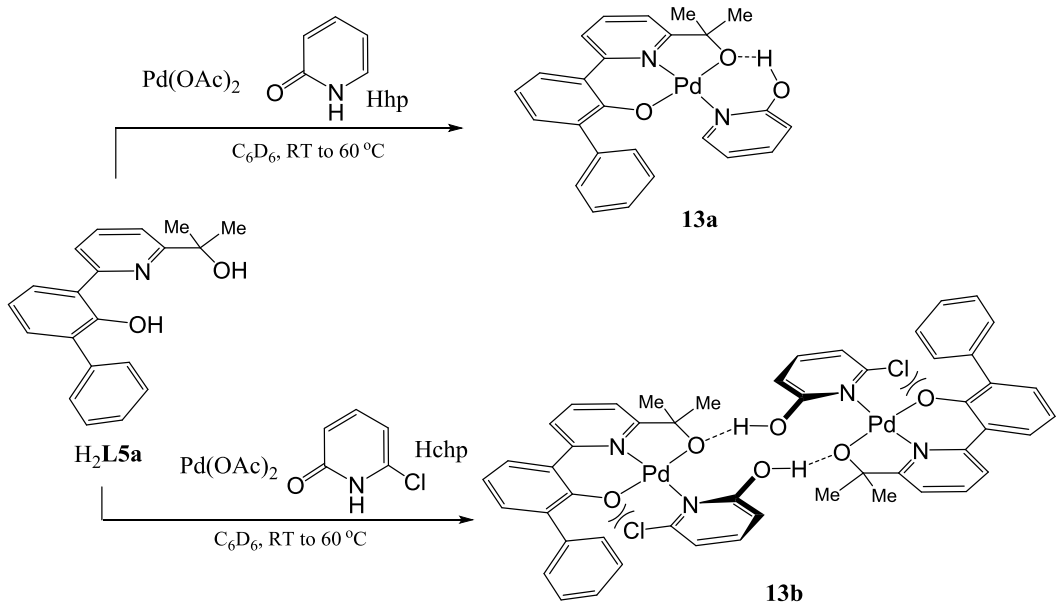

Scheme 3.6. Reaction of H_2**L5a** with 2-pyridones Hxhp (x = H, Cl).

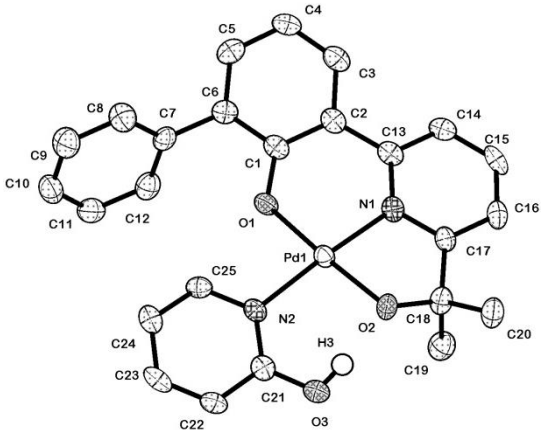

Figure 3.8. Molecular structure of **13a** including a partial atom numbering scheme. All hydrogen atoms have been omitted for clarity.

Table 3.5. Selected bond lengths [Å] and bond angles [°] of **13a**

	Selected bond lengths	
	Molecule A	*Molecule B*
Pd(1)-O(1)	1.972(3)	1.965(3)
Pd(1)-N(1)	1.961(3)	1.976(3)
Pd(1)-O(2)	1.990(3)	1.985(3)
Pd(1)-N(2)	2.057(3)	2.066(3)
O(3)-C(21)	1.311(5)	1.318(5)
	Selected bond angles	
O(2)-Pd(1)-N(1)	83.21(13)	83.59(13)
O(2)-Pd(1)-O(1)	176.34(14)	177.09(13)
N(1)-Pd(1)-O(1)	93.30(13)	93.64(14)
O(2)-Pd(1)-N(2)	94.19(13)	93.73(13)
O(1)-Pd(1)-N(2)	89.24(13)	89.10(13)

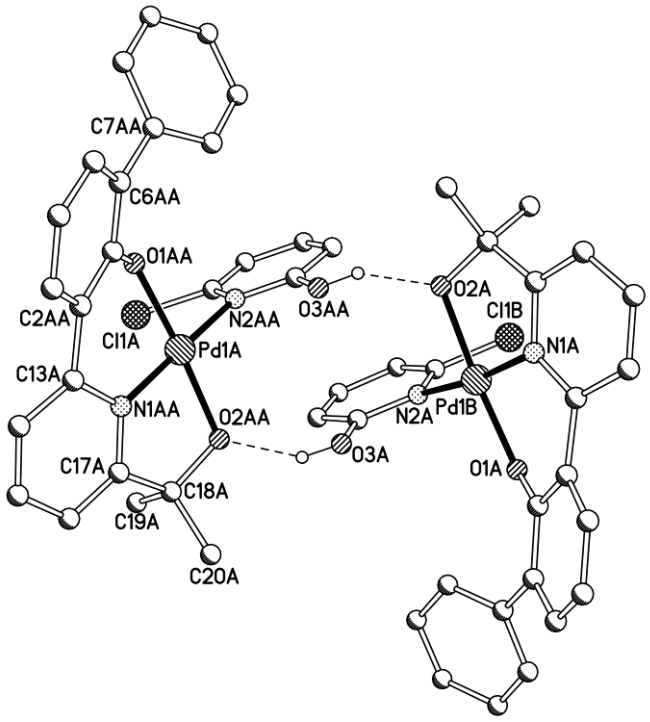

Figure 3.9. Molecular structure of **13b** including a partial atom numbering scheme. All hydrogen atoms have been omitted for clarity

Table 3.6. Selected bond lengths [Å] and bond angles [º] of **13b**

	Selected bond lengths	
	Molecule A	*Molecule B*
Pd(1)-O(1)	1.974(4)	1.981(4)
Pd(1)-N(1)	1.978(5)	1.952(5)
Pd(1)-O(2)	2.001(4)	2.013(4)
Pd(1)-N(2)	2.082(5)	2.065(5)
O(3)-C(21)	1.287(6)	1.334(7)
	Selected bond angles	
O(2)-Pd(1)-N(1)	82.47(19)	82.07(19)
O(2)-Pd(1)-O(1)	175.75(16)	175.44(16)
N(1)-Pd(1)-O(1)	93.71(19)	93.50(19)
O(2)-Pd(1)-N(2)	90.90(17)	95.01(17)
O(1)-Pd(1)-N(2)	92.84(16)	89.31(17)

3.2.5. Attempted preparation of symmetrical ONO-palladium complexes

Given the varied reactivity of unsymmetrical H_2**L5** towards palladium(II) acetate, it was of interest to compare this reactivity with their symmetrical counterparts namely, 2,2'-(pyridine-2,6-diyl)diphenol (H_2**L6**) and 2,2'-(pyridine-2,6-diyl)bis(propan-2-ol) (H_2**L7**) (Fig 3.10). Unexpectedly inspection of the various chemical databases revealed no evidence for well-defined products obtained using these two previously reported ligand

systems. To explore their reactivity we treated H_2**L6** or H_2**L7** with palladium(II) acetate under the same conditions as we used with H_2**L5**. Unfortunately no clean products could be isolated. It should be noted that related pyridine diols with palladium have been reported and have been found to coordinate through the pyridine nitrogen with the OH groups pendant (Fig. 3.11).[44]

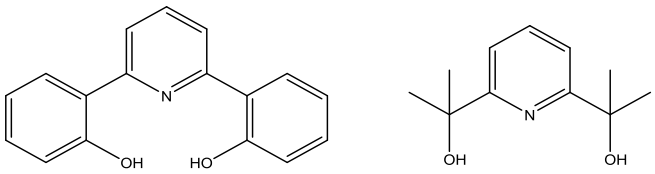

H_2**L6** H_2**L7**

Figure 3.10. Symmetrical ONO pincer ligands H_2**L6** and H_2**L7**

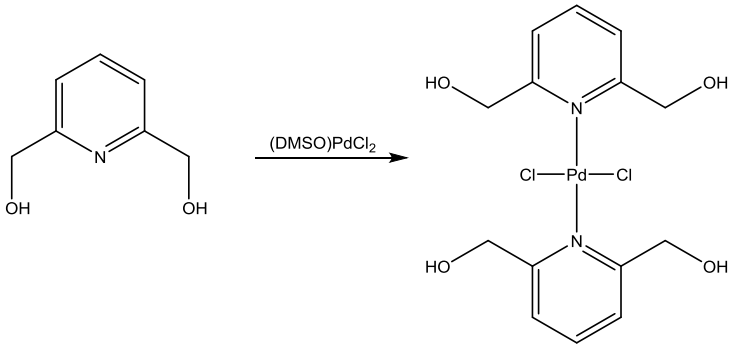

Scheme 3.7. Previously reported reaction of a symmetrical di-alcohol ligand with a palladium(II) salt

It would appear that the hybrid pyridine-based unsymmetrical ligands H_2**L5a**-H_2**L5d** developed in this work are more effectively designed to meet the square planar requirements of palladium(II); their increased flexibility allows more efficient binding and deprotonation.

3.2.6. Attempted protonation of 10a

To test the proton acceptor capacity of complex **10a**, we attempted several reactions with different acids named HBF_4 and HCl in the presence of pyridine (Scheme 3.8). We were expecting some selectivity of the different oxygen donor groups towards protonation. Unfortunately, it was found that acidification with one equivalent of acid led to protonation of both alkoxide and phenoxide oxygen resulting into decomplexation of ligand from the palladium centre and reformation of free H_2**L5a**.

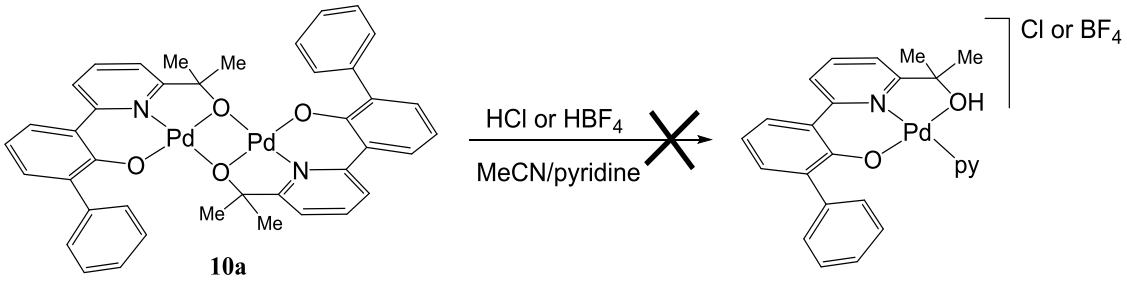

Scheme 3.8 Attempted reaction of **10a** with HCl or HBF_4

3.2.7 Reaction of 11a with MeI or bromotoluene

Palladium(IV) chemistry is currently a topical area due to the role of such high oxidation state species in catalytic reactions involving Pd(II)/Pd(IV) catalytic cycles. However, due to their instability there are relatively few examples of well-defined Pd(IV) complexes to explain such reaction pathways.[49] Recently Vicente has demonstrated the involvement of palladium(IV) chemistry in Heck-type reactions using pyridine-based tridentate pincers (Fig. 3.11). [50]

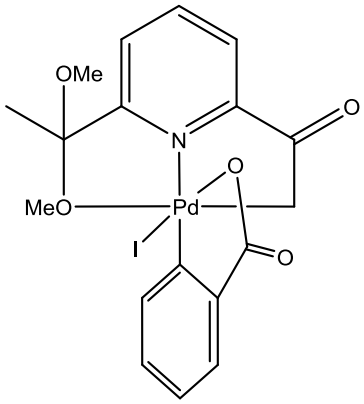

Figure 3.11. Palladium(IV) pincer complex

To explore the potential for the ONO-Pd species generated in this work, mono-palladium complex **12a** was selected to examine its potential to support a palladium(IV) framework. However, it was found that the prolonged reaction of **12a** with stoichiometric amounts of methyl iodide or 4-bromotoluene in toluene resulted in decomposition leading to decomplexation of the ligand (Scheme 3.11). We are uncertain as to the mechanism of decomposition.

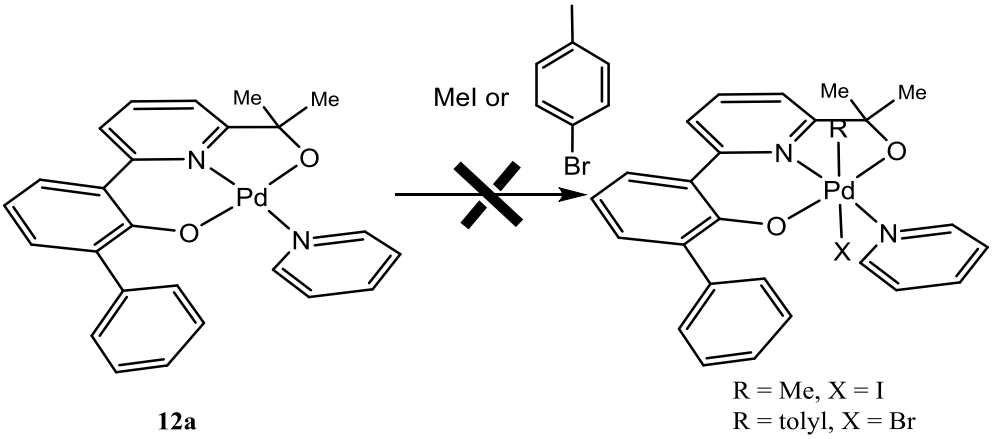

Scheme 3.11 Attempted reaction of **12a** with methyl iodide or bromotoluene

3.3. Conclusions

In summary, a series of novel unsymmetrical ONO'-type pro-ligands, H_2**L5a**, H_2**L5b**, H_2**L5c** and H_2**L5d**, have been prepared and fully characterised. Double deprotonation of H_2**L5a** and H_2**L5b** occurs on reaction with palladium(II) acetate leading to the dipalladium complexes [**L5a**Pd]$_2$ (**10a**) and [**L5b**Pd]$_2$ (**10b**), respectively. With the less sterically bulky, H_2**L5c** and H_2**L5d**, the tetrameric palladium complexes [**L5c**Pd]$_4$ (**11a**) and [**L5d**Pd]$_4$ (**11b**) have been isolated. The X-ray structures of **10a**, **11a** and **11b** reveal the alkoxide moiety in **L5** acts as the bridging ligand in each case. Cleavage of the alkoxide bridges in **10a** can be achieved by reaction with the strong donor ligands, pyridine and 3,5-dimethylpyridine, to give **L5a**Pd(NC_5H_5) (**12a**) and **L5a**Pd(NC_5H_3-3,5-Me_2) (**12b**). By contrast, **L5a**Pd(NC_5H_3-3,5-Cl_2) (**12c**) could not be isolated using a similar route. However, **12c** can be prepared using a one-pot reaction containing $Pd(OAc)_2$, 3,5-dichloropyridine and H_2**L5** which is also applicable to the synthesis of **12a** but not **12b**. Neutral pyridone ligands have also been amenable to a one-pot synthetic approach yielding the pyridinol complexes **L5a**Pd(Hxhp) (x = H (**13a**), Cl (**13b**)). Notably the X-ray structures of **13a** and **13b** reveal the pyridinol OH to serve as hydrogen bond donor to an alkoxide-oxygen acceptor either intra- or inter-molecularly, respectively. Attempted protonation of **10a** led to decomplexation of the pro-ligand while attempted oxidative addition reactions of **12a** with methyl iodide or bromotoluene resulted in decomposition.

3.4. References

1. *CHAPTER 1 - Organometallic pincer-type complexes: recent applications in synthesis and catalysis A2 - Morales-Morales, David*, Elsevier Science B.V., Amsterdam, 2007.
2. H. Aghabozorg, F. Manteghi, M. Ghadermazi, M. Mirzaei, A. R. Salimi, A. Shokrollahi, S. Derki and H. Eshtiagh-Hosseini, *J. Mol. St.*, 2009, **919**, 381-388.
3. Y.-Y. Xu, J.-G. Lin, J. Yao, S. Gao, H.-Z. Zhu and Q.-J. Meng, *Inorg. Chem. Comm.*, 2008, **11**, 1422-1425.
4. J. Chakraborty, H. Mayer-Figge, W. S. Sheldrick and P. Banerjee, *Polyhedron*, 2006, **25**, 3138-3144.
5. Z. Derikvand, M. M. Olmstead, A. Shokrollahi and F. Zarghampour, *synth. react. inorg. met.-org. nano-metal chem.*, 2015, **45**, 104-111.
6. H. Aghabozorg, M. Ghadermazi, F. Manteghi and B. Nakhjavan, *Z. Anorg. Allg. Chem.*, 2006, **632**, 2058-2064.
7. D. Griffith, A. Chopra, H. Muller-Bunz and C. J. Marmion, *Dalton Trans.*, 2008, 6933-6939.
8. F. Borbone, U. Caruso, R. Centore, A. De Maria, A. Fort, M. Fusco, B. Panunzi, A. Roviello and A. Tuzi, *Eur. J. Inorg. Chem.*, 2004, **2004**, 2467-2476.
9. F. Cariati, U. Caruso, R. Centore, W. Marcolli, A. D. Maria, B. Panunzi, A. Roviello and A. Tuzi, *Inorg. Chem.*, 2002, **41**, 6597-6603.
10. K. Ha, *Acta Crysta. Sec. E.*, 2012, **68**, m454.
11. M. Bagherzadeh, N.-a. Mousavi, M. Zare, S. Jamali, A. Ellern and L. K. Woo, *Inorg. Chim. Acta*, 2016, **451**, 227-232.
12. Y. Boutadla, D. L. Davies, S. A. Macgregor and A. I. Poblador-Bahamonde, *Dalton Trans.*, 2009, 5820-5831.
13. D. Wang, P. Y. Zavalij and A. N. Vedernikov, *Organometallics*, 2013, **32**, 4882-4891.
14. J. Zhang, E. Khaskin, N. P. Anderson, P. Y. Zavalij and A. N. Vedernikov, *Chem. Comm.*, 2008, 3625-3627.
15. W.-H. Wang, J. T. Muckerman, E. Fujita and Y. Himeda, *New J. Chem.*, 2013, **37**, 1860-1866.
16. C. S. Yeung and V. M. Dong, *Chem. Rev.*, 2011, **111**, 1215-1292.
17. C.-L. Sun, B.-J. Li and Z.-J. Shi, *Chem. Rev.*, 2011, **111**, 1293-1314.
18. J. Wencel-Delord, T. Droge, F. Liu and F. Glorius, *Chem. Soc. Rev.*, 2011, **40**, 4740-4761.
19. T. C. Boorman and I. Larrosa, *Chem. Soc. Rev.*, 2011, **40**, 1910-1925.
20. T. W. Lyons and M. S. Sanford, *Chem. Rev.*, 2010, **110**, 1147-1169.
21. E. I. Negishi, *Angew. Chem., Int. Ed.*, 2011, **50**, 6738-6764.
22. A. Suzuki, *Angew. Chem., Int. Ed.*, 2011, **50**, 6722-6737.
23. *Cooperating Ligands in Catalysis*, Wiley-VCH Verlag GmbH & Co. KGaA, 2015.
24. N. Kuhl, M. N. Hopkinson, J. Wencel-Delord and F. Glorius, *Angew. Chem., Int. Ed.*, 2012, **51**, 10236-10254.
25. S. R. Neufeldt and M. S. Sanford, *Acc. Chem. Res.*, 2012, **45**, 936-946.
26. K. M. Engle, T.-S. Mei, M. Wasa and J.-Q. Yu, *Acc. Chem. Res.*, 2012, **45**, 788-802.
27. P. Sehnal, R. J. K. Taylor and I. J. S. Fairlamb, *Chem. Rev.*, 2010, **110**, 824-889.
28. R. Giri, J. Liang, J.-G. Lei, J.-J. Li, D.-H. Wang, X. Chen, I. C. Naggar, C. Guo, B. M. Foxman and J.-Q. Yu, *Angew. Chem., Int. Ed.*, 2005, **44**, 7420-7424.
29. C. J. Vickers, T.-S. Mei and J.-Q. Yu, *Org. Lett.*, 2010, **12**, 2511-2513.
30. A. Vignesh, N. S. P. Bhuvanesh and N. Dharmaraj, *J. Org. Chem.*, 2016, **82**, 887–892.
31. V. Arumugam, W. Kaminsky and D. Nallasamy, *RSC Advances*, 2015, **5**, 77948-77957.
32. F. Juliá-Hernández, A. Arcas, D. Bautista and J. Vicente, *Organometallics*, 2012, **31**, 3736-3744.
33. F. Juliá-Hernández, A. Arcas and J. Vicente, *Tetrahedron Lett.*, 2014, **55**, 1141-1144.
34. O. Adeyi, W. B. Cross, G. Forrest, L. Godfrey, E. G. Hope, A. McLeod, A. Singh, K. Singh, G. A. Solan, Y. Wang and L. A. Wright, *Dalton Trans.*, 2013, **42**, 7710-7723.
35. H.-K. Yip, T.-F. Lai and C.-M. Che, *J. Chem. Soc., Dalton Trans.*, 1991, 1639-1641.

36. B.-H. Xia, C.-M. Che and Z.-Y. Zhou, *Chem. Eur. J.*, 2003, **9**, 3055-3064.
37. Q.-J. Pan, H.-X. Zhang, X. Zhou, H.-G. Fu and H.-T. Yu, *J. Phys. Chem. A*, 2007, **111**, 287-294.
38. S. Clément, S. M. Aly, D. Bellows, D. Fortin, C. Strohmann, L. Guyard, A. S. Abd-El-Aziz, M. Knorr and P. D. Harvey, *Inorg. Chem.*, 2009, **48**, 4118-4133.
39. S. Iwatsuki, T. Itou, H. Ito, H. Mori, K. Uemura, Y. Yokomori, K. Ishihara and K. Matsumoto, *Dalton Trans.*, 2006, 1497-1504.
40. V. G. Zaitsev, D. Shabashov and O. Daugulis, *J. Am. Chem. Soc.*, 2005, **127**, 13154-13155.
41. J. E. Bercaw, A. C. Durrell, H. B. Gray, J. C. Green, N. Hazari, J. A. Labinger and J. R. Winkler, *Inorg. Chem.*, 2010, **49**, 1801-1810.
42. *The Chemistry of Pincer Compounds*, Elsevier Science, Amsterdam, 2007.
43. N. Selander and K. J. Szabó, *Chem. Rev.*, 2011, **111**, 2048-2076.
44. A. Klein, S. Elmas and K. Butsch, *Eur. J. Inorg. Chem.*, 2009, **2009**, 2271-2281.
45. F. Baker and E. C. C. Baly, *Journal of the Chemical Society, Transactions*, 1907, **91**, 1122-1132.
46. P. Beak, F. S. Fry, J. Lee and F. Steele, *J. Am. Chem. Soc.*, 1976, **98**, 171-179.
47. H. W. Yang and B. M. Craven, *Acta Crystallogr. Sect. C*, 1998, **54**, 912-920.
48. K. Modig, B. G. Pfrommer and B. Halle, *Phys. Rev. Lett.*, 2003, **90**, 075502.
49. L.-M. Xu, B.-J. Li, Z. Yang and Z.-J. Shi, *Chem. Soc. Rev.*, 2010, **39**, 712-733.
50. F. Juliá-Hernández, A. Arcas and J. Vicente, *Chem. Eur. J.*, 2012, **18**, 7780-7786.

Chapter 4

Cyclopalladated 6-phenyl-2-pyridone complexes: synthesis, reactivity and C-H halogenation

Chapter 4
Cyclopalladated 6-phenyl-2-pyridone complexes: synthesis, reactivity and C-H halogenation

4.1 Introduction

4.1.1 Importance of CH activation

CH activation has been an area of intense research over the last two decades due, in part, to the broad range of applications and huge availability of hydrocarbon feedstocks.[1-4] With regard to applications, it can present a key step in synthesis such as in coupling reactions in which more complex molecules can be readily generated. In addition, CH activation is a vital step in catalysis and functionalisation of aryl motifs.[5-7]

Bi-aryl compounds represent an important class of organic compounds as they form part of the molecular structure of many pharmaceuticals and agro-chemicals compounds.[8] Therefore, efficient aryl-aryl coupling strategies based on organometallic chemistry have been given high priority. Traditionally coupling reactions were developed using stoichiometric amounts of transition metal reagents. Later highly efficient coupling reactions were developed that typically make use of an aryl halide and an aryl-organometallic compound in the presence of a suitable catalyst (Scheme 4.1).[9]

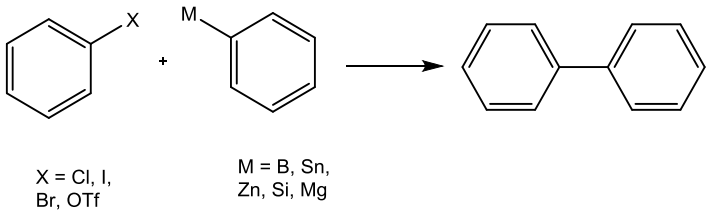

Scheme 4.1. Synthesis of biphenyl using various coupling precursors

A greener approach is proposed by considering the CH unit as a functional group rather than functionalising it with other active groups (e.g., halides or triflate). Therefore, CH activation and subsequent functionalisation under moderate conditions represents a desirable process.

4.1.2 Types of CH activation

There are several CH activations mechanisms known and these have been thoroughly studied. The main mechanisms which are well understood are 1) oxidative addition, 2) sigma bond metathesis, 3) 1,2-addition, 4) electrophilic CH activation, 5) Ambiphilic Metal Ligand Activation (AMLA) or Concerted Metalation-Deprotonation (CMD).

4.1.2.1 Oxidative addition

As the name oxidative addition suggests the metal centre ends up being oxidised by +2 units.[10] Electron rich metal atoms with vacant coordination sites undergo oxidative addition resulting in metal hydride and metal carbon bonds (Scheme 4.2).

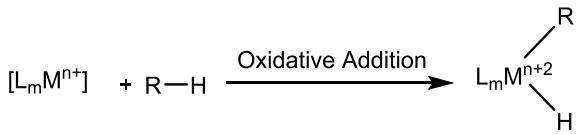

Scheme 4.2. Oxidative addition of alkyl/aryl-hydrogen bond to the metal atom.[3]

The oxidation addition of aryl-hydrogen and alkyl-hydrogen bonds to $Ru(dmpe)_2$ was reported first in 1965 by Chatt and Davison (Scheme 4.3).[11]

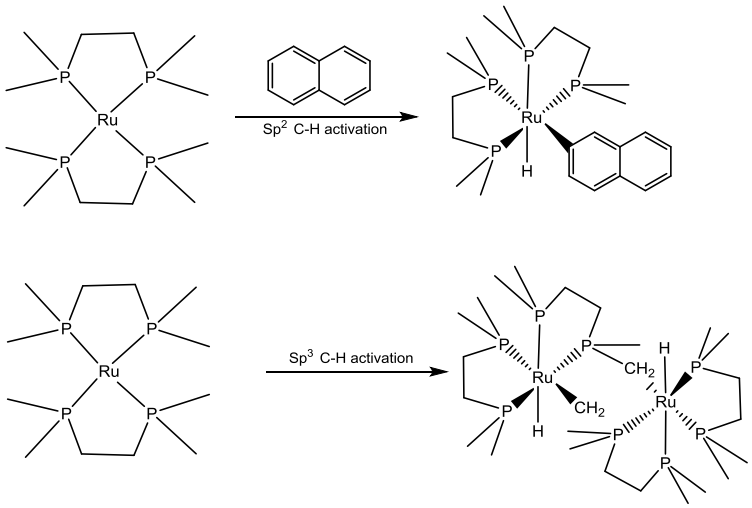

Scheme 4.3. Oxidative addition of sp^2 and sp^3 C-H bonds on a metal centre.[11]

4.1.2.2 Sigma bond metathesis (SBM)

In the Sigma bond metathesis CH activation mechanism two sigma bonds are broken and two new sigma bonds are formed. The reaction occurs via a four membered transition state (Scheme 4.4) and the metal's oxidation state remains unchanged after the reaction. The early transition metals with no *d* electrons, that are unable to undergo oxidative addition, usually proceed via a sigma bond metathesis.[12-14]

Scheme 4.4. Sigma bond metathesis (SBM). [3]

Watson reported the first example of sigma bond metathesis when a methyl ligand in $(Cp^*)_2LuMe$ was replaced by $^{13}CH_3$ using ^{13}C-labelled CH_4 (Scheme 4.5).[15]

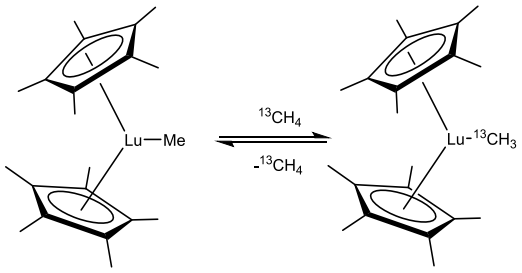

Scheme 4.5. Sigma bond metathesis of $(Cp^*)_2LuMe$ with $^{13}CH_4$.[15]

4.1.2.3 1,2-Addition

In the 1,2-addition mechanism the C-H bond is added to a metal-ligand in similar manner to that of sigma bond metathesis but involves π–electrons instead of σ-electrons (Scheme 4.6).

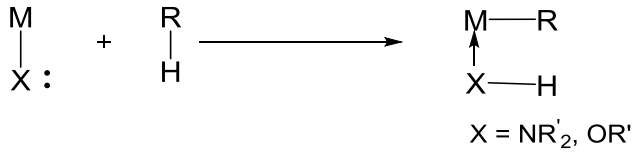

Scheme 4.6. CH activation via a 1,2-addition mechanism

Periana *et al.* in 2005 reported CH activation of benzene via 1,2-addition using the iridium acac complex **A** shown in Scheme 4.7. The reaction involved dissociation of a methanol molecule and coordination of benzene ring to the complex. In the CH activation step a four membered transition state is formed with the benzene-CH partially bound to the OMe ligand. The resulting methanol ligand then dissociates after abstracting a benzene proton and neutral donor pyridine coordinates at the vacant site to give **B**.[16]

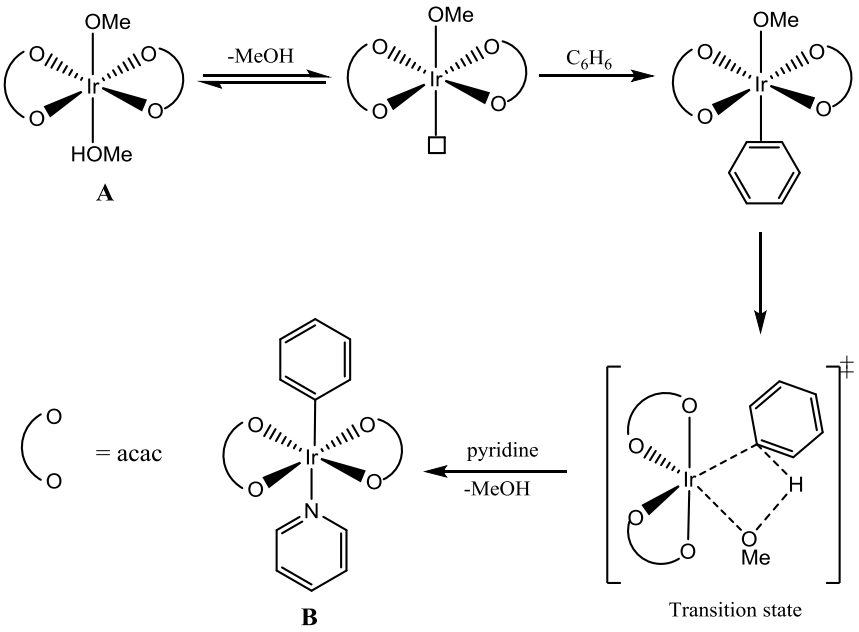

Scheme 4.7. 1,2-Addition in CH-activation of benzene.[16]

4.1.2.4 Electrophilic CH activation

In electrophilic CH activation, the metal atom is electrophilic and reacts with an electron rich carbon atom followed by the removal of an H atom (Scheme 4.8).

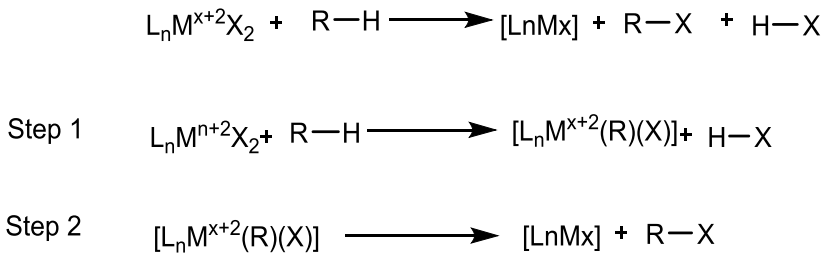

Scheme 4.8. Electrophilic CH activation mechanism[3]

Shilov first reported the exchange of a methane hydrogen by D/H in D_2O in a solution of K_2PtCl_4.[17] The following research led to the oxidation of methane to methanol also known as Shilov chemistry (Scheme 4.9).[18]

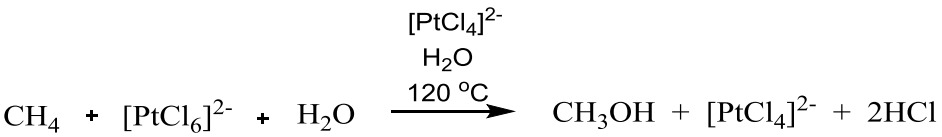

Scheme 4.9. Shilov's methane electrophilic oxidation to form methanol[18]

The requirement for a stoichiometric amount of an expensive Pt(IV) oxidant to allow the reaction to take place makes this approach less commercially viable.

4.1.2.5 Ambiphilic Metal Ligand Activation (AMLA/CMD)

The term Ambiphilic Metal Ligand Activation (AMLA) was used first coined by Davies *et al.* in 2006, while a similar process referred to as Concerted Metalation Deprotonation (CMD) was introduced by Fagnou in the same year.[19, 20] AMLA or CMD is a CH activation mechanism in which an electrophilic metal centre and an internal base cooperate in a concerted fashion to form 4- or 6-membered transition states (Fig. 4.1).[19, 21] In the case of the 6-membered transition state, the acetate bound molecule can act as the internal base for the removal of a C-H proton.

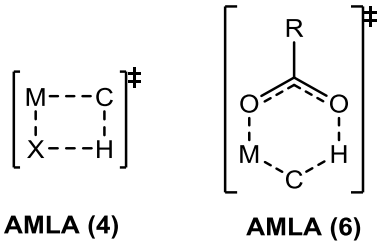

Figure 4.1. Transition states involved in AMLA/CMD CH activation

Originally, the mechanism of CH activation of N,N-dimethylbenzylamine (DMBA) by palladium(II) acetate were investigated by Ryabov (Fig. 4.2). It was found that the rate limiting step involved a six-membered transition state with the pendant oxygen atom of the acetate able to abstract a H atom from the aryl C-H bond.[22, 23]

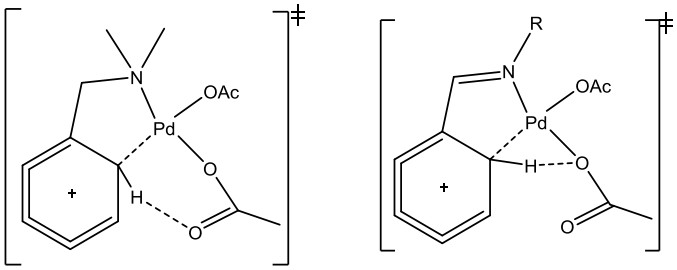

Figure 4.2. AMLA/CMD type interactions

4.1.3 Reactivity of phenyl-pyridines towards $Pd(OAc)_2$ and use in CH-halogenation (Cl vs Br vs F)

The 2-arylpyridine motif is an important building block in the synthesis of complex valuable molecules and the first step usually involves the halogenation of the aryl group (Scheme 4.10). Once halogenated they can be easily transformed to the desired compounds by making use of techniques such as coupling reactions, using Grignard reagents, nucleophilic substitutions or organolithiations.[24-30] Aryl halogen compounds are also highly sought after in biologically active compounds due to the properties they impart on a molecule.[31]

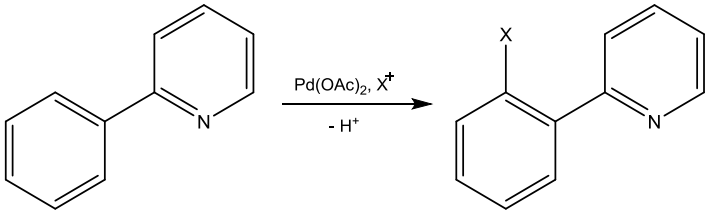

Scheme 4.10. Palladium catalysed halogenation of 2-phenylpyridine (X = halogen)

Due to many uses of halogenated aryls, considerable research has focused on using 2-phenylpyridine as a test material for exploring potential CH activation and halogenation strategies (Scheme 4.11).[32-34] The proposed mechanism involves the abstraction of a proton by an internal base followed by electrophilic addition of halogen forcing palladium into a higher oxidation state. The resulting octahedral palladium(IV) undergoes reductive elimination to form the halogenated product.[34] Transition metal catalysed halogenation is highly desirable due to many advantages such as less harsh conditions and more functional group tolerance.[32, 35, 36]

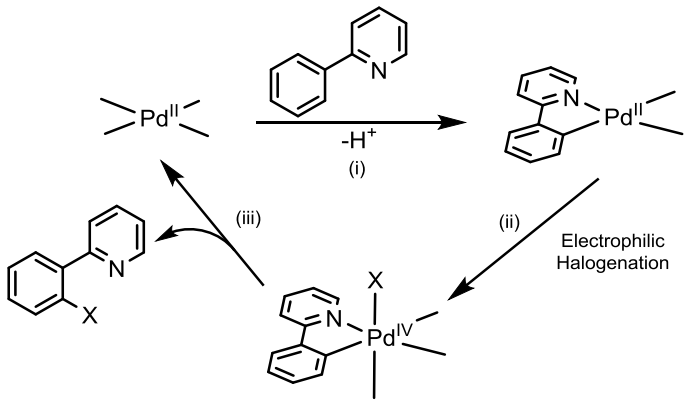

Scheme 4.11. Proposed mechanism of electrophilic halogenation of phenylpyridine.[35]

Using palladium(II) acetate as catalyst and an oxidising halogenating source such as NBS or NCS, many examples of *ortho* halogenation of phenylpyridines have been reported.[32, 35, 37] Most of them have proposed a Pd(II)/Pd(IV) catalytic cycle involved in the transformation.

Late stage aryl fluorination is highly sought after due to the use of such fluorinated compounds in pharmaceuticals and agrochemicals.[38, 39] However it is relatively scarce due to its challenging nature. Fluorination of phenylpyridine using palladium(II) acetate as catalyst and selectfluor as oxidising agent has not so far been reported. However using N-fluorobenzenesulfonimide (NFSI) as an electrophilic fluorine source, ligand directed fluorination using palladium acetate catalyst has been reported leading to ortho-fluorination of an aryl group (Scheme 4.12).[40]

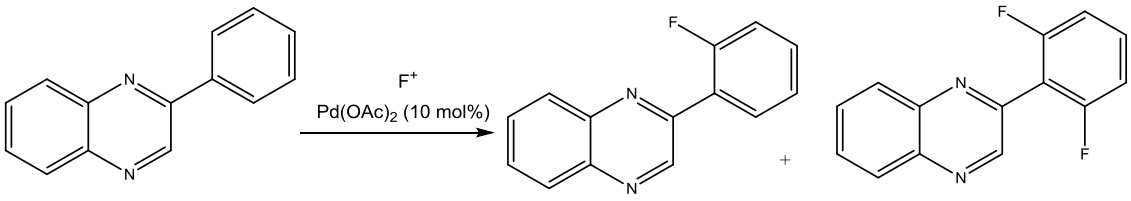

Scheme 4.12. Palladium(II) acetate catalysed fluorination using NFSI as fluorinating reagent

4.1.4 2-Pyridones and their reactivity with platinum group metals

2-Pyridones are important motifs in numerous biological systems, natural products dyes and as fluorescent materials due to their broad range of properties.[41-43] The characteristic structure of 2-pyridones is ideal to exhibit features such as hydrogen bonding, tautomerism, acid-base reactions (to impart pH switchibility) and water solubility (Fig. 4.3).[44] Indeed 2-pyridone can also exist in the 2-pyridinol tautomeric form and various factors have been shown to influence which form is preferred.

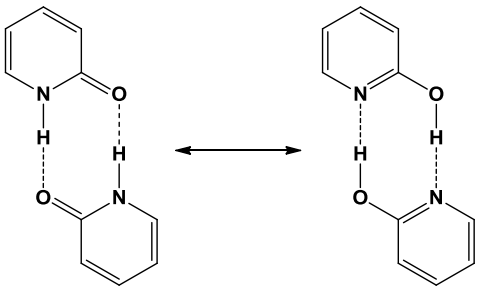

Figure 4.3. Tautomerism and hydrogen-bonded assembly in 2-pyridones

Substituted 2-pyridones have therapeutic value but have been less studied due, in part, to the difficulty in accessing them chemically.[45] In particular, aryl-substituted pyridones have found use in many therapeutically challenging fields such as anticancer agents. For example, 1-methyl-7-phenyl-1,2,3,4-tetrahydro-1,6-naphthyridin-5-one has shown promising results in the inhibition of tankyrases (Fig. 4.4a).[46] Aryl-substituted pyridones have also shown antiviral activity against HIV (Fig. 4.4b) and are likely to be further investigated in other challenging therapeutic applications.[46]

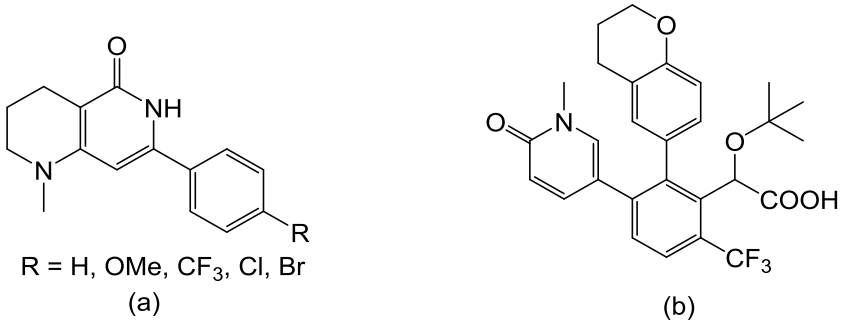

Figure 4.4. (a) 1-Methyl-7-phenyl-1,2,3,4-tetrahydro-1,6-naphthyridin- 5-one and (b) antiviral agent against HIV[46]

Surprisingly, the 6-phenyl-2-pyridone (H_2**L8**) member of the 2-pyridone family has been the subject of relatively few reports associated with C-H activation of the aryl group (Fig. 4.5). It is plausible that the presence of the oxygen group at the 2-position may have been considered as detrimental to the coordination of the N-directing group during the metal-mediated CH transformation. Indeed, previous findings for the reactions of first row transition metals with 2-pyridones have seen the formation of products involving metal-oxygen bond formation.[47] Nevertheless there have been some reports that will be highlighted in the next section.

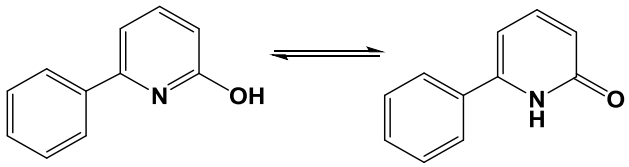

Figure 4.5. Tautomerism in 6-phenyl-2-pyridone (H_2**L8**)

Complexation reactions of simple 2-pyridones with platinum group metals have been thoroughly studied.[47-49] Many examples are known in which deprotonation occurs and the resulting 2-pyridonate ligand can bridge across metal centres or act as a chelating ligand via the nitrogen and the oxygen donor atoms (Fig. 4.6(a)-(c)).[50] For example, Flood *et al*.

have reported a N,O-chelated pyridonate osmium complex that under suitable conditions can undergo mer-fac isomerization of the PMe_3 ligands (Fig. 4.6(b)) whilst maintaining the N,O-chelation of the pyridonate (Figure 4.6).[51]

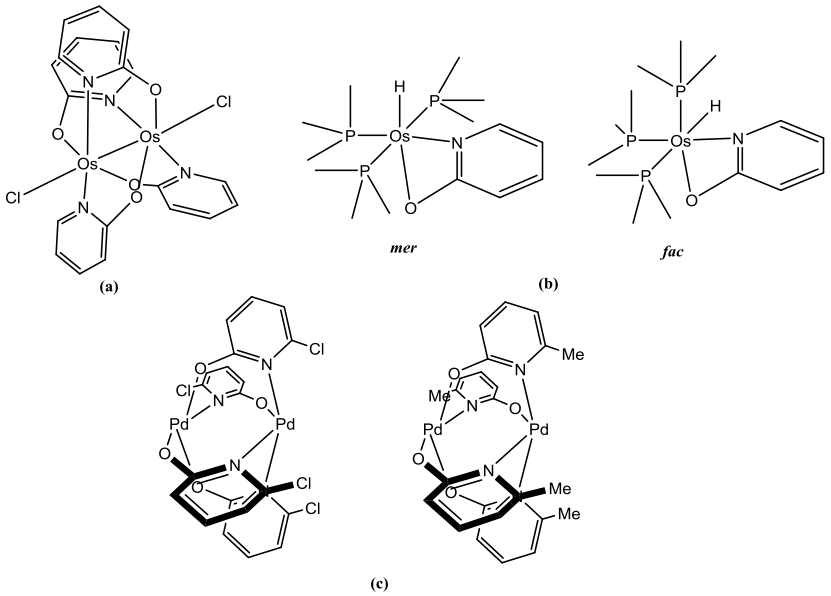

Figure 4.6. Monoanionic 2-pyridonate acting (a) as a NO-bridging ligand with osmium.[50] (b) as chelating ligand with osmium and [51] (c) as a NO-bridging ligand with palladium.[52]

On the other hand, complexation of 2-pyridone does not necessarily result in deprotonation. For example, a Cp*Ir (Fig. 4.7) bearing a neutral 2-hydroxypyridine can be readily synthesised and moreover it is an excellent (pre-)catalyst for the oxidant-free oxidation of alcohols. It is considered that the hydroxyl proton on the pyridine ligand helps the generation of the species that is thought to contain a chelated 2-pyridonate.[53]

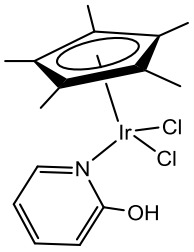

Figure 4.7. Cp^*IrCl_2(2-hydroxypyridine) pre-catalyst used in the dehydrogenation of alcohols

By contrast, 6-phenyl-2-pyridone (H_2**L8**) has received much less attention with regard to its reactivity towards platinum group metals.[52, 54, 55] Fujita *et al.* have demonstrated that

H_2**L8** undergoes C-H activation on reaction with an iridium(III) half-sandwich complex (Fig. 4.8(a)). Indeed the cyclometallated iridium species, containing an intact 2-pyridinol unit, is an efficient catalyst for the oxidation of primary and secondary alcohols.[55] By comparison, it was reported that the phenyl-pyridine iridium analogue showed far less activity for the same transformation (Fig. 4.8(b)).[53]

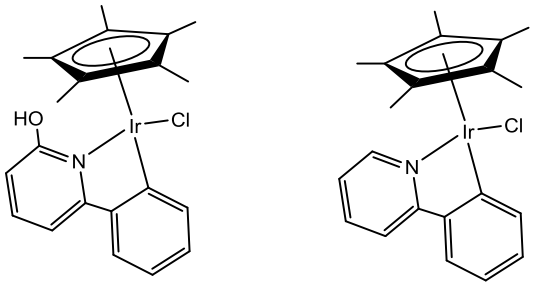

Figure 4.8. (a) 6-Phenyl-2-pyridone-based [CpIrCl(6-(C_6H_4)-2-OH-C_5H_3N)] and its (b) 2-phenylpyridine analogue [CpIrCl(6-(C_6H_4)-C_5H_4N)].

4.2 Aims and objectives

Given the rarity of reactions of platinum groups metals with 6-phenyl-2-pyridone (H_2**L8** in Fig. 4.5) and the apparent absence of reactivity with palladium(II), the first aim in this chapter is to develop its palladium(II) chemistry with a view to promoting CH activation. In particular the reactivity of H_2**L8** towards palladium(II) acetate and palladium(II) chloride will be investigated on a stoichiometric level with different relative ratios of pro-ligand to palladium(II). All the resultant complexes will be fully characterised using spectroscopic ($^1H/^{13}C$ NMR, IR), spectrometric (ESIMS, TOFMS) and single crystal X-ray diffraction techniques.

As a second aim of the chapter, the controlled halogenation (Br, Cl or F) of H_2**L8** will be attempted with or without a palladium catalyst using reagents such as NBS, NCS, selectfluor as oxidants. In addition, selected ONN and ONO palladium(II) pincer complexes prepared in chapter 2 and 3 will be explored for their reactivity towards H_2**L8**. Furthermore, the selected palladium(II) pincer complexes will also be evaluated in their own right as catalysts in the halogenations of H_2**L8** and these results compared with those obtained using palladium(II) acetate.

4.3 Results and discussion

4.3.1 Synthesis of 6-phenyl-2-pyridone (H_2L8)

We have found the reported syntheses of 6-phenyl-2-pyridone (H_2**L8**), unreliable[56-59] and instead have used a three step synthesis from 2,6-dibromopyridine that can deliver gram quantities of the target compound (Scheme 4.12).

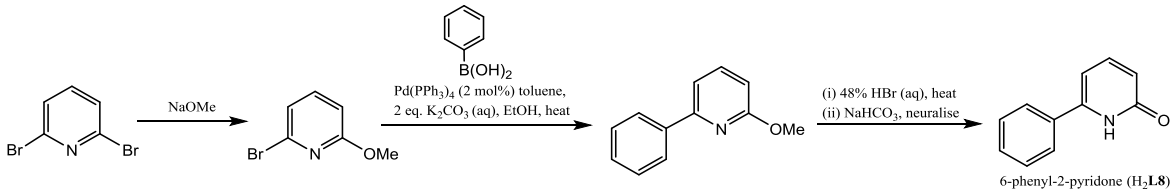

Scheme 4.12. Three step synthesis of 6-phenyl-2-pyridone (H_2**L8**)

The spectroscopic properties of 6-phenyl-2-pyridone agree with those previously reported.[60] In addition, its single crystal X-ray structure has been determined.

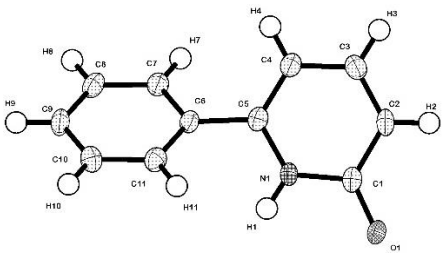

Figure 4.9a Molecular structure of H_2**L8** with full atom numbering

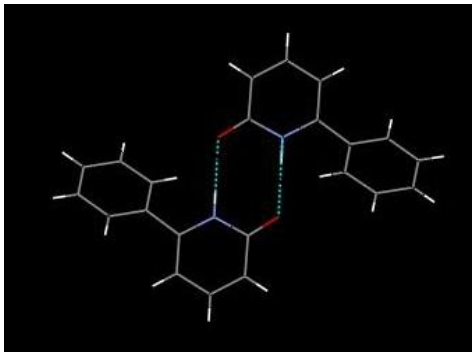

Figure 4.9b Hydrogen bonding between two neighbouring molecules

Table 4.1. Selected bond distances (Å) and angles (°) for H_2**L8**

Bond length	
O(1)-C(1)	1.254(2)
N(1)-C(5)	1.371(2)
N(1)-C(1)	1.378(2)
C(5)-C(6)	1.483(2)
C(2)-C(3)	1.360(2)
Bond angles	
O(1)-C(1)-N(1)	119.96(15)
C(5)-N(1)-C(1)	124.52(14)
N(1)-C(5)-C(6)	117.19(14)
C(5)-C(4)-C(3)	119.09(15)
C(7)-C(6)-C(5)	120.21(14)

The structure of H_2**L8** consists of a 2-pyridone heterocycle with a phenyl group positioned at the 6-position (Fig. 4.9a). Support for the presence of the pyridone form is given by

O(1)-C(1) bond distance of 1.254(2) Å which is consistent with double bond character. The torsion angle between the pyridone and phenyl ring is 43.5(2)^{o} which is similar to that seen in phenyl-pyridine. As expected the X-ray structure reveals pairs of molecules linked together through hydrogen bonding interactions with the pyridone NH as the donor and the carbonyl O as acceptor (Fig. 4.9b).

In the ^{1}H NMR spectrum (recorded in $CDCl_3$ at room temperature) of H_2**L8** the NH peak is seen as a broad resonance at 10.35 ppm while the C=O carbon is seen at 164.0 ppm in the ^{13}C NMR spectrum. In the IR spectrum the υ(C=O) band is visible at 1739 cm^{-1} supportive of the presence of the pyridone tautomer at room temperature.

4.3.2 Stoichiometric reactions of H_2L8 with palladium(II) acetate

Reaction of H_2**L8** with one molar equivalent of palladium(II) acetate at room temperature gave the acetate-bridged dimer [Pd(κ^2-H**L8**)(μ-OAc)]$_2$ (**14**) in good yield (Scheme 4.13). Complex **14** has been characterised spectroscopically and has been the subject of a single crystal X-ray diffraction study.

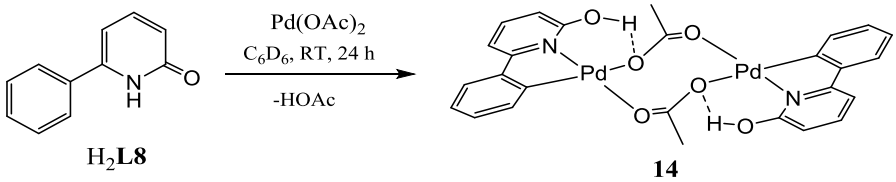

Scheme 4.13. Synthesis of **14**

Crystals of **14** suitable for the X-ray diffraction study were grown by slow diffusion of petroleum ether into a solution of the complex in dichloromethane. A view of the structure is given in Fig. 4.10; selected bond distances and angles are collected in Table 4.2. The structure of **14** consists of two palladium centres that are linked together by two acetate ligands with each metal centre bound by a N,C-chelating phenyl-pyridinol. The geometry at each palladium is distorted square planar. The pyridinol form in **14** is supported by the length of the C(16)-O(6) bond of 1.297(7) Å, which is longer than the corresponding bond distance found in free pyridone H_2**L8** (1.254(2) Å). In addition, each pyridinol hydrogen atom is involved in a hydrogen bonding interaction with an acetate oxygen atom. The torsion angle between the pyridine and phenyl ring is significantly reduced (1.9(8)^{o}) as compared to 43.5(2)^{o} in H_2**L8** so as to facilitate NC-chelate formation with palladium.

The C(26)-Pd(2)-N(2) bite angle formed by the five-membered NC-chelate ring is 81.27(19)^{o} while the O(5)-Pd(2)-O(3) angle is 86.91(14)^{o}, highlighting the distortion from square planar geometry at palladium(II). Similar structural features apparent in **14** have been observed in acetate-bridged phenyl-pyridine-containing analogues.[61]

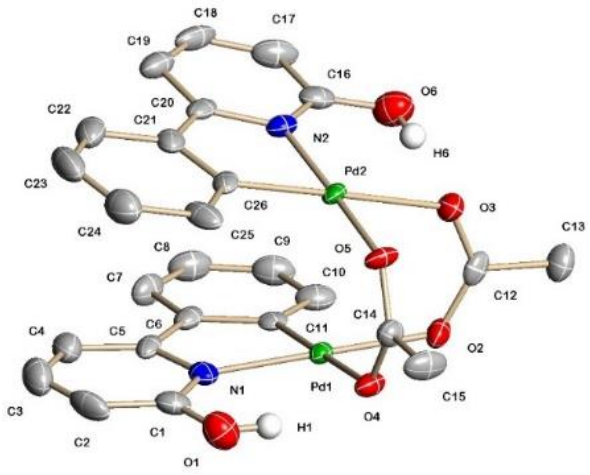

Figure 4.10. The molecular structure of **14** with full atom numbering; H atoms have been omitted for clarity.

Table 4.2. Selected bond distances (Å) and angles (^{o}) for **14**

Bond length	
Pd(2)-C(26)	1.980(5)
Pd(2)-N(2)	2.034(4)
Pd(2)-O(5)	2.069(3)
C(16)-N(2)	1.341(7)
O(6)-C(16)	1.297(7)
Bond angles	
C(26)-Pd(2)-N(2)	81.27(19)
C(26)-Pd(2)-O(5)	94.66(18)
N(2)-Pd(2)-O(5)	175.34(14)
O(26)-Pd(2)-O(3)	177.69(17)
O(2)-C(12)-O(3)	126.2(5)

The ^{1}H NMR spectrum of **14** shows a singlet at 2.27 ppm for the acetate methyl groups confirming the symmetry in the palladium dimer. Hydrogen bonding interactions were supported by downfield shift of the OH signal (9.63 ppm). Furthermore, the CH-activated carbon is supported by a downfield ^{13}C NMR signal at 184.4 ppm. The palladium-palladium distance in **14** of 2.877 Å, is notably longer than in the acetate-bridged dipalladium phenylpyridine complex (2.555 Å),[36] but is significantly smaller than the sum of the van der Waals radii of palladium (3.26 Å).

AMLA/CMD[19] is a well-established mechanism for CH activation and operates via metal and ligand (internal base) cooperation and is presumed to be occurring in this case (Fig. 4.11). Further hydrogen bonding between the pyridinol OH and the palladium bound acetate oxygen atom supports the possibility of agostic interactions.

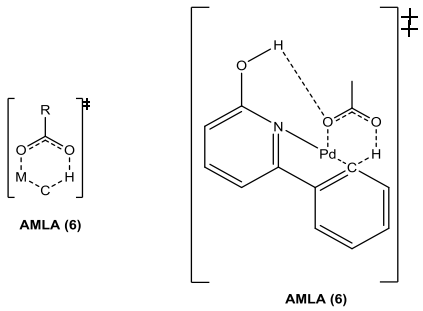

Figure 4.11. Possible AMLA-type transition state for the CH activation of H_2**L8** by $Pd(OAc)_2$

The reaction of two equivalents of H_2**L8** in benzene at room temperature with palladium(II) acetate gave [Pd(μ-H**L8**)(κ^2-H**L8**)]$_2$ (**15**) in high yield (Scheme 4.14). Complex **15** has been characterised spectroscopically and has been the subject of a single crystal X-ray diffraction study.

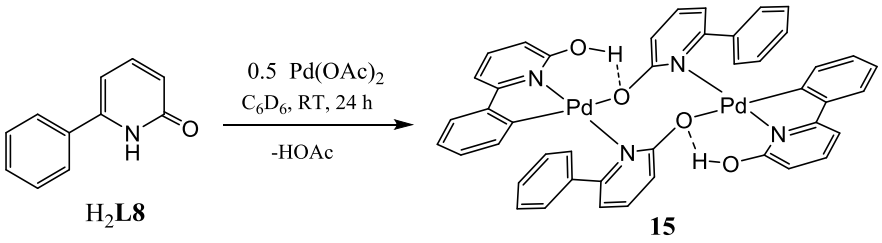

Scheme 4.14. Synthesis of **15**

Crystals of **15** suitable for the X-ray determination were grown by slow diffusion of hexane into a dichloromethane solution of the complex. A view of the structure is shown in Fig. 4.12; selected lengths and angles are compiled in Table 4.3. The structure consists of a square planar palladium dimer bridged by two molecules of 6-phenyl-2-pyridonate. The bridging pyridonates are bound to one palladium by anionic oxygen and to the other by neutral pyridine nitrogen dative bond (Fig 4.3). The CH-activated phenylpyridinols are bound in the pyridinol form and are involved in hydrogen bonding with the oxygen atom of the bridging pyridonate. The torsion angle between the palladium pyridinol plane and bridging phenylpyridonate is 82.7(6)^o [C(11)-Pd(1)-N(4)-C(38)]. The palladium-

palladium distance is 2.840 Å and is slightly smaller than observed in the acetate-bridged dimer **14** (2.877 Å).

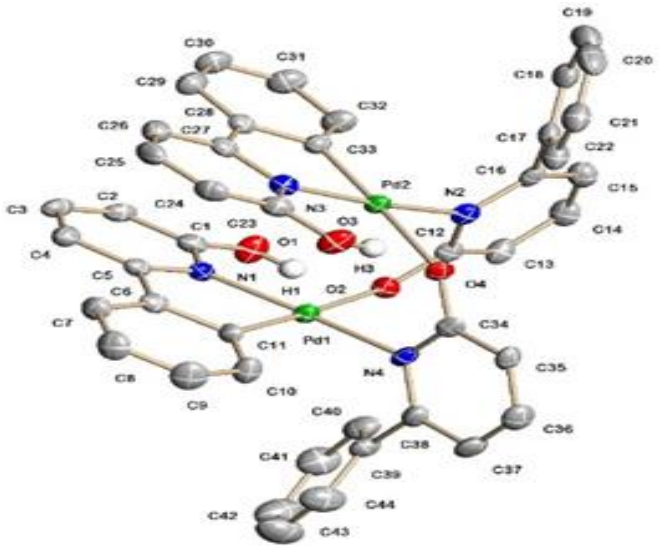

Figure 4.12. Molecular structure of **15** with full atom numbering; H atoms have been omitted for clarity.

Table 4.3. Selected bond distances (Å) and angles (°) for **15**

Bond length	
Pd(1)-C(11)	1.967(7)
Pd(1)-N(1)	2.041(5)
O(3)-C(23)	1.321(8)
O(4)-C(34)	1.298(8)
Pd(1)-O(2)	2.159(5)
Bond angles	
C(11)-Pd(1)-N(4)	92.4(3)
C(11)-Pd(1)-N(1)	82.1(3)
N(4)-Pd(1)-N(1)	173.9(2)
C(11)-Pd(1)-O(2)	177.69(17)
N(4)-Pd(1)-O(2)	90.5(2)

The downfield shift of the pyridinol OH (12.35 ppm) in the ^{1}H NMR spectrum of **15** supports hydrogen bonding between the pyridinol proton and the oxygen bound to the palladium centre. Complex **15** shows a protonated peak in its mass spectrum (ASAP) and no carbonyl (C=O) peak in its IR spectrum as compared to a υ(C=O) peak at 1739 for free H_2**L8**.

Interestingly, on standing acetate-bridged **14** in C_6D_6 solution for several days saw the gradual formation of a new complex [Pd(μ:κ^2-**L8**)]$_4$ (**16**). This reaction could be accelerated by heating the benzene solution resulting in the elimination of acetic acid

(Scheme 4.15). Complex **16** has been characterised spectroscopically and has been the subject of a single crystal X-ray diffraction study.

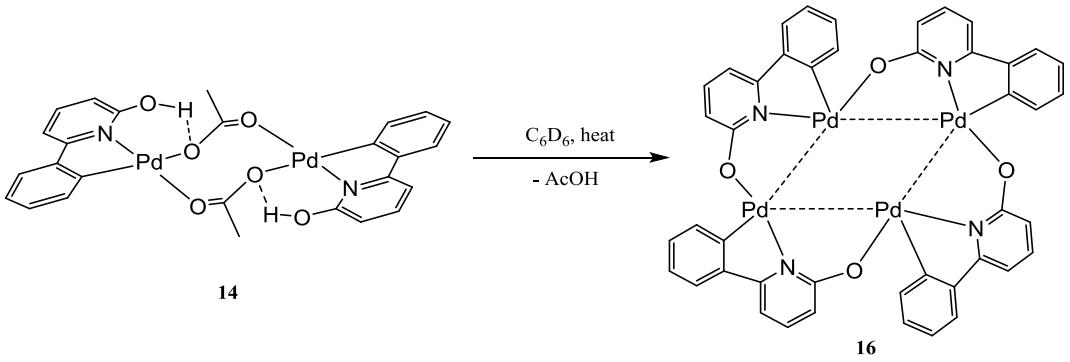

Scheme 4.15. Synthesis of **16**

Crystals of **16** suitable for the X-ray determination were grown by slow evaporation of a C_6D_6 solution of the complex. A view of the structure is shown in Fig. 4.13; selected bond lengths and angles are compiled in Table 4.4. Complex **16** consists of four palladium centres with four CH activated 6-phenyl-2-pyridonates that bridge via a pyridonate dative nitrogen and an oxygen donor atom. All the phenylpyridonates are ortho-CH-activated and the palladium-palladium distance of 2.6602(12) Å is shorter than their van Waals radii (3.26 Å) and also shorter that the corresponding distance found in previously reported dimers.[62-67] One pair of 6-phenyl-2-pyridonates are almost orthogonal to the other pair [C(1)-C(6)-C(7)-N(1) 107.8(2)^o]. In addition each C-coordinated phenyl ring is close to co-planar [C(1)-C(6)-C(7)-N(1) 1.6(7)^o] with respect to the pyridonate ring so as to facilitate efficient coordination with the square planar palladium. The Pd-C bond distance is shorter ((1.959(5) Å) than that of an average Pd-C single bond of 2.10 Å.[68]

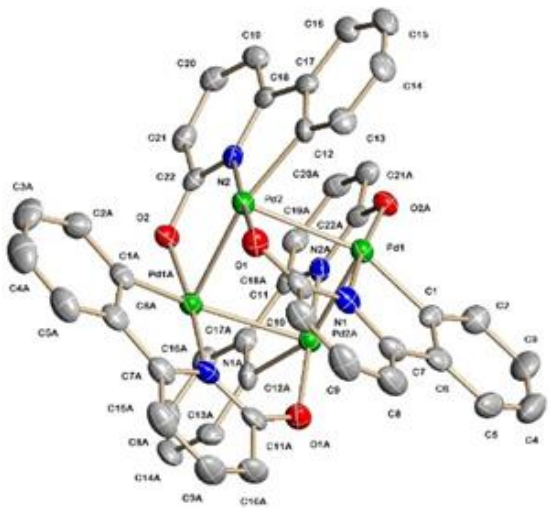

Figure 4.13. Molecular structure of **16** with full atom numbering; H atoms have been omitted for clarity.

Table 4.4. Selected bond distances (Å) and angles (°) for **16**

Bond lengths	
Pd(1)-C(1)	1.959(5)
Pd(1)-N(1)	2.017(4)
Pd(2)-O(1)	2.010(4)
O(1)-C(11)	1.285(6)
Pd(1)···Pd(2)	2.6602(12)
Bond angles	
C(1)-Pd(1)-O(2)#1	93.3(2)
C(1)-Pd(1)-N(1)	82.3(2)
N(1)-Pd(1)-Pd(2)	83.23(13)
Pd(2)-Pd(1)-Pd(2)#1	90.00(4)
O(2)#1-Pd(1)-N(1)	174.72(16)

The ^{1}H NMR spectrum of **16** shows no evidence for a downfield shifted NH/OH peak which is in agreement with deprotonation of the pyridone. In addition, the ^{13}C NMR spectrum confirms the symmetry in the tetrameric structure with a single C-Pd resonance at 171.5 ppm.

There are only a few reported square-based palladium(II) tetramers in the literature. The one which most closely resembles **16** is $[Pd_2(\mu\text{-}O_2CCH_3)_2(\mu\text{-}CO)]_2$ (Fig**.** 4.14). The Pd···Pd distance in **16** (2.6602(12) Å) is comparable to that found in $[Pd_2(\mu\text{-}O_2CCH_3)_2(\mu\text{-}CO)]_2$ (2.663 Å).[69]

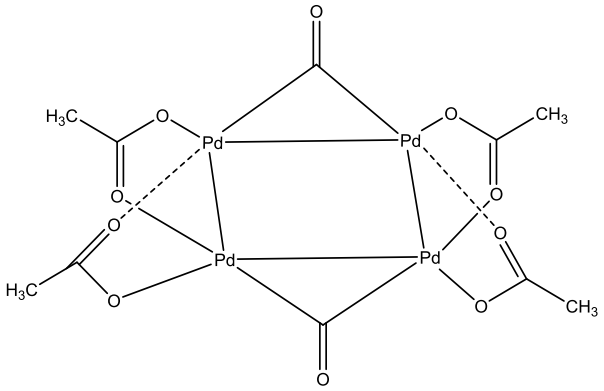

Figure 4.14. Representation of $[Pd_2(\mu\text{-}O_2CCH_3)_2(\mu\text{-}CO)]_2$.[69]

4.3.3 Reactions of H_2L8 towards bis(acetonitrile)dichloropalladium(II)

The reaction of H_2**L8** with $(MeCN)_2PdCl_2$ was also carried out with various ratios of ligand to metal; however a 2:1 ratio of ligand to metal gave the cleanest product. Hence reaction of $(MeCN)_2PdCl_2$ with two equivalents of H_2**L8** in chloroform at room temperature afforded $[PdCl(\kappa^2\text{-}H\mathbf{L8})(\kappa^1\text{-}H_2\mathbf{L8})]$ (**17**) in high yield (Scheme 4.16).

Complex **17** has been characterised spectroscopically and has been the subject of a single crystal X-ray diffraction study.

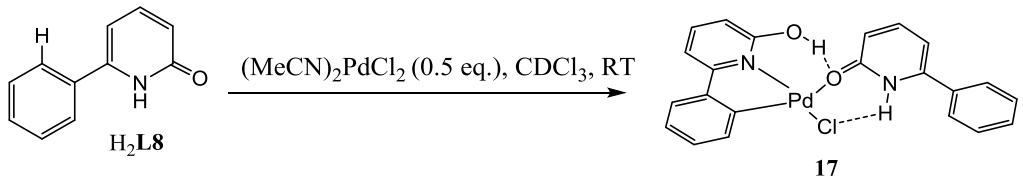

Scheme 4.16. Synthesis of **17**

A view of **17** is shown in Fig 4.15; selected bond distance and angles are collected in Table 4.5. The structure consists of a single palladium centre bound by a NC-chelating phenylpyridinol, an O-bound phenylpyridone and a chloride ligand to complete a distorted square planar geometry. The aryl CH-activated carbon of the NC-chelating phenylpyridinol is trans to the O-bound phenylpyridone. As expected the two carbon oxygen bond distances in **17** are significantly different with C(1)-O(1) at 1.273(6) Å corresponding to the O-bound phenylpyridone and C(2)-O(12) at 1.320(6) Å to the NC-chelating phenylpyridinol. No unusual features are noted for the Pd-Cl bond length [2.319(15) Å] which is comparable to the Pd-Cl bond in $(Hmp)_2PdCl_2$ [2.320 Å].[70]

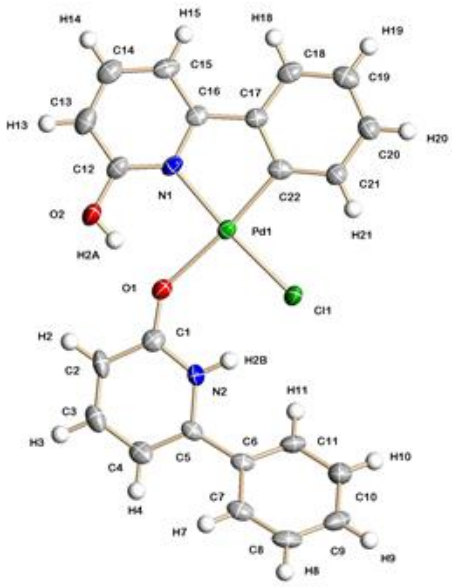

Figure 4.15. Molecular structure of **17** with full numbering scheme

Table 4.5. Selected bond distances (Å) and angles (°) for **17**

Bond lengths	
Pd(1)-C(22)	1.976(5)
Pd(1)-N(1)	2.067(4)
Pd(1)-O(1)	2.170(4)
Pd(1)-Cl(1)	2.319(15)
O(1)-C(1)	1.273(6)
O(2)-C(12)	1.320(6)
C(12)-N(1)	1.336(6)
C(1)-N(2)	1.347(7)
Bond angles	
C(22)-Pd(1)-N(1)	81.7(2)
N(1)-Pd(1)-O(1)	92.62(16)
C(22)-Pd(1)-Cl(1)	93.51(17)
N(1)-Pd(1)-C(1)	172.22(13)
O(1)-Pd(1)-Cl(1)	91.92(10)

4.3.4 Selective halogenation of H_2L8

(a) Bromination of H_2L8

H_2**L8** has proved amenable to selective bromination on the 6-phenyl-2-pyridone skeleton under a range of conditions using stoichiometric amounts of various sources of bromine in the presence or absence of catalyst (Scheme 4.17). Thus, mono-bromination at the pyridone ring with liquid bromine at low temperature affords 6-(C_6H_5)-3-BrC_5H_2N-2-O (H_2**L8**-3-Br) and trace quantities of the 5-substituted isomer (H_2**L8**-5-Br). Under more forcing conditions (120 °C) using NBS as the oxidant (2-3 equivalents), dibromination at the 3- and 5-positions of the pyridone ring occurs to give 6-(C_6H_5)-3,5-Br_2C_5HN-2-O (H**L8**-3,5-Br_2). On the other hand, when the reaction with NBS (3.1 eq.) is performed in acetonitrile at 120 °C in the presence of palladium acetate(II) (5 mol%), tribromination takes place to afford 6-(2-BrC_6H_4)-3,5-Br_2C_5HN-2-O (o-Br-**L8**-3,5-Br_2), in which *ortho*-bromination of the phenyl ring as well as dibromination of the pyridone ring has taken place. The formation of o-Br-**L8**-3,5-Br_2) makes use of conditions similar to that employed for the *ortho*-bromination of phenylpyridine.[35]

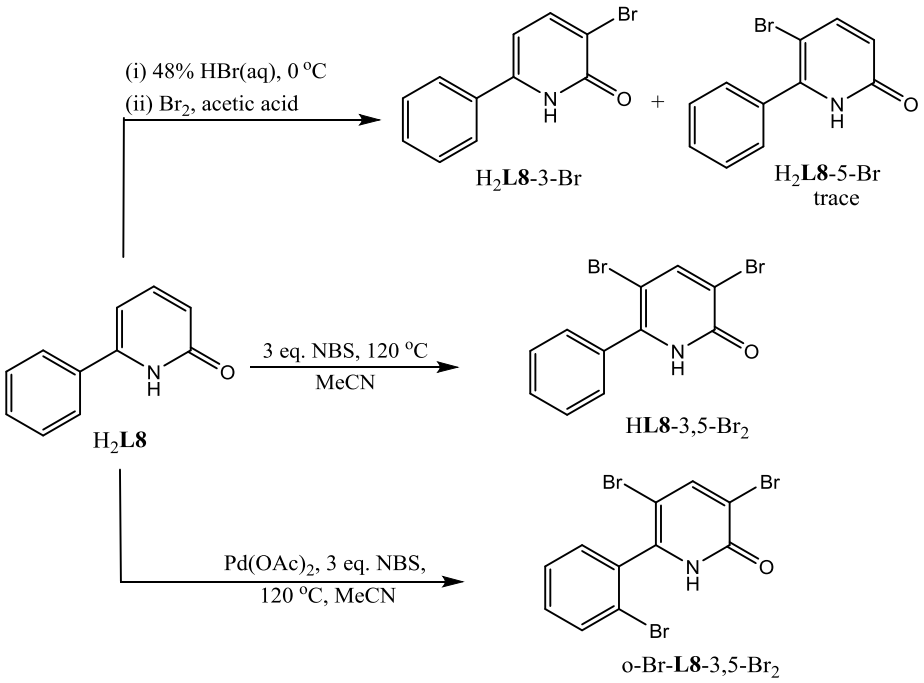

Scheme 4.17. Selective bromination reactions of H_2**L8**

Compounds H_2**L8**-3-Br, H**L8**-3,5-Br_2 and o-Br-**L8**-3,5-Br_2 have been characterised by $^1H/^{13}C$ and IR spectroscopy, mass spectrometry and melting point determinations. In addition all three compounds have been the subject of single crystal X-ray diffraction studies. Each compound, H_2**L8**-3-Br, H**L8**-3,5-Br_2 and o-Br-**L8**-3,5-Br_2, adopts the pyridone form which is confirmed by the carbonyl peaks which fall in the range 160.0-161.0 ppm in the ^{13}C NMR spectra. The amine NH peaks come downfield between 9.82-10.19 ppm which suggests strong hydrogen-bonding between molecules.

Crystals of H_2**L8**-3-Br, H**L8**-3,5-Br_2 and o-Br-**L8**-3,5-Br_2 suitable for the X-ray determinations were grown by slow evaporation of a saturated methanol solution of the corresponding compound. Views of each are shown in Figs. 4.16, 4.17 and 4.18; selected bond lengths and angles are compiled in Tables 4.6 and 4.7. Each structure consists of 2-pyridone unit substituted at the 6-position by an aryl group. In H_2**L8**-3-Br the 3-position of the 2-pyridone unit is substituted by a bromo group, in H**L8**-3,5-Br_2 bromo substituents are present at the 3 and 5 positions, while o-Br-**L8**-3,5-Br_2 resembles H**L8**-3,5-Br_2 but with a bromo substituent additionally on the ortho-position of the phenyl group. Like H_2**L8**, all three brominated structures prefer the pyridone form in the solid state as is evident from the C-O bond lengths [range: 1.241(10) - 1.245(6) Å]. In addition, the

presence of the sterically bulky ortho-substituted bromo group in o-Br-**L8**-3,5-Br_2 leads to the greatest torsion angle between the pyridone and phenyl ring at 70.7(8)°.

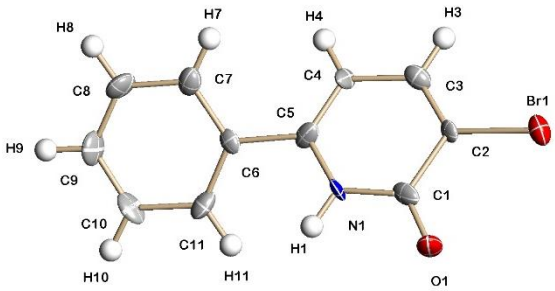

Figure 4.16. Molecular structure of H_2**L8**-3-Br with full atom numbering.

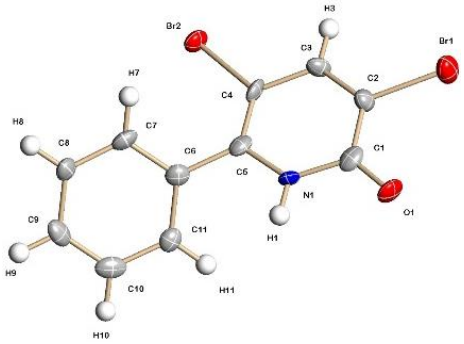

Figure 4.17. Molecular structure of H**L8**-3,5-Br_2 with full atom numbering.

Table 4.6. Selected bond distances (Å) and angles (°) for H_2**L8**-3-Br and H**L8**-3,5-Br_2

	Bond lengths	
	H_2**L8**-3-Br	H**L8**-3,5-Br_2
Br(1)-C(2)	1.837(11)	1.868(10)
Br(2)-C(4)	-	1.892(9)
O(1)-C(1)	1.241(10)	1.242(11)
N(1)-C(1)	1.377(10)	1.379(12)
C(5)-C(6)	1.516(14)	1.468(13)
	Bond angles	
C(11)-C(6)-C(5)	119.6(8)	119.9(8)
C(1)-C(2)-Br(1)	116.3(7)	117.8(7)
C(3)-C(4)-Br(2)	-	115.9(7)
N(1)-C(5)-C(6)	117.9(8)	116.2(8)
O(1)-C(1)-N(1)	122.6(7)	120.2(9)

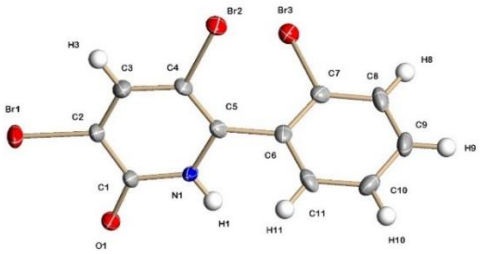

Figure 4.18. Molecular structure of o-Br-**L8**-3,5-Br_2 with full atom numbering.

Table 4.7. Selected bond distances (Å) and angles (°) for o-Br-**L8**-3,5-Br_2

Bond lengths	
Br(1)-C(2)	1.878(5)
Br(2)-C(4)	1.882(5)
O(1)-C(1)	1.245(6)
N(1)-C(1)	1.377(6)
Br(3)-C(7)	1.892(5)
C(5)-C(6)	1.485(7)
Bond angles	
C(11)-C(6)-C(5)	119.7(5)
C(1)-C(2)-Br(1)	116.5(4)
C(3)-C(4)-Br(2)	118.8(4)
N(1)-C(5)-C(6)	115.4(5)
O(1)-C(1)-N(1)	120.4(5)

The precise mechanism for the tri-bromination of H_2**L8** to give o-Br-**L8**-3,5-Br_2 is uncertain but a possible catalytic cycle is depicted in Scheme 4.18. In (i) both dibromination of the pyridone ring and CH-activation of the phenyl group occur to give a tetrametallic species that resembles **16**. This square planar tetramer then undergoes electrophilic bromination in (ii) to form a palladium(IV) complex which then decomposes by reductive elimination (iii) to give o-Br-**L8**-3,5-Br_2 and regenerate the active catalyst. If we compare this proposed mechanism with earlier reported mechanisms (e.g., Scheme 4.11) for the palladium acetate-mediated halogenation of 2-phenylpyridine,[34] the main difference is the capacity of 6-phenyl-2-pyridonate to act as bridging ligand. This results in halogenation of four molecules in one cycle which may be the possible reason for the higher isolated yields as compared to those reported.

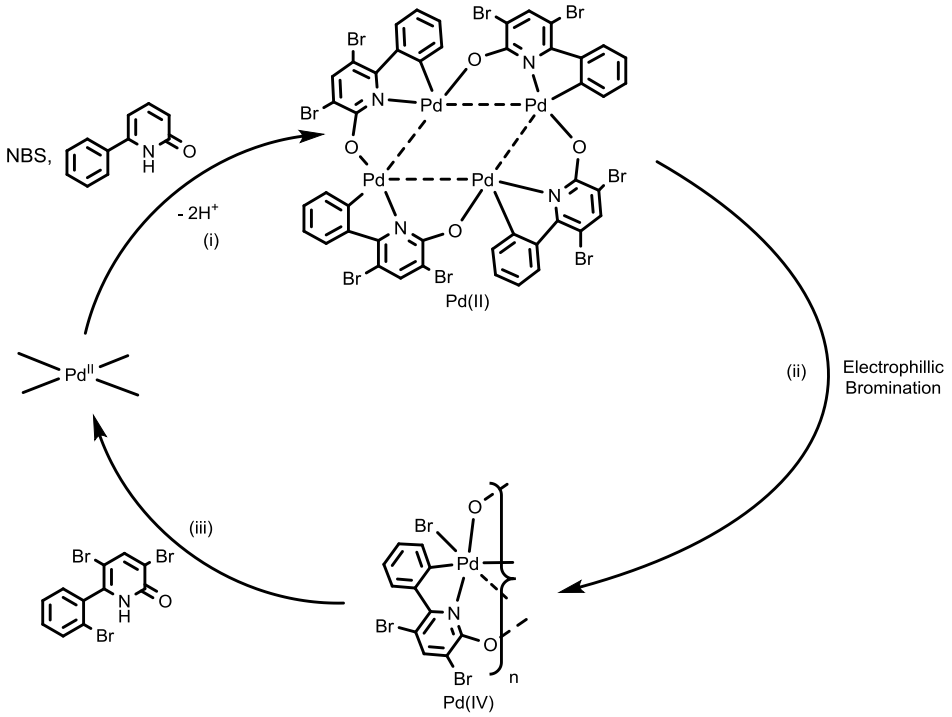

Scheme 4.18 Proposed mechanism for palladium(II)-catalysed tri-bromination of H_2**L8**

(b) Chlorination of H_2L8

The chlorination of a 2-pyridone ring and at the *ortho* position of 6-substituted phenyl group is desirable for synthesis of biological important compunds.[71] It is observed that using a similar protocol as that described above, chlorination of H_2**L8** could be achieved by using *N*-chlorosuccinamide (NCS) as oxidant with palladium(II) acetate as catalyst at 120 ^oC to form tri-chlorinated 6-(2-ClC_6H_4)-3,5-Cl_2C_5HN-2-O (o-Cl-**L8**-3,5-Cl_2) Similarly, dichlorination at the 3- and 5-positions of the pyridone ring occurs to give 6-(C_6H_5)-3,5-Cl_2C_5HN-2-O (H**L8**-3,5-Cl_2) with NCS as oxidant (Scheme 4.19). Single crystals suitable for an X-ray diffraction study were grown by slow evaporation of a methanol solution. A view of the structure is given in Fig. 4.19; selected bond distances and angles are collected in Table 4.8.

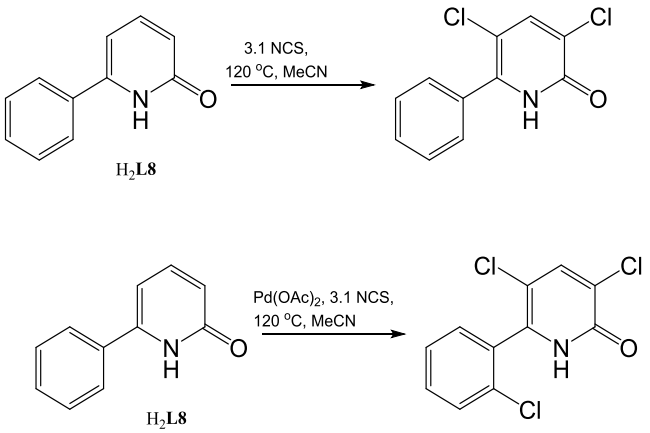

Scheme 4.19. Synthesis of tri-chlorinated o-Cl-**L8**-3,5-Cl_2

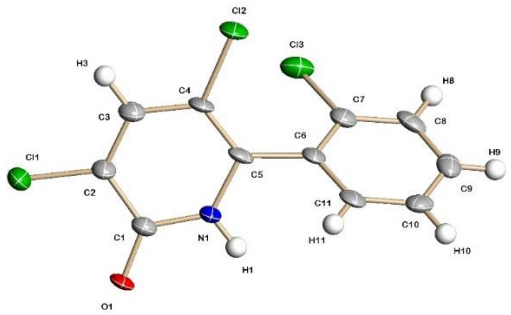

Figure 4.19. Molecular structure of o-Cl-**L8**-3,5-Cl_2 with full atom numbering.

Table 4.8. Selected bond distances (Å) and angles (°) for o-Cl-**L8**-3,5-Cl_2

Bond lengths	
C(1)-C(2)	1.719(5)
Cl(2)-C(4)	1.730(5)
O(1)-C(1)	1.246(5)
N(1)-C(1)	1.360(6)
Cl(3)-C(7)	1.734(5)
C(5)-C(6)	1.484(6)
Bond angles	
C(11)-C(6)-C(5)	119.5(4)
C(1)-C(2)-Cl(1)	116.9(3)
C(3)-C(4)-Cl(2)	117.5(3)
N(1)-C(5)-C(6)	114.7(4)
O(1)-C(1)-N(1)	120.8(4)

As with o-Br-**L8**-3,5-Br_2, the molecular structure of o-Cl-**L8**-3,5-Cl_2 reveals the heterocyclic unit to adopt the pyridone form with an O(1)-C(1) distance of 1.246(5) Å. The torsion angle between the phenyl and pyridone is increased from 43.5(2)° in H_2**L8** to 60.6(7)° in o-Cl-**L8**-3,5-Cl_2 but less than that in o-Br-**L8**-3,5-Br_2 (70.7(8)°) consistent

with steric properties of this halide. As expected, the ^{1}H NMR pattern of peaks in the aromatic region is similar in both o-Cl-**L8**-3,5-Cl_2 and o-Br-**L8**-3,5-Br_2 with a singlet for the 1H (pyridone ring) at 7.55 and 7.39 ppm along with a multiplet for the 5Hs belonging to the phenyl ring at 7.55 and 7.32 ppm, respectively.

(c) Fluorination of H_2L8

Fluorination of H_2**L8** was also attempted using 3.1 equivalents of Selectfluor as fluorinating reagent and 5 mol% of palladium(II) acetate as catalyst leading to the isolation of 6-(2-C_6H_5)-5,5-F_2-6-OH-C_5H_2NH-2-O. In this case difluorination had occurred at the 5-position of the pyridone ring along with hydroxylation at the 6-position; however, no fluorination was observed on the phenyl ring (Scheme 4.20). The loss of planarity within the heterocyclic unit may have contributed towards the lack of *ortho*-CH activation and fluorination. Notably, when the reaction of H_2**L8** with Selectfluor was conducted in the absence of palladium(II) acetate the same product, 6-(2-C_6H_5)-5,5-F_2-6-OH-C_5H_2NH-2-O was afforded. Notably, a similar type of difluorination of a fused 2-pyridone ring was reported in the preparation of anti-cancer compounds with Selectfluor as fluorinating agent.[72]

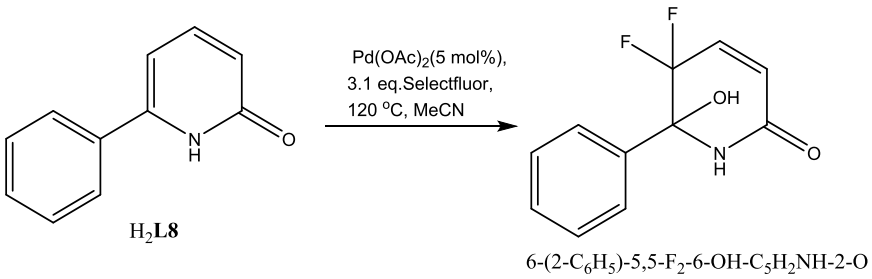

H_2**L8**

6-(2-C_6H_5)-5,5-F_2-6-OH-C_5H_2NH-2-O

Scheme 4.20. Reaction of H_2**L8** with selectfluor in the presence of $Pd(OAc)_2$

An X-ray determination was performed on a single crystal of 6-(2-C_6H_5)-5,5-F_2-6-OH-C_5H_2NH-2-O grown by slow evaporation of methanol. A view of the structure is shown in Fig 4.20; selected bond distances and bond angles are collected in Table 4.9. The structure reveals that carbonyl group is still intact with the C(3)-O(2) bond length of 1.245(3) Å, whereas the C(1)-C(2) distance 1.543(4) is now consistent with a single bond. In addition, the N(1)-C(2) distance of 1.449(3) Å shows single bond character higlighting the loss of aromaticity in the heterocycle.

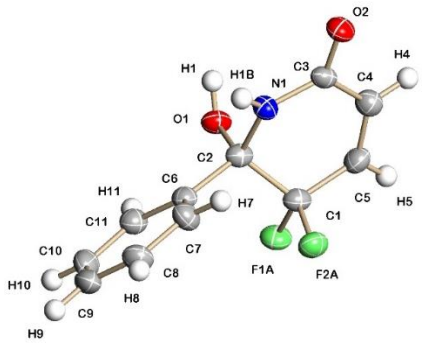

Figure 4.20. Molecular structure of 6-(2-C_6H_5)-5,5-F_2-6-OH-C_5H_2NH-2-O with full atom numbering.

Table 4.9. Selected bond distances (Å) and angles (°) for 6-(2-C_6H_5)-5,5-F_2-6-OH-C_5H_2NH-2-O

Bond lengths	
C(1)-C(2)	1.543(4)
C(1)-C(5)	1.492(4)
C(1)-F(1A)	1.359(3)
C(1)-F(2A)	1.373(3)
O(1)-C(2)	1.424(3)
O(2)-C(3)	1.245(3)
N(1)-C(2)	1.449(3)
Bond angles	
C(5)-C(1)-C(2)	112.9(2)
O(2)-C(3)-N(1)	121.5(2)
C(7)-C(6)-C(2)	121.4(2)
O(1)-C(2)-N(1)	110.9(2)
F(1A)-C(1)-F(2A)	105.52(19)

Confirmation of the gem-fluoride arrangement in 6-(2-C_6H_5)-5,5-F_2-6-OH-C_5H_2NH-2-O is shown by two mutually coupled doublets peaks -118.61 and -97.67 ppm in the ^{19}F NMR spectrum. In the ^{1}H NMR spectrum a broad NH peak at 9.21 ppm is observed along with a hydroxy peak at 7.59 ppm.

As with the palladium-catalysed reaction of 2-phenylpyridine with selectfluor, the reaction of H_2**L8** did not result fluorination of the phenyl group.[40] The possible reason for non-fluorination at the ortho position could be due to the loss of planarity in the heterocycle. Furthermore, it is apparent that pyridone ring is too reactive towards selectfluor with the consequence that the fluorinated heterocycle could electronically influence the ortho-fluorination.

4.3.5 Reactivity of H_2L8 with ONO'-Pd pincer complex 10a

In Chapter 3, we have seen some reactivity of the ONO'-palladium pincer complexes with a range of simple 2-pyridones *e.g.*, 2-pyridone, 6-methyl-2-pyridone, 6-chloro-2-pyridone and 6-fluoro-2-pyridone. To extend this chemistry we now explore the reactivity of (**L5a**Pd)$_2$ (**10a**) towards H_2**L8**. Unexpectedly, the reaction of **10a** with H_2**L8** at elevated temperature in toluene gave CH-activated **15** along with the loss of free H_2**L5a** in good yield (Scheme 4.21). The reaction product, **15**, is the same species as that formed when palladium(II) acetate is reacted with two equivalents of H_2**L8** (see Scheme 4.14). It would seem likely that the oxygen atom in coordinated **L5a** ligand in **15** serves as an internal base in an AMLA-type process in a manner similar to that seen for acetate when using $Pd(OAc)_2$ (see later).

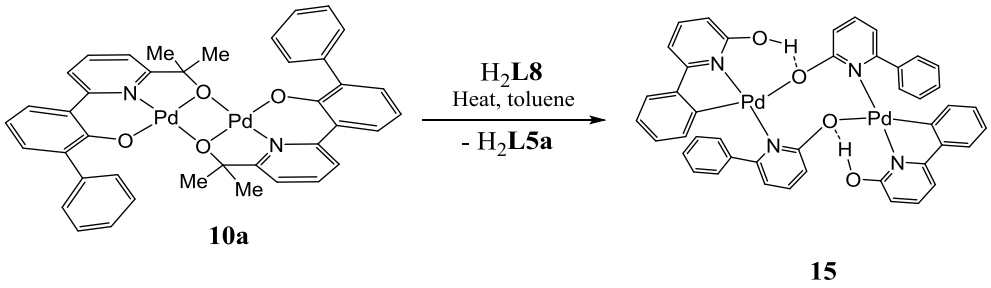

Scheme 4.21. Reaction of **10a** with H_2**L8**

4.3.6 Reactivity of H_2L8 with ONN-Pd pincer complex 4a and related

In Chapter 2, **L4**PdOAc (**4a**) was shown to readily undergo acetate exchange reactions with a variety of 2-pyridones. With a view to exploring the potential of the NNO-ligand **L4** in **4a** to act as an internal base to abstract an *ortho*-CH proton in H_2**L8**, **4a** was reacted with H_2**L8** in toluene at room temperature affording phenylpyridonate-containing **L4**Pd(H**L8**) (**18**) in reasonable yield (Scheme 4.22). Complex **18** has been characterised spectroscopically and has been the subject of a single crystal X-ray study.

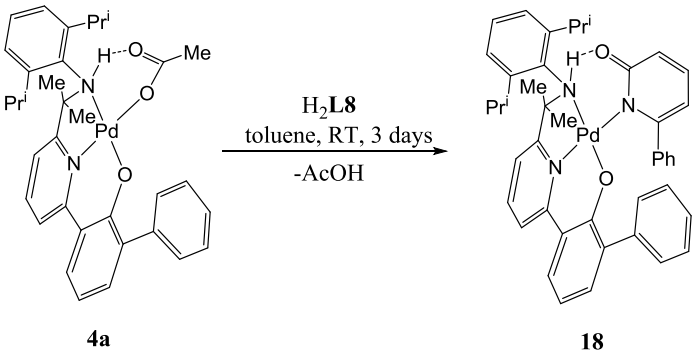

4a **18**

Scheme 4.22 Reaction of **4a** with H_2**L8**

Single crystals suitable for an X-ray determination were grown by layering a dichloromethane solution of **18** with hexane. The molecular structure is shown in Fig 4.21; selective bond distances and bond angles are compiled in Table 4.10. The structure shows monoanionic H**L8** to be coordinated to the palladium centre via the pyridonate nitrogen atom [Pd(1)-N(3) 2.057(2) Å], while the NNO ligand, **L4**, uses all its three donor atoms to complete a distorted square planar geometry. The torsion angle between the NNO-palladium plane and the pyridonate ring is *ca.* 18^o off orthogonal [O(1)-Pd(1)-N(3)-C(32) 108.69(17)^o] suggesting the pocket created by the pincer ligand is not big enough to accommodate H**L8** in a pseudo-planar fashion that would have enabled a potential *ortho*-CH hydrogen bonding interaction with the phenolate-O atom. Nevertheless, it may be possible at higher temperatures to de-coordinate either the NH or the phenolate oxygen arm on the pincer ligand to allow *ortho*-activation of H**L8**. Despite the tilting of the pyridonate unit, the pyridonate-O atom still undergoes a hydrogen bonding interaction with the NH donor of the pincer ligand (HN···O 2.938 Å).

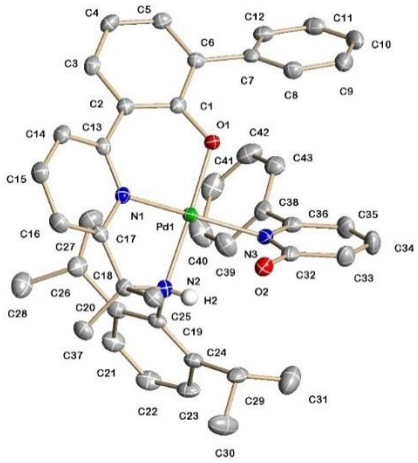

Figure 4.21. Molecular structure of **18** with full atom numbering; H atoms have been omitted for clarity

Table 4.10. Selected bond distances (Å) and angles (°) for **18**

Bond lengths	
Pd(1)-O(1)	1.9697(17)
Pd(1)-N(1)	1.977(2)
Pd(1)-N(2)	2.042(2)
Pd(1)-N(3)	2.057(2)
O(2)-C(32)	1.260(3)
Bond angles	
O(1)-Pd(1)-N(1)	94.08(8)
O(1)-Pd(1)-N(2)	177.06(7)
N(1)-Pd(1)-N(2)	83.19(8)
O(1)-Pd(1)-N(3)	87.56(7)
N(1)-Pd(1)-N(3)	168.35(8)

In an attempt to reduce the steric hindrance imposed by pincer ligand **L4** on the coordination mode exhibited by H**L8** in **18**, we set about synthesizing [(2-(C_6H_4O)-6-{CMe_2NH(2,6-*i*-$Pr_2C_6H_3$)}C_5H_3N)]Pd(H**L8**) (**19**), which contains no pendant phenyl group on the phenolate moiety. Hence reaction of [(2-(C_6H_4O)-6-{CMe_2NH(2,6-*i*-$Pr_2C_6H_3$)}C_5H_3N)]Pd(OAc) with H_2**L8** in toluene at room temperature gave **19** in satisfactory yield (Scheme 4.23). Complex **19** has been characterised spectroscopically and has been the subject of a single crystal X-ray study.

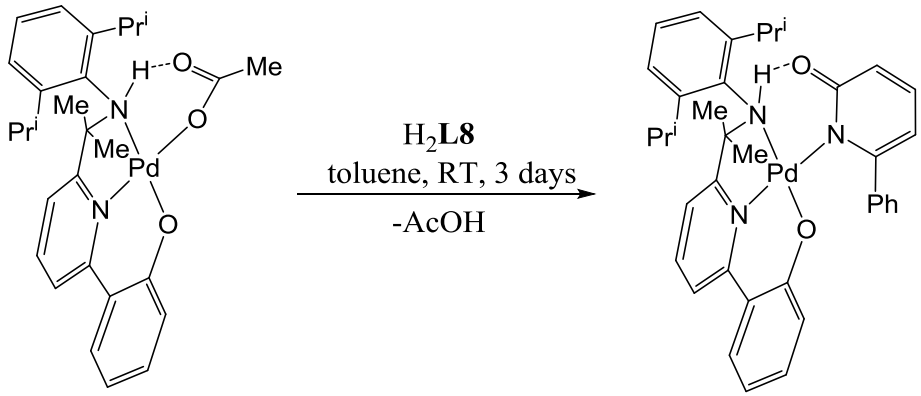

19

Scheme 4.23 Reaction of less bulky [(2-(C_6H_4O)-6-{CMe_2NH(2,6-*i*-$Pr_2C_6H_3$)}C_5H_3N)]Pd(OAc) with H_2**L8**

Single crystals suitable for an X-ray determination were grown by layering a dichloromethane solution of **19** with hexane. The molecular structure of **19** is shown in Fig 4.22; selective bond distances and bond angles are compiled in Table 4.11. As with **18**, H**L8** is bound to the palladium centre by the pyridonate nitrogen atom without any evidence for *ortho*-CH activation of the phenyl ring in H**L8** having occurred. Unexpectedly, the corresponding torsion angle between the NNO-palladium plane and the pyridonate ring indicates that it is more tilted in **19** as compared with that in **18** (11^{o} off orthogonal in **19** *vs.* 18^{o} in **18**), with the result that the NH···$O_{pyridonate}$ interaction is reduced in comparison with that see in **18** (2.938 Å (**18**) *vs.* 3.094 Å (**19**))..

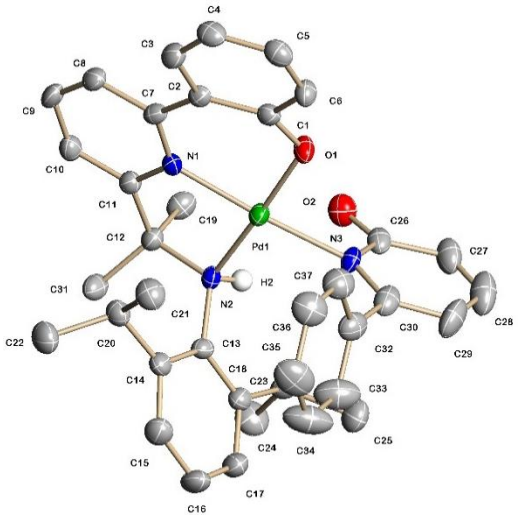

Figure 4.22. Molecular structure of **18** with full atom numbering; H atoms have been omitted for clarity

Table 4.11. Selected bond distances (Å) and angles (^{o}) for **19**

Bond lengths	
Pd(1)-O(1)	1.964(2)
Pd(1)-N(1)	1.987(3)
Pd(1)-N(2)	2.035(3)
Pd(1)-N(3)	2.057(2)
O(2)-C(26)	1.267(4)
Bond angles	
O(1)-Pd(1)-N(1)	93.72(12)
O(1)-Pd(1)-N(2)	176.91(11)
N(1)-Pd(1)-N(2)	84.29(12)
O(1)-Pd(1)-N(3)	88.18(11)
N(1)-Pd(1)-N(3)	171.55(12)

4.3.7 Catalytic bromination of H_2**L8** using Pd-pincer complexes and comparison with palladium(II) acetate

Given the ability of ONO'-containing **10** to stoichiometrically CH-activate H_2**L8** (see Scheme 4.21), along with the facile reactivity of NNO-bearing **4a** towards H_2**L8** (see Scheme 4.22), it was of interest to screen selected palladium(II) pincer complexes developed in this thesis as catalysts for the bromination of H_2**L8**. The resulting findings can then be compared with the results obtained using palladium(II) acetate as catalyst.

Specifically, seven different palladium pincer complexes were chosen namely **9a**, **9b**, **9c**, **10a**, **11b**, **12b** and **12c**, three of which contain NNO-ligands (**9a** – **9c**) and the remaining four ONO-ligands (**10a**, **11b**, **12b** and **12c**). For **9a**-**9c** the effect of counterion (PF_6 vs. BF_4 vs OTf) was being probed while **12b** and **12c** the nature of the monodentate pyridine ligand was being examined; for **10a** and **11b** the size of the cluster as well as the electronic properties were being tested. In all cases the screening was performed under identical conditions: stirred solutions under nitrogen in acetonitrile at 120 ^oC in a sealed vessel for 16 hours (entries 1 – 9, Table 4.12).

Table 4.12. Catalytic evaluation of a range of NNO-Pd and ONN-Pd complexes in the bromination of H_2**L8**

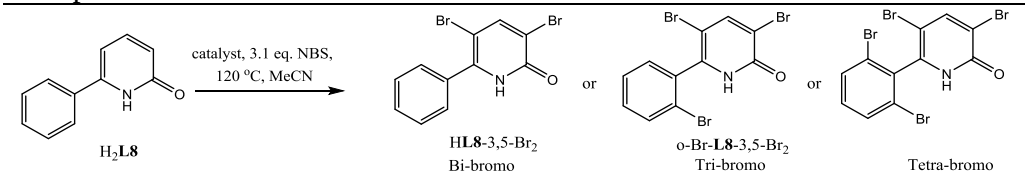

H_2**L8** | H**L8**-3,5-Br_2 Bi-bromo | o-Br-**L8**-3,5-Br_2 Tri-bromo | Tetra-bromo

Entry	Catalyst (5 mol%)	Dibromo % conversion	Tribromo % conversion	Tetrabromo % conversion
1.	-	100	0	0
2.	$Pd(OAc)_2$	0	100	0
3.	[**L4**Pd(MeCN)]PF_6 (**9a**)	84	16	0
4.	[**L4**Pd(MeCN)]BF_4 (**9b**)	83	17	0
5.	[**L4**Pd(MeCN)]OTf (**9c**)	79	21	0
6.	**L5a**Pd(3,5-Cl_2py) (**12b**)	86	14	0
7.	**L5a**Pd(3,5-Me_2py) (**12c**)	95	5	0
8.	(**L5a**Pd)$_2$ (**10a**)	85	15	0
9.	(**L5d**Pd)$_4$ (**11b**)	85	15	0

Reaction conditions: H_2**L8** was heated with 3.1 NBS, [Pd] 5 mol% at 120 °C in closed vessel for 16 h. The conversion was determined using ^{1}H NMR spectroscopy.

On inspection of the data, all pincer complexes give a mixture of di- and tri-brominated products (entries 3-9); there is no evidence for a tetra-brominated species for any of the runs. Unlike palladium(II) acetate (entry 2), none of the pincer complexes achieve 100% conversion to the tri-brominated species. Indeed the best conversions (16 – 21%) are achieved using the ONN-type palladium(II) pincer salts, **9a** – **9c** (entries 3-5). Nevertheless, it is clear that both the ONN and ONO'-type pincer ligands when bound to palladium are capable of acting as proton acceptors in manner akin to acetate in the CH-bromination; for comparative purposes without catalyst 100% di-bromination resulted (entry 1). The better performance of **9a** - **9c** may be due to the lability of the acetonitrile ligands or to their increased solubility due to the presence of the N-2,6-diisopropylphenyl group.

4.4 Conclusions

The reaction of 6-phenyl-2-pyridone (H_2**L8**) with palladium(II) acetate using different stoichiometric ratios of H_2**L8** has been studied. The acetate-bridged complex [Pd(κ^2-H**L**)(μ-OAc)]$_2$ (**14**) was formed with one equivalent of H_2**L8** whereas the dimeric palladium complex [Pd(μ-H**L**)(κ^2-H**L**)]$_2$ (**15**) was the main product when two equivalents were used. On prolonged standing **14** underwent further reaction affording the tetrameric square-shaped cluster [Pd(μ:κ^2-**L8**)]$_4$ (**16**) with the loss of acetic acid. CH-activation of H_2**L8** could also be achieved on reaction with (MeCN)$_2$PdCl$_2$ generating [PdCl(κ^2-H**L8**)(κ^1-H_2**L8**)] (**17**).

The selective halogenation (Br, Cl or F) of H_2**L8** was achieved by varying the stoichiometry of the halogenating reagent and palladium(II) acetate catalyst. Mono-bromo (H_2**L8**-3-Br), di-bromo (H**L8**-3,5-Br$_2$) and tri-brominated (o-Br-**L8**-3,5-Br$_2$) pyridones were synthesised by using Br_2 or NBS as the brominating reagent with or without catalyst. Similarly, tri-chlorinated pyridone, o-Cl-**L8**-3,5-Cl$_2$, was synthesised by heating with NCS and palladium(II) acetate as the catalyst (5 mol%). Extension of this approach to the trifluorination of H_2**L8** using Selectfluor as the fluorinating reagent and palladium(II) acetate as the catalyst was unsuccessful yielding 6-(2-C_6H_5)-5,5-F_2-6-OH-

C_5H_2NH-2-O in which difluorination of the 5-position of the pyridone ring occurred and no fluorination of the phenyl group.

To explore the reactivity of H_2**L8** towards pincer complexes already prepared in this thesis, we examined its reaction with (**L5a**Pd)$_2$ (**10**) and **L4**PdOAc (**4a**). For **10**, ligand displacement occurred forming CH-activated **15**, while for **4a** the acetate group was substituted for phenyl pyridonate, H**L8**, to give **18**; no evidence of a CH-activated phenyl group was observed in the latter reaction.

Given the capacity of palladium(II) acetate to act as an effective catalyst in the tri-bromination of H_2**L8**, it was of interest to explore a selection of the pincer complexes developed in this thesis as catalysts in their own right towards the tri-bromination of H_2**L8**. In all the cases screened, the major product identified was the di-brominated pyridone, H**L8**-3,5-Br_2. Nevertheless, substantial amounts of the tri-brominated product, o-Br-**L8**-3,5-Br_2, were detected (up to 21% with **9c**). Overall, it was found that palladium(II) acetate is the best catalyst to mediate the tri-bromination of H_2**L8**.

4.5 References

1. R. G. Bergman, *Nature*, 2007, **446**, 391-393.
2. R. H. Crabtree, *J. Chem. Soc., Dalton Trans.*, 2001, DOI: 10.1039/B103147N, 2437-2450.
3. J. A. Labinger and J. E. Bercaw, *Nature*, 2002, **417**, 507-514.
4. A. E. Shilov and G. B. Shul'pin, *Chem. Rev.*, 1997, **97**, 2879-2932.
5. T. W. Lyons and M. S. Sanford, *Chem. Rev.*, 2010, **110**, 1147-1169.
6. D. A. Colby, R. G. Bergman and J. A. Ellman, *Chem. Rev.*, 2010, **110**, 624-655.
7. G. P. Chiusoli, M. Catellani, M. Costa, E. Motti, N. Della Ca' and G. Maestri, *Coord. Chem. Rev.*, 2010, **254**, 456-469.
8. D. Y. K. Chen and S. W. Youn, *Chem. Eur. J.*, 2012, **18**, 9452-9474.
9. D. Alberico, M. E. Scott and M. Lautens, *Chem. Rev.*, 2007, **107**, 174-238.
10. A. H. Janowicz and R. G. Bergman, *J. Am. Chem. Soc.*, 1982, **104**, 352-354.
11. J. Chatt and J. M. Davidson, *J. Chem. Soc. (Resumed)*, 1965, DOI: 10.1039/JR9650000843, 843-855.
12. P. L. Watson, *J. Am. Chem. Soc.*, 1983, **105**, 6491-6493.
13. M. E. Thompson, S. M. Baxter, A. R. Bulls, B. J. Burger, M. C. Nolan, B. D. Santarsiero, W. P. Schaefer and J. E. Bercaw, *J. Am. Chem. Soc.*, 1987, **109**, 203-219.
14. D. Balcells, E. Clot and O. Eisenstein, *Chem. Rev.*, 2010, **110**, 749-823.
15. P. L. Watson and G. W. Parshall, *Acc. Chem. Res.*, 1985, **18**, 51-56.
16. W. J. Tenn, K. J. H. Young, G. Bhalla, J. Oxgaard, W. A. Goddard and R. A. Periana, *J. Am. Chem. Soc.*, 2005, **127**, 14172-14173.
17. G. NF, M. Tyabin, A. Shilov and S. AA, 1969.
18. N. Gol'dshleger, V. Es'kova, A. Shilov and A. Shteinman, *Zh Fiz Khim*, 1972, **46**, 1353-1354.
19. Y. Boutadla, D. L. Davies, S. A. Macgregor and A. I. Poblador-Bahamonde, *Dalton Trans.*, 2009, 5820-5831.
20. S. I. Gorelsky, D. Lapointe and K. Fagnou, *J. Am. Chem. Soc.*, 2008, **130**, 10848-10849.
21. S. I. Gorelsky, D. Lapointe and K. Fagnou, *J. Am. Chem. Soc.*, 2008, **130**, 10848-10849.
22. A. D. Ryabov, I. K. Sakodinskaya and A. K. Yatsimirsky, *J. Chem. Soc., Dalton Trans.*, 1985, DOI: 10.1039/DT9850002629, 2629-2638.
23. A. D. Ryabov, *Chem. Rev.*, 1990, **90**, 403-424.
24. J. Ruiz, N. Sotomayor and E. Lete, *Org. Lett.*, 2003, **5**, 1115-1117.
25. B. J. Wakefield, *Appl. Organomet. Chem.*, 1998, **12**, 879-879.
26. *Reaction intermediates*, Wiley, 1985.
27. M. R. Crampton, *Organic Reaction MechanismsOrganic Reaction Mechanisms*, Wiley, New York.
28. F. Roudesly, J. Oble and G. Poli, *J. Mol. Catal. A: Chem.*, 2017, **426, Part B**, 275-296.
29. P. Ruiz-Castillo and S. L. Buchwald, *Chem. Rev.*, 2016, **116**, 12564-12649.
30. M. N. a. S. A., *Chem. Rev.*, 1995, **95**.
31. A. Butler and J. V. Walker, *Chem. Rev.*, 1993, **93**, 1937-1944.
32. D. C. Powers, D. Y. Xiao, M. A. L. Geibel and T. Ritter, *J. Am. Chem. Soc.*, 2010, **132**, 14530-14536.
33. D. C. Powers and T. Ritter, *Nat Chem*, 2009, **1**, 302-309.
34. N. R. Deprez and M. S. Sanford, *J. Am. Chem. Soc.*, 2009, **131**, 11234-11241.

35. D. Kalyani, A. R. Dick, W. Q. Anani and M. S. Sanford, *Org. Lett.*, 2006, **8**, 2523-2526.
36. D. C. Powers, M. A. L. Geibel, J. E. M. N. Klein and T. Ritter, *J. Am. Chem. Soc.*, 2009, **131**, 17050-17051.
37. S. Korwar, K. Brinkley, A. R. Siamaki, B. F. Gupton and K. C. Ellis, *Org. Lett.*, 2015, **17**, 1782-1785.
38. S. Purser, P. R. Moore, S. Swallow and V. Gouverneur, *Chem. Soc. Rev.*, 2008, **37**, 320-330.
39. P. Jeschke, *Chem. Bio. Chem.*, 2004, **5**, 570-589.
40. S.-J. Lou, D.-Q. Xu, A.-B. Xia, Y.-F. Wang, Y.-K. Liu, X.-H. Du and Z.-Y. Xu, *Chem. Commun.*, 2013, **49**, 6218-6220.
41. C. S. Peng and A. Tokmakoff, *J. Phy. Chem. Lett.*, 2012, **3**, 3302-3306.
42. M. M. Heravi and H. Hamidi, *J. Iranian Chem. Soc.*, 2013, **10**, 265-273.
43. M. Sellstedt, A. Nyberg, E. Rosenbaum, P. Engström, M. Wickström, J. Gullbo, S. Bergström, L. B. Å. Johansson and F. Almqvist, *Eur. J. Org. Chem.*, 2010, **2010**, 6171-6178.
44. W.-H. Wang, J. T. Muckerman, E. Fujita and Y. Himeda, *New J. Chem.*, 2013, **37**, 1860-1866.
45. E. E. Anagnostaki, A. D. Fotiadou, V. Demertzidou and A. L. Zografos, *Chem. Commun.*, 2014, **50**, 6879-6882.
46. K. Kumpan, A. Nathubhai, C. Zhang, P. J. Wood, M. D. Lloyd, A. S. Thompson, T. Haikarainen, L. Lehtiö and M. D. Threadgill, *Bioorg. Med Chem*, 2015, **23**, 3013-3032.
47. J. M. Rawson and R. E. P. Winpenny, *Coord. Chem. Rev.*, 1995, **139**, 313-374.
48. F. A. Cotton and J. L. Thompson, *J. Am. Chem. Soc.*, 1980, **102**, 6437-6441.
49. F. A. Cotton, K. R. Dunbar and M. Matusz, *Inorg. Chem.*, 1986, **25**, 1585-1589.
50. F. A. Cotton and J. L. Thompson, *Inorg. Chim. Acta*, 1980, **44**, L247-L248.
51. T. C. Flood, J. K. Lim and M. A. Deming, *Organometallics*, 2000, **19**, 2310-2317.
52. D. P. Bancroft, F. A. Cotton, L. R. Falvello and W. Schwotzer, *Inorg. Chem.*, 1986, **25**, 1015-1021.
53. K.-i. Fujita, N. Tanino and R. Yamaguchi, *Organic Letters*, 2006, **9**, 109-111.
54. L. Schäffler, U. R. Werz and G. Maas, *Inorg. Chim. Acta*, 2005, **358**, 3152-3158.
55. K.-i. Fujita, T. Yoshida, Y. Imori and R. Yamaguchi, *Org. Lett.*, 2011, **13**, 2278-2281.
56. C. L. Smith, C. Hirschhäuser, G. K. Malcolm, D. J. Nasrallah and T. Gallagher, *Synlett*, 2014, **25**, 1904-1908.
57. US20070185156A1, 2007.
58. F. Kröhnke, W. Zecher, J. Curtze, D. Drechsler, K. Pfleghar, K. E. Schnalke and W. Weis, *Angew. Chem. Int. Ed.*, 1962, **1**, 626-632.
59. S. Yogi, K. Hokama and O. Tsuge, *Bull. Chem. Soc. Jpn.*, 1987, **60**, 335-342.
60. H. W. Yang and B. M. Craven, *Acta. Crysta. Sec. B*, 1998, **54**, 912-920.
61. J. E. Bercaw, A. C. Durrell, H. B. Gray, J. C. Green, N. Hazari, J. A. Labinger and J. R. Winkler, *Inorg. Chem.*, 2010, **49**, 1801-1810.
62. H.-K. Yip, T.-F. Lai and C.-M. Che, *J. Chem. Soc., Dalton Trans.*, 1991, 1639-1641.
63. B.-H. Xia, C.-M. Che and Z.-Y. Zhou, *Chem. Eur. J.*, 2003, **9**, 3055-3064.
64. Q.-J. Pan, H.-X. Zhang, X. Zhou, H.-G. Fu and H.-T. Yu, *J. Phys. Chem. A*, 2007, **111**, 287-294.
65. V. G. Zaitsev, D. Shabashov and O. Daugulis, *J. Am. Chem. Soc.*, 2005, **127**, 13154-13155.

66. S. Iwatsuki, T. Itou, H. Ito, H. Mori, K. Uemura, Y. Yokomori, K. Ishihara and K. Matsumoto, *Dalton Trans.*, 2006, 1497-1504.
67. S. Clément, S. M. Aly, D. Bellows, D. Fortin, C. Strohmann, L. Guyard, A. S. Abd-El-Aziz, M. Knorr and P. D. Harvey, *Inorg. Chem.*, 2009, **48**, 4118-4133.
68. A. Crispini and M. Ghedini, *J. Chem. Soc., Dalton Trans.*, 1997, DOI: 10.1039/A604494H, 75-80.
69. I. I. Moiseev, *J. Organomet. Chem.*, 1995, **488**, 183-190.
70. J. G. Małecki and A. Maroń, *Transition Met. Chem.*, 2011, **36**, 297-305.
71. J. S. Debenham, C. B. Madsen-Duggan, J. Wang, X. Tong, J. Lao, T. M. Fong, M.-T. Schaeffer, J. C. Xiao, C. C. R. R. Huang, C.-P. Shen, D. Sloan Stribling, L. P. Shearman, A. M. Strack, D. Euan MacIntyre, J. J. Hale and T. F. Walsh, *Bioorg. Med. Chem. Lett.*, 2009, **19**, 2591-2594.
72. P.-P. Kung, E. Rui, S. Bergqvist, P. Bingham, J. Braganza, M. Collins, M. Cui, W. Diehl, D. Dinh, C. Fan, V. R. Fantin, H. J. Gukasyan, W. Hu, B. Huang, S. Kephart, C. Krivacic, R. A. Kumpf, G. Li, K. A. Maegley, I. McAlpine, L. Nguyen, S. Ninkovic, M. Ornelas, M. Ryskin, S. Scales, S. Sutton, J. Tatlock, D. Verhelle, F. Wang, P. Wells, M. Wythes, S. Yamazaki, B. Yip, X. Yu, L. Zehnder, W.-G. Zhang, R. A. Rollins and M. Edwards, *J. Med. Chem.*, 2016, **59**, 8306-8325.

Chapter 5
Experimental

Chapter 5
Experimental

5.1 General

All experiments were performed under an air free inert atmosphere of dry nitrogen using standard Schlenk techniques unless otherwise stated. Solvents were distilled under nitrogen from appropriate drying agents.[202] The infrared spectra were recorded in the solid state with Universal ATR sampling accessories on a Perkin Elmer Spectrum One FTIR instrument. NMR spectra were recorded on a Bruker DRX400 spectrometer at 400.13 (^{1}H) and 100.61 MHz (^{13}C) at room temperature; chemical shifts (ppm) are referred to the residual protic solvent peaks and coupling constants are expressed in hertz (Hz). Melting points (Mp) were measured on a Gallenkamp melting point apparatus (model MFB-595) in open capillary tubes and were uncorrected. ESI mass spectra were recorded on a micromass Quattra LC spectrometer in either MeCN or MeOH; FAB mass spectra (including high resolution) were recorded on a Kratos Concept spectrometer with NBA as matrix or on Water Xevo QToF mass spectrometer equipped with an atmospheric solids analysis probe (ASAP). Elemental analyses were conducted at London Metropolitan University.

The reagents 2-phenylphenol, 2,6-dibromopyridine, *n*-butyllithium (1.6M in hexane) trimethylaluminium (2M solution in toluene), boron tribromide (1M solution in dichloromethane), silver triflate, silver tetrafluoroborate, silver hexafluorophosphate, 2-hydroxypyridine, 6-methyl-2-pyridinol, 6-chloro-2-hydroxypyridine, SelectFluor^{TM}, N-bromo-succinimide (NBS), N-chloro-succinimide (NCS), pentafluorophenol, 2-iodobenzoic acid, 3,5-dichloropyridine, 3,5-lutidine and aqueous 48% HBr were purchased from Aldrich Chemical Co. and used without further purification. 2,6-Diisopropylaniline was distilled under inert conditions immediately prior to use. The compounds tetrakis(triphenylphosphine)palladium(0),[203] 2-hydroxybiphenyl-3-ylboronic acid,[204] 2-methoxybiphenyl-3-ylboronic acid,[204] 6-fluoro-2-hydroxypyridine,[205] 2-bromo-6-methoxypyridine,[206] 2-bromo-6-formylpyridine,[207] 2-bromo-6-acetylpyridine,[207] 6-phenyl-2-methoxypyridine[208] and bis(acetonitrile)dichloropalladium(II)[203] were prepared using literature procedures. $Pd(OAc)_2$ was provided on loan from Johnson Matthey PLC. All other chemicals were obtained commercially and used without further purification.

5.2 Chapter 2 Experimental

5.2.1 Synthesis of 2-(3'-phenyl-2'-phenol)-6-acetylpyridine

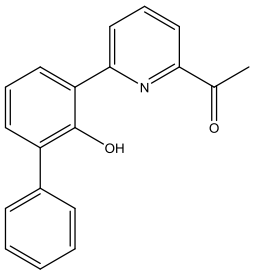

A Schlenk flask equipped with stir bar was evacuated and backfilled with nitrogen and loaded with 2-bromo-6-acetylpyridine (1.571 g, 7.85 mmol), $Pd(PPh_3)_4$ (0.181 g, 0.157 mmol), toluene (30 mL) and an aqueous 2M solution of potassium carbonate (7.9 mL, 15.7 mmol). The mixture was stirred at room temperature for 15 min. followed by the addition of 2-hydroxy-biphenyl-3-ylboronic acid (2.185 g, 10.21 mmol, 1.3 eq) in ethanol (20 mL). The solution was heated to 90 °C and stirred at this temperature for 72 h. On cooling to room temperature hydrogen peroxide (0.65 mL, 30 wt. % in water) was added and the solution left to stir for 1 h. Following extraction with diethyl ether (3 x 100 mL) and washing with a brine solution (1 x 50 mL), the combined organic extracts were dried over magnesium sulfate. Filtration followed by removal of the solvent on the rotary evaporator gave the crude product as a viscous brown oil. The catalyst residues were removed by a short silica column using a mixture composed of dichloromethane:hexane (80:20) as the eluent affording 2-(3'-phenyl-2'-phenoxy)-6-acetylpyridine as a yellow oil (1.612 g, 71%). ^{1}H NMR (400 MHz, $CDCl_3$): δ [ppm] 2.68 (s, 3H, Me), 6.97 (t, J_{HH} 7.7, 1H, Ar-H), 7.26-7.41 (m, 4H, Ar-*H*), 7.58-7.61 (m, 2H, Ar-H), 7.78 (dd, J_{HH} 8.0, 1.6, 1H, Ar-H), 7.91-7.98 (m, 2H, Py-H), 8.11 (dd, J_{HH} 7.5, 1.8, 1H, Py-H), 13.97 (s, 1H, Ar-OH). ^{13}C{^{1}H} NMR (100 MHz, $CDCl_3$): δ 25.3 (*Me*C=O), 117.6 (C), 118.0, 118.8, 122.3, 125.1, 126.14, 127.1, 128.5 (CH), 130.3 (C), 132.3 (CH), 137.2 (C), 137.8 (CH), 148.9 (C), 155.8 (C), 156.5(C), 196.5 (*C*Me=O). IR (cm^{-1}): 1700 (C=O). ESIMS: *m/z* 290 $[M+H]^+$. HRMS (ESI): calcd for $C_{19}H_{16}NO_2$ $[M+H]^+$ 290.1181, found 290.1187.

5.2.2 Synthesis of (3'-phenyl-2'-phenoxy)-6-formylpyridine

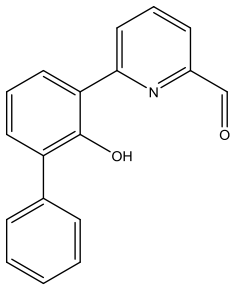

Step 1 (Suzuki coupling): A Schlenk flask equipped with stir bar was charged with 2-bromo-6-formylpyridine (2.180 g, 11.7 mmol), $Pd(PPh_3)_4$ (0.269 g, 0.23 mmol), toluene (30 mL) and an aqueous 2M solution of potassium carbonate (12.0 mL, 23.4 mmol). The mixture was stirred at room temperature for 15 min. followed by the addition of 2-methoxybiphenyl-3-ylboronic acid (3.470 g, 15.2 mmol, 1.3 eq.) in ethanol (20 mL). The solution was heated to 90 °C and stirred at this temperature for 42 h. On cooling to room temperature hydrogen peroxide (10 mL, 30 wt% in water) was added and the solution left to stir for 1 h. Following extraction with diethyl ether (3 x 100 mL) and washing with a brine solution (1 × 50 mL), the combined organic extracts were dried over magnesium sulfate. Filtration followed by removal of the solvent on the rotary evaporator gave the crude product as a viscous brown oil. The catalyst residues were removed by a short silica column using a mixture of dichloromethane–hexane (80:20) as the eluent affording 2-(2-methoxybiphenyl-3-yl)-6-formylpyridine as a yellow oil (2.920 g, 86%). ^{1}H NMR (400 MHz, $CDCl_3$): δ 3.27 (s, 3H, OMe), 7.11–7.41 (m, 5H, Ar-H), 7.56–7.65 (m, 2H, Ar-H), 7.85 (dd, J_{HH} 7.7, 1.8, 1H, Py-H), 7.92–7.96 (m, 2H, Py-H, Ar-H), 8.13 (dd, J_{HH} 6.9, 1.4, 1H, Py-H), 10.16 (s, 1H, C*H*O). ^{13}C{^{1}H} NMR (100 MHz, $CDCl_3$): δ 61.0 (OCH3), 118.8, 123.7, 125.9, 126.9, 127.3, 128.2, 129.8, 131.4, 132.2, 134.9, 136.0, 137.3, 151.7, 154.6, 156.0, 192.8 (C*H*O). IR (cm^{-1}): 1712 (C=O), 1585 ($C=N_{pyridine}$). ESIMS: *m/z* 290 [M + H]+. HRMS (FAB): calcd for $C_{19}H_{15}NO_2$ $[M + H]^+$ 290.11770, found 290.11775.

Step 2 (Deprotection): A Schlenk flask equipped with stir bar was initially evacuated and backfilled with nitrogen and then charged with 2-(2-methoxybiphenyl-3-yl)-6-formylpyridine (2.380 g, 8.24 mmol), dichloromethane (40 mL) and the solution cooled to −78 °C. A 1M solution of boron tribromide in dichloromethane (18 mL, 18 mmol) was

added at −78 °C forming an orange solution. The solution was allowed to warm to room temperature and left to stir overnight. Water (40 mL) was added carefully and the mixture neutralised with potassium carbonate. The organic layer was separated and the aqueous phase washed repeatedly with chloroform (3 × 100 mL). All organic extracts were combined and the solvent removed on the rotary evaporator yielding 2-(3-biphenyl-2-ol)-6-formylpyridine as a green/gold foamy solid (1.830 g, 81%). Mp: 67–68 °C. ^{1}H NMR (400 MHz, $CDCl_3$): δ 6.96 (t, J_{HH} 6.8, 1H, Ar-H), 7.21–7.39 (m, 4H, Ar-H), 7.55 (d, J_{HH} 6.8, 2H, Ar-H), 7.86 (d, J_{HH} 7.7, 1H, Ar-H/Py-H), 7.92 (d, J_{HH} 7.7, 1H, Ar-H/Py-H), 8.07 (t, J_{HH} 7.7, 1H, Py-H), 8.13 (d, J_{HH} 6.9, 1H, Py-H), 10.17 (s, 1H, CHO), 14.22 (br s, 1H, OH). ^{13}C{^{1}H} NMR (100 MHz, $CDCl_3$): δ 117.2, 118.1, 118.7, 119.6, 123.3, 125.0, 126.3, 127.1, 128.9, 133.5, 137.0, 149.0, 156.3, 158.2, 189.8 (CH=O). IR (cm^{-1}): 1712 (C=O), 1591 ($C{=}N_{pyridine}$). ESIMS (+ve): m/z 276 $[M + H]^+$. ESIMS (−ve): *m/z* 274 $[M-H]^+$. HRMS (FAB): calcd for $C_{18}H_{14}NO_2$ $[M\ ]^+$ 275.09463, found 275.09469.

5.2.3 Synthesis of HL1

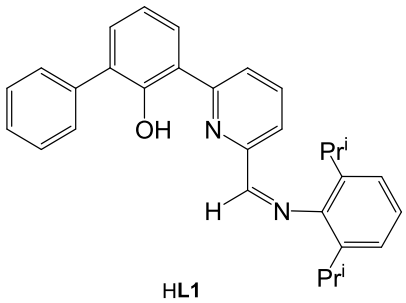

HL1

To a small round bottomed flask equipped with stir bar was added 2-(3-biphenyl-2-ol)-6-formylpyridine (1.83 g, 6.65 mmol), 2,6-diisopropylaniline (1.76 g, 9.98 mmol, 1.5 eq) and ethanol (13 mL). The suspension was stirred and heated to 40°C and after 15 min. a catalytic amount of formic acid was added. After further stirring at 40°C overnight a yellow precipitate formed which was allowed to cool to room temperature. The precipitate was filtered, washed with ethanol and further dried under reduced pressure to give H**L1** as a yellow solid (1.99 g, 69%). Yellow plates of H**L3** suitable for an X-ray determination were grown by slow evaporation of a methanol solution. Mp: 127-130 ºC. ^{1}H NMR (400 MHz, $CDCl_3$): δ 1.18 (d, $^{3}J_{HH}$ 6.9, 12H, $CH(CH_3)_2$), 2.95 (sept, $^{3}J_{HH}$ 6.9, 2H, $CH(CH_3)_2$), 7.04 (t, $^{3}J_{HH}$ 7.7, 1H, Ar-*H*), 7.10 (m, 3H, Ar-*H*), 7.35 (t, $^{3}J_{HH}$ 7.4, 1H, Ar-*H*), 7.35 (m, 3H, Ar-*H*), 7.66 (d, $^{3}J_{HH}$ 7.1, 2H, Ar-*H*), 7.88 (dd, $^{3}J_{HH}$ 8.1, $^{4}J_{HH}$ 1.4, 1H, Ar-*H*), 8.03 (t, $^{3}J_{HH}$ 7.9, 1H,

Ar-*H*), 8.11 (d, $^{3}J_{HH}$ 7.7, 1H, Ar-*H*), 8.24 (d, $^{3}J_{HH}$ 7.5, 1H, Ar-*H*), 8.33 (s, 1H, N=C*H*), 14.2 (br s, 1H, OH). $^{13}C\{^{1}H\}$ NMR (100 MHz, $CDCl_3$): δ 23.4 ($CH(CH_3)_2$), 27.9 ($CH(CH_3)_2$), 118.8 (C), 118.9, 119.2, 121.3, 123.1 (CH), 124.7 (C), 126.0, 127.0, 128.1, 129.5 (CH), 131.4 (C), 133.0 (CH), 137.0 (C), 138.4 (CH), 138.6, 148.2, 150.9, 157.0, 158.2 (C), 161.0 (N=*C*-H), IR (cm^{-1}): 2962 (C-H), 2600 (br, OH), 1641 ($C=N_{imine}$), 1589 ($C=N_{pyridine}$). ESI MS: *m/z* 435 $[(M+H)]^+$, 457 $[(M+Na)]^+$. HRMS (FAB): calcd. $C_{30}H_{31}N_2O$ $[M+H]^+$ 435.24286, found 435.24247.

5.2.4 Synthesis of HL2

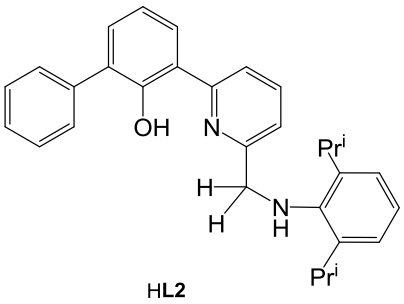

HL2

Two Schlenk flasks equipped with stir bars were evacuated and back filled with nitrogen. To one of the flasks was added lithium aluminium hydride (0.131 g, 3.46 mmol) and dry tetrahydrofuran (10 mL) and the resulting suspension stirred and cooled to 0 °C. To the second flask was added H**L1** (0.300 g, 0.69 mmol) and dry tetrahydrofuran (10 mL) and the contents stirred until dissolution. The solution of H**L1** was then transferred *via* cannular (dropwise) to the cooled $LiAlH_4$ suspension. The reaction mixture was allowed to warm to room temperature and stirred for 90 min. Water (2 mL) was carefully added followed by chloroform (30 mL) and more water (30 mL). The organic phase was separated and the aqueous layer extracted with chloroform. All organic extracts were combined and dried over magnesium sulfate. Filtration followed by removal of the solvent under reduced pressure gave H**L2** as a yellow brown oil (1.21 g, 76%). ^{1}H NMR (300 MHz, $CDCl_3$): δ 1.21 (d, $^{3}J_{HH}$ 6.8, 12H, $CH(CH_3)_2$), 3.28 (sept, $^{3}J_{HH}$ 6.8, 2H, $CH(CH_3)_2$), 3.45 (s, 1H, N-H), 4.22 (s, 2H, NH-CH_2), 6.89 (t, $^{3}J_{HH}$ 7.7, 1H, Ar-*H*), 7.0 (m, 3H, Ar-*H*), 7.24 (t, $^{3}J_{HH}$ 8.1, 1H, Ar-*H*), 7.30-7.40 (m, 4H, Ar-H/Py-*H*), 7.57 (d, $^{3}J_{HH}$ 7.0, 2H, Ar-*H*), 7.80-7.70 (m, 3H, Ar-*H*), 15.2 (br s, 1H, OH). $^{13}C\{^{1}H\}$ NMR (400 MHz, $CDCl_3$): δ 21.4 ($CH(CH_3)_2$), 23.2 ($CH(CH_3)_2$), 26.7 ($CH(CH_3)_2$), 55.4 ($NHCH_2$), 117.0, 117.5, 117.6, 118.0, 118.8, 121.7, 122.6, 123.4, 124.8, 125.9, 127.0, 128.5, 130.1, 131.4, 131.6, 137.4, 137.5, 139.2, 141.1,

141.9, 155.5, 155.3, 156.8. IR (cm^{-1}): 2962 (C-H), 2600 (br, OH), 1592 ($C=N_{pyridine}$), 1589. ESI MS (+ve): *m/z* 437 $[M+H]^+$. ESI MS (+ve): *m/z* 435 $[M-H]^+$. HRMS (FAB): calcd for $C_{30}H_{33}N_2O$ $[M+H]^+$ 437.2593, found 437.2599.

5.2.5 Synthesis of HL3

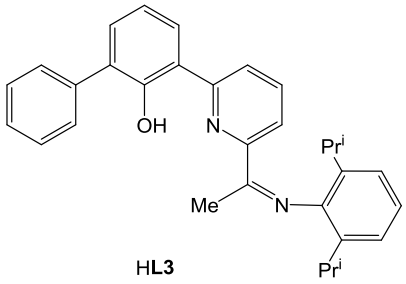

HL3

A 50 mL round bottom flask equipped with a stir bar was charged with 2-(3'-phenyl-2'-phenoxy)-6-acetylpyridine (0.733 g, 2.54 mmol), 2,6-diisopropylaniline (0.674 g, 3.81 mmol, 1.5 eq.) and absolute ethanol (7 mL). The solution was stirred at 100 ^oC for 15 min. before the addition of 1-2 drops of glacial acetic acid. After heating to reflux at 100 ^oC for 72 h, the reaction mixture was allowed to cool down to room temperature. A pale yellow precipitate formed which was filtered, washed with methanol and further dried under reduced pressure to give H**L3** as a pale yellow solid (0.895 g, 78%). Yellow plates of H**L3** suitable for and X-ray determination were grown by slow evaporation of a methanol solution. ^1H NMR (400 MHz, $CDCl_3$): δ [ppm] 1.13 (d, J_{HH} 6.7, 6H, $CH(CH_3)_2$), 1.15 (d, J_{HH} 6.1, 6H, $CH(CH_3)_2$), 2.23 (s, 3H, $N=C(CH_3)$), 2.70 (sept, J_{HH} 6.8, 2H, $CH(CH_3)_2$), 7.03 (t, 1H, J_{HH} 7.6, Ar-H), 7.10-7.18 (m,3H, Ar-H), 7.32-7.36 (m, 1H, Ar-H), 7.40 (dd, J_{HH} 7.6, 1.6, 1H, Ar-H), 7.42 (m, 2H, Ar-H), 7.65-7.67 (m, 2H, Ar-H), 7.88 (dd, J_{HH} 8.1, 1.6, 1H, Ar-H), 8.00 (t, J_{HH} 7.7, 1H, Py-H), 8.10 (d, J_{HH} 7.6, 1H, py-H), 8.34 (dd, J_{HH} 7.8, J_{HH} 0.8, 1H, Py-H), 14.45 (s, 1H, Ar-OH). $^{13}C\{^1H\}$ NMR (100 MHz, $CDCl_3$): δ 17.5 (CMe=N), 22.9, 23.2 (CH_3), 28.4 (CH), 118.9 (CH), 119.1 (C), 119.4, 120.9, 123.1, 123.9, 126.0, 127.1, 128.1, 129.6 (CH), 131.2 (C), 132.9 (CH), 135.7 (C), 138.4 (CH), 138.5, 146.0 (C), 153.1 (C), 156.9 (C), 157.1 (C), 164.8 (CMe=N). IR (cm^{-1}): 2960 (C-H), 1634 ($C=N_{imine}$), 1566 ($C=N_{pyridine}$). ESI MS: *m/z* 449 $[M+H]^+$, 471 $[M+Na]^+$. TOF MS(ES+): calcd for $C_{31}H_{32}NO_2$ $[M+H]^+$ 449.2593, found 449.2610.

5.2.6 Synthesis of HL4

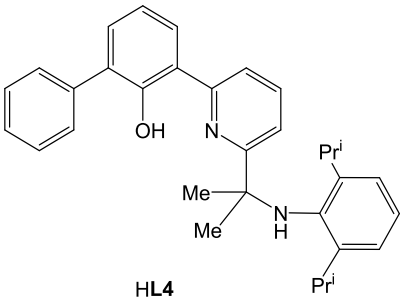

HL4

A Schlenk flask equipped with stir bar was evacuated and backfilled with nitrogen and charged with H**L3** (0.646 g, 1.44 mmol) and toluene (10 mL). A 2M trimethylaluminium solution (4.32 mL, 8.64 mmol, 6 eq.) was added dropwise and the solution stirred and heated to 110 ^{o}C for 96 h. On cooling to room temperature, deionised water (10 mL) was added very slowly. After stirring for 2 h the organic layer was separated and the aqueous layer extracted with diethylether (3 x 30 mL). All organic extracts were combined and dried over magnesium sulfate. Following filtration, the solvent was removed under reduced pressure affording H**L4** as a yellow-brown solid (0.508 g, 76%). ^{1}H NMR (400 MHz, $CDCl_3$): δ [ppm] 1.05 (d, J_{HH} 6.8, 12H, CH(CH_3)$_2$), 1.54 (s, 6H, NH-C(CH_3)$_2$), 3.03 (sept, J_{HH} 6.8, 2H, CH(CH_3)$_2$), 3.38 (br s, 1H, (NH)), 6.99 (t, J_{HH} 7.8, 1H, Ar-H), 7.04-7.06 (m, 3H, Ar-H), 7.29-7.34 (m, 1H, Ar-H), 7.38 (dd, J_{HH} 7.5, 1.6 1H, Ar-H), 7.40-7.44 (m, 3H, Ar-H), 7.65-7.70 (m, 3H, Ar-H), 7.84-7.86 (m, 3H, py-H), 14.95 (s, 1H, Ar-OH). ^{13}C{^{1}H} NMR (100 MHz, $CDCl_3$): δ 23.8 (CH_3), 28.4 (CH(Me_2)), 29.2 (CH_3), 59.1 (N-C(Me_2)), 117.2, 118.2, 118.5, 119.3(C), 123.1, 124.5, 125.8, 126.9, 128.0, 129.6, 131.0 (C), 132.5, 138.0, 138.6, 139.7, 145.5, 156.8, 157.4 (C), 166.1 (CMe=N). ESI MS: *m/z* 465 [M+H]$^{+}$. TOF MS(ES+): calcd for $C_{32}H_{36}N_2O$ [M+H]$^{+}$ 465.2906, found 465.2908.

5.2.7 Synthesis of 1a

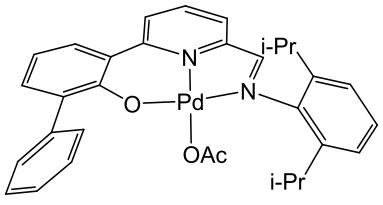

1a

A Schlenk flask equipped with stir bar was evacuated and backfilled with nitrogen and loaded with $Pd(OAc)_2$ (0.065 g, 0.29 mmol), H**L1** (0.126 g, 0.29 mmol) and dry toluene (10 mL). After stirring at 60 ºC overnight, the reaction mixture was cooled to room temperature and filtered through a celite pad and the pad thoroughly washed with dichloromethane. The filtrate was concentrated to *ca.* 1 mL whereupon diethyl ether (*ca.* 8 mL) was added. The resulting precipitate was filtered and dried under reduced pressure forming **1a** as a dark red powder (0.175 g, 91%). Red blocks suitable for an X-ray diffraction study could be grown by slow diffusion of hexane into a dichloromethane solution of the complex. Mp: > 260 ºC. ^{1}H NMR (400 MHz, $CDCl_3$): δ 1.11 (d, $^3J_{HH}$ 6.9, 6H, $CH(CH_3)_2$), 1.33 (d, $^3J_{HH}$ 6.9, 6H, $CH(CH_3)_2$), 1.65 (s, 3H, O=C-CH_3), 3.43 (sept, $^3J_{HH}$ 6.7, 2H, $CH(CH_3)_2$), 6.83 (t, $^3J_{HH}$ 8.1, 1H, Ar-*H*), 7.18 (d, $^3J_{HH}$ 7.6, 1H, Ar-*H*), 7.22 (d, $^3J_{HH}$ 7.8, 2H, Ar-*H*), 7.30 (m, 3H, Ar-*H*), 7.40 (d, $^3J_{HH}$ 7.0, 1H, Ar-H), 7.64 (d, $^3J_{HH}$ 7.1, 1H, Ar-*H*), 7.76 (d, $^3J_{HH}$ 7.1, 2H, Ar-*H*), 7.88 (d, $^3J_{HH}$ 8.5, 1H, Py-*H*), 8.02 (s, 1H, $N=C_{imine}$-*H*), 8.15 (t, $^3J_{HH}$ 8.3, 1H, Py-*H*), 8.52 (d, $^3J_{HH}$ 8.8, 1H, Py-*H*). ^{13}C{^{1}H} NMR (100 MHz, $CDCl_3$): δ 21.3 (H_3C-C=O), 21.9 ($CH(CH_3)_2$), 24.2 ($CH(CH_3)_2$), 27.5 ($CH(CH_3)_2$), 114.9 (CH), 119.3 (C), 122.4, 123.6, 125.5, 125.9, 126.5, 127.3, 127.6, 129.0, 132.5 (CH), 133.3 (C), 136.6 (CH), 138.9 (C), 140.2 (CH), 141.0, 151.1, 151.7, 160.4 (C), 165.0 (N_{imine}=CH), 176.5 (Me-*C*=O). IR (cm^{-1}): 2961 (C-H), 1615 ($C=N_{imine}$), 1582 $(COO)_{asymm}$/$C=N_{pyridine}$), 1383 $(COO)_{symm}$. FAB MS *m/z*: 539 $[M\text{-}OAc]^+$, 598 $[M]^+$. Anal calcd for ($C_{32}H_{32}N_2O_3Pd$): C, 64.97; H, 5.35; N, 4.68. Found: C, 64.88; H, 5.21; N, 4.72%.

5.2.8 Synthesis of 1b

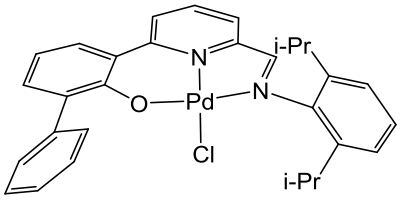

1b

Method 1. A Schlenk flask equipped with stir bar was evacuated and backfilled with nitrogen and loaded with $PdCl_2(NCMe)_2$ (0.060 g, 0.231 mmol), H**L1** (0.110 g, 0.254 mmol) and tetrahydrofuran (25 mL). After stirring overnight at room temperature, the reaction mixture was concentrated to *ca.* 2 mL and hexane (15 mL) added. The precipitate was filtered, washed with hexane and dried under reduced pressure to give **1b** as a dark red

powder (0.084 g, 53%). Red blocks suitable for an X-ray diffraction study could be grown by slow diffusion of hexane into a dichloromethane solution of the complex. Mp: > 260 ºC. ^{1}H NMR (300 MHz, $CDCl_3$): δ 1.00 (d, $^{3}J_{HH}$ 6.9, 6H, CH(CH_3)$_2$), 1.34 (d, $^{3}J_{HH}$ 6.6, 6H, CH(CH_3)$_2$), 3.22 (sept, $^{3}J_{HH}$ 7.0, 2H, CH(CH$_3$)$_2$), 6.83 (dd, $^{3}J_{HH}$ 8.4, 7.2, 1H, Ar-*H*), 7.21 (m, 3H, Ar-*H*), 7.35 (m, 3H, Ar-*H*), 7.53 (dd, $^{3}J_{HH}$ 7.2, $^{4}J_{HH}$ 1.6, 1H, Ar-*H*), 7.77 (dd, $^{3}J_{HH}$ 7.2, $^{4}J_{HH}$ 0.9, 1H, Ar-*H*), 7.86 (d, $^{3}J_{HH}$ 7.1, 2H, Py/Ar-*H*), 7.90 (dd, $^{3}J_{HH}$ 8.6, $^{4}J_{HH}$ 1.6, 1H, Ar-*H*), 7.99 (s, 1H, N=C-*H*), 8.16 (dd, $^{3}J_{HH}$ 8.7, 7.2, 1H, Py-*H*), 8.51 (d, $^{3}J_{HH}$ 8.7, 1H, Py-*H*). ^{13}C {^{1}H} NMR (75 MHz, $CDCl_3$): δ 22.1 (CH(*C*H$_3$)$_2$), 22.6 (CH(*C*H$_3$)$_2$), 27.6 (*C*H(CH$_3$)$_2$), 115.4, 119.5, 122.4, 124.4 (CH), 125.6 (C), 126.4, 126.6 (CH), 127.6, 127.7 (C), 129.1, 132.9 (CH), 133.4, 137.0, 138.8 (C), 139.6 (CH), 142.6 (C), 151.1 (CH), 151.4, 159.9 (C), 166.8 (N=CH). IR (cm^{-1}): 2961 (C-H), 1614 (C=N$_{imine}$), 1589 (C=N$_{pyridine}$). FAB MS *m/z*: 539 [M-Cl]$^{+}$, 575 [M+H]$^{+}$. Anal calcd for ($C_{30}H_{29}N_2OPdCl$): C, 62.62; H, 5.08; N, 4.87. Found: C, 62.61; H, 5.00; N, 4.81%.

Method 2. A round bottomed flask equipped with stirrer bar was loaded with **1a** (0.323 g, 0.054 mmol), chloroform (10 mL) and a saturated solution of brine (10 mL) added. After stirring vigorously at room temperature overnight the organic phase was separated and the aqueous phase washed with chloroform (3 x 10 mL). All organic extracts were combined and dried over magnesium sulfate. Following filtering, all volatiles were removed under reduced pressure affording **1b** as a red powders (0.031 g, 98%). The spectroscopic data obtained for **1b** were consistent with that given above.

5.2.9 Synthesis of 2a

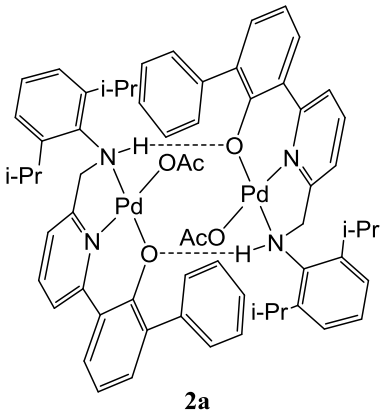

2a

A Schlenk flask equipped with stir bar was evacuated and backfilled with nitrogen and loaded with $Pd(OAc)_2$ (0.065 g, 0.29 mmol), H**L2** (0.126 g, 0.29 mmol) and dry toluene (10 mL). After stirring at 0 °C overnight, the reaction mixture was filtered through a celite pad and the pad thoroughly washed with dichloromethane. The filtrate was concentrated to *ca.* 1 mL whereupon diethyl ether (*ca.* 8 mL) was added. The resulting precipitate was filtered and dried under reduced pressure forming **2a** as a yellow powder (0.100 g, 58%). Yellow plates of **2a** suitable for an X-ray diffraction study could be grown by slow diffusion of hexane into a dichloromethane solution of the complex. Mp: > 260 °C. ^{1}H NMR (400 MHz, $CDCl_3$): δ 1.16 (d, $^3J_{HH}$ 6.8, 3H, CH(CH_3)$_2$), 1.17 (d, $^3J_{HH}$ 6.4, 3H, CH(CH_3)$_2$), 1.33 (d, $^3J_{HH}$ 6.5, 3H, CH(CH_3)$_2$), 1.58 (s, 3H, C(O)CH_3), 1.68 (d, $^3J_{HH}$ 6.8, 3H, CH(CH_3)$_2$), 3.24 (sept, $^3J_{HH}$ 6.7, 1H, CH(CH$_3$)$_2$), 4.16 (dd, $^2J_{HH}$ 17.3, $^3J_{HH}$ 9.2, 1H, HN-CH_aH$_b$), 4.58 (dd, $^2J_{HH}$ 17.2, $^3J_{HH}$ 10.0, 1H, HN-CH$_a$$H_b$), 5.21 (sept, $^3J_{HH}$ 6.7, 1H, CH(CH$_3$)$_2$), 6.77 (t, $^3J_{HH}$ 7.8, 1H, Ar-*H*), 6.84 (t, $^3J_{HH}$ 7.6, 1H, Ar-*H*), 7.07 (dd, $^3J_{HH}$ 6.4, $^4J_{HH}$ 3.2, 1H, Ar-*H*), 7.18 (t, $^3J_{HH}$ 7.2, 1H, Ar-H), 7.20-7.32 (m, 4H, Ar-H), 7.52 (dd, $^3J_{HH}$ 7.8, $^4J_{HH}$ 1.6, 1H, Ar-H), 7.54 (br t, $^3J_{HH}$ 8.0, 1H, *H*N-CH$_a$H$_b$), 7.73-7.79 (m, 3H, Py/Ar-H), 7.89 (d, $^3J_{HH}$ 8.0, 1H, Py-H). ^{13}C{^{1}H} NMR (75 MHz, $CDCl_3$) δ 21.5 (H$_3$*C*-C=O), 22.3 (CH(*C*H$_3$)$_2$), 23.5 (CH(*C*H$_3$)$_2$), 23.6 (CH(*C*H$_3$)$_2$), 24.9 (CH(*C*H$_3$)$_2$), 27.0 (*C*H(CH$_3$)$_2$), 27.7 (*C*H(CH$_3$)$_2$), 62.3 (HN-*C*H$_2$), 114.5, 114.9, 119.7, 122.6, 123.2, 125.1, 126.4, 126.5, 128.1, 128.9, 131.7, 132.5, 137.2, 137.8, 139.22, 140.0, 141.8, 152.8, 160.1, 161.2, 177.3 (Me-*C*=O). IR (cm^{-1}): 3224 (NH), 2954 (C-H), 1585 (COO_{asymm}/$C=N_{pyridine}$), 1384 (COO_{symm}). ESI MS: *m/z* 1141 [M_2-OAc], 541 [M-OAc]. FAB MS *m/z* 601 [M+H]$^+$, 534 [M-OAc]$^+$. Anal calcd for ($C_{32}H_{34}N_2O_3Pd$): C, 63.95; H, 5.70; N, 4.66. Found: C, 64.01; H, 5.55; N, 4.89%.

5.2.10 Synthesis of 2b

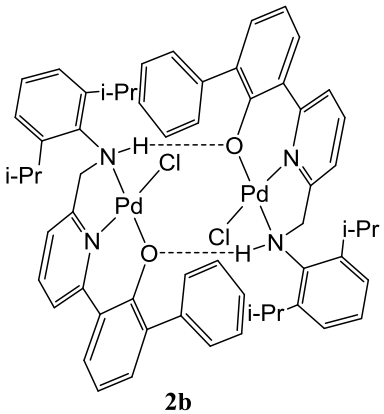

2b

A round bottomed flask equipped with stirrer bar was loaded with **2a** (0.032 g, 0.054 mmol), chloroform (10 mL) and a saturated solution of brine (10 mL) added. After stirring vigorously at room temperature overnight the organic phase was separated and the aqueous phase washed with chloroform (3 x 10 mL). All organic extracts were combined and dried over magnesium sulfate. Following filtering, all volatiles were removed under reduced pressure affording **2b** as yellowy brown powder (0.026 g, 87%). Yellow blocks suitable for an X-ray diffraction study could be grown by slow diffusion of hexane into a dichloromethane solution of the complex. Mp: > 260 ºC. ^{1}H NMR (400 MHz, $CDCl_3$): δ 0.73 (d, $^{3}J_{HH}$ 6.8, 3H, CH(CH_3)$_2$), 1.02 (br s, 3H, CH(CH_3)$_2$), 1.20 (br s, 3H, CH(CH_3)$_2$), 1.48 (d, $^{3}J_{HH}$ 6.5, 3H, CH(CH_3)$_2$), 3.34 (dd, $^{2}J_{HH}$ 17.7, $^{3}J_{HH}$ 1.8, 1H, HN-CH_aH$_b$), 3.72 (br s, 1H, CH(CH$_3$)$_2$), 4.21 (sept, $^{3}J_{HH}$ 6.5, 1H, CH(CH$_3$)$_2$), 4.99 (dd, $^{2}J_{HH}$ 17.7, $^{3}J_{HH}$ 7.9, 1H, HN-CH$_a$$H_b$), 5.98 (br, s, 1H, HN-CH$_2$), 6.60 (t, $^{3}J_{HH}$ 7.5, 1H, Ar-H), 7.05-7.24 (m, 7H, Py/Ar-H), 7.26 (t, $^{3}J_{HH}$ 7.5, 2H, Ar-H), 7.35 (br s, 2H, Py-H), 7.88 (d, $^{3}J_{HH}$ 8.1, 2H, Ar-H). IR (cm^{-1}): 3223 (NH), 2955 (CH), 1598 (C=N$_{pyridine}$). ESI MS *m/z* 1118 [M$_2$-Cl]$^+$, 539 [M-Cl]$^+$. FABMS *m/z* 574 [M]$^+$, 539 [M-Cl]$^+$. Anal Calcd for (C$_{30}$H$_{31}$N$_2$OPdCl): C, 62.40; H, 5.41; N, 4.85. Found: C, 62.69; H, 5.25; N, 4.92%.

5.2.11 Synthesis of 3a

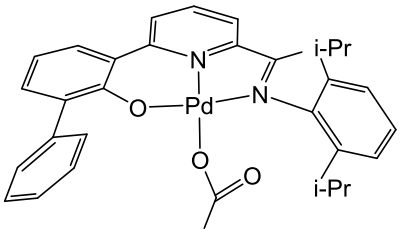

3a

A small Schlenk flask equipped with stir bar was evacuated and backfilled with nitrogen. The flask was charged with H**L3** (0.100 g, 0.223 mmol), Pd(OAc)$_2$ (0.050 g, 0.223 mmol) and dry toluene (10 ml). After stirring at 60 ºC for two days, the reaction mixture was filtered through celite pad and the pad thoroughly washed with dichloromethane. The filtrate was dried under reduced pressure to give crude **3a** as red solid (0.122 g, 82%). Orange blocks of **3a** suitable for an X-ray diffraction study could be grown by slow diffusion of hexane into a dichloromethane solution of the complex. ^{1}H NMR (400 MHz, $CDCl_3$): δ 1.05 (d, J_{HH} 6.9, 6H, CH(CH_3)$_2$), 1.37 (d, J_{HH} 6.9, 6H, CH(CH_3)$_2$), 1.50 (s, 3H,

CH_3CO_2), 2.21 (s, 3H, NCMe), 3.22 (sept, J_{HH} 6.7, 2H, $CH(CH_3)_2$), 6.83 (t, J_{HH} 8.1, 1H, Ar-H), 8.05 (t, J_{HH} 8.3, 1H, Py-H), 8.52 (d, J_{HH} 8.8, 1H, Py-H). Mp: > 260 °C. IR (cm^{-1}): 2960 (C-H), 1610 $(C=N)_{imine}$, 1589 $(COO)_{asymm}/C=N_{pyridine}$), 1385 $(COO)_{symm.}$ ESIMS: *m/z* 1171 [M_2 − OAc], 555 [M − OAc]. FABMS *m/z* 615 $[M + H]^+$, 554 $[M - OAc]^+$. Anal Calcd for ($C_{33}H_{34}N_2O_3Pd$): C, 64.44; H, 5.90; N, 4.55. Found: C, 64.09; H, 5.75; N, 4.79%.

5.2.12 Synthesis of 3b

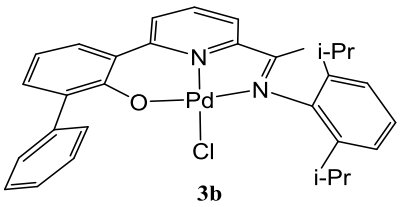

3b

A round bottomed flask equipped with stirrer bar was loaded with **3a** (0.100 g, 0.163 mmol), chloroform (10 mL) and a saturated solution of brine (10 mL) was added. After stirring vigorously at room temperature overnight the organic phase was separated and the aqueous phase washed with chloroform (3 x 10 mL). All organic extracts were combined and dried over magnesium sulfate. Following filtering, all volatiles were removed under reduced pressure affording **3b** as a red powder (0.091 g, 95%). ^1H NMR (400 MHz, $CDCl_3$): δ 1.10 (d, J_{HH} 7.0, 6H, $CH(CH_3)_2$), 1.39 (d, J_{HH} 6.7, 6H, $CH(CH_3)_2$), 2.25 (s, 3H, $C(CH_3)$), 3.16 (sept, J_{HH} 6.7, 2H, $CH(CH_3)_2$), 6.82 (dd, J_{HH} 8.2, 2.0 2H, ArH), 6.99 (m, 1 H, ArH), 7.13 (m, 3H, ArH), 7.26 (m, 1 H, ArH), 7.35 (m, 2 H, ArH), 7.67 (d, J_{HH} 7.4, 1 H, ArH), 7.73 (d, J_{HH} 7.0, 1H, ArH), 7.97 (d, J_{HH} 7.0 , 1H, ArH), 8.26 (t, J_{HH} 8.0, 1H, ArH), 8.42 (d, J_{HH} 8.0, 1H, ArH). Mp: > 260 °C. IR (cm^{-1}): 2960 (C-H), 1610 $(C=N)_{imine}$, 1589 $C=N_{pyridine}$).. ESIMS: *m/z* 555 [M − Cl]. FABMS *m/z* 554 $[M - Cl]^+$.

5.2.13 Synthesis of 3c

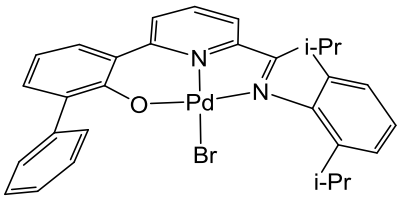

3c

A round bottomed flask equipped with stirrer bar was loaded with **3a** (0.100 g, 0.163 mmol), chloroform (10 mL) and a saturated solution of sodium bromide (10 mL) was added. After stirring vigorously at room temperature overnight the organic phase was separated and the aqueous phase washed with chloroform (3 x 10 mL). All organic extracts were combined and dried over magnesium sulfate. Following filtering, all volatiles were removed under reduced pressure affording **3c** as a red powder (0.092 g, 89%).

NMR (400 MHz, CDCl3): δ 1.10 (d, J_{HH} 7.0, 6H, CH(CH_3)$_2$), 1.45 (d, J_{HH} 6.7, 6H, CH(CH_3)$_2$), 2.21 (s, 3H, C(CH_3)), 3.03 - 3.15 (m, 2H, C*H*(CH_3)$_2$), 6.84 (dd, J_{HH} 8.2, 7.0, 1H, ArH), 7.18 - 7.25 (m, 3H, ArH), 7.29 - 7.38 (m, 3H, ArH), 7.47 (dd, J_{HH} 7.0, 1.6, 1H, ArH), 7.72 (d, J_{HH} 7.0, 1H, ArH), 7.79 (dd, J_{HH} 8.2, 1.6, 1H, ArH), 7.88 (dd, J_{HH} 8.2, 1.2, 2H, ArH), 8.13 (dd, J_{HH} 8.6, 7.8, 1H, ArH), 8.46 (d, J_{HH} 8.2, 1H, ArH). Mp: > 260 °C. IR (cm^{-1}): 2960 (C-H), 1611 $(C=N)_{imine}$. ESI MS: *m/z* 554 [M − Br].

5.2.14 Synthesis of 4a

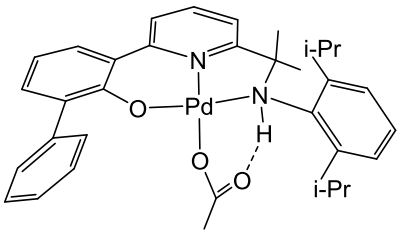

4a

A small Schlenk flask equipped with stir bar was evacuated and backfilled with nitrogen. The flask was charged with H**L4** (0.100 g, 0.215 mmol), $Pd(OAc)_2$ (0.048 g, 0.215 mmol) and dry toluene (10 ml). After stirring at 60 ºC for two days, the reaction mixture was filtered through a celite pad and the pad thoroughly washed with dichloromethane. The filtrate was dried under reduced pressure to give crude **4a** as red solid (0.120 g, 89%).

Orange coloured crystals of **4a**·OH_2 suitable for an X-ray diffraction study were grown by slow diffusion of petroleum ether into a chloroform solution of the complex. Alternatively, crystals of the non-solvated **4a** could be grown by slow evaporation of a concentrated benzene solution. Mp. > 188 ^{o}C (decomposed). ^{1}H NMR (400 MHz, $CDCl_3$): δ 0.83 (d, $^{3}J_{HH}$ 6.9, 3H, CH(CH_3)$_a$), 1.25 (d, J_{HH} 6.5, 3H, CH(CH_3)$_b$), 1.27 (d, J_{HH} 6.8, 3H, CH(CH_3)$_b$), 1.29 (s, 3H, O=C(O)-CH_3), 1.69 (d, J_{HH} 6.7, 3H, CH(CH_3)$_a$), 1.95 (s, 3H, C(*Me*)$_2$), 2.42 (s, 3H, C(*Me*)$_2$), 3.25 (sept, J_{HH} 6.6, 1H, CH_b(CH_3)), 3.53 (sept, J_{HH} 6.8, 1H, CH_a(CH_3)), 6.78 (dd, J_{HH} 8.2, 7.3, 1H, Ar-H), 6.94 (m, 1H, py-H), 7.09 (dd, J_{HH} 7.6, 1.7, 1H, Ar-H), 7.13 (dd, J_{HH} 7.7, 1.7, 1H, Ar-H), 7.18-7.23 (m, 2H, Ar-H), 7.31 (t, J_{HH} 7.4, 2H, Ar-H), 7.37 (dd, J_{HH} 7.2, 1.7, 1H, Ar-H), 7.54 (dd, J_{HH} 8.2, 1.7, 1H, Ar-H), 7.76-7.79 (m, 2H, Ar-H), 7.84-7.85 (m, 2H, py-H), 8.72 (s, 1H, NH). ^{13}C{^{1}H} NMR (100 MHz, $CDCl_3$): δ 22.8 (H_3*C*COO), 23.1 (CH(*C*H_3)$_2$), 24.9 (CH(*C*H_3)$_2$), 25.1 (CH_3), 25.2 (CH(*C*H_3)$_2$), 25.6 (CH_3), 28.3 (CH(*C*H_3)$_2$), 28.7 (*C*H(CH_3)$_2$), 33.4 (*C*H(CH_3)$_2$), 72.5 (*C*(CH_3)$_2$), 116.1, 116.7, 121.5, 124.6, 125.2, 125.7, 126.3, 127.4, 127.8, 128.9, 129.9, 133.2, 133.4, 135.6, 138.9, 139.7, 143.8, 144.2, 153.9, 170.1, 180.1 (H_3C*C*OO). IR (cm^{-1}): 3212 (NH), 2957 (C-H), 1594 (COO_{asymm}/C=$N_{pyridine}$), 1371 (COO_{symm}). ESI MS *m/z*: 610 [M-OAc+MeCN]$^{+}$, 596 [M-OAc+Na]$^{+}$. FAB MS *m/z*: 628 [M-H]$^{+}$, 569 [M-OAc]$^{+}$. Anal calcd for ($C_{32}H_{32}N_2O_3Pd$): C, 64.91; H, 6.09; N, 4.45. Found: C, 64.78; H, 6.13; N, 4.54%.

5.2.15 Synthesis of 4b

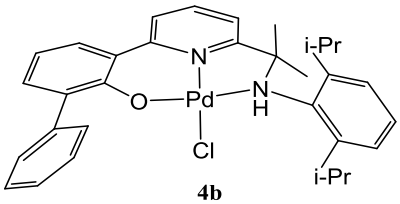

4b

A 50 mL round bottom flask equipped with stirrer bar was loaded with **4a** (0.045 g, 0.072 mmol) and a saturated solution of brine (10 mL) added. After stirring vigorously at room temperature overnight the organic phase was separated and the aqueous phase washed with chloroform (3 x 10 mL). All organic extracts were combined and dried over magnesium sulphate. Following filtering, all volatiles were removed under reduced pressure affording **4b** as an orange red solid (0.041 g, 94%). Orange–red coloured crystals were grown by slow diffusion of petroleum ether into a dichloromethane solution of the complex. Mp. > 300 ^{o}C. ^{1}H NMR (400 MHz, $CDCl_3$): δ 0.91 (d, J_{HH} 6.8, 3H, CH(*CH*$_3$)$_a$, 1.31 (s, 3H,

NHC(CH_3)), 1.32 (d, J_{HH} 7.2, 3H, CH(CH_3)$_b$), 1.47 (d, J_{HH} 6.5, 3H, CH(CH_3)$_b$, 1.62 (d, J_{HH} 6.7, 3H, CH(CH_3)$_a$), 2.25 (s, 3H, NHC(CH_3), 3.12 (sept, J_{HH} 6.6, 1H, CH^b(CH_3)$_2$), 3.29 (sept, J_{HH} 6.8, 1H, CH^a(CH_3)$_2$), 6.22 (s, 1H, NHC(CH_3)$_2$), 6.78 (dd, J_{HH} 7.3, 8.2, 1H, Ar-H), 6.94 (dd, J_{HH} 7.3, 1.4, 1H, py-H), 7.12-7.23 (m, 4H, Ar-H), 7.32 (t, J_{HH} 7.9, 2H, Ar-H), 7.36 (dd, J_{HH} 7.2, 1.6, 1H, Ar-H), 7.54 (dd, J_{HH} 8.3, 1.6, 1H, Ar-H), 7.80 (dd, J_{HH} 1.32, 8.4, 2H, Ar-H), 7.88 (m, 2H, Ar-H/Py-H). $^{13}C\{^1H\}$ NMR (100 MHz, $CDCl_3$): δ 21.5 (CH(CH_3)$_2$), 23.6 (CH(CH_3)$_2$, 23.6 (CH(CH_3)$_2$, 23.8 (CH_3), 24.4 (CH(CH_3)$_2$, 27.9 (CH_3), 28.1 (CH(CH_3)$_2$, 33.2 (CH(CH_3)$_2$), 72.0 (C(CH_3)$_2$), 115.1, 115.8 120.8, 123.5, 123.5, 124.65, 125.2, 126.5, 126.8, 128.1, 129.0, 132.1, 132.8, 134.7, 138.2, 138.7, 141.3, 141.9, 152.1, 160.9, 167.7. ESI MS: *m/z*: 611 $[M\text{-}Cl+MeCN]^+$. FAB MS *m/z*: 604 $[M]^+$, 569 $[M\text{-}Cl]^+$. IR (cm^{-1}): 3299 (NH), 2963 (CH), 1588 ($C{=}N_{pyridine}$). Anal calcd for ($C_{32}H_{39}N_2OClPd{\cdot}CH_2Cl_2{\cdot}1/3H_2O$): C, 57.32; H, 5.89; N, 3.93. Found: C, 57.14; H, 4.00; N, 4.27%.

5.2.16 Synthesis of 4c

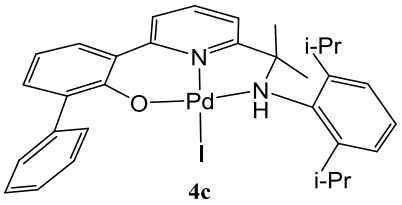

4c

A 50 ml round bottom flask equipped with stirrer bar was loaded with **4a** (0.045 g, 0.072 mmol) and a saturated aqueous solution of sodium iodide (10 mL) added. After stirring vigorously at room temperature overnight the organic phase was separated and the aqueous phase was washed with dichloromethane (3 x 10 mL). All organic extracts were combined and dried over magnesium sulphate. Following filtering, all volatiles were removed under reduced pressure affording **4c** as orange red solid (0.041g, 91%). Orange–red coloured crystals were grown by slow diffusion of petroleum ether into a dichloromethane solution of the complex. Mp > 300 ^oC (decomposed). ^1H NMR (400 MHz, $CDCl_3$): δ 0.78 (d, J_{HH} 7.0, 3H, CH(CH_3)$^a{}_2$, 1.20 (s, 3H, NHC(CH_3)), 1.26 (d, J_{HH} 6.7, 3H, CH(CH_3)^b), 1.46 (d, J_{HH} 6.3, 3H, CH(CH_3)^b, 1.48 (d, J_{HH} 7.0, 3H, CH(CH_3)^a), 2.12 (s, 3H, NHC(CH_3), 2.96 (sept, J_{HH} 6.6, 1H, CH^b(CH_3)$_2$), 3.55 (sept, J_{HH} 6.6, 1H, CH^a(CH_3)$_2$), 6.05 (s, 1H, NHC(CH_3)$_2$), 6.72 (t, J_{HH} 7.3, 8.2, 1H, Ar-H), 6.94 (d, J_{HH} 7.4, 1H, py-H), 7.05 (m, 2H, Ar-H), 7.14 (m, 2H, Ar-H), 7.25 (m, 3H, Ar-H) 7.51 (dd, J_{HH} 8.2, 1.6, 1H, Ar-H), 7.70 (m,

2H, Ar-*H*), 7.87 (m, 2H, Ar-H/Py-H). $^{13}C\{^{1}H\}$ NMR (100 MHz, $CDCl_3$): δ 23.0, 24.9, 25.1, 25.2, 25.5, 29.0, 29.6, 34.5, 74.5, 116.8, 122.4, 124.4, 124.9, 125.9, 126.7, 127.6, 127.8, 128.4, 129.4, 130.5, 133.8, 135.2, 136.6, 139.6, 139.7, 142.1, 142.0, 142.2, 143.7, 153.1, 161.8, 167.7. ESI MS *m/z*: 611 $[M\text{-}I+MeCN]^+$. FAB MS *m/z*: 569 $[M\text{-}I]^+$.

5.2.17 Synthesis of 5a

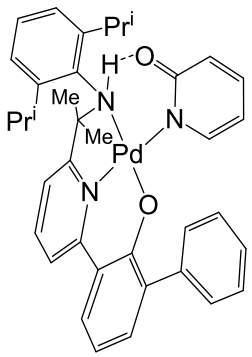

5a

A small Schlenk flask equipped with stir bar was evacuated and backfilled with nitrogen and loaded with $Pd(OAc)_2$ (0.024 g, 0.108 mmol), H**L4** (0.050 g, 0.108 mmol) and dry toluene (10 mL). After overnight stirring at 60 ^oC, the reaction mixture was cooled down to room temperature and 2-hydroxypyridine (Hhp) (0.010 g, 0.108 mmol) added. After stirring overnight at room temperature the reaction mixture was filtered through a celite pad and the pad thoroughly washed with dichloromethane. The filtrate was concentrated and dried under reduced pressure forming a red solid (0.059 g, 82%). Orange–red coloured crystals suitable for and X-ray determination were grown by slow diffusion of petroleum ether into a dichloromethane solution of the complex. ^1H NMR (400 MHz, $CDCl_3$): δ 0.72 (d, J_{HH} 6.8, 3H, $CH(CH_3)_2$), 1.12 (d, J_{HH} 6.3, 3H, $CH(CH_3)_2$), 1.25 (s, 3H, NH-$C(CH_3)_2$), 1.26 (d, J_{HH} 6.0, 3H, $CH(CH_3)_2$), 1.42 (d, J_{HH} 6.8, 3H, $CH(CH_3)_2$), 2.44 (s, 3H, NH-$C(CH_3)_2$), 3.49 (sept, J_{HH} 6.5, 1H, $CH(CH_3)_2$), 4.27 (sept, J_{HH} 6.8 1H, $CH(CH_3)_2$), 5.48 (td, J_{HH} 6.5, 1.4, 1H, Ar-H), 6.13 (dd, J_{HH} 8.6, 0.8, 1H, Ar-H), 6.72 (dd, J_{HH} 5.8, 1.64, 1H, py-H), 7.79 (dd, J_{HH} 8.2, 7.2, 1H, Ar-H), 6.97-7.03 (m, 4H, Ar-H), 7.11 (t, J_{HH} 7.7, 1H, py-H), 7.20-7.25 (m, 3H, Ar-H), 7.34 (dd, J_{HH} 7.2, 1.8, 1H, Ar-H), 7.46-7.49 (m, 2H, Ar-H), 7.60 (dd, J_{HH} 8.4, 1.7, Ar-H), 7.85-7.93 (m, 2H, py-H), 10.38 (s, 1H, NH). $^{13}C\{^{1}H\}$ NMR (100 MHz, $CDCl_3$): δ 22.9 ($CH(CH_3)_2$, 25.0 ($CH(CH_3)_2$, 25.4 (CH_3), 25.9 ($CH(CH_3)_2$, 28.6 (CH_3), 28.8 ($CH(CH_3)_2$, 33.3 ($CH(CH_3)_2$, 72.3 ($C(CH_3)_2$, 106.8, 108.5, 115.6, 115.8, 116.9,

121.4, 124.3, 125.3, 126.1, 127.5, 128.4, 129.7, 129.9, 132.9, 133.9, 134.7, 136.6, 137.9, 138.9, 140.4, 144.9, 145.1, 147.4, 154.2, 170.2, 170.8. FAB MS *m/z*: 664 $[M]^+$, 569 $[M\text{-}Hhp]^+$. ESI MS: *m/z*: 664 $[M]^+$.

5.2.18 Synthesis 5b

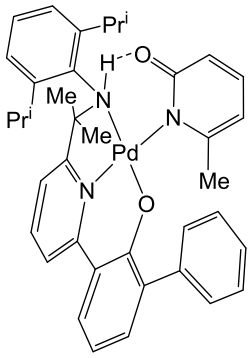

5b

Employing a similar procedure to that described for **5a** using $Pd(OAc)_2$ (0.024 g, 0.108 mmol), H**L4** (0.050 g, 0.108 mmol) and 6-methyl-2-hydroxypyridine (Hmhp) gave **5b** as a red solid (0.061 g, 84%). Red blocks suitable for an X-ray diffraction study could be grown by slow diffusion of hexane into a dichloromethane solution of the complex. Mp: > 260 ºC. ^{1}H NMR (400 MHz, $CDCl_3$): δ 0.81 (d, J_{HH} 6.7, 3H, CH(CH_3)$_2$), 0.85 (d, J_{HH} 6.4, 3H, CH(CH_3)$_2$), 1.19 (d, J_{HH} 6.6, 3H, CH(CH_3)$_2$), 1.35 (s, 3H, C(CH_3)$_2$), 1.45 (d, J_{HH} 6.7, 3H, CH(CH_3)$_2$), 1.74 (s, 3H, C(CH_3)$_2$), 2.54 (s, 3H, (CH_3)), 3.49 (m, 2H, C*H*(CH_3)$_2$), 5.53 (d, J_{HH} 6.7, 1H, Hmhp-H), 6.15 (d, J_{HH} 8.7, 1H, Hmhp-*H*), 6.76 (dd, J_{HH} 7.3, 8.1, 1H, Hmhp-*H*), 6.98 (m, 2H, Ar-*H*), 7.09 (m, 2H, Ar-*H*), 7.40 (dd, J_{HH} 7.2, 1.7, 1H, Ar-*H*), 7.48 (m, 2H, Ar-*H*), 7.62 (dd, J_{HH} 8.2, 1.6, 1H, Ar-*H*), 7.88 (m, 2H, Ar-*H*), 9.53 (s, 1H, NH). ESI MS *m/z*: 678 $[M]^+$. FABMS *m/z*: 678 $[M]^+$, 569 $[M\text{-}mhp]^+$. Anal calcd for ($C_{38}H_{41}N_3O_2Pd\cdot0.5CH_2Cl_2$): C, 64.17; H, 5.87; N, 4.92. Found: C, 64.71; H, 6.46; N, 5.81%.

5.2.19 Synthesis of 5c

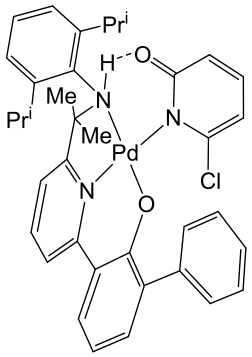

5c

Employing a similar procedure to that described for **5a** using $Pd(OAc)_2$ (0.024 g, 0.108 mmol), H**L4** (0.050 g, 0.108 mmol) and 2-chloro-6-hydroxypyridine (Hchp) gave **5c** as a red solid (0.061 g, 84%). Red blocks of **5c** suitable for an X-ray diffraction study could be grown by slow diffusion of hexane into a dichloromethane solution of the complex. ^{1}H NMR (400 MHz, $CDCl_3$): δ 0.77 (d, J_{HH} 6.9, 3H, $CH(CH_3)$), 0.88 (d, J_{HH} 6.9, 3H, $CH(CH_3)$), 1.21 (d, J_{HH} 6.6, 3H), 1.31 (s, 3H, CH_3), 1.50 (d, J_{HH} 6.6, 3H, CH_3), 2.56 (s, 3H, CH_3), 3.38 (sept, J_{HH} 6.5, 1H, $CH(CH_3)$), 3.62 (sept, J_{HH} 6.7, 1H, $CH(CH_3)$), 5.80 (d, J_{HH} 6.5, 1H, Pyridone-H), 6.20 (dd, J_{HH} 8.6, 1.0, Ar-H), 6.76 (dd, J_{HH} 7.2, 1.7, 1H, Ar-H), 6.95-7.17 (m, 8H, Ar-H), 7.37 (dd, J_{HH} 7.2, 1.7, 1H, Ar-H), 7.54 (m , 2H, Ar-H), 7.61 (dd, J_{HH} 8.2, 1.7, 1H, Ar-H), 7.86 (m, 2H, Ar-H), 9.05 (s, 1H, NH). $^{13}C\{^1H\}$ NMR (100 MHz, $CDCl_3$): 23.6 ($CH(CH_3)_2$, 24.8 ($CH(CH_3)_2$, 24.9 ($CH_3)_2$, 25.0 ($CH(CH_3)_2$, 25.1 ($CH_3)_2$, 28.2 ($CH(CH_3)_2$, 28.5 (*C*$H(CH_3)_2$, 34.1 (*C*$H(CH_3)_2$, 73.0 (*C*$(CH_3)_2$, 106.8, 113.6, 115.7, 116.6, 121.5, 124.6, 124.8, 125.6, 125.7, 127.0, 127.5, 128.9, 129.8, 133.1, 133.9, 136.3, 139.0, 139.1, 140.0, 143.3, 143.8, 147.5, 153.6, 162.2, 169.7, 171.7. ESI MS *m/z*: 698 $[M+H]^+$. FABMS *m/z*: 698 $[M+H]^+$, 569 $[M\text{-chp}]^+$.

5.2.20 Synthesis 5d

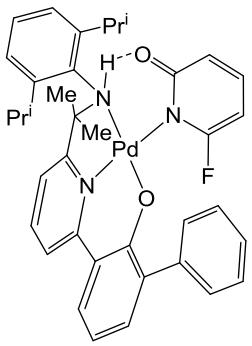

5d

Employing a similar procedure to that described for **5a** using $Pd(OAc)_2$ (0.024 g, 0.108 mmol), H**L4** (0.050 g, 0.108 mmol) and 6-fluoro-2-hydroxypyridine (Hfhp) (0.012 g, 0.108 mmol) gave **5d** as a red solid (0.065 g, 89%). Red-orange blocks of **5d** suitable for an X-ray diffraction study could be grown by slow diffusion of hexane into a dichloromethane solution of the complex. ^{1}H NMR (400 MHz, $CDCl_3$): δ 0.73 (d, J_{HH} 6.8, 3H, CH_3), 0.91 (d, J_{HH} 6.4, 3H, CH_3), 1.16 (d, J_{HH} 6.7, 3H, CH_3), 1.20 (s, 3H, (CH_3)), 1.50 (d, J_{HH} 6.7, 3H, CH_3), 2.39 (s, 3H, CH_3), 3.34 (sept, J_{HH} 6.5, 1H, $CH(CH_3)$), 3.78 (sept, J_{HH} 6.7, 1H, $CH(CH_3)$), 5.28 (d, J_{HH} 7.4, 1H, pyridone-H), 5.99 (d, J_{HH} 8.5, 1H, pyridone-H), 6.69 (dd, J_{HH} 8.2, 7.2, 1H, pyridone-H), 6.90 (m, 2H, Ar-H), 7.05 (m,7H, Ar-H), 7.25 (dd, J_{HH} 7.2, 1.7, 1H, Ar-H), 7.41 (m, 2H, py-H), 7.55 (dd, J_{HH} 8.3, 1.6, 1H, py-H), 7.81 (m, 2H, Ar-H), 9.27 (s, 1H, NH). ^{13}C{^{1}H} NMR (100 MHz, $CDCl_3$): δ 23.2 ($CH(CH_3)_2$, 24.8 ($CH(CH_3)_2$, 25.0 ($CH_3)_2$, 25.3 ($CH(CH_3)_2$, 28.4 ($CH_3)_2$, 28.6 ($CH(CH_3)_2$, 33.6, 72.8 (*C*H($CH_3)_2$, 89.1 (*C*H($CH_3)_2$, 89.4 (*C* ($CH_3)_2$, 111.1, 115.8, 116.6, 121.5, 123.8, 125.0, 125.5, 125.8, 127.1, 127.7, 129.0, 129.5, 133.2, 134.2, 136.0, 138.9, 140.0, 140.5, 140.6, 143.9, 144.4, 153.6, 161.9, 163.7, 170.1, 170.6. ^{19}F{^{1}H} NMR (376 MHz, $CDCl_3$) δ 69.27. ^{19}F NMR: δ 69.26 (F, J_{FH} 8.4). ESI MS *m/z*: 682 $[M]^+$, 610 [M-fhp+MeCN], 569 [M-fhp], TofMS: calcd 682.2061, found : 682.2093. Anal calcd for ($C_{37}H_{38}FN_3O_2Pd$): C, 65.15; H, 5.61; N, 6.16. Found: C, 65.12; H, 5.62; N, 6.13%.

5.2.21 Synthesis of 6

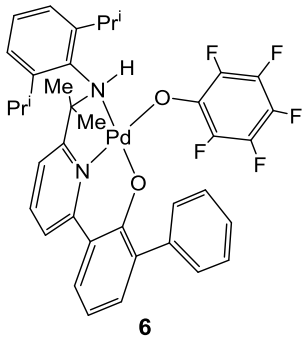

6

A small Schlenk flask equipped with stir bar was evacuated and backfilled with nitrogen and loaded with **4a** (0.040 g, 0.064 mmol), pentafluorophenol (0.012 g, 0.064 mmol) and dry toluene (10 mL). After overnight stirring at room temperature, the reaction mixture was dried under reduced pressure to afford **6** as red solid (0.042 g, 87%). ^{1}H NMR (400 MHz, $CDCl_3$): δ 0.95 (d, J_{HH} 6.8, 3H, $CH(CH_3)_2$), 1.18 (d, J_{HH} 6.6, 3H, $CH(CH_3)_2$), 1.32 (d, J_{HH} 6.6, 3H, $CH(CH_3)_2$), 1.36 (s, 3H, $C(CH_3)_2$), 1.64 (d, J_{HH} 6.6, $CH(CH_3)_2$), 2.37 (s, 3H, $C(CH_3)_2$), 3.06-3.14 (m, 2H, $CH(CH_3)_2$), 6.41 (s, 1H, N*H*), 6.70 (dd, J_{HH} 8.2, 7.2, 1H, Ar-H), 6.93 (dd, J_{HH} 6.5, 2.3, 1H, py-H), 7.06 (dd, J_{HH} 7.6, 1.6, 1H, Ar-H), 7.13-7.23 (m, 6H, Ar-H), 7.28-7.30 (m, 2H, Ar-H), 7.56 (dd, J_{HH} 8.4, 1.7, 1H, Ar-H), 7.85-7.86 (m, 2H, py-H). ^{13}C{^{1}H} NMR (100 MHz, $CDCl_3$): δ 22.7 ($CH(CH_3)_2$, 24.1 ($CH(CH_3)_2$, 24.2 ($C(CH_3)_2$, 25.3 ($CH(CH_3)_2$, 28.9 ($CH(CH_3)_2$ 29.2 ($CH(CH_3)_2$, 34.5 ($C(CH_3)_2$), 115.7, 115.9, 121.7, 123.0, 124.3, 125.8, 125.9, 127.0, 127.5, 127.8, 128.8, 129.0, 130.0, 133.6, 134.3, 135.2, 138.5, 139.7, 142.2, 142.7, 154.1, 169.5. ^{19}F{^{1}H} NMR (376 MHz, $CDCl_3$) δ -178.55 (m, 1F), -168.92 (t, J_{FH} 24, 2F), -162.32 (dd, J_{FH} 24, 8, 2F). IR (cm^{-1}): 3299 (NH), 2962 (CH), 1596 ($C{=}N_{pyridine}$), 1499 (983 (CF). Anal calcd for ($C_{38}H_{35}F_5N_2O_2Pd$): C, 60.60; H, 5.68; N, 3.72. Found: C, 60.75; H, 4.73; N, 3.75%.

5.2.22 Synthesis of 7a

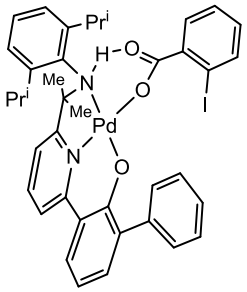

7a

A small Schlenk flask equipped with stir bar was evacuated and backfilled with nitrogen and loaded with **4a** (0.030 g, 0.048 mmol), 2-iodobenzoic acid (0.012 g, 0.048 mmol) and dry toluene (10 mL). After overnight stirring at room temperature, the reaction mixture was dried under reduced pressure to afford **7a** as a yellow-orange solid (0.030 g, 76%). Red-orange blocks of **7a** suitable for an X-ray diffraction study could be grown by slow diffusion of hexane into a dichloromethane solution of the complex. Mp. > 270 ^{o}C. ^{1}H NMR (400 MHz, $CDCl_3$): δ 0.80 (d, J_{HH} 6.6, 3H, CH(CH_3)$_2$), 1.00 (d, J_{HH} 6.3, 3H, CH(CH_3)$_2$), 1.18 (d, J_{HH} 6.6, 3H, CH(CH_3)$_2$), 1.23 (s, 3H, C(CH_3)$_2$), 1.68 (d, J_{HH} 6.7, 3H, CH(CH_3)$_2$), 2.34 (s, 3H, C(CH_3)$_2$), 3.17 (sept, J_{HH} 6.6, 1H, CH(CH_3)$_2$), 3.88 (sept, J_{HH} 6.7, 1H, CH(CH_3)$_2$), 6.71 (t, J_{HH} 7.7, 1H, Ar-H), 6.83-6.87 (m, 2H, Ar/Py-H), 6.96-7.17 (m, 7H, Ar-H), 7.27-7.29 (m, 1H, Ar-H), 7.44 (dd, J_{HH} 8.2, 1.7, 1H, Ar-H), 7.47 (dd, J_{HH} 7.7, 1.7, 1H, Ar-H), 7.68-7.70 (m, 2H, Ar-H), 7.73-7.77 (m, 3H, Ar/Py-H), 8.18 (s, 1H, NH). ^{13}C{^{1}H} NMR (100 MHz, $CDCl_3$): δ 21.9 (CH(CH_3)$_2$), 23.7 (CH(CH_3)$_2$), 24.3 (C(CH_3)$_2$, 24.4 (CH(CH_3)$_2$), 24.7 (CH(CH_3)$_2$), 27.4 (C(CH_3)$_2$), 28.0 (CH(CH_3)$_2$), 32.6 (CH(CH_3)$_2$), 71.5 (C(CH_3)$_2$), 115.2, 115.7, 120.6 (CH), 123.9 (C), 124.4, 124.6, 125.2, 126.0, 126.5, 126.9, 128.1, 128.8, 129.1, 129.7 132.3 (CH), 132.6, 134.7 (C), 138.0 (CH), 138.7 (C), 139.0 (CH), 140.1, 142.8, 143.4, 153.2, 161.6, 169.0, 173.5 (C). ESIMS *m/z*: 817 $[M]^+$, 610 $[M\text{-}OOCC_6H_4I]^+$. FABMS *m/z*: 817 $[M]^+$, 610 $[M\text{-}OOCC_6H_4I]^+$.

5.2.23 Synthesis of 7b

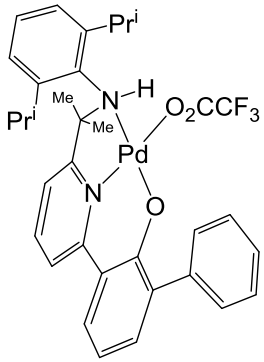

7b

To a small glass vial was added **4a** (0.010 g, 0.016 mmol) and the contents dissolved in C_6D_6 (0.5 mL) forming in an orange solution. To this solution was added trifluoroacetic acid (0.002 g, 0.016 mmol, 1 eq.) and the reaction mixture sonicated for 15 min. The ^{1}H NMR spectrum was recorded and showed complete consumption of the starting material. The reaction mixture was filtered through a celite plug and the filtrate layered with petroleum ether forming **7b** as red crystals (0.008 g, 73%). Mp. > 300 ^{o}C.^{1}H NMR (400 MHz, $CDCl_3$): δ 0.87 (d, J_{HH} 7.0, 3H, CH(CH_3)$_2$), 1.25 (d, J_{HH} 6.3, 3H, CH(CH_3)$_2$), 1.30 (d, J_{HH} 6.7, 3H, CH(CH_3)$_2$), 1.31 (s, 3H, C(CH_3)$_2$), 1.68 (d, J_{HH} 7.0, 3H, CH(CH_3)$_2$), 2.41 (s, 3H, C(CH_3)$_2$), 3.13 (sept, J_{HH} 6.0, 1H, CH(CH_3)$_2$), 3.52 (sept, J_{HH} 6.7, 1H, CH(CH_3)$_2$), 6.83 (t, J_{HH} 7.6, 1H, Ar-H), 6.96 (dd, J_{HH} 5.9, 2.7, 1H, Ar-H), 7.12 (dd, J_{HH} 7.8, 1.6, 1H, Ar-H), 7.17 (dd, J_{HH} 7.4, 1.6, 1H, Ar-H), 7.25 (m, 2H, Ar-H), 7.32 (m, 2H, Ar-H), 7.40 (dd, J_{HH} 7.0, 1.6, 1H, Ar-H), 7.56 (dd, J_{HH} 8.2, 1.6, 1H, Ar-H), 7.63 (br s, 1H, NH), 7.74 (m, 2H, Ar-H), 7.88 (m, 2H, Ar-H).^{13}C{^{1}H} NMR (100 MHz, $CDCl_3$): δ 22.8, 24.6, 25.1, 25.6, 28.2, 28.9, 33.7, 72.8, 116.7, 116.9, 122.0, 125.2, 125.9, 126.5, 127.6, 128.9, 129.8, 133.4, 134.9, 139.1, 139.4, 143.3, 143.8, 153.8, 161.8, 169.9. IR (cm^{-1}): 3299 (NH), 1596 (C=N$_{pyridine}$). ESIMS *m/z*: 569 [M-CF_3COO]$^+$, 610 [M- CF_3COO+MeCN]$^+$. FABMS *m/z*: 569 [M- CF_3COO]$^+$.

5.2.24 Synthesis of 7c

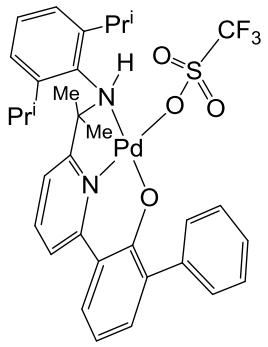

7c

To a small glass vial was added **4a** (0.010 g, 0.016 mmol) and the contents dissolved in C_6D_6 (0.5 mL) forming in an orange solution. To this solution was added triflic acid (14 µl, 0.016 mmol, 1 eq.) and the reaction mixture sonicated for 15 min. The ^{1}H NMR spectrum was recorded and showed complete consumption of the starting material. The reaction mixture was filtered through a celite plug and the filtrate layered with petroleum ether forming **7c** as red/orange crystals (0.009 g, 75%). Mp. > 300 ^{o}C. ^{1}H NMR (400 MHz, $CDCl_3$): δ 0.93 (d, J_{HH} 5.9, 3H, CH(*CH*$_3$)$_2$), 1.17 (s, 3H, C(*CH*$_3$)$_2$), 1.24 (m, 12H, CH(*CH*$_3$)$_2$), 1.53 (d, J_{HH} 7.0, 3H, CH(*CH*$_3$)$_2$), 3.18 (sept, J_{HH} 6.9, C*H*(CH$_3$)$_2$), 3.55 (sept, J_{HH} 7.0, C*H*(CH$_3$)$_2$), 6.74 (br s, 1H, NH), 6.85 (t, J_{HH} 8.0, 1H, ArH), 7.09 (m, 3H, ArH), 7.22 (m, 6H, ArH), 7.36 (m, 2H, ArH), 7.92 (m, 1H, ArH). ^{19}F{^{1}H} NMR (376 MHz, $CDCl_3$): δ 77.62. IR (cm^{-1}): 3299 (NH), 1596 (C=N$_{pyridine}$). ESIMS *m/z*: 569 [M-CF_3SO_3]$^+$, 149 [CF_3SO_3]. FABMS *m/z*: 569 [M-CF_3SO_3]$^+$, 149 [CF_3SO_3].

5.2.25 Synthesis of 8

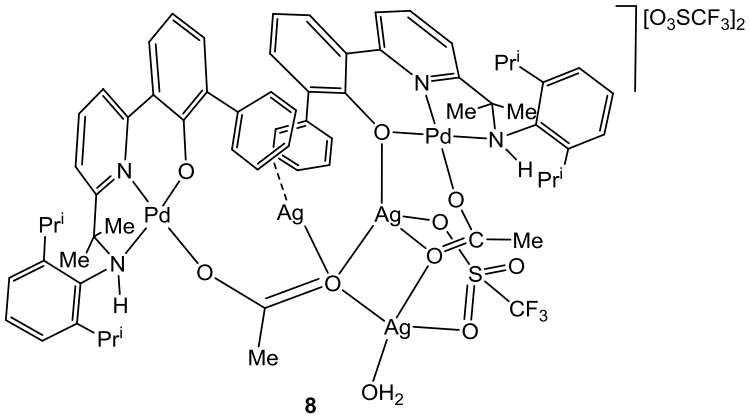

8

To a small glass vial was added **4a** (0.010 g, 0.016 mmol) and the contents dissolved in $CDCl_3$ (0.5 mL) forming in an orange solution. To this solution was silver triflate (0.020 g, 0.040 mmol, 5 eq.) and the reaction mixture sonicated for 15 min and left for three days at room temperature. The ^{1}H NMR spectrum was recorded and showed complete consumption of the starting material. The reaction mixture was filtered through a celite plug and the filtrate layered with petroleum ether forming **8** as yellow orange crystals (0.011 g, 79%). Mp. > 300 ^{o}C (decomposed). ^{1}H NMR (400 MHz, CD_3CN): 0.87 (d, J_{HH} 6.7, 3H, CH(CH_3)$_2$), 1.23 (d, J_{HH} 6.7, 3H, CH(CH_3)$_2$), 1.28 (s, 3H, C(CH_3)$_2$), 1.29 (d, J_{HH} 7.2, 3H, CH(CH_3)$_2$), 1.60 (d, J_{HH} 6.7, 3H, CH(CH_3)$_2$), 2.28 (s, 3H, C(CH_3)$_2$), 3.15 (sept, J_{HH} 6.7, 1H, C*H*(CH_3)$_2$), 3.60 (sept, J_{HH} 7.0, 1H, C*H*(CH_3)$_2$), 6.78 (m, 1H, ArH), 7.21 (m, 2H, ArH), 7.31 (m, 4H, ArH) 7.69 (m, 3H, ArH), 8.00 (m, 2H, ArH), 8.04 (br s, 1H, N*H*). ^{19}F{^{1}H} NMR (376 MHz, $CDCl_3$): δ 77.47. ESIMS: *m/z* 569 [M-CF_3SO_3]$^+$, 149 [CF_3SO_3]. TofMS: calcd 719.1410, found 719.1429 [**L4**PdO_3SCF_3].$^+$

5.2.26 Synthesis of 9a

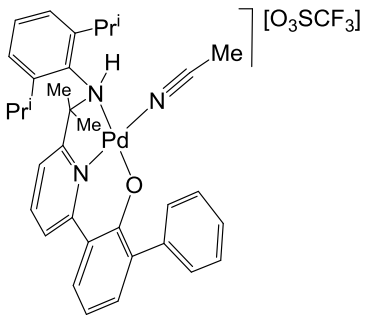

9a

To a small glass vial was added **4b** (0.010 g, 0.016 mmol) and the contents dissolved in CD_3CN (0.5 mL) forming in an orange solution. To this solution was silver triflate (0.006 g, 0.022 mmol, 1.4 eq.) and the reaction mixture sonicated for 15 min and left for three days at room temperature. The ^{1}H NMR spectrum was recorded and showed complete consumption of the starting material. The reaction mixture was filtered through a celite plug and the filtrate layered with petroleum ether forming **9a** as yellow orange crystals (0.010 g, 83%). Mp. > 300 ^{o}C. ^{1}H NMR (400 MHz, $CDCl_3$): δ 0.92 (d, J_{HH} 6.7, 3H, CH(CH_3)$_2$), 1.25 (d, J_{HH} 7.0, 3H, CH(CH_3)$_2$), 1.28 (s, 3H, NHC(CH_3)), 1.35 (d, J_{HH} 3H, CH(CH_3)$_2$), 1.48 (d, J_{HH} 7.1, 3H, CH(CH_3)$_2$), 2.01 (s, 3H, NHC(CH_3)), 2.07 (s, 3H, MeCN), 3.16 (sept, J_{HH} 7.0, 1H, CH(CH_3)$_2$), 3.24 (sept, J_{HH} 6.7, 1H, CH(CH_3)$_2$), 6.84 (br s, 1H, NH), 7.05 (t,

J_{HH} 7.6, 1H, ArH), 7.16 (m, 2H, ArH), 7.27 (m, 6H, ArH), 7.42 (m, 2H, ArH), 7.63 (d, J_{HH} 7.8, 1H, ArH), 8.19 (m, 1H, ArH), 8.26 (t, J_{HH} 8.0, 1H, ArH). $^{19}F\{^{1}H\}$ NMR (376 MHz, $CDCl_3$): δ 77.33. ESIMS: *m/z* 610 [M- $CF_3SO_3]^+$, 149 [CF_3SO_3]. FABMS *m/z*: 610 [M-$CF_3SO_3]^+$

5.2.27 Synthesis of 9b

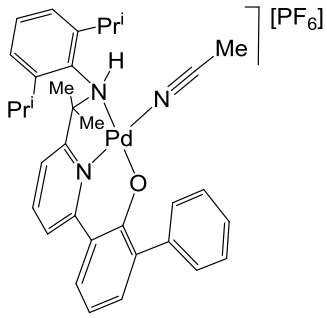

9b

To a small glass vial was added **4b** (0.010 g, 0.016 mmol) and the contents dissolved in CD_3CN (0.5 mL) forming in an orange solution. To this solution was silver hexafluorophosphate (0.006 g, 0.022 mmol, 1.4 eq.) and the reaction mixture sonicated for 15 min and left for three days at room temperature. The ^{1}H NMR spectrum was recorded and showed complete consumption of the starting material. The reaction mixture was filtered through a celite plug and the filtrate layered with petroleum ether forming **9b** as a yellow orange solid (0.009 g, 82%). Mp. > 270 ^{o}C (decomposed). ^{1}H NMR (400 MHz, $CDCl_3$): δ 1.05 (d, J_{HH} 7.0, 3H, CH(CH_3)$_2$), 1.30 (d, J_{HH} 6.7, 3H, CH(CH_3)$_2$), 1.35 (d, J_{HH} 7.2, 3H, CH(CH_3)$_2$), 1.36 (s, 3H, NHC(CH_3)), 1.60 (d, J_{HH} 6.7, 3H, CH(CH_3)$_2$), 2.05 (s, 3H, NHC(CH_3)), 3.15 (sept, J_{HH} 6.7, 1H, C*H*(CH_3)$_2$), 3.49 (sept, J_{HH} 7.0, 1H, C*H*(CH_3)$_2$), 6.35 (br s, 1H, N*H*), 6.93 (dd, J_{HH} 8.2, 7.0, 1H, ArH), 7.29 (m, 3H, ArH), 7.36 (m, 5H, ArH), 7.58 (m, 2H, ArH), 7.78 (dd, J_{HH} 8.6, 1.6, 1H, ArH), 8.13 (dd, J_{HH} 8.4, 7.6, 1H, ArH), 8.21 (dd, J_{HH} 8.0, 2.0, 1H, ArH). $^{13}C\{^{1}H\}$ NMR (100 MHz, $CDCl_3$): δ 20.7, 22.3, 22.4, 22.7, 22.8, 26.7, 27.4, 32.0, 116.3, 117.4, 121.4, 122.8, 123.3, 124.5, 125.7, 126.4, 126.5, 127.1, 127.3, 128.8, 132.0, 132.7, 140.0, 140.3, 141.0, 151.1, 156.2, 168.6. $^{19}F\{^{1}H\}$ NMR (376 MHz, $CDCl_3$): δ 72.93 (J_{PF} 706.9). FABMS: *m/z* 610 [M-$PF_6]^+$.

5.2.28 Synthesis of 9c

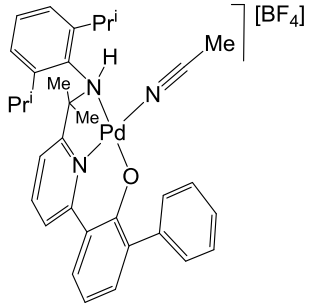

9c

To a small glass vial was added **4b** (0.010 g, 0.016 mmol) and the contents dissolved in CD_3CN (0.5 mL) forming in an orange solution. To this solution was silver tetrafluoroborate (0.005 g, 0.024 mmol, 1.4 eq.) and the reaction mixture sonicated for 15 min and left for three days at room temperature. The ^1H NMR spectrum was recorded and showed complete consumption of the starting material. The reaction mixture was filtered through a celite plug and the filtrate layered with petroleum ether forming **9c** as a yellow orange solid (0.010 g, 83%). Mp. > 300 ^oC. ^1H NMR (400 MHz, CD_3CN): δ 1.05 (d, J_{HH} 6.7, 3H, CH(CH_3)$_2$), 1.30 (d, J_{HH} 6.7, 3H, CH(CH_3)$_2$), 1.35 (d, J_{HH} 3H, CH(CH_3)$_2$), 1.59 (d, J_{HH} 7.0, 3H, CH(CH_3)$_2$), 2.14 (s, 6H, NHC(CH_3)), 3.08 (sept, J_{HH} 7.2, 1H, C*H*(CH_3)$_2$), 3.41 (sept, J_{HH} 6.7, 1H, C*H*(CH_3)$_2$)) 6.93 (dd, J_{HH} 8.2, 7.0, 1H, ArH), 7.30 (m, 4H, ArH), 7.37 (m, 5H, ArH), 7.57 (dd, J_{HH} 8.2, 2.0, 1H, ArH), 7.78 (dd, J_{HH} 8.2, 1.6, 1H, ArH), 8.13 (m, 1H, ArH), 8.21 (m, 1H, ArH). $^{19}F\{^1H\}$ NMR (376 MHz, $CDCl_3$): δ 151.84. ESIMS: *m/z* 569 $[M\text{-}MeCN\text{-}BF_4]^+$.

5.3 Chapter 3 Experimental

5.3.1 Synthesis of H_2L5a

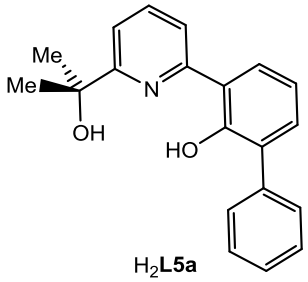

H_2**L5a**

A Schlenk flask equipped with stir bar was evacuated and backfilled with nitrogen and charged with 2-(3'-phenyl-2'-phenoxy)-6-acetylpyridine (0.320 g, 1.12 mmol) and toluene (10 mL). A 2M trimethylaluminium solution in toluene (2.8 mL, 5.53 mmol, 5 eq.) was added dropwise and the solution stirred and heated to 110 ^{o}C for 48 h. On cooling to room temperature, deionised water (10 mL) was added very slowly followed by stirring for 2 h at room temperature. The organic layer was separated and the aqueous layer was extracted with dichloromethane (3 x 30 mL). All organic extracts were combined and dried over magnesium sulfate. Following filtration, the solvent was removed under reduced pressure affording H_2**L5a** as a pale yellow-brown solid (0.330 g, 97%). Mp. 230 ^{o}C. ^{1}H NMR (400 MHz, $CDCl_3$): δ 1.57 (s, 6H, (CH_3), 2.01 (br s, 1H, OH), 6.90 (t, J_{HH} 7.7, 1H, Ar-H), 7.09 (m, 1H, Ar-H), 7.16 (m, 1H, Ar-H), 7.26 (m, 2H, Ar-H), 7.29 (dd, J_{HH} 7.4, 1.6, 1H, Ar-H), 7.36 (m, 2H, Ar-H), 7.49 (dd, J_{HH} 6.4, 2.3, 1H, Ar-H), 7.59 (m, 2H, Ar-H), 7.73 (dd, J_{HH} 8.0, 1.7, 1H, Ar-H), 7.76 (m, 2H, Ar-H), 14.54 (s, 1H, Ar-OH). ^{13}C{^{1}H} NMR (100 MHz, $CDCl_3$): δ 28.2 (*C*H_3), 71.2 (*C*(CH_3)$_2$), 114.7, 115.4, 116.5, 117.0, 123.7, 124.8, 125.9, 127.4, 128.8, 130.4, 136.4, 154.6, 154.9, 162.0. IR (cm^{-1}): 2972 (C-H), 2563 (OH), 1569 (C=$N_{pyridine}$). ESI MS: *m/z* 306 [M+H], 304 [M-H], 305 [M]. TOFMS calcd 306.1494, found 306.1497.

5.3.2 Synthesis of H_2L5b

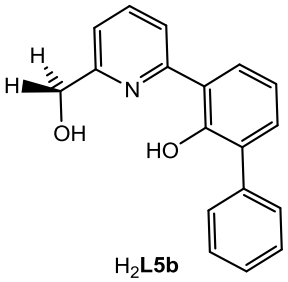

H_2**L5b**

Two small Schlenk flasks equipped with stir bars were evacuated and backfilled with nitrogen. One flask was charged with $LiAlH_4$ (0.103 g, 2.724 mmol, 5 eq.) in dry THF (10 mL) and the resulting suspension cooled to 0 ^oC with stirring. The second flask was charged with 2-(3'-phenyl-2'-phenoxy)-6-formylpyridine (0.150 g, 0.545 mmol, 1 eq.) and dry THF (20 mL) and its contents transferred by cannula to the cooled $LiAlH_4$ suspension. The combined reaction mixture was warmed to room temperature for 20 mins and the progress of reaction monitored by ESIMS. After completion of the reaction, water (0.6 mL) was added carefully followed by chloroform (20 mL) and more water (30 mL). The aqueous phase was separated and extracted with chloroform. All organic extracts were combined and dried over magnesium sulphate. All volatiles were removed under reduced pressure to give H_2**L5b** as a light orange solid (0.094 g, 63%). Mp. 210-220 ^oC. ^1H NMR (400 MHz, $CDCl_3$): δ 4.52 (s, 2H, (CH_2)), 6.83 (t, J_{HH} 7.6, 1H, ArH), 7.11 (m, 1H, ArH), 7.23 (m, 2H, ArH), 7.33 (t, 8.0, 2H, ArH), 7.52 (m, 2H, ArH), 7.61 (m, 3H, ArH), 14.78 (s, 1H, OH). $^{13}C\{^1H\}$ NMR (100 MHz, $CDCl_3$): δ 63.6 (CH_2), 116.8, 117.4, 117.8, 124.8, 125.9, 127.1, 128.5, 130.1, 131.5, 137.4, 137.5, 156.0, 156.1, 156.2. IR (cm^{-1}): 2972 (C-H), 2563 (OH), 1569 ($C=N_{pyridine}$). ESI MS: *m/z* 278 $[M]^+$. TOF MS(ES+): calcd [M+H] 278.1181, found 278.1192.

5.3.3 Synthesis of H_2L5c

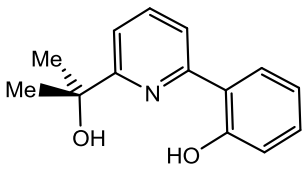

H_2**L5c**

A Schlenk flask equipped with stir bar was evacuated and backfilled with nitrogen and charged with 2-phenoxy-6-acetylpyridine (0.100 g, 0.469 mmol) and toluene (10 mL). A 2M trimethylaluminium solution in toluene (1.172 mL, 2.345 mmol, 5 eq.) was added dropwise and the solution stirred and heated to 110 ^oC for 48 h. On cooling to room temperature, deionised water (10 mL) was added very slowly followed by stirring for 2 h at room temperature. The organic layer was separated and the aqueous layer was extracted with dichloromethane (3 x 30 mL). All organic extracts were combined and dried over magnesium sulfate. Following filtration, the solvent was removed under reduced pressure affording H_2**L5c** as a pale yellow-brown solid (0.095 g, 88%). Mp. 210 ^oC. ^1H NMR (400

MHz, $CDCl_3$): δ 1.50 (s, 6H, (CH_3)$_2$), 2.59 (br s, 1H, OH), 6.81 (m, 1H, ArH), 6.90 (m, 1H, ArH), 7.19 (m, 1H, ArH), 7.46 (d, J_{HH} 7.8, 1H, ArH), 7.68 (m, 3H, ArH), 13.65 (br s, 1H, OH). IR (cm^{-1}): 2972 (C-H), 2563 (OH), 1569 ($C=N_{pyridine}$). ESI MS: *m/z* 229 $[M]^+$.

5.3.4 Synthesis of H_2L5d

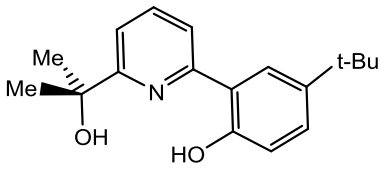

H_2**L5d**

A Schlenk flask equipped with stir bar was evacuated and backfilled with nitrogen and charged with 2-(5'-*t*-butyl-2'-phenoxy)-6-acetylpyridine (0.300 g, 1.11 mmol) and toluene (10 mL). A 2M trimethylaluminium solution in toluene (2.8 mL, 5.569 mmol, 5 eq.) was added dropwise and the solution stirred and heated to 110 ^oC for 48 h. On cooling to room temperature, deionised water (10 mL) was added very slowly followed by stirring for 2 h at room temperature. The organic layer was separated and the aqueous layer was extracted with dichloromethane (3 x 30 mL). All organic extracts were combined and dried over magnesium sulfate. Following filtration, the solvent was removed under reduced pressure affording H_2**L5d** as pale yellow-brown solid (0.231 g, 72%). Mp. 215 ^oC. ^1H NMR (400 MHz, $CDCl_3$): δ 1.27 (s, 9H, C(CH_3)$_3$), 1.58 (s, 6H, C(CH_3)$_2$), 2.30 (br. s, 1H, OH), 6.87 (d, J_{HH} 8.5, 1H, Ar-H), 7.28 (dd, J_{HH} 8.6, 2.5, 1H, Py-H), 7.47 (dd, J_{HH} 7.4, 1.3, 1H, Py-H), 7.74 (m, 3H, Ar/Py-H), 14.10 (s, 1H, OH). $^{13}C\{^1H\}$ NMR (100 MHz, $CDCl_3$): δ 30.5 (CH_3), 31.6 (CH_3), 34.2, 73.6, 116.7,117.3, 117.9, 118.1, 122.8, 128.9, 138.6, 141.5, 157.0, 157.3, 164.3. IR (cm^{-1}): 2972 (C-H), 2563 (OH), 1569 ($C=N_{pyridine}$). ESI MS: *m/z* 286 [M+], 284 [M-2H]. TOF MS(ASAP+): calcd for $C_{18}H_{23}NO_2$ $[M]^+$ 286.1807, found 286.1807.

5.3.5 Synthesis of 10a

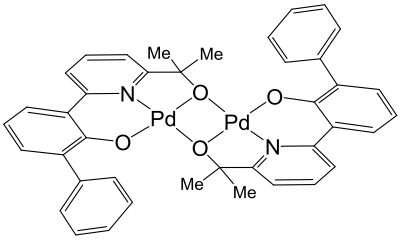

10a

A small Schlenk flask equipped with stir bar was evacuated and backfilled with nitrogen and loaded with H_2**L5a** (0.065 g, 0.215 mmol), $Pd(OAc)_2$ (0.048 g, 0.215 mmol) and dry toluene (10 mL). The reaction mixture was stirred for 2 days at room temperature resulting in a pale yellow suspension. The solid was allowed to settle for 30 min and washed with hexane (5 mL). The solid was then dissolved in excess of DCM and filtered through celite. Solvent was removed from filtrate to get **10a** as pale yellow solid (0.110 g, 76%). Mp. > 220 ^{o}C (decomposed). ^{1}H NMR (400 MHz, $CDCl_3$): δ 1.45 (s, 12H, C(CH_3)$_2$), 6.63-6.69 (m, 3H, Ar-H), 7.15 (dd, J_{HH} 7.0, 1.7, 2H, Ar-H), 7.19-7.24 (m, 2H, Ar-H), 7.29-7.33 (m, 5H, Ar-H), 7.41-7.44 (m, 4H, Ar-H), 7.55-7.58 (m, 2H, Ar-H), 7.65-7.68 (m, 4H, Ar-H). ^{13}C{^{1}H} NMR (100 MHz, $CDCl_3$): Sample insufficiently soluble. ESI MS: *m/z* 821 $[M+H]^+$, 862 $[M+MeCN]^+$, 900 $[M+2MeCN]^+$. FAB MS *m/z*: 410 $[1/2M]^+$.

5.3.6 Synthesis of 10b

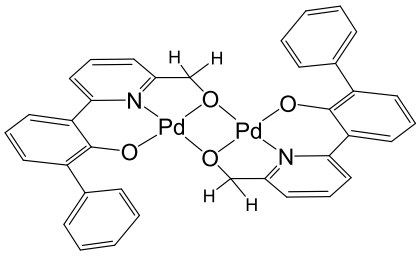

10b

A small Schlenk flask equipped with stir bar was evacuated and backfilled with nitrogen and loaded with H_2**L5b** (0.065 g, 0.235 mmol), $Pd(OAc)_2$ (0.053 g, 0.235 mmol) and dry toluene (10 mL). The reaction mixture was stirred for 2 days at room temperature resulting in pale yellow suspension. The reaction mixture was stirred for 2 days at room temperature resulting in a pale yellow suspension. The solid was allowed to settle for 30 min and washed with hexane (5 mL). The solid was then dissolved in excess of DCM and filtered through celite. Solvent was removed from filtrate to get **10b** as pale yellow solid. (0.129 g, 72 %).

Mp. > 220 ^{o}C (decomposed). ^{1}H NMR (400 MHz, $CDCl_3$): δ 4.54 (s, 2H, (CH_2)), 6.12 (d, J_{HH} 7.0, 1H, Ar-H), 6.72 (t, J_{HH} 7.6, 1H, Ar-H), 7.18 (m, 2H, Ar-H), 7.25 (m, 1H, Ar-H), 7.53 (m, 6H, Ar-H). ^{13}C{^{1}H} NMR (100 MHz, $CDCl_3$): Sample insufficiently soluble. ESI MS: *m/z* 764 $[M+H]^+$. FAB MS *m/z*: 764 $[M]^+$, 599 [$(L5b)_2$Pd-OAc], 640 [[$(L5b)_2$Pd-OAc+MeCN].

5.3.7 Synthesis of 11a

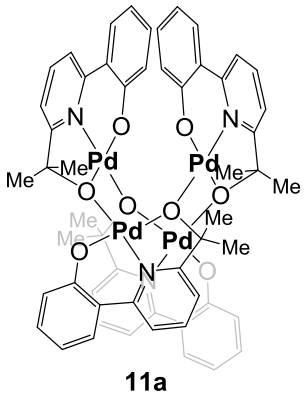

11a

A small Schlenk flask equipped with stir bar was evacuated and backfilled with nitrogen and loaded with H_2**L5c** (0.065 g, 0.284 mmol), $Pd(OAc)_2$ (0.063 g, 0.284 mmol) and dry toluene (10 mL). The reaction mixture was stirred for 2 days at room temperature resulting in a pale yellow suspension. The reaction mixture was stirred for 2 days at room temperature resulting in a pale yellow suspension. The solid was allowed to settle for 30 min and washed with hexane (5 mL). The solid was then dissolved in excess of DCM and filtered through celite. Solvent was removed from filtrate to get **11a** as pale yellow solid. (0.080 g, 84%). Mp. > 240 ^{o}C (decomposed). ^{1}H NMR (400 MHz, DMSO): δ 1.52 (s, 6H, C(CH_3)$_2$), 6.63 (t, J_{HH} 7.4, 1H, Ar-H), 6.85 (d, J_{HH} 7.8, 1H, Ar-H), 7.62 (m, 2H, Ar-H), 7.81 (d, J_{HH} 8.2, 1H, Ar-H), 7.97 (m, 2H, Ar-H). ^{13}C{^{1}H} NMR (100 MHz, $CDCl_3$): sample insufficiently soluble. ESI MS: 379 [L5cPd+MeCN], TofMS: 669.0058 $[1/2M]^+$.

5.3.8 Synthesis of 11b

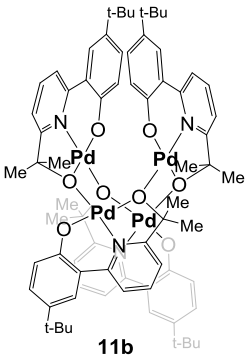

11b

A small Schlenk flask equipped with stir bar was evacuated and backfilled with nitrogen and loaded with H_2**L5d** (0.065 g, 0.227 mmol), $Pd(OAc)_2$ (0.051 g, 0.227 mmol) and dry toluene (10 mL). The reaction mixture was stirred for 2 days at room temperature resulting in a pale yellow suspension. The reaction mixture was stirred for 2 days at room temperature resulting in a pale yellow suspension. The solid was allowed to settle for 30 min and washed with hexane (5 mL). The solid was then dissolved in excess of DCM and filtered through celite. Solvent was removed from filtrate to get **11b** as pale yellow solid. (0.070 g, 89 %). Mp. > 250 ^oC (decomposed). ^1H NMR (400 MHz, $CDCl_3$): δ 1.46 (s, 9H, $C(CH_3)_3$), 1.57 (s, 6H, $C(CH_3)_2$), 7.32 (m, 1H, ArH), 7.41 (dd, J_{HH} 7.2, 2.3, 1H, ArH), 7.47 (m, 2H, ArH), 7.57 (d, J_{HH} 7.8, 1H, ArH), 7.94 (d, J_{HH}, 2.3, 1H, ArH). $^{13}C\{^1H\}$ NMR (100 MHz, $CDCl_3$): sample insufficiently soluble. ESI MS 431 [L5dPd+MeCN], Tof(asap) 431.8749 [L5dPd+H+MeCN]

5.3.9 Synthesis of 12a

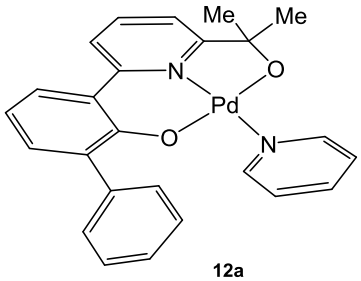

12a

A small Schlenk flask equipped with stir bar was evacuated and backfilled with nitrogen and loaded with H_2**L5a** (0.030 g, 0.098 mmol), $Pd(OAc)_2$ (0.022 g, 0.098 mmol), pyridine (0.008 g, 0.108 mmol, 1.1 eq) and dry toluene (10 mL). The reaction mixture was stirred

for 2 days at 60 °C. The reaction mixture was allowed to cool to room temperature and all volatiles removed under reduced pressure to afford **12a** as a brown solid (0.043 g, 89%). Red-orange blocks of **12a** suitable for an X-ray diffraction study could be grown by slow diffusion of hexane into a dichloromethane solution of the complex. Mp. > 230 °C (decomposed). ^{1}H NMR (400 MHz, C_6D_6): δ 1.87 (s, 6H, C(CH_3)$_2$), 6.36 (dd, 7.6, 1.1, 1H, Ar-H), 6.49 (m, 2H, ArH), 6.78 (tt, 7.6, 1.6, 1H, ArH), 6.85 (dd, 7.0, 8.2, 1H, ArH), 7.00 (t, 1H, 7.8, ArH), 7.34 (m, 4H, ArH), 7.51 (dd, 1H, J_{HH} 7.0, 1.7, ArH), 7.62 (dd, 1H, 8.4, 1.6, ArH), 7.79 (m, 2H, ArH), 8.89 (m, 2H, ArH). ^{13}C{^{1}H} NMR (100 MHz, $CDCl_3$): 32.0 (C(CH_3)$_2$), 82.3 (C(CH_3)$_2$), 114.2, 115.6, 118.5, 123.1 (CH), 23.2 9 (C), 125.0, 126.5, 128.5, 129.2, 131.0 (CH), 133.8(C), 136.9 (CH), 140.6 (C), 148.7 (CH), 151.9, 161.2, 177.4 (C). IR (cm^{-1}): 1548 ($C=N_{pyridine}$). ESI MS (MeCN): *m/z* 489 $[M]^+$, 451 $[M\text{-}Py+MeCN]^+$, 941 $[2M\text{-}Py+MeCN+H]^+$, 979 $[2M+H]^+$. FAB MS: *m/z* 489 $[M]^+$, 978 $[2M]^+$.

5.3.9 Synthesis of 12b

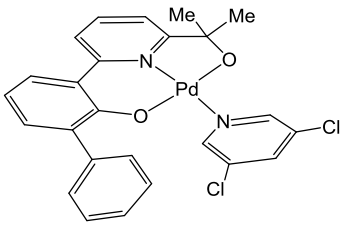

12b

A small Schlenk flask equipped with stir bar was evacuated and backfilled with nitrogen and loaded with H_2**L5a** (0.030 g, 0.098 mmol), $Pd(OAc)_2$ (0.022 g, 0.098 mmol), 3,5-dichloropyridine (0.016 g, 0.108 mmol, 1.1 eq) and dry toluene (10 mL). The reaction mixture was stirred for 2 days at 60 °C. The reaction mixture was allowed to cool to room temperature and all volatiles removed under reduced pressure to afford **12b** as a brown solid (0.045 g, 81%). Red-orange blocks of **12b** suitable for an X-ray diffraction study were grown by slow diffusion of hexane into a dichloromethane solution of the complex. Mp. > 270 °C (decomposed). ^{1}H NMR (400 MHz, C_6D_6): δ 1.45 (s, 6H, C(CH_3)$_2$,), 6.63-6.69 (m, 2H, Ar-H), 6.87 (dd, J_{HH} 5.5, 3.4, 1H, Ar-H), 7.15 (dd, J_{HH} 7.0, 1.7, 1H, Ar-H), 7.31 (t, 1H, J_{HH} 7.4, 1H, Ar-H), 7.35-7.36 (m, 1H, Ar-H), 7.41-7.44 (m, 2H, Ar-H), 7.50-7.52 (m, 1H, Ar-H), 7.57 (dd, J_{HH} 8.4, 1.7, 1H, Ar-H), 7.65-7.66 (m, 2H, Ar/py-H), 7.76 (m, 1H, Ar/py-H), 8.52 (d, 2.1, 1H, Ar-H). ESI MS: *m/z* 558 $[M]^+$.

5.3.10 Synthesis of 12c

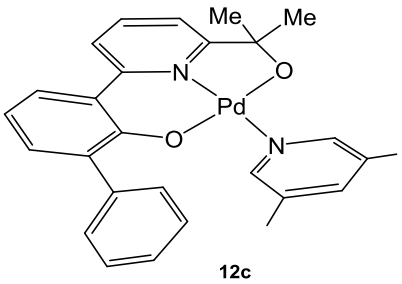

12c

A small Schlenk flask equipped with stir bar was evacuated, backfilled with nitrogen and loaded with **10a** (0.030 g, 0.037 mmol), 3,5-lutidine (0.008 g, 0.072 mmol, 2eq.) and toluene (10 mL). The reaction mixture was stirred at 60 ^{o}C for 2 days. Following celite filtration, all volatiles were removed under pressure to afford **12c** as a red solid (0.030 g, 80%). Mp. > 220 ^{o}C (decomposed). ^{1}H NMR (400 MHz, C_6D_6): δ 1.65 (s, 6H, $C(CH_3)_2$, 1.93 (s, 6H, (CH_3),), 6.64 (dd, 1H, J_{HH} 8.2, 7.0, ArH), 6.78 (dd, 1H, J_{HH} 7.0, 2.0, ArH), 7.19 (m, 4H, ArH), 7.46 (m, 3H, ArH), 7.63 (m, 2H, ArH), 8.01 (s, 2H, PyH), 8.21 (s, 1H, PyH). ESI MS: *m/z* 517 $[M]^+$, 559 [M+H+MeCN]

5.3.11 Synthesis of 13a

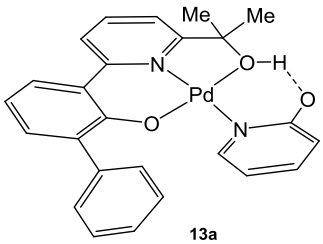

13a

A small Schlenk flask equipped with stir bar was evacuated, backfilled with nitrogen and loaded with H_2**L5a** (0.030 g, 0.098 mmol), $Pd(OAc)_2$ (0.022 g, 0.098 mmol), 2-hydroxypyridine (Hhp) (0.010 g, 0.108 mmol, 1.1 eq.) and toluene (10 mL). The reaction mixture was stirred at 60 ^{o}C for 2 days. All volatiles were removed under pressure to afford **13a** as a red solid (0.041 g, 83%). Mp. > 280 ^{o}C (decomposed). ^{1}H NMR (400 MHz, $CDCl_3$): δ 1.77 (s, 6H, $C(CH_3)_2$), 6.08-6.12 (m, 1H, Ar-H), 6.49-6.52 (m, 1H, Ar-H), 6.78

(dd, J_{HH} 8.1, 7.2, 1H, Ar-H), 6.94 (t, J_{HH} 4.2, 1H, Py-H), 7.27 (dd, J_{HH} 8.1, 1.7, 1H, Ar-H), 7.35-7.44 (m, 5H, Ar-H), 7.48-7.51 (m, 2H, Ar-H), 7.64 (dd, J_{HH} 8.2, 1.7, 1H, Ar-H), 7.81-7.82 (m, 2H, Py-H), 15.75 (br. s, 1H, OH). $^{13}C\{^{1}H\}$ NMR (100 MHz, $CDCl_3$): 32.0 ($C(CH_3)_2$), 84.4 ($C(CH_3)_2$), 113.1, 113.5, 115.9, 116.7, 120.3 (CH), 124.4 (C), 126.3, 127.8, 129.4, 130.1, 132.4 (CH), 134.9 (C), 138.5, 140.3 (CH), 141.2 (C), 146.3 (CH), 152.8, 161.6, 163.6, 163.9, 173.2 (C). ESI MS: *m/z* 507 $[M+2H]^+$. FAB MS *m/z* 505 $[M]^+$.

5.3.12 Synthesis of 13b

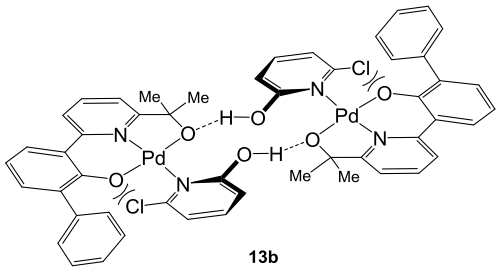

13b

Employing a similar procedure to that described for **13a** using $Pd(OAc)_2$ (0.022 g, 0.098 mmol), H**L5a** (0.030 g, 0.098 mmol**)** and 6-chloro-2-hydroxypyridine (Hchp) (0.014 g, 0.098 mmol) gave **13b** as a red solid (0.047 g, 89%). Red-orange blocks of **13b** suitable for an X-ray diffraction study were grown by slow diffusion of hexane into a dichloromethane solution of the complex. Mp. > 220 ºC (decomposed). ^{1}H NMR (400 MHz, C_6D_6): δ 1.53 (s, 6H, $C(CH_3)_2$), 5.90 (d, J_{HH} 7.4, 1H, Ar-H), 5.98-6.04 (m, 2H, Ar-H), 6.17 (d, J_{HH} 8.4, 1H, Ar-H), 6.44-6.53 (m, 2H, Py-H), 6.62 (t, J_{HH} 7.5, 1H, Ar-H), 6.80-6.87 (m, 1H, Ar-H), 7.07-7.15 (m, 1H, Ar-H), 7.21-7.30 (m, 3H, Ar-H), 7.80-7.82 (m, 2H, Py-H), 10.7 (br. s, 1H, OH). ESI MS: *m/z* 451 $[M\text{-chp}+MeCN]^+$, FABMS: *m/z* 451 $[M\text{-chp}+MeCN]^+$. Anal calcd for ($C_{38}H_{35}F_5N_2O_2Pd$): C, 59.77; H, 4.39; N, 5.55. Found: C, 59.38; H, 4.29; N, 5.53%.

5.4 Experimental of Chapter 4

5.4.1 Synthesis of 6-phenyl-2-pyridone (H_2L8)

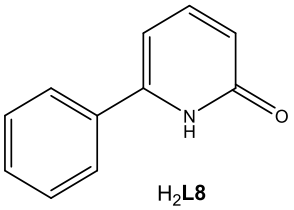

H_2**L8**

A 10 mL round bottom flask equipped with stir bar and reflux condenser was loaded with 6-phenyl-2-methoxy pyridine (103 mg, 0.557 mmol) and aqueous 48% HBr (2.5 mL, 22 mmol, 40 eq). The reaction mixture was stirred at reflux for 4 h. The solution was then allowed to cool to room temperature and neutralised with a saturated aqueous solution of $NaHCO_3$. The product was extracted with diethyl ether (3 x 50 mL), dried over $MgSO_4$. Following filtration and drying under reduced pressure, H_2**L8** was obtained as a white solid (62 mg, 65%). Crystals suitable for an X-ray determination were grown by prolonged standing of a methanol solution of H_2**L8** at room temperature. Mp: 196-197 ^oC. ^1H NMR (400 MHz, $CDCl_3$): δ 6.40 (d, J_{H-H} 7.0, 1H), 6.47 (d, J_{H-H} 8.0, 1H), 7.42 (m, 4H), 7.56 (m, 2H), 10.35 (br NH, 1H). $^{13}C\{^1H\}$ NMR (100 MHz, $CDCl_3$): δ 103.8 (CH), 117.7 (CH), 125.7 (CH), 128.1 (CH), 129.0 (CH), 132.5 (C), 140.3 (CH), 146.0 (C), 164.3 (C=O). ESI MS: *m/z* 172 $[M+H]^+$. HR MS: Calcd for $C_{11}H_9NO$ $[M+H]^+$ 172.0762, found 172.0762. IR (cm^{-1}): 3033, 2857, 2787, 1739 (C=O), 1643, 1612. The spectroscopic data were consistent with that previously reported.[193]

5.4.2 Synthesis of [(HL8))Pd(μ-CH_3COO)]$_2$ (14)

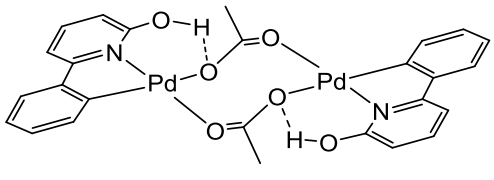

14

A glass vial was loaded with H_2**L8** (60 mg, 0.35 mmol), $Pd(OAc)_2$ (78 mg, 0.35 mmol, 1 eq) and dry toluene (6 mL). The reaction mixture was sonicated for 15 min to allow complete dissolution of the solids affording a dark red solution. After standing at room temperature for three days orange crystals formed on the base of the vial. The toluene was decanted and the crystals of **14** were dried under reduced pressure (65 mg, 55 %). Crystals

of **14** suitable for the X-ray diffraction study were grown by slow diffusion of petroleum ether into a solution of the complex in dichloromethane. Mp. > 250 ºC. ^{1}H NMR (400 MHz, $CDCl_3$): δ 2.27 (s, 6H, CMe=O), 5.95 (d, J_{H-H} 8.3, 2H, Py-H), 6.72 (m, 4H, Py-H, Ar- H), 6.84 (m, 6H, Ar-H), 7.28 (t, J_{HH} 7.3, 2H, Py-H), 9.63 (OH). ^{13}C {^{1}H} NMR (100 MHz, $CDCl_3$): δ 25.01 (CMe=O), 109.2 (CH), 109.3 (CH), 122.6 (CH), 124.6 (CH), 128.2 (CH), 129.0 (CH), 140.1 (CH), 145.1, 147.3, 161.4, 164.9, 184.4 (C). IR (cm^{-1}): 3051, 1680, 1620, 1570, 1552. Anal calcd for ($C_{26}H_{22}N_2O_6Pd_2$): C, 46.52; H, 3.30; N, 4.17. Found: C, 46.61; H, 3.21; N, 4.23%.

5.4.3. Synthesis of [Pd(μ-HL8)(κ^2-HL8)]$_2$ (15)

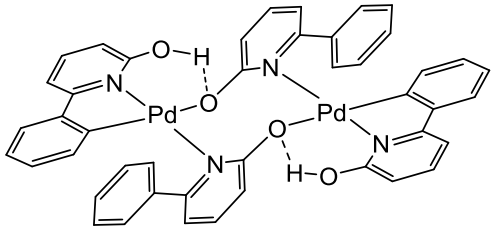

15

A small Schlenk flask that had been evacuated and backfilled with nitrogen was loaded with a stir bar, $Pd(OAc)_2$ (34 mg, 0.15 mmol), H_2**L8** (53 mg, 0.31 mmol, 2 eq) and dry toluene (5 mL). The resulting dark orange solution was left to stir at room temperature for three days affording a yellow suspension. The solution was decanted and the solid collected and dried under reduced pressure affording **15** as a yellow solid (50 mg, 72%). Single crystals of **15** suitable for an X-ray determination were grown by slow diffusion of hexane into a dichloromethane solution of the complex. Mp: > 250 ºC. ^{1}H NMR (400 MHz, $CDCl_3$: δ 5.67 (d, J_{H-H} 8.3 Hz, 1H, Py-H), 5.85 (d, J_{H-H} 7.7 Hz, 1H, Py-H), 6.46 (d, J_{H-H} 7.4 Hz, 1H, Py-H), 6.66 (m, 5H), 7.08 (t, J_{H-H} 7.8 Hz, 1H, Py-H), 7.37 (t, J_{H-H} 7.1, 2H), 7.44 (t, J_{H-H} 7.2 Hz, 1H, Ar-H) 7.49 (t, J_{H-H} 7.7 Hz, 1H, Py-H), 7.97 (d, J_{H-H} 7.2 Hz, 2H, Ar-H), 12.35 (OH, 1H). ^{13}C {^{1}H} NMR (125 MHz, $CDCl_3$): δ 108.2 (Py-CH), 109.7 (Py-CH), 113.8 (Ar-CH), 115.8 (Ar-CH), 122.6 (Ar-CH), 123.3 (Ar-CH), 127.9 (Ar-CH), 128.0 (Ar-CH), 128.4 (Py-CH), 129.3 (Ar-CH), 133.2 (Py-CH), 139.0 (Py-CH), 139.1 (Py-CH), 141.8, 145.6, 149.1, 158.9, 161.0, 166.5, 169.8 (C). IR (cm^{-1}): 3051, 1682, 1593, 1568. HRMS (ASAP): calcd for $C_{44}H_{32}N_4O_4Pd_2$ $[M+H]^+$ 893.0595, found 893.0577. Anal calcd for ($C_{26}H_{22}N_2O_6Pd$): C, 59.14; H, 3.61; N, 6.27. Found: C, 58.84; H, 3.50; N, 6.18%.

5.4.4 Synthesis of [Pd(μ:κ^2-L8)]$_4$ (16)

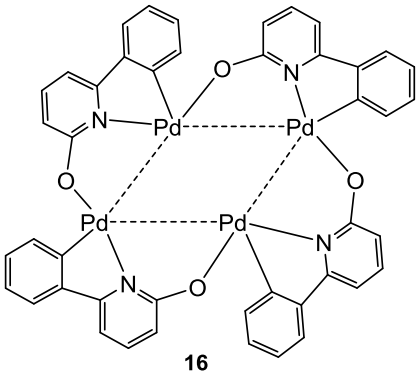

16

A glass vial was loaded with **14** (13.0 mg, 0.0194 mmol) and dissolved in C_6D_6 (0.5 mL). The contents was transferred to an NMR tube and sonicated for 15 min affording a dark orange solution. This solution was then left to stand at room temperature and the reaction progress monitored by ^{1}H NMR spectroscopy. After 3 days the resulting light orange solution was passed through a celite filter and the solvent removed under reduced pressure. Crystallisation of the orange residue from dichloromethane/hexane afforded orange needles of **16** (3.1 mg, 58%). ^{1}H NMR (400 MHz, $CDCl_3$): δ 5.92 (dd, J_{HH} 8.6, 0.9, 1H), 6.74 (dd, J_{HH} 7.4, 1.0, 1H), 6.93 (m, 2H), 7.01 (m, 1H), 7.17 (m, 1H), 7.37 (d, J_{HH} 7.7, 1H). ^{13}C{^{1}H} (125 MHz, $CDCl_3$): δ 105.6 (Py-CH), 115.1 (Py-CH), 123.4 (Ar-CH), 127.4 (Ar-CH), 128.6 (Ar-CH), 131.1, (Ar-H), 138.3 (Py-CH), 145.5, 147.0, 159.9, 171.5 (C). Anal calcd for ($C_{44}H_{28}N_4O_4Pd_4$): C, 48.11; H, 2.61; N, 5.32. Found: C, 47.94; H, 2.56; N, 5.08%.

5.4.5 Synthesis of [PdCl(κ^2-HL8)(κ^1-H$_2$L8)] (17)

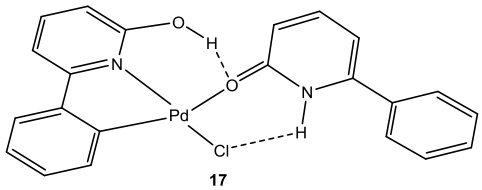

17

A glass vial was loaded with $(MeCN)_2PdCl_2$ (4.29 mg, 0.017 mmol), H_2**L8** (5.72 mg, 0.035 mmol, 2 eq) and $CDCl_3$ (0.5 mL) and sonicated to dissolve all solid starting materials. The contents of the vial was transferred to an NMR tube and the progress of the reaction monitored using ^{1}H NMR spectroscopy. After 5 days of standing at room temperature a pink solid precipitated. This solid was filtered through a celite pad and the filtrate left to slowly evaporate. After several days pale yellow crystals of **17** were formed (4.7 mg, 59%). ^{1}H NMR (400 MHz, $CDCl_3$): δ 6.49 (d, J_{HH} 8.6, 1H), 6.64 (m, 1H), 6.79

(m, 1H), 6.91 (td, J_{HH} 8.0, 2.0, 1H), 6.98 (td, J_{HH} 8.0, 1.1, 1H), 7.07 (d, J_{HH} 7.2, 1H), 7.22 (dd, J_{HH} 8.1, 2.2, 1H), 7.46 (m, 4H), 7.57 (t, J_{HH} 8.1, 1H), 7.72 (m, 4H), 13.11 (s, 1H). FAB MS: *m/z* 448 [M-Cl]. Anal calcd for ($C_{22}H_{17}ClN_2O_2Pd$): C, 54.68; H, 3.55; N, 5.80. Found: C, 54.88; H, 3.50; N, 6.11%.

5.4.6 Synthesis of 3-bromo-6-phenyl-2-pyridone (H_2L8-3-Br)

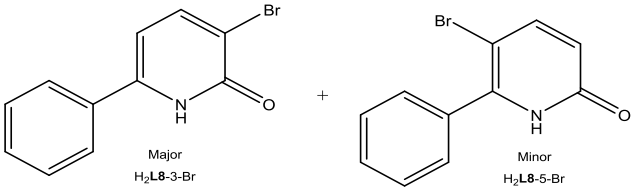

A clean dry 25 mL round bottom flask equipped with stir bar was loaded with H_2**L8** (0.074 g, 0.433 mmol), aqueous 48% HBr (1 mL) and cooled to 0 ^oC. On stirring for few minutes a thick white slurry was formed. To this slurry, bromine (0.073 g, 0.457 mmol, 1.06 eq) in glacial acetic acid (0.5 mL) was added dropwise forming a yellow/orange suspension. After the addition of the bromine was complete, the suspension was stirred for an additional 10 min at 0 ^oC. The ice bath was then removed and the suspension stirred at room temperature for 5 min followed by the addition of water (10 mL) to form a cloudy suspension with a white solid. This suspension was stirred for another 1 h at room temperature and filtered using a Hirsch funnel affording H_2**L8**-3-Br as a white solid. Following washing with cold water (40 mL), the product was dried under reduced pressure overnight (60 mg, 55%). Mp: 238 – 240 ^oC. ^1H NMR (400 MHz, CD_2Cl_2): δ 6.32 (d, J_{HH} 7.1 Hz, 1H, Py-H), 7.43 (m, 3 H, Ar-H), 7.57 (m, 2H, Ar-H), 7.78 (d, J_{HH} 7.2 Hz, 1H, Py-H), 10.19 (NH). Small peaks (*ca.* 5%) were seen on the baseline of the ^1H NMR spectrum corresponding to the 5-substituted isomer. $^{13}C\{^1H\}$ (125 MHz, CD_2Cl_2): δ 105.2 (Py-CH), 114.4 (C), 126.9 (Ar-CH), 129.6 (Ar-CH), 130.7 (Ar-CH), 133.1 (C), 143.7 (Py-CH), 146.8 (C), 161.0 (C=O). IR (cm^{-1}): 2905, 2832, 1610, 1595, 1573, 752, 691. ESI MS: 250/252 $[M+H]^+$. HRMS: Calcd for $C_{11}H_8BrNO$ $[M+H]^+$ 249.9875, found 249.9868.

5.4.7 Synthesis of 3,5-dibromo-6-phenyl-2-pyridone (HL8-3,5-Br_2)

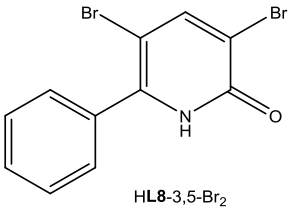

H**L8**-3,5-Br_2

A small Schlenk flask equipped with stir bar was evacuated and backfilled with nitrogen. H_2**L8** (42 mg, 0.246 mmol, 1 eq), NBS (132 mg, 0.74 mmol, 3 eq) and dry MeCN (5 mL) were loaded into the flask. This vessel was sealed under a under nitrogen atmosphere, and the reaction mixture stirred and heated to 120 ^oC. On reaching the desired temperature a homogeneous orange solution formed. After 16 h at 120 ^oC, the mixture was allowed cool to room temperature. The remaining residue was dissolved in dichloromethane (10 mL) and passed through celite pad. The organic filtrate was washed with water (3 x 5 mL) and dried over magnesium sulphate. All volatiles were removed from the filtrate under reduced pressure affording H**L8**-3,5-Br_2 as an off-white solid (79 mg, 89%). Mp: > 250 ^oC. ^1H NMR (400 MHz, $CDCl_3$): δ 7.52 (m, 5H), 7.99 (s, 1H). ESI MS: 330 $[M+H]^+$. HRMS: Calcd for $C_{11}H_8NOBr_2$ $[M+H]^+$ 329.8974, found 329.8953.

5.4.8 Synthesis of 6-(2-bromophenyl)-3,5-dibromo-2-pyridone (o-Br-L8-3,5-Br_2)

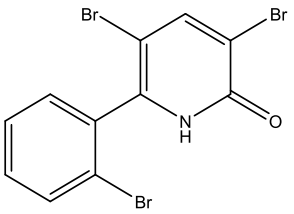

o-Br-**L8**-3,5-Br_2

A small Schlenk flask equipped with a stir bar was evacuated and backfilled with nitrogen. H_2**L8** (42 mg, 0.246 mmol), NBS (132 mg, 0.74 mmol, 3 eq), $Pd(OAc)_2$ (2.8 mg, 0.012 mmol, 0.05 eq) and dry acetonitrile (5 mL) were loaded into the flask. The vessel was sealed under a nitrogen atmosphere and the reaction mixture stirred and heated to 120 ^oC. On reaching 120 ^oC the reaction mixture became a homogeneous solution. After 16 h, the vessel was cooled to room temperature. The residue was dissolved in of dichloromethane (10 mL) and passed through a celite pad. The filtrate was washed with water (3 x 5 mL) and dried over magnesium sulphate. All volatiles were removed from

the filtrate under reduced pressure affording the crude product as a red solid. Purification by column chromatography using an 8:2 mixture dichloromethane to ethyl acetate as eluent gave o-Br-**L8**-3,5-Br_2 as a pale yellow solid (85 mg, 85%). Crystals suitable for an X-ray determination were grown by slow evaporation of a methanol solution of o-Br-**L8**-3,5-Br_2. Mp: > 270 ºC. ^{1}H NMR (400 MHz, $CDCl_3$): δ 7.26 (m, 1H), 7.32 (m, 1H), 7.39 (m, 1H), 7.64 (d, J_{HH} 7.2, 1H), 7.92 (s, 1H), 9.82 (br, NH). $^{13}C\{^1H\}$ NMR (125 MHz, MeOD): δ 101.1 (C), 116.2 (C), 123.1 (C), 129.0 (CH), 132.3 (CH), 133.2 (CH), 134.1 (CH), 136.2 (C), 146.4 (C), 147.7 (CH), 160.1 (C=O). ESI MS: 408 $[M+H]^{+\cdot}$ HRMS: Calcd for $C_{11}H_8NOBr_3$ $[M+H]^+$ 407.8058, found 407.8068.

5.4.9 Synthesis of 6-phenyl-3,5-dichloro-2-pyridone (L8-3,5-Cl_2)

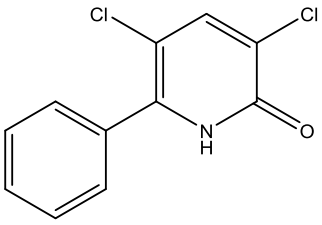

L8-3,5-Cl_2

A Schlenk flask equipped with a stir bar was evacuated and backfilled with nitrogen. H_2**L8** (42 mg, 0.246 mmol), NCS (98 mg, 0.738 mmol, 3 eq), and dry MeCN (5 mL) were loaded into the flask. The vessel was sealed under a nitrogen atmosphere and the reaction mixture stirred and heated to 120 ºC. On reaching 120 ºC all reagents had dissolved forming a dark orange solution. After 16 h, the reaction mixture was cooled to room temperature affording a suspension. More acetonitrile (5 mL) was added and the mixture filtered affording crude **L8**-3,5-Cl_2 as a dark brown solid. Purification by column chromatography using an 8:2 mixture dichloromethane to ethyl acetate as eluent gave **L8**-3,5-Cl_2 as a pale yellow solid (50 mg, 85%). ^{1}H NMR (400 MHz, $CDCl_3$): δ 7.46 (m, 5H), 7.61 (s, 1H), 10.38 (br. s, 1H, NH). $^{13}C\{^1H\}$ NMR (100 MHz, $CDCl_3$): Sample insufficiently soluble. ESI MS: *m/z* 239 $[M]^+$. HRMS: Calcd for $C_{11}H_8NOCl_3$ $[M]^+$, Calculated 239.9983, found 239.9984.

5.4.10 Synthesis of 6-(2-dichlorophenyl)-3,5-dichloro-2-pyridone (o-Cl-L8-3,5-Cl_2)

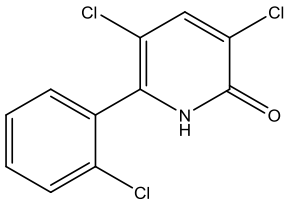

o-Cl-**L8**-3,5-Cl_2

A Schlenk flask equipped with a stir bar was evacuated and backfilled with nitrogen. H_2**L8** (42 mg, 0.246 mmol), NCS (98 mg, 0.738 mmol, 3 eq), $Pd(OAc)_2$ (2.8 mg, 0.012 mmol, 0.05 eq) and dry MeCN (5 mL) were loaded into the flask. The vessel was sealed under a nitrogen atmosphere and the reaction mixture stirred and heated to 120 ^oC. On reaching 120 ^oC all reagents had dissolved forming a dark orange solution. After 16 h, the reaction mixture was cooled to room temperature affording a suspension. More acetonitrile (5 mL) was added and the mixture filtered affording crude o-Cl-**L8**-3,5-Cl_2 as a dark brown solid. Purification by column chromatography using an 8:2 mixture dichloromethane to ethyl acetate as eluent gave o-Cl-**L8**-3,5-Cl_2 as a pale yellow solid (61 mg, 91%). Crystals suitable for an X-ray determination were grown by slow evaporation of a methanol solution of o-Cl-**L8**-3,5-Cl_2. ^1H NMR (400 MHz, $CDCl_3$): δ 7.53 (m, 2H), 7.58 (m, 2H), 7.69 (s, 1H), 10.43 (br. s, 1H, NH). $^{13}C\{^1H\}$ NMR (100 MHz, $CDCl_3$): Sample insufficiently soluble. ESI MS: *m/z* 274 $[M]^+$. HRMS: Calcd for $C_{11}H_8NOCl_3$ $[M]^+$, Calculated 273.9593, found 273.9582.

5.4.11 Synthesis of 6-(2-C_6H_5)-5,5-F_2-6-OH-C_5H_2NH-2-O

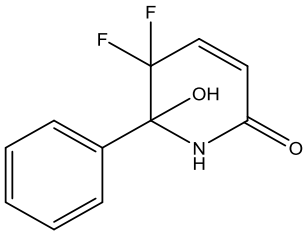

6-(2-C_6H_5)-5,5-F_2-6-OH-C_5H_2NH-2-O

A Schlenk flask equipped with stir bar was evacuated and backfilled with nitrogen. H_2**L8** (41 mg, 0.246 mmol), SelectFluor (264 mg, 0.75 mmol, 3 eq) and dry acetonitrile (6 mL) were loaded into the flask. The vessel was sealed under a nitrogen atmosphere and the reaction mixture stirred and heated to 120 ^oC. On reaching 120 ^oC a clear orange solution formed. After 16 h, the vessel was allowed to cool to room temperature. The solvent was

removed under reduced pressure affording a brown solid. Chloroform (10 mL) was added to dissolve the DABCO by-product and the remaining solid filtered affording 6-(2-C_6H_5)-5,5-F_2-6-OH-C_5H_2NH-2-O as a fine yellow powder (49 mg, 89%). ^{1}H NMR (400 MHz, $CDCl_3$): δ 6.22 (br, OH), 6.30 (m, 1H), 6.65 (m, 1H), 7.47 (m, 3H), 7.65 (m, 2H). ^{19}F{^{1}H} NMR (376 MHz, $CDCl_3$): -98 (d, J_{FF} 279), -118 (d, J_{FF} 279). ESI MS: *m/z* 225 $[M]^+$, HRMS (ASAP): calcd for $C_{11}H_9NO_2F_2$ $[M+MeCN+Na-H]^+$ 288.1370.

5.4.12 Synthesis of 18

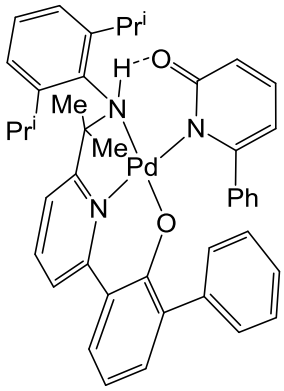

18

To a small glass vial was added **4a** (0.010 g, 0.016 mmol) and the contents dissolved in C_6D_6 (0.5 mL) forming an orange solution. To this solution was added H_2**L8** (0.003 g, 0.016 mmol, 1 eq.) and the reaction mixture sonicated for 15 min. The ^{1}H NMR spectrum was recorded and showed 47% consumption of the starting material. The reaction mixture was filtered through a celite plug and the filtrate layered with petroleum ether forming **18** as red crystals (0.008 g, 73%). Mp. > 300 ^{o}C.^{1}H NMR (400 MHz, $CDCl_3$): δ 0.79 (d, J_{HH} 6.7, 3H, CH(CH_3)$_2$), 0.87 (d, J_{HH} 7.0, 3H, CH(CH_3)$_2$), 0.88 (d, J_{HH} 7.2, 3H, CH(CH_3)$_2$), 1.17 (d, J_{HH} 6.7, 3H, CH(CH_3)$_2$), 1.47 (s, 3H, C(CH_3)$_2$), 2.28 (sept, J_{HH} 6.7, 1H, C*H*(CH_3)$_2$), 2.54 (s, 3H, C(CH_3)$_2$), 3.54 (sept, J_{HH} 6.0, 1H, C*H*(CH_3)$_2$), 6.43 (dd, J_{HH} 8.6, 1.2, 1H, Ar-H), 6.47 (dd, J_{HH} 7.0, 0.8, 1H, Ar-H), 6.55 (dd, J_{HH} 9.4, 0.8, 1H, Ar-H), 6.62 (dd, J_{HH} 8.2, 7.0, 1H, Ar-H), 6.88 (m, 3H, Ar-H), 7.06 (m, 4H, Ar-H), 7.17 (m, 3H, Ar-H), 7.49 (m, 3H, Ar-H), 7.63 (m, 3H, Ar-H), 7.76 (m, 2H, Ar-H), 8.95 (br s, 1H, NH). IR (cm^{-1}): 3299 (NH), 1596 (C=$N_{pyridine}$). ESIMS *m/z*: 740 $[M]^+$, FABMS *m/z*: calculated 740.2468, found 740.2526.

5.4.13 Synthesis of 19

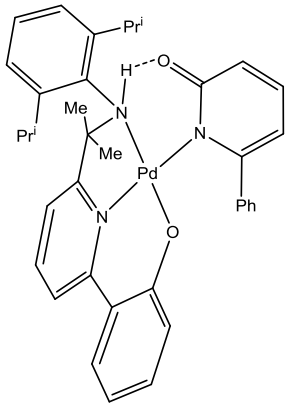

19

To a small glass vial was added [(2-(C_6H_4O)-6-{CMe_2NH(2,6-*i*-$Pr_2C_6H_3$)}C_5H_3N)]Pd(OAc) (0.010 g, 0.016 mmol) and the contents dissolved in C_6D_6 (0.5 mL) forming an orange solution. To this solution was added H_2**L8** (0.003 g, 0.016 mmol, 1 eq.) and the reaction mixture sonicated for 15 min. The ^{1}H NMR spectrum was recorded and showed 47% consumption of the starting material. The reaction mixture was filtered through a celite plug and the filtrate layered with petroleum ether forming **19** as red crystals (0.006 g, 60%).Mp. > 300 ^{o}C.^{1}H NMR (400 MHz, C_6D_6): δ 0.67 (d, J_{HH} 8.0, 3H, CH(CH_3)$_2$), 0.89 (d, J_{HH} 6.3, 3H, CH(CH_3)$_2$), 1.00 (s, 3H, C(CH_3)$_2$), 1.19 (d, J_{HH} 8.0, 3H, CH(CH_3)$_2$), 1.90 (s, 3H, C(CH_3)$_2$), 2.28 (sept, J_{HH} 6.0, 1H, C*H*(CH_3)$_2$), 3.85 (sept, J_{HH} 7.0, 1H, C*H*(CH_3)$_2$), 5.95 (dd, J_{HH} 7.0, 0.8, 2H, ArH), 6.47 (dd, J_{HH} 8.0, 4.0, 2H, ArH), 6.79 (m, 3H, ArH), 6.87 (m, 6H, ArH), 7.63 (m, 5H, ArH)), 9.46 (br s, 1H, N*H*). ESIMS *m/z*: 624 $[M]^+$. FABMS *m/z*: mass 624.1690 found 624.1696

5.4.14 Catalytic screening of 9a-c, 10a, 11b, 12b and 12c in the CH-bromination of H_2L8

A small Schlenk flask equipped with small stir bar was evacuated and backfilled with nitrogen. H_2**L8** (0.031 g, 0.181 mmol), NBS (0.100 g, 0.546 mmol, 3.1 eq.), palladium(II) pincer complex (0.009 mmol, 5 mol%) and dry MeCN (5 mL) were loaded into the flask. This vessel was sealed under nitrogen and stirred and heated to 120 ^{o}C. After 16 h, the vessel was cooled to room temperature and the volatiles removed under reduced. The residue was dissolved in dichloromethane (30 mL) and washed with water (3 x 20 mL). 1,3,5-Trimethoxybenzene was added as a standard (0.175 mmol) to the dichloromethane solution and all the volatiles removed under reduced pressure. A small amount of the solid

residue was dissolved in $CDCl_3$ (0.5 mL) and the ^1H NMR spectrum recorded. The percentage conversion to product could be determined by comparison to the standard.

5.5 Crystallographic Studies

All crystallographic data were collected on a Bruker APEX 2000 CCD diffractometer. Details of data collection, refinement and crystal data are listed in Tables 5.1 – 5.37. The data were corrected for Lorentz and polarisation effects and empirical absorption corrections applied. Structure solution by direct methods and structure refinement based on full-matrix least-squares on F^2 employed SHELXTL version 6.10. Hydrogen atoms were included in calculated positions (C-H = 0.96 – 1.00 Å) riding on the bonded atom with isotropic displacement parameters set to 1.5 U_{eq}(C) for methyl H atoms and 1.2 U_{eq}(C) for all other H atoms. All non-H atoms were refined with anisotropic displacement parameters

Table 5.1. Crystal data and structure refinement for H**L1**.

Identification code	09050	
Empirical formula	C34 H40 N2 O2	
Formula weight	508.68	
Temperature	150(2) K	
Wavelength	0.71073 Å	
Crystal system	Triclinic	
Space group	P-1	
Unit cell dimensions	a = 8.9542(16) Å	α= 89.451(3)°.
	b = 12.028(2) Å	β= 85.613(4)°.
	c = 14.082(3) Å	γ = 81.432(4)°.
Volume	1495.3(5) $Å^3$	
Z	2	
Density (calculated)	1.130 Mg/m^3	
Absorption coefficient	0.070 mm^{-1}	
F(000)	548	
Crystal size	0.25 x 0.23 x 0.12 mm^3	
Theta range for data collection	2.24 to 25.00°.	
Index ranges	-10<=h<=10, -14<=k<=14, -16<=l<=16	
Reflections collected	10849	
Independent reflections	5210 [R(int) = 0.0850]	
Completeness to theta = 25.00°	99.1 %	
Absorption correction	Empirical	
Max. and min. transmission	0.9917 and 0.9828	
Refinement method	Full-matrix least-squares on F^2	
Data / restraints / parameters	5210 / 0 / 303	
Goodness-of-fit on F^2	0.825	
Final R indices [I>2sigma(I)]	R1 = 0.0613, wR2 = 0.1362	
R indices (all data)	R1 = 0.1155, wR2 = 0.1513	
Largest diff. peak and hole	0.291 and -0.244 $e.Å^{-3}$	

Table 5.2. Crystal data and structure refinement for H**L3**.

Identification code	13031n	
Empirical formula	C31 H32 N2 O	
Formula weight	448.59	
Temperature	150(2) K	
Wavelength	0.71073 Å	
Crystal system	Orthorhombic	
Space group	Pna2(1)	
Unit cell dimensions	a = 22.238(8) Å	α= 90°.
	b = 13.302(5) Å	β= 90°.
	c = 8.410(3) Å	γ = 90°.
Volume	2487.7(16) $Å^3$	
Z	4	
Density (calculated)	1.198 Mg/m^3	
Absorption coefficient	0.072 mm^{-1}	
F(000)	960	
Crystal size	0.25 x 0.11 x 0.05 mm^3	
Theta range for data collection	1.78 to 25.00°.	
Index ranges	0<=h<=26, 0<=k<=15, -10<=l<=10	
Reflections collected	4369	
Independent reflections	2354 [R(int) = 0.1295]	
Completeness to theta = 25.00°	100.0 %	
Absorption correction	Empirical	
Max. and min. transmission	0.981 and 0.066	
Refinement method	Full-matrix least-squares on F^2	
Data / restraints / parameters	2354 / 1 / 312	
Goodness-of-fit on F^2	0.864	
Final R indices [I>2sigma(I)]	R1 = 0.0685, wR2 = 0.1197	
R indices (all data)	R1 = 0.1693, wR2 = 0.1498	
Absolute structure parameter	?	
Largest diff. peak and hole	0.203 and -0.265 $e.Å^{-3}$	

Table 5.3. Crystal data and structure refinement for **1a**.

Identification code	09097	
Empirical formula	C65 H66 Cl2 N4 O6 Pd2	
Formula weight	1282.92	
Temperature	150(2) K	
Wavelength	0.71073 Å	
Crystal system	Monoclinic	
Space group	P2(1)/c	
Unit cell dimensions	a = 15.311(2) Å	α= 90°.
	b = 11.6253(17) Å	β= 90.364(4)°.
	c = 32.923(5) Å	γ = 90°.
Volume	5860.0(15) $Å^3$	
Z	4	
Density (calculated)	1.454 Mg/m^3	
Absorption coefficient	0.760 mm^{-1}	
F(000)	2632	
Crystal size	0.14 x 0.10 x 0.09 mm^3	
Theta range for data collection	1.81 to 26.00°.	
Index ranges	-18<=h<=18, -14<=k<=14, -40<=l<=40	
Reflections collected	45009	
Independent reflections	11515 [R(int) = 0.2017]	
Completeness to theta = 26.00°	99.9 %	
Absorption correction	Empirical	
Max. and min. transmission	0.831 and 0.593	
Refinement method	Full-matrix least-squares on F^2	
Data / restraints / parameters	11515 / 0 / 720	
Goodness-of-fit on F^2	0.841	
Final R indices [I>2sigma(I)]	R1 = 0.0699, wR2 = 0.1035	
R indices (all data)	R1 = 0.1671, wR2 = 0.1271	
Largest diff. peak and hole	0.740 and -0.698 $e.Å^{-3}$	

Table 5.4. Crystal data and structure refinement for **1b**.

Identification code	10031	
Empirical formula	C30 H29 Cl N2 O Pd	
Formula weight	575.40	
Temperature	150(2) K	
Wavelength	0.71073 Å	
Crystal system	Monoclinic	
Space group	P2(1)/c	
Unit cell dimensions	a = 9.941(4) Å	α= 90°.
	b = 12.678(5) Å	β= 97.076(7)°.
	c = 20.671(8) Å	γ = 90°.
Volume	2585.3(17) $Å^3$	
Z	4	
Density (calculated)	1.478 Mg/m^3	
Absorption coefficient	0.847 mm^{-1}	
F(000)	1176	
Crystal size	0.33 x 0.27 x 0.18 mm^3	
Theta range for data collection	1.89 to 26.00°.	
Index ranges	-12<=h<=12, -15<=k<=15, -25<=l<=25	
Reflections collected	19633	
Independent reflections	5077 [R(int) = 0.1370]	
Completeness to theta = 26.00°	99.9 %	
Absorption correction	Empirical	
Max. and min. transmission	0.831 and 0.421	
Refinement method	Full-matrix least-squares on F^2	
Data / restraints / parameters	5077 / 0 / 374	
Goodness-of-fit on F^2	0.994	
Final R indices [I>2sigma(I)]	R1 = 0.0706, wR2 = 0.1377	
R indices (all data)	R1 = 0.1214, wR2 = 0.1552	
Largest diff. peak and hole	1.420 and -0.639 $e.Å^{-3}$	

Table 5.5. Crystal data and structure refinement for **2a**.

Identification code	10001	
Empirical formula	C33 H36 Cl2 N2 O3 Pd	
Formula weight	685.94	
Temperature	150(2) K	
Wavelength	0.71073 Å	
Crystal system	Monoclinic	
Space group	P2(1)/c	
Unit cell dimensions	a = 13.471(3) Å	α= 90°.
	b = 14.913(3) Å	β= 108.732(4)°.
	c = 16.595(4) Å	γ = 90°.
Volume	3157.1(12) $Å^3$	
Z	4	
Density (calculated)	1.443 Mg/m^3	
Absorption coefficient	0.792 mm^{-1}	
F(000)	1408	
Crystal size	0.15 x 0.13 x 0.04 mm^3	
Theta range for data collection	1.60 to 26.00°.	
Index ranges	-16<=h<=16, -18<=k<=18, -20<=l<=20	
Reflections collected	24097	
Independent reflections	6204 [R(int) = 0.1722]	
Completeness to theta = 26.00°	99.9 %	
Absorption correction	Empirical	
Max. and min. transmission	0.802 and 0.496	
Refinement method	Full-matrix least-squares on F^2	
Data / restraints / parameters	6204 / 0 / 375	
Goodness-of-fit on F^2	0.860	
Final R indices [I>2sigma(I)]	R1 = 0.0644, wR2 = 0.0905	
R indices (all data)	R1 = 0.1428, wR2 = 0.1070	
Largest diff. peak and hole	0.546 and -0.739 $e.Å^{-3}$	

Table 5.6. Crystal data and structure refinement for **2b**.

Identification code	10016	
Empirical formula	C39 H54 Cl N2 O2 Pd	
Formula weight	724.69	
Temperature	150(2) K	
Wavelength	0.71073 Å	
Crystal system	Triclinic	
Space group	P-1	
Unit cell dimensions	a = 10.5900(16) Å	α= 92.595(3)°.
	b = 10.9142(16) Å	β= 95.184(3)°.
	c = 14.160(2) Å	γ = 105.297(3)°.
Volume	1568.1(4) $Å^3$	
Z	2	
Density (calculated)	1.535 Mg/m^3	
Absorption coefficient	0.717 mm^{-1}	
F(000)	762	
Crystal size	0.18 x 0.13 x 0.12 mm^3	
Theta range for data collection	1.94 to 26.00°.	
Index ranges	-13<=h<=13, -13<=k<=13, -17<=l<=17	
Reflections collected	12345	
Independent reflections	6069 [R(int) = 0.0958]	
Completeness to theta = 26.00°	98.6 %	
Absorption correction	Empirical	
Max. and min. transmission	0.831 and 0.513	
Refinement method	Full-matrix least-squares on F^2	
Data / restraints / parameters	6069 / 0 / 320	
Goodness-of-fit on F^2	0.873	
Final R indices [I>2sigma(I)]	R1 = 0.0584, wR2 = 0.1216	
R indices (all data)	R1 = 0.0849, wR2 = 0.1289	
Largest diff. peak and hole	0.984 and -0.690 $e.Å^{-3}$	

Table 5.7. Crystal data and structure refinement for **3b**.

Identification code	15054	
Empirical formula	C31 H31 Cl N2 O Pd	
Formula weight	589.43	
Temperature	150(2) K	
Wavelength	0.71073 Å	
Crystal system	Monoclinic	
Space group	P2(1)/c	
Unit cell dimensions	a = 9.8163(17) Å	α= 90°.
	b = 12.530(2) Å	β= 93.803(4)°.
	c = 21.819(4) Å	γ = 90°.
Volume	2677.9(8) $Å^3$	
Z	4	
Density (calculated)	1.462 Mg/m^3	
Absorption coefficient	0.819 mm^{-1}	
F(000)	1208	
Crystal size	0.18 x 0.12 x 0.03 mm^3	
Theta range for data collection	1.87 to 26.00°.	
Index ranges	-12<=h<=12, -15<=k<=15, -26<=l<=26	
Reflections collected	20619	
Independent reflections	5255 [R(int) = 0.1382]	
Completeness to theta = 26.00°	99.9 %	
Absorption correction	Empirical	
Max. and min. transmission	0.831 and 0.567	
Refinement method	Full-matrix least-squares on F^2	
Data / restraints / parameters	5255 / 0 / 330	
Goodness-of-fit on F^2	0.928	
Final R indices [I>2sigma(I)]	R1 = 0.0591, wR2 = 0.1074	
R indices (all data)	R1 = 0.0900, wR2 = 0.1200	
Largest diff. peak and hole	1.360 and -1.486 $e.Å^{-3}$	

Table 5.8. Crystal data and structure refinement for **3c**.

Identification code	15038	
Empirical formula	C31 H31 Br N2 O Pd	
Formula weight	633.89	
Temperature	150(2) K	
Wavelength	0.71073 Å	
Crystal system	Monoclinic	
Space group	P2(1)/c	
Unit cell dimensions	a = 9.977(6) Å	α= 90°.
	b = 12.531(8) Å	β= 94.956(10)°.
	c = 21.605(13) Å	γ = 90°.
Volume	2691(3) $Å^3$	
Z	4	
Density (calculated)	1.565 Mg/m^3	
Absorption coefficient	2.201 mm^{-1}	
F(000)	1280	
Crystal size	0.30 x 0.09 x 0.02 mm^3	
Theta range for data collection	1.88 to 26.00°.	
Index ranges	-11<=h<=12, -15<=k<=15, -26<=l<=26	
Reflections collected	20094	
Independent reflections	5292 [R(int) = 0.1879]	
Completeness to theta = 26.00°	100.0 %	
Absorption correction	Empirical	
Max. and min. transmission	0.831 and 0.379	
Refinement method	Full-matrix least-squares on F^2	
Data / restraints / parameters	5292 / 0 / 331	
Goodness-of-fit on F^2	1.082	
Final R indices [I>2sigma(I)]	R1 = 0.1071, wR2 = 0.2274	
R indices (all data)	R1 = 0.1817, wR2 = 0.2558	
Extinction coefficient	0.0118(13)	
Largest diff. peak and hole	1.925 and -1.158 $e.Å^{-3}$	

Table 5.9. Crystal data and structure refinement for **4a**·OH_2

Identification code	12121	
Empirical formula	C102 H116 N6 O10 Pd3	
Formula weight	1905.21	
Temperature	150(2) K	
Wavelength	0.71073 Å	
Crystal system	Monoclinic	
Space group	P2(1)/c	
Unit cell dimensions	a = 25.178(11) Å	α= 90°.
	b = 37.050(16) Å	β= 101.394(10)°.
	c = 11.257(5) Å	γ = 90°.
Volume	10295(8) $Å^3$	
Z	4	
Density (calculated)	1.229 Mg/m^3	
Absorption coefficient	0.574 mm^{-1}	
F(000)	3952	
Crystal size	0.28 x 0.07 x 0.03 mm^3	
Theta range for data collection	1.84 to 25.00°.	
Index ranges	-29<=h<=29, -44<=k<=44, -13<=l<=13	
Reflections collected	74858	
Independent reflections	18104 [R(int) = 0.4530]	
Completeness to theta = 25.00°	99.9 %	
Absorption correction	Empirical	
Max. and min. transmission	0.862 and 0.669	
Refinement method	Full-matrix least-squares on F^2	
Data / restraints / parameters	18104 / 0 / 1046	
Goodness-of-fit on F^2	0.829	
Final R indices [I>2sigma(I)]	R1 = 0.0958, wR2 = 0.1926	
R indices (all data)	R1 = 0.3224, wR2 = 0.2573	
Largest diff. peak and hole	0.842 and -1.609 $e.Å^{-3}$	

Table 5.10. Crystal data and structure refinement for **4a**

Identification code	14002	
Empirical formula	C34 H38 N2 O3 Pd	
Formula weight	629.06	
Temperature	150(2) K	
Wavelength	0.71073 Å	
Crystal system	Monoclinic	
Space group	P2(1)/c	
Unit cell dimensions	a = 10.4373(15) Å	α= 90°.
	b = 15.856(2) Å	β= 93.447(3)°.
	c = 17.709(3) Å	γ = 90°.
Volume	2925.4(7) $Å^3$	
Z	4	
Density (calculated)	1.428 Mg/m^3	
Absorption coefficient	0.672 mm^{-1}	
F(000)	1304	
Crystal size	0.18 x 0.07 x 0.05 mm^3	
Theta range for data collection	1.73 to 26.00°.	
Index ranges	-12<=h<=12, -19<=k<=19, -21<=l<=21	
Reflections collected	22741	
Independent reflections	5756 [R(int) = 0.1837]	
Completeness to theta = 26.00°	100.0 %	
Absorption correction	Empirical	
Max. and min. transmission	0.831 and 0.602	
Refinement method	Full-matrix least-squares on F^2	
Data / restraints / parameters	5756 / 1 / 368	
Goodness-of-fit on F^2	0.712	
Final R indices [I>2sigma(I)]	R1 = 0.0609, wR2 = 0.0862	
R indices (all data)	R1 = 0.1601, wR2 = 0.1063	
Largest diff. peak and hole	0.744 and -1.002 $e.Å^{-3}$	

Table 5.11. Crystal data and structure refinement for **4b**

Identification code	13005	
Empirical formula	C33 H37 Cl3 N2 O Pd	
Formula weight	690.40	
Temperature	150(2) K	
Wavelength	0.71073 Å	
Crystal system	Triclinic	
Space group	P-1	
Unit cell dimensions	a = 10.546(2) Å	α= 95.268(4)°.
	b = 12.444(3) Å	β= 110.131(3)°.
	c = 12.911(3) Å	γ = 90.841(4)°.
Volume	1582.2(6) $Å^3$	
Z	2	
Density (calculated)	1.449 Mg/m^3	
Absorption coefficient	0.868 mm^{-1}	
F(000)	708	
Crystal size	0.23 x 0.12 x 0.09 mm^3	
Theta range for data collection	1.65 to 26.00°.	
Index ranges	-13<=h<=12, -15<=k<=15, -15<=l<=15	
Reflections collected	12477	
Independent reflections	6137 [R(int) = 0.0740]	
Completeness to theta = 26.00°	98.9 %	
Absorption correction	Empirical	
Max. and min. transmission	0.831 and 0.538	
Refinement method	Full-matrix least-squares on F^2	
Data / restraints / parameters	6137 / 0 / 368	
Goodness-of-fit on F^2	0.964	
Final R indices [I>2sigma(I)]	R1 = 0.0476, wR2 = 0.0957	
R indices (all data)	R1 = 0.0633, wR2 = 0.1011	
Largest diff. peak and hole	0.889 and -0.938 $e.Å^{-3}$	

Table 5.12. Crystal data and structure refinement for **4c**

Identification code	13081	
Empirical formula	C34 H37 Cl6 I N2 O Pd	
Formula weight	935.66	
Temperature	150(2) K	
Wavelength	0.71073 Å	
Crystal system	Monoclinic	
Space group	P2(1)/n	
Unit cell dimensions	a = 14.627(3) Å	α= 90°.
	b = 16.778(4) Å	β= 103.966(4)°.
	c = 15.762(3) Å	γ = 90°.
Volume	3753.8(13) $Å^3$	
Z	4	
Density (calculated)	1.656 Mg/m^3	
Absorption coefficient	1.774 mm^{-1}	
F(000)	1856	
Crystal size	0.32 x 0.16 x 0.03 mm^3	
Theta range for data collection	1.71 to 26.00°.	
Index ranges	-18<=h<=17, -20<=k<=20, -19<=l<=19	
Reflections collected	29120	
Independent reflections	7370 [R(int) = 0.1316]	
Completeness to theta = 26.00°	100.0 %	
Absorption correction	Empirical	
Max. and min. transmission	0.831 and 0.590	
Refinement method	Full-matrix least-squares on F^2	
Data / restraints / parameters	7370 / 0 / 412	
Goodness-of-fit on F^2	0.836	
Final R indices [I>2sigma(I)]	R1 = 0.0512, wR2 = 0.0745	
R indices (all data)	R1 = 0.1013, wR2 = 0.0852	
Largest diff. peak and hole	0.708 and -0.822 $e.Å^{-3}$	

Table 5.13. Crystal data and structure refinement for **5a**

Identification code	12123	
Empirical formula	C39 H43 N3 O4 Pd	
Formula weight	724.16	
Temperature	150(2) K	
Wavelength	0.71073 Å	
Crystal system	Monoclinic	
Space group	P2(1)/n	
Unit cell dimensions	a = 12.6746(19) Å	α= 90°.
	b = 10.5982(16) Å	β= 96.364(4)°.
	c = 26.668(4) Å	γ = 90°.
Volume	3560.2(9) $Å^3$	
Z	4	
Density (calculated)	1.351 Mg/m^3	
Absorption coefficient	0.564 mm^{-1}	
F(000)	1504	
Crystal size	0.13 x 0.10 x 0.08 mm^3	
Theta range for data collection	1.54 to 25.99°.	
Index ranges	-15<=h<=15, -13<=k<=13, -32<=l<=32	
Reflections collected	27345	
Independent reflections	6993 [R(int) = 0.1796]	
Completeness to theta = 25.99°	99.9 %	
Absorption correction	Empirical	
Max. and min. transmission	0.831 and 0.556	
Refinement method	Full-matrix least-squares on F^2	
Data / restraints / parameters	6993 / 0 / 431	
Goodness-of-fit on F^2	0.786	
Final R indices [I>2sigma(I)]	R1 = 0.0626, wR2 = 0.0860	
R indices (all data)	R1 = 0.1433, wR2 = 0.1042	
Largest diff. peak and hole	0.596 and -0.621 $e.Å^{-3}$	

Table 5.14. Crystal data and structure refinement for **5b**

Identification code	13002	
Empirical formula	C152 H170 N12 O11 Pd4	
Formula weight	2766.60	
Temperature	150(2) K	
Wavelength	0.71073 Å	
Crystal system	Monoclinic	
Space group	P2(1)/n	
Unit cell dimensions	a = 15.699(2) Å	α= 90°.
	b = 10.8745(16) Å	β= 109.911(3)°.
	c = 20.628(3) Å	γ = 90°.
Volume	3311.1(8) $Å^3$	
Z	1	
Density (calculated)	1.387 Mg/m^3	
Absorption coefficient	0.601 mm^{-1}	
F(000)	1438	
Crystal size	0.20 x 0.13 x 0.06 mm^3	
Theta range for data collection	2.00 to 26.00°.	
Index ranges	-19<=h<=19, -13<=k<=13, -25<=l<=25	
Reflections collected	25484	
Independent reflections	6510 [R(int) = 0.1531]	
Completeness to theta = 26.00°	99.9 %	
Absorption correction	Empirical	
Max. and min. transmission	0.8311 and 0.611	
Refinement method	Full-matrix least-squares on F^2	
Data / restraints / parameters	6510 / 3 / 413	
Goodness-of-fit on F^2	0.824	
Final R indices [I>2sigma(I)]	R1 = 0.0599, wR2 = 0.0973	
R indices (all data)	R1 = 0.1244, wR2 = 0.1141	
Largest diff. peak and hole	0.871 and -0.887 $e.Å^{-3}$	

Table 5.15. Crystal data and structure refinement for **5d**

Identification code	13033	
Empirical formula	C37 H38 F N3 O2 Pd	
Formula weight	682.10	
Temperature	150(2) K	
Wavelength	0.71073 Å	
Crystal system	Orthorhombic	
Space group	Pbca	
Unit cell dimensions	a = 12.921(5) Å	α= 90°.
	b = 20.810(8) Å	β= 90°.
	c = 23.105(9) Å	γ = 90°.
Volume	6213(4) $Å^3$	
Z	8	
Density (calculated)	1.458 Mg/m^3	
Absorption coefficient	0.642 mm^{-1}	
F(000)	2816	
Crystal size	0.22 x 0.20 x 0.18 mm^3	
Theta range for data collection	1.76 to 26.00°.	
Index ranges	-15<=h<=15, -24<=k<=25, -28<=l<=28	
Reflections collected	46573	
Independent reflections	6104 [R(int) = 0.1094]	
Completeness to theta = 26.00°	100.0 %	
Absorption correction	Empirical	
Max. and min. transmission	0.831 and 0.728	
Refinement method	Full-matrix least-squares on F^2	
Data / restraints / parameters	6104 / 0 / 403	
Goodness-of-fit on F^2	1.014	
Final R indices [I>2sigma(I)]	R1 = 0.0523, wR2 = 0.1349	
R indices (all data)	R1 = 0.0865, wR2 = 0.1491	
Largest diff. peak and hole	2.869 and -0.396 $e.Å^{-3}$	

Table 5.16. Crystal data and structure refinement for **7a**

Identification code	13069	
Empirical formula	C39 H39 I N2 O3 Pd	
Formula weight	817.02	
Temperature	150(2) K	
Wavelength	0.71073 Å	
Crystal system	Monoclinic	
Space group	P2(1)/c	
Unit cell dimensions	a = 9.340(2) Å	α= 90°.
	b = 41.778(11) Å	β= 102.915(6)°.
	c = 8.691(2) Å	γ = 90°.
Volume	3305.4(15) Å3	
Z	4	
Density (calculated)	1.642 Mg/m3	
Absorption coefficient	1.537 mm-1	
F(000)	1640	
Crystal size	0.18 x 0.08 x 0.06 mm3	
Theta range for data collection	1.95 to 26.00°.	
Index ranges	-11<=h<=11, -51<=k<=51, -10<=l<=10	
Reflections collected	26122	
Independent reflections	6502 [R(int) = 0.1622]	
Completeness to theta = 26.00°	99.9 %	
Absorption correction	Empirical	
Max. and min. transmission	0.831 and 0.610	
Refinement method	Full-matrix least-squares on F2	
Data / restraints / parameters	6502 / 0 / 421	
Goodness-of-fit on F2	0.830	
Final R indices [I>2sigma(I)]	R1 = 0.0601, wR2 = 0.0856	
R indices (all data)	R1 = 0.1334, wR2 = 0.1029	
Largest diff. peak and hole	0.749 and -0.941 e.Å-3	

Table 5.17. Crystal data and structure refinement for **7b**

Identification code	13088	
Empirical formula	C34 H35 F3 N2 O3 Pd	
Formula weight	683.04	
Temperature	150(2) K	
Wavelength	0.71073 Å	
Crystal system	Monoclinic	
Space group	P2(1)/n	
Unit cell dimensions	a = 12.566(3) Å	α= 90°.
	b = 16.814(3) Å	β= 104.565(4)°.
	c = 14.486(3) Å	γ = 90°.
Volume	2962.2(10) $Å^3$	
Z	4	
Density (calculated)	1.532 Mg/m^3	
Absorption coefficient	0.684 mm^{-1}	
F(000)	1400	
Crystal size	0.12 x 0.10 x 0.05 mm^3	
Theta range for data collection	1.89 to 26.00°.	
Index ranges	-15<=h<=15, -20<=k<=20, -17<=l<=17	
Reflections collected	23251	
Independent reflections	5830 [R(int) = 0.1601]	
Completeness to theta = 26.00°	99.9 %	
Absorption correction	Empirical	
Max. and min. transmission	0.831 and 0.579	
Refinement method	Full-matrix least-squares on F^2	
Data / restraints / parameters	5830 / 0 / 394	
Goodness-of-fit on F^2	0.819	
Final R indices [I>2sigma(I)]	R1 = 0.0590, wR2 = 0.0824	
R indices (all data)	R1 = 0.1196, wR2 = 0.0968	
Largest diff. peak and hole	0.728 and -1.364 $e.Å^{-3}$	

Table 5.18. Crystal data and structure refinement for **8**

Identification code	13080	
Empirical formula	C75 H82 Ag3 Cl12 F9 N4 O16 Pd2 S3	
Formula weight	2524.44	
Temperature	150(2) K	
Wavelength	0.71073 Å	
Crystal system	Triclinic	
Space group	P-1	
Unit cell dimensions	a = 13.906(4) Å	α= 78.049(5)°.
	b = 14.598(4) Å	β= 78.004(5)°.
	c = 23.233(6) Å	γ = 80.442(5)°.
Volume	4476(2) $Å^3$	
Z	2	
Density (calculated)	1.873 Mg/m^3	
Absorption coefficient	1.551 mm^{-1}	
F(000)	2508	
Crystal size	0.32 x 0.14 x 0.11 mm^3	
Theta range for data collection	1.62 to 26.00°.	
Index ranges	-16<=h<=17, -17<=k<=18, -28<=l<=28	
Reflections collected	35290	
Independent reflections	17350 [R(int) = 0.0941]	
Completeness to theta = 26.00°	98.7 %	
Absorption correction	Empirical	
Max. and min. transmission	0.831 and 0.591	
Refinement method	Full-matrix least-squares on F^2	
Data / restraints / parameters	17350 / 1041 / 1015	
Goodness-of-fit on F^2	0.809	
Final R indices [I>2sigma(I)]	R1 = 0.0619, wR2 = 0.1194	
R indices (all data)	R1 = 0.1174, wR2 = 0.1325	
Largest diff. peak and hole	1.116 and -0.699 $e.Å^{-3}$	

Table **5.19.** Crystal data and structure refinement for **10a**

Identification code	13046	
Empirical formula	C52 H46 N2 O4 Pd2	
Formula weight	975.71	
Temperature	150(2) K	
Wavelength	0.71073 Å	
Crystal system	Monoclinic	
Space group	P2(1)/n	
Unit cell dimensions	a = 5.8696(15) Å	α= 90°.
	b = 22.606(6) Å	β= 94.689(5)°.
	c = 15.824(4) Å	γ = 90°.
Volume	2092.6(9) $Å^3$	
Z	2	
Density (calculated)	1.549 Mg/m^3	
Absorption coefficient	0.909 mm^{-1}	
F(000)	992	
Crystal size	0.20 x 0.18 x 0.05 mm^3	
Theta range for data collection	1.57 to 26.00°.	
Index ranges	-7<=h<=7, -26<=k<=27, -19<=l<=19	
Reflections collected	16306	
Independent reflections	4100 [R(int) = 0.1010]	
Completeness to theta = 26.00°	99.4 %	
Absorption correction	Empirical	
Max. and min. transmission	0.831 and 0.510	
Refinement method	Full-matrix least-squares on F^2	
Data / restraints / parameters	4100 / 5 / 273	
Goodness-of-fit on F^2	0.954	
Final R indices [I>2sigma(I)]	R1 = 0.0545, wR2 = 0.1106	
R indices (all data)	R1 = 0.0853, wR2 = 0.1195	
Largest diff. peak and hole	1.304 and -0.949 $e.Å^{-3}$	

Table 5.20. Crystal data and structure refinement for **11a**

Identification code	15072	
Empirical formula	C56 H52 N4 O8 Pd4	
Formula weight	1334.62	
Temperature	150(2) K	
Wavelength	0.71073 Å	
Crystal system	Tetragonal	
Space group	P-42(1)c	
Unit cell dimensions	a = 12.1803(16) Å	α= 90°.
	b = 12.1803(16) Å	β= 90°.
	c = 16.090(3) Å	γ = 90°.
Volume	2387.0(6) $Å^3$	
Z	2	
Density (calculated)	1.857 Mg/m^3	
Absorption coefficient	1.546 mm^{-1}	
F(000)	1328	
Crystal size	0.23 x 0.09 x 0.08 mm^3	
Theta range for data collection	2.10 to 26.99°.	
Index ranges	-15<=h<=15, -15<=k<=15, -20<=l<=20	
Reflections collected	19416	
Independent reflections	2608 [R(int) = 0.0833]	
Completeness to theta = 26.99°	99.9 %	
Absorption correction	Empirical	
Max. and min. transmission	0.831 and 0.674	
Refinement method	Full-matrix least-squares on F^2	
Data / restraints / parameters	2608 / 0 / 165	
Goodness-of-fit on F^2	0.974	
Final R indices [I>2sigma(I)]	R1 = 0.0338, wR2 = 0.0674	
R indices (all data)	R1 = 0.0539, wR2 = 0.0724	
Absolute structure parameter	-0.01(7)	
Largest diff. peak and hole	0.712 and -0.483 $e.Å^{-3}$	

Table 5.21. Crystal data and structure refinement for **11b**

Identification code	15065	
Empirical formula	C337 H392 N16 O32 Pd16	
Formula weight	6881.07	
Temperature	150(2) K	
Wavelength	0.71073 Å	
Crystal system	Monoclinic	
Space group	P2(1)/c	
Unit cell dimensions	a = 15.293(4) Å	α= 90°.
	b = 35.159(8) Å	β= 116.784(4)°.
	c = 15.712(4) Å	γ = 90°.
Volume	7542(3) $Å^3$	
Z	1	
Density (calculated)	1.515 Mg/m^3	
Absorption coefficient	0.998 mm^{-1}	
F(000)	3518	
Crystal size	0.36 x 0.14 x 0.03 mm^3	
Theta range for data collection	1.56 to 26.00°.	
Index ranges	-18<=h<=18, -43<=k<=43, -19<=l<=19	
Reflections collected	58383	
Independent reflections	14814 [R(int) = 0.0811]	
Completeness to theta = 26.00°	99.9 %	
Absorption correction	Empirical	
Max. and min. transmission	0.831 and 0.616	
Refinement method	Full-matrix least-squares on F^2	
Data / restraints / parameters	14814 / 32 / 941	
Goodness-of-fit on F^2	1.001	
Final R indices [I>2sigma(I)]	R1 = 0.0451, wR2 = 0.1003	
R indices (all data)	R1 = 0.0655, wR2 = 0.1067	
Largest diff. peak and hole	1.350 and -0.795 $e.Å^{-3}$	

Table 5.22. Crystal data and structure refinement for **12a**

Identification code	13038	
Empirical formula	C25 H22 N2 O2 Pd	
Formula weight	488.85	
Temperature	150(2) K	
Wavelength	0.71073 Å	
Crystal system	Monoclinic	
Space group	P2(1)/n	
Unit cell dimensions	a = 22.507(8) Å	α= 90°.
	b = 6.562(2) Å	β= 102.520(6)°.
	c = 28.359(9) Å	γ = 90°.
Volume	4089(2) $Å^3$	
Z	8	
Density (calculated)	1.588 Mg/m^3	
Absorption coefficient	0.932 mm^{-1}	
F(000)	1984	
Crystal size	0.39 x 0.06 x 0.04 mm^3	
Theta range for data collection	1.47 to 26.00°.	
Index ranges	-27<=h<=27, -8<=k<=8, -33<=l<=34	
Reflections collected	30777	
Independent reflections	8009 [R(int) = 0.1483]	
Completeness to theta = 26.00°	99.8 %	
Absorption correction	Empirical	
Max. and min. transmission	0.831 and 0.612	
Refinement method	Full-matrix least-squares on F^2	
Data / restraints / parameters	8009 / 62 / 545	
Goodness-of-fit on F^2	0.892	
Final R indices [I>2sigma(I)]	R1 = 0.0654, wR2 = 0.1211	
R indices (all data)	R1 = 0.1435, wR2 = 0.1449	
Largest diff. peak and hole	0.966 and -0.836 $e.Å^{-3}$	

Table 5.23. Crystal data and structure refinement for **12b**

Identification code	13061	
Empirical formula	C27 H24 Cl2 N2 O4 Pd	
Formula weight	617.78	
Temperature	150(2) K	
Wavelength	0.71073 Å	
Crystal system	Triclinic	
Space group	P-1	
Unit cell dimensions	a = 8.057(3) Å	α= 106.660(7)°.
	b = 11.909(4) Å	β= 99.085(8)°.
	c = 14.463(5) Å	γ = 106.264(8)°.
Volume	1232.7(8) $Å^3$	
Z	2	
Density (calculated)	1.664 Mg/m^3	
Absorption coefficient	1.008 mm^{-1}	
F(000)	624	
Crystal size	0.33 x 0.15 x 0.03 mm^3	
Theta range for data collection	1.52 to 26.00°.	
Index ranges	-9<=h<=9, -14<=k<=14, -17<=l<=17	
Reflections collected	9843	
Independent reflections	4793 [R(int) = 0.1064]	
Completeness to theta = 26.00°	98.9 %	
Absorption correction	Empirical	
Max. and min. transmission	0.831 and 0.460	
Refinement method	Full-matrix least-squares on F^2	
Data / restraints / parameters	4793 / 0 / 328	
Goodness-of-fit on F^2	0.888	
Final R indices [I>2sigma(I)]	R1 = 0.0661, wR2 = 0.1159	
R indices (all data)	R1 = 0.1095, wR2 = 0.1296	
Largest diff. peak and hole	1.101 and -1.057 $e.Å^{-3}$	

Table 5.24. Crystal data and structure refinement for **13a**

Identification code	13043	
Empirical formula	C25 H22 N2 O3 Pd	
Formula weight	504.85	
Temperature	150(2) K	
Wavelength	0.71073 Å	
Crystal system	Monoclinic	
Space group	P2(1)	
Unit cell dimensions	a = 7.494(2) Å	α= 90°.
	b = 23.410(7) Å	β= 90.654(5)°.
	c = 12.000(4) Å	γ = 90°.
Volume	2105.1(11) $Å^3$	
Z	4	
Density (calculated)	1.593 Mg/m^3	
Absorption coefficient	0.912 mm^{-1}	
F(000)	1024	
Crystal size	0.37 x 0.20 x 0.13 mm^3	
Theta range for data collection	1.70 to 27.00°.	
Index ranges	-9<=h<=9, -29<=k<=29, -15<=l<=15	
Reflections collected	17735	
Independent reflections	8873 [R(int) = 0.0420]	
Completeness to theta = 27.00°	99.8 %	
Absorption correction	Empirical	
Max. and min. transmission	0.831 and 0.684	
Refinement method	Full-matrix least-squares on F^2	
Data / restraints / parameters	8873 / 1 / 565	
Goodness-of-fit on F^2	0.993	
Final R indices [I>2sigma(I)]	R1 = 0.0359, wR2 = 0.0663	
R indices (all data)	R1 = 0.0408, wR2 = 0.0687	
Absolute structure parameter	-0.01(2)	
Largest diff. peak and hole	0.846 and -0.654 $e.Å^{-3}$	

Table 5.25. Crystal data and structure refinement for **13b**

Identification code	13050	
Empirical formula	C49 H53 Cl N2 O3 Pd	
Formula weight	859.78	
Temperature	150(2) K	
Wavelength	0.71073 Å	
Crystal system	Monoclinic	
Space group	P2(1)/n	
Unit cell dimensions	a = 15.302(3) Å	α= 90°.
	b = 13.009(3) Å	β= 96.614(5)°.
	c = 34.156(7) Å	γ = 90°.
Volume	6754(2) $Å^3$	
Z	8	
Density (calculated)	1.691 Mg/m^3	
Absorption coefficient	0.684 mm^{-1}	
F(000)	3584	
Crystal size	0.26 x 0.18 x 0.08 mm^3	
Theta range for data collection	1.20 to 25.00°.	
Index ranges	-18<=h<=18, -15<=k<=15, -40<=l<=40	
Reflections collected	48143	
Independent reflections	11893 [R(int) = 0.1395]	
Completeness to theta = 25.00°	99.9 %	
Absorption correction	Empirical	
Max. and min. transmission	0.831 and 0.600	
Refinement method	Full-matrix least-squares on F^2	
Data / restraints / parameters	11893 / 0 / 581	
Goodness-of-fit on F^2	0.803	
Final R indices [I>2sigma(I)]	R1 = 0.0546, wR2 = 0.1194	
R indices (all data)	R1 = 0.1014, wR2 = 0.1279	
Largest diff. peak and hole	0.568 and -0.720 $e.Å^{-3}$	

Table 5.26. Crystal data and structure refinement for H_2**L8**

Identification code	14012	
Empirical formula	C11 H9 N O	
Formula weight	171.19	
Temperature	150(2) K	
Wavelength	0.71073 Å	
Crystal system	Triclinic	
Space group	P-1	
Unit cell dimensions	a = 6.1264(15) Å	α= 105.758(4)°.
	b = 8.461(2) Å	β= 97.473(4)°.
	c = 8.639(2) Å	γ = 102.181(4)°.
Volume	412.85(17) $Å^3$	
Z	2	
Density (calculated)	1.377 Mg/m^3	
Absorption coefficient	0.089 mm^{-1}	
F(000)	180	
Crystal size	0.43 x 0.33 x 0.24 mm^3	
Theta range for data collection	2.50 to 25.00°.	
Index ranges	-7<=h<=7, -10<=k<=10, -10<=l<=10	
Reflections collected	2967	
Independent reflections	1438 [R(int) = 0.0371]	
Completeness to theta = 25.00°	99.0 %	
Absorption correction	Empirical	
Max. and min. transmission	0.969 and 0.679	
Refinement method	Full-matrix least-squares on F^2	
Data / restraints / parameters	1438 / 0 / 118	
Goodness-of-fit on F^2	1.054	
Final R indices [I>2sigma(I)]	R1 = 0.0515, wR2 = 0.1347	
R indices (all data)	R1 = 0.0566, wR2 = 0.1396	
Largest diff. peak and hole	0.256 and -0.327 $e.Å^{-3}$	

Table 5.27. Crystal data and structure refinement for H_2**L8**-3Br

Identification code	13095	
Empirical formula	C11 H8 Br N O	
Formula weight	250.09	
Temperature	150(2) K	
Wavelength	0.71073 Å	
Crystal system	Orthorhombic	
Space group	Pca2(1)	
Unit cell dimensions	a = 12.527(3) Å	α= 90°.
	b = 10.481(2) Å	β= 90°.
	c = 14.733(3) Å	γ = 90°.
Volume	1934.4(7) $Å^3$	
Z	8	
Density (calculated)	1.718 Mg/m^3	
Absorption coefficient	4.212 mm^{-1}	
F(000)	992	
Crystal size	0.26 x 0.15 x 0.08 mm^3	
Theta range for data collection	2.53 to 25.99°.	
Index ranges	-15<=h<=15, -12<=k<=12, -18<=l<=18	
Reflections collected	14385	
Independent reflections	3779 [R(int) = 0.0908]	
Completeness to theta = 25.99°	99.9 %	
Absorption correction	Empirical	
Max. and min. transmission	0.894 and 0.405	
Refinement method	Full-matrix least-squares on F^2	
Data / restraints / parameters	3779 / 1 / 249	
Goodness-of-fit on F^2	0.953	
Final R indices [I>2sigma(I)]	R1 = 0.0542, wR2 = 0.1168	
R indices (all data)	R1 = 0.0745, wR2 = 0.1243	
Absolute structure parameter	0.25(2)	
Largest diff. peak and hole	1.234 and -0.528 $e.Å^{-3}$	

Table 5.28. Crystal data and structure refinement for H**L8**-3,5-Br_2

Identification code	15116	
Empirical formula	C11 H7 Br2 N O	
Formula weight	329.00	
Temperature	150(2) K	
Wavelength	0.71073 Å	
Crystal system	Triclinic	
Space group	P-1	
Unit cell dimensions	a = 3.969(2) Å	α= 111.989(8)°.
	b = 11.698(6) Å	β= 97.542(9)°.
	c = 12.294(6) Å	γ = 94.823(9)°.
Volume	519.2(5) $Å^3$	
Z	2	
Density (calculated)	2.104 Mg/m^3	
Absorption coefficient	7.774 mm^{-1}	
F(000)	316	
Crystal size	0.19 x 0.06 x 0.02 mm^3	
Theta range for data collection	1.81 to 26.00°.	
Index ranges	-4<=h<=4, -14<=k<=14, -14<=l<=15	
Reflections collected	4076	
Independent reflections	2019 [R(int) = 0.0846]	
Completeness to theta = 26.00°	99.2 %	
Absorption correction	Empirical	
Max. and min. transmission	0.928 and 0.487	
Refinement method	Full-matrix least-squares on F^2	
Data / restraints / parameters	2019 / 0 / 136	
Goodness-of-fit on F^2	0.929	
Final R indices [I>2sigma(I)]	R1 = 0.0723, wR2 = 0.1630	
R indices (all data)	R1 = 0.1043, wR2 = 0.1747	
Largest diff. peak and hole	1.682 and -1.195 e.$Å^{-3}$	

Table 5.29. Crystal data and structure refinement for o-Br-**L8**-3,5-Br_2

Identification code	15076	
Empirical formula	C11 H6 Br3 N O	
Formula weight	407.90	
Temperature	150(2) K	
Wavelength	0.71073 Å	
Crystal system	Triclinic	
Space group	P-1	
Unit cell dimensions	a = 5.0517(10) Å	α= 111.689(3)°.
	b = 10.306(2) Å	β= 94.175(3)°.
	c = 12.288(2) Å	γ = 91.769(3)°.
Volume	591.7(2) $Å^3$	
Z	2	
Density (calculated)	2.289 Mg/m^3	
Absorption coefficient	10.201 mm^{-1}	
F(000)	384	
Crystal size	0.17 x 0.14 x 0.05 mm^3	
Theta range for data collection	1.79 to 27.00°.	
Index ranges	-6<=h<=6, -13<=k<=13, -15<=l<=15	
Reflections collected	5006	
Independent reflections	2545 [R(int) = 0.0509]	
Completeness to theta = 27.00°	98.1 %	
Absorption correction	Empirical	
Max. and min. transmission	0.894 and 0.431	
Refinement method	Full-matrix least-squares on F^2	
Data / restraints / parameters	2545 / 0 / 145	
Goodness-of-fit on F^2	0.974	
Final R indices [I>2sigma(I)]	R1 = 0.0479, wR2 = 0.1112	
R indices (all data)	R1 = 0.0604, wR2 = 0.1153	
Largest diff. peak and hole	1.383 and -0.838 $e.Å^{-3}$	

Table 5.30. Crystal data and structure refinement for o-Cl-**L8**-3,5-Cl_2

Identification code	15150	
Empirical formula	C11 H6 Cl3 N O	
Formula weight	274.52	
Temperature	150(2) K	
Wavelength	0.71073 Å	
Crystal system	Monoclinic	
Space group	P2(1)/c	
Unit cell dimensions	a = 13.274(8) Å	α= 90°.
	b = 10.693(7) Å	β= 101.963(12)°.
	c = 7.744(5) Å	γ = 90°.
Volume	1075.4(11) $Å^3$	
Z	4	
Density (calculated)	1.696 Mg/m^3	
Absorption coefficient	0.824 mm^{-1}	
F(000)	552	
Crystal size	0.10 x 0.08 x 0.04 mm^3	
Theta range for data collection	1.57 to 26.00°.	
Index ranges	-16<=h<=16, -13<=k<=13, -9<=l<=9	
Reflections collected	8233	
Independent reflections	2113 [R(int) = 0.1409]	
Completeness to theta = 26.00°	99.9 %	
Absorption correction	Empirical	
Max. and min. transmission	0.928 and 0.050	
Refinement method	Full-matrix least-squares on F^2	
Data / restraints / parameters	2113 / 0 / 145	
Goodness-of-fit on F^2	0.926	
Final R indices [I>2sigma(I)]	R1 = 0.0692, wR2 = 0.1506	
R indices (all data)	R1 = 0.1038, wR2 = 0.1635	
Largest diff. peak and hole	0.689 and -0.873 $e.Å^{-3}$	

Table 5.31. Crystal data and structure refinement for 6-(2-C_6H_5)-5,5-F_2-6-OH-C_5H_2NH-2-O

Identification code	15131	
Empirical formula	C11 H9 F2 N O2	
Formula weight	225.19	
Temperature	150(2) K	
Wavelength	0.71073 Å	
Crystal system	Monoclinic	
Space group	P2(1)/c	
Unit cell dimensions	a = 9.4571(17) Å	α= 90°.
	b = 7.9066(14) Å	β= 96.823(3)°.
	c = 27.244(5) Å	γ = 90°.
Volume	2022.7(6) $Å^3$	
Z	8	
Density (calculated)	1.479 Mg/m^3	
Absorption coefficient	0.126 mm^{-1}	
F(000)	928	
Crystal size	0.32 x 0.15 x 0.08 mm^3	
Theta range for data collection	1.51 to 26.00°.	
Index ranges	-11<=h<=11, -9<=k<=9, -33<=l<=32	
Reflections collected	15223	
Independent reflections	3979 [R(int) = 0.0736]	
Completeness to theta = 26.00°	99.9 %	
Absorption correction	Empirical	
Max. and min. transmission	0.962 and 0.730	
Refinement method	Full-matrix least-squares on F^2	
Data / restraints / parameters	3979 / 0 / 291	
Goodness-of-fit on F^2	0.948	
Final R indices [I>2sigma(I)]	R1 = 0.0583, wR2 = 0.1442	
R indices (all data)	R1 = 0.0879, wR2 = 0.1545	
Largest diff. peak and hole	1.327 and -0.241 $e.Å^{-3}$	

Table 5.32. Crystal data and structure refinement for **14**

Identification code	14033	
Empirical formula	C26 H22 N2 O6 Pd2	
Formula weight	671.26	
Temperature	150(2) K	
Wavelength	0.71073 Å	
Crystal system	Triclinic	
Space group	P-1	
Unit cell dimensions	a = 9.863(5) Å	α= 100.292(11)°.
	b = 10.016(5) Å	β= 111.794(7)°.
	c = 13.265(8) Å	γ = 97.959(8)°.
Volume	1166.7(11) $Å^3$	
Z	2	
Density (calculated)	1.911 Mg/m^3	
Absorption coefficient	1.589 mm^{-1}	
F(000)	664	
Crystal size	0.43 x 0.36 x 0.08 mm^3	
Theta range for data collection	1.71 to 27.00°.	
Index ranges	-12<=h<=12, -12<=k<=12, -16<=l<=16	
Reflections collected	9609	
Independent reflections	4963 [R(int) = 0.0365]	
Completeness to theta = 27.00°	97.4 %	
Absorption correction	Empirical	
Max. and min. transmission	0.831 and 0.586	
Refinement method	Full-matrix least-squares on F^2	
Data / restraints / parameters	4963 / 0 / 327	
Goodness-of-fit on F^2	1.094	
Final R indices [I>2sigma(I)]	R1 = 0.0451, wR2 = 0.1089	
R indices (all data)	R1 = 0.0543, wR2 = 0.1134	
Largest diff. peak and hole	1.470 and -1.033 e.$Å^{-3}$	

Table 5.33. Crystal data and structure refinement for **15**

Identification code	14067	
Empirical formula	C45 H33 Cl3 N4 O4 Pd2	
Formula weight	1012.90	
Temperature	150(2) K	
Wavelength	0.71073 Å	
Crystal system	Monoclinic	
Space group	P2(1)/n	
Unit cell dimensions	a = 11.443(4) Å	α= 90°.
	b = 28.611(10) Å	β= 111.677(6)°.
	c = 13.203(5) Å	γ = 90°.
Volume	4017(2) $Å^3$	
Z	4	
Density (calculated)	1.675 Mg/m^3	
Absorption coefficient	1.145 mm^{-1}	
F(000)	2024	
Crystal size	0.35 x 0.22 x 0.10 mm^3	
Theta range for data collection	1.81 to 26.00°.	
Index ranges	-13<=h<=14, -35<=k<=34, -16<=l<=16	
Reflections collected	31103	
Independent reflections	7887 [R(int) = 0.1701]	
Completeness to theta = 26.00°	99.9 %	
Absorption correction	Empirical	
Max. and min. transmission	0.831 and 0.622	
Refinement method	Full-matrix least-squares on F^2	
Data / restraints / parameters	7887 / 0 / 523	
Goodness-of-fit on F^2	0.984	
Final R indices [I>2sigma(I)]	R1 = 0.0563, wR2 = 0.0999	
R indices (all data)	R1 = 0.0826, wR2 = 0.1093	
Largest diff. peak and hole	1.576 and -1.982 $e.Å^{-3}$	

Table 5.34. Crystal data and structure refinement for **16**

Identification code	14003	
Empirical formula	C44 H28 N4 O4 Pd4	
Formula weight	1102.30	
Temperature	150(2) K	
Wavelength	0.71073 Å	
Crystal system	Monoclinic	
Space group	C2/c	
Unit cell dimensions	a = 19.239(10) Å	α= 90°.
	b = 12.081(6) Å	β= 107.061(9)°.
	c = 15.660(8) Å	γ = 90°.
Volume	3480(3) $Å^3$	
Z	4	
Density (calculated)	2.104 Mg/m^3	
Absorption coefficient	2.089 mm^{-1}	
F(000)	2144	
Crystal size	0.43 x 0.16 x 0.06 mm^3	
Theta range for data collection	2.02 to 27.00°.	
Index ranges	-24<=h<=23, -15<=k<=15, -19<=l<=19	
Reflections collected	14334	
Independent reflections	3812 [R(int) = 0.0660]	
Completeness to theta = 27.00°	99.9 %	
Absorption correction	Empirical	
Max. and min. transmission	0.831 and 0.603	
Refinement method	Full-matrix least-squares on F^2	
Data / restraints / parameters	3812 / 0 / 253	
Goodness-of-fit on F^2	1.031	
Final R indices [I>2sigma(I)]	R1 = 0.0453, wR2 = 0.1012	
R indices (all data)	R1 = 0.0685, wR2 = 0.1093	
Largest diff. peak and hole	1.334 and -0.671 e.$Å^{-3}$	

Table 5.35. Crystal data and structure refinement for **17**.

Identification code	14043	
Empirical formula	C22 H17 Cl N2 O2 Pd	
Formula weight	483.23	
Temperature	150(2) K	
Wavelength	0.71073 Å	
Crystal system	Monoclinic	
Space group	P2(1)/n	
Unit cell dimensions	a = 8.0105(18) Å	α= 90°.
	b = 16.587(4) Å	β= 91.366(5)°.
	c = 13.840(3) Å	γ = 90°.
Volume	1838.4(7) $Å^3$	
Z	4	
Density (calculated)	1.746 Mg/m^3	
Absorption coefficient	1.176 mm^{-1}	
F(000)	968	
Crystal size	0.30 x 0.10 x 0.05 mm^3	
Theta range for data collection	1.92 to 26.00°.	
Index ranges	-9<=h<=9, -20<=k<=20, -16<=l<=17	
Reflections collected	14237	
Independent reflections	3612 [R(int) = 0.1200]	
Completeness to theta = 26.00°	99.9 %	
Absorption correction	Empirical	
Max. and min. transmission	0.831 and 0.575	
Refinement method	Full-matrix least-squares on F^2	
Data / restraints / parameters	3612 / 0 / 253	
Goodness-of-fit on F^2	0.898	
Final R indices [I>2sigma(I)]	R1 = 0.0534, wR2 = 0.0927	
R indices (all data)	R1 = 0.0896, wR2 = 0.1022	
Largest diff. peak and hole	0.938 and -0.653 $e.Å^{-3}$	

Table 5.36. Crystal data and structure refinement for **18.**

Identification code	14063	
Empirical formula	C87 H88 Cl2 N6 O4 Pd2	
Formula weight	1565.33	
Temperature	150(2) K	
Wavelength	0.71073 Å	
Crystal system	Triclinic	
Space group	P-1	
Unit cell dimensions	a = 12.754(2) Å	α= 79.663(3)°.
	b = 12.771(2) Å	β= 84.270(3)°.
	c = 23.038(4) Å	γ = 89.478(3)°.
Volume	3672.7(12) $Å^3$	
Z	2	
Density (calculated)	1.415 Mg/m^3	
Absorption coefficient	0.620 mm^{-1}	
F(000)	1620	
Crystal size	0.44 x 0.42 x 0.22 mm^3	
Theta range for data collection	1.60 to 27.00°.	
Index ranges	-16<=h<=16, -16<=k<=16, -29<=l<=29	
Reflections collected	30967	
Independent reflections	15731 [R(int) = 0.0409]	
Completeness to theta = 27.00°	98.1 %	
Absorption correction	Empirical	
Max. and min. transmission	0.831 and 0.577	
Refinement method	Full-matrix least-squares on F^2	
Data / restraints / parameters	15731 / 0 / 922	
Goodness-of-fit on F^2	0.976	
Final R indices [I>2sigma(I)]	R1 = 0.0383, wR2 = 0.0838	
R indices (all data)	R1 = 0.0513, wR2 = 0.0885	
Largest diff. peak and hole	0.756 and -0.549 $e.Å^{-3}$	

Table 5.37. Crystal data and structure refinement for **19**.

Identification code	14101	
Empirical formula	C37 H43 N3 O4 Pd	
Formula weight	700.14	
Temperature	150(2) K	
Wavelength	0.71073 Å	
Crystal system	Monoclinic	
Space group	P2(1)/n	
Unit cell dimensions	a = 9.675(3) Å	α= 90°.
	b = 33.738(9) Å	β= 112.475(5)°.
	c = 10.850(3) Å	γ = 90°.
Volume	3272.6(15) $Å^3$	
Z	4	
Density (calculated)	1.421 Mg/m^3	
Absorption coefficient	0.611 mm^{-1}	
F(000)	1456	
Crystal size	0.39 x 0.15 x 0.10 mm^3	
Theta range for data collection	2.12 to 26.00°.	
Index ranges	-11<=h<=11, -41<=k<=41, -13<=l<=13	
Reflections collected	25554	
Independent reflections	6419 [R(int) = 0.1046]	
Completeness to theta = 26.00°	99.8 %	
Absorption correction	Empirical	
Max. and min. transmission	0.831 and 0.675	
Refinement method	Full-matrix least-squares on F^2	
Data / restraints / parameters	6419 / 4 / 412	
Goodness-of-fit on F^2	0.871	
Final R indices [I>2sigma(I)]	R1 = 0.0480, wR2 = 0.0739	
R indices (all data)	R1 = 0.0809, wR2 = 0.0816	
Largest diff. peak and hole	0.655 and -0.813 $e.Å^{-3}$	

Appendix

Synthesis of *trans*-[Pd(OAc)$_2$(3,5-lutidine)]

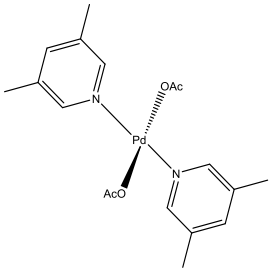

In a small glass vile $Pd(OAc)_2$ (0.042 g, 0.186 mmol), 3,5-lutidine (0.040 g, 0.372 mmol, 2 eq.) and dry toluene (5 mL) was added and sonicated for 30 min and left for 24 h at room temperature. Light yellow precipitates were filtered and dissolved in chloroform. Solvents were removed to get bright yellow solid. ^{1}H NMR (400 MHz, $CDCl_3$): δ 1.85 (s, 6H, 2x CH3), 2.29 (s, 12H, 4 x CH3), 7.36 (s, 2H, py-H), 8.32 (s, 4H, py-H). $^{13}C\{^1H\}$ NMR (100 MHz, $CDCl_3$): 18.3 (CH_3), 23.3 (CH_3), 134.2, 139.8, 148.7, 178.0. ESIMS: *m/z* 319 [Pd(3,5-lutidine)$_2$], 379 [Pd(3,5-lutidine)$_2$OAc], 437 [M^+-2H], HRMS [Pd(3,5-lutidine)$_2$OAc] calculated 379.0638 found 379.0631

Postgraduate activities

Internal Seminars

16/01/2013	John Slattery, University of York
23/01/2013	Prof. Sabine Flitsch, University of Manchester
06/02/2013	Prof. Nicholas Tomkinson, University of Strathclyde
13/02/2013	Dr Miles Congreve, Head of Chemistry, Heptares Therapeutics
06/03/2013	Prof Andrew Wilson, University of Leeds
16/10/2013	Dr Ramon Rios Torres, University of Southampton
22/10/2013	Professor Maya Shankar Singh, Banaras Hindu University, India
13/11/2013	Professor Lee Cronin, Regius Chair of Chemistry University of Glasgow
20/11/2013	Professor Oliver Einsle, University of Freiburg, Germany
05/02/2014	Prof. Ian Baxendale, University of Durham
05/03/2014	Prof. Carl Redshaw, University of Hull
08/10/2014	Prof Gareth Williams, Durham University
03/12/2014	Prof Graham Hutchins, University of Huddersfield
12/02/2015	Professor Simon Lancaster, University of East Anglia
13/04/2015	Prof Ed Tate, Imperial College, London
14/06/2016	Professor Ming Bao, School of Petroleum and Chemical Engineering, Dalian University of Technology

Internal Symposia

University of Leicester Department of Chemistry Postgraduate Research Symposia:

2013: Oral presentation given: "Palladium pincers with H-bond donor and acceptor capacities"

Publications/Posters

"From discrete monomeric complexes to hydrogen bonded dimeric assemblies based on sterically encumbered square planar palladium(II) ONN-pincers" O. Adeyi, W. B. Cross, G. Forrest, L. Godfrey, E. G. Hope, A. McLeod, A. Singh, K. Singh, G. A. Solan, Y. Wang and L. A. Wright, *Dalton Trans*., 2013, **42**, 7710.

"Probing non-covalent interactions using functionalised pyridine-based pincers" Dalton transactions conference in Warwick, April 2014